Phenomenological aspects of bimetric theory

Marvin Lüben

München 2021

Phenomenological aspects of bimetric theory

Marvin Lüben

Dissertation
an der Fakultät für Physik
der Ludwig–Maximilians–Universität
München

vorgelegt von
Marvin Lüben
aus Gifhorn

München, den 20. April 2021

Erstgutachter: Prof. Dr. Jochen Weller
Zweitgutachter: Prof. Dr. Dieter Lüst
Tag der mündlichen Prüfung: 14. Juni 2021

Contents

In aller Kürze

Wir beschäftigen uns mit der von Hassan und Rosen präsentierten geistfreien bimetrischen Gravitationstheorie, welche eine Erweiterung der Allgemeinen Relativitätstheorie darstellt. Diese Theorie postuliert zusätzlich zum gewöhnlichen masselosen Spin-2 Teilchen ein weiteres massives Spin-2 Teilchen, welche vollständig nichtlinearen (Selbst-)Interaktionen unterliegen. Wir schlagen ein neues vereinheitlichendes Rahmenwerk vor, das uns erlaubt, die Theorie konsistent und umfassend mithilfe theoretischer und beobachtungsbezogener Überlegungen einzuschränken. Dieses Rahmenwerk fußt auf den folgenden Parametern, die eine direkte physikalische Interpretation ermöglichen: die Masse des Spin-2 Teilchens, seine Kopplungsstärke an Standardteilchen, sowie die effektive kosmologische Konstante. Wir ermitteln theoretische Einschränkungen an diese Parameter, welche eine konsistente kosmische Expansionsgeschichte garantieren, d.h. reellwertig, nicht-singulär und ohne Higuchi-Geist. Ferner bestimmen wir solche Parameterkombinationen, die zu wohl-definierten kosmologischen Perturbationen mithilfe des Vainshtein-Mechanismus führen. Nach diesen formellen Überlegungen, stellen wir unsere Theorie kosmologischen und lokalen Gravitationstests sorfältig gegenüber. Wir finden heraus, daß die bimetrische Gravitationstheorie genauso gut zu diesen beobachteten Daten passt wie das kosmologische Standardmodell. Aus theoretischer Perspektive impliziert das eine Präferenz für die selbst-beschleunigenden bimetrischen Modelle, welche keine Vakuumenergie beinhalten. Interessanterweise ist die Theorie mit den Beobachtungen selbst dann vereinbar, wenn das massive Spin-2 Teilchen äußerst schwer ist. Unsere Untersuchungen liefern die bisher umfassendsten und stringentesten Einschränkungen an diese Theorie. Zu guter Letzt betrachten wir das frühe Universum und beschäftigen uns mit Konsequenzen des massiven Spin-2 Teilchens auf die kosmische Inflation. Wir zeigen, daß Unitarität eine obere Schranke an die Steigung des Inflatonpotentials impliziert, welche die aus der de Sitter-Sumpfland-Vermutung resultierende untere Schranke ergänzt.

Abstract

We are concerned with ghost-free bimetric theory due to Hassan and Rosen, an extension of General Relativity. The theory proposes to supplement the usual massless spin-2 field with an additional massive spin-2 field, which (self-)interact fully nonlinearly. We propose a new unified framework, which allows to consistently and comprehensively constrain bimetric theory by means of theoretical and observational considerations. Our framework builds upon the following physically interpretable parameters: the mass of the spin-2 field, its coupling strength to ordinary matter, and the effective cosmological constant. We compute theoretical constraints on these parameters to ensure a viable cosmic expansion history, i.e. real-valued, non-singular, and devoid of the Higuchi ghost. We then identify those parameter combinations that are a priori consistent on the level of cosmological perturbations due to the Vainshtein screening mechanism. Building upon these formal considerations, we perform a thorough confrontation of bimetric theory with cosmological and local tests of gravity. We find that bimetric theory generally fits the observed data as good as the cosmological standard model, signalling a theoretical preference for the self-accelerating models devoid of vacuum energy. Interestingly, even a heavy spin-2 field is perfectly consistent with the observed data. Our investigations yield the to date most comprehensive and stringent constraints on bimetric theory. We finally move to the early universe and explore consequences of a massive spin-2 field on cosmic inflation. We show that unitarity leads to an upper bound in the inflaton potential, which complements the lower swampland de Sitter bound.

Acknowledgements

My endless gratitude goes to Dieter Lüst and Jochen Weller for their supervision and advice. Your warm personalities, scientific advise and continuing support, in particular during the difficult periods, allowed me to enjoy doing research to the fullest, which ultimately led to this thesis.

I am extremely grateful to Angnis Schmidt-May without whom not a single line of this thesis would have been written. In particular, I want to thank you for giving me absolute research freedom and encouraging guidance at the same time.

This work would not have been possible without my other former and current collaborators, Yashar Akrami, Luca Amendola, Angelo Caravano, Edvard Mörtsell, Juri Smirnov, and Adam Solomon. Thank you for sharing your knowledge and enthusiasm with me.

I want to thank Ralph Blumenhagen, Martin Kerscher, Thomas Kuhr, and Georg Raffelt, for being members of my doctoral examination committee.

I am infinitely grateful to my dear office mates, Verónica Errasti Díez and Julio Méndez-Zavaleta, for the great and fun time together with endless discussions and numerous night shifts. Your friendship and encouragement are essential to this work.

Further, I am deeply thankful to Elisa Ferreira and Azadeh Maleknejad for their selfless support on various occasions. I am honored to know you and having discussed some mysterious of our Universe with you.

I thank all my fellow students and other colleagues including but not limited to Henk Bart, Lasha Berezhiani, Max Brinkmann, Giordano Cintia, Alessandra Gnecchi, Nicolás González Albornoz, Brage Gording, Nico Hamaus, Daniela Herschmann, Daniel Kläwer, Andriana Makridou, Chrysoula Markou, David Osten, Georgia Pollina, Ariadna Ribes Metidieri, and Florian Wolf. I very much enjoyed the great work atmosphere and supportive environment you created. Special thanks to Thomas Hahn for his infinite patience regarding my numerous technical issues and to Corina Brunnlechner, Monika Goldammer, and Annette Sturm for their ever present help.

Last but not least I want to express my deep gratitude to Max Brinkmann, Angelo Caravano, Marcus Högas, Julio Méndez-Zavaleta, and especially Verónica Errasti Díez, whose careful reading of and benevolent criticism on the previous manuscripts brought this thesis into a digestible form.

I wish you only the best with all my heart for hopefully many exciting years ahead.

Part I

Introduction and review

Chapter 1

Introduction

Owing to its all-permeating manifestation in our everyday life experience, we all are familiar with gravity. Therefore, it is not surprising that gravity was the first force of nature to be uncovered: Newton established the famous Inverse-Square-Law of the gravitational force in his 1687 published Principia [1]. Gravity rules the falling of an apple from a tree and the orbiting of planets around the Sun. Going further, gravity is the dominating force on the largest observable scales and as such determines the evolution of the Universe as a whole. Nonetheless, even centuries after its discovery, our comprehension of gravity is challenged precisely on these cosmological scales. Overwhelming observational evidence suggests that the Universe is primarily filled with exotic forms of matter and energy, which lack a fundamental description as of yet. It is the purpose of this thesis to contribute to the ongoing efforts to provide an explanation for these enigmatic cosmic constituents and to thereby deepen our understanding of gravity itself.

The modern foundation of gravity is Einstein's theory of General Relativity (GR) [2–4]. GR proposes to consider gravity as a consequence of spacetime deformations, which in turn result from the presence of mass/energy. The theory building principles are equivalence (namely, an observer freely falling in a gravitational field locally measures flat Minkowski spacetime) and general covariance (that is, the freedom to choose coordinates). GR withstands solar system tests to remarkable precision. Further, various of the theory's predictions have been observationally confirmed. The historical success of correctly describing the precession of Mercury's orbit [5] has been complemented by the prediction and subsequent detection of, for example, gravitational lensing [6, 7], gravitational waves [8–11] and most recently black holes [12, 13].

Despite these successes, the theory is severely challenged at both the largest and smallest scales. Let us begin by briefly revisiting some of the most prominent obstacles at large scales. In order to account for the apparent enhancement of gravity on (extra)galactic scales, first observed by Zwicky [14] and more accurately by Rubin et al. [15,16], an exotic matter component dubbed *dark matter* is introduced. The measured acceleration of the cosmic expansion at present times [17,18] suggests that gravity becomes weaker at even larger, cosmological scales. This is accounted for by the introduction of an exotic energy component with negative pressure baptised *dark energy*. Even though dark matter admits a particle interpretation, which has led to the ongoing postulation of many theoretically consistent models and in turn to multiple efforts for their direct detection, it hitherto has failed to receive any experimental evidence outside gravity. On the other hand, dark energy can be modelled by a cosmological constant, but the fine-tuning problem [19,20] and more recently its claimed quantum inconsistency [21–28] theoretically disfavours or even rules out such scenario, respectively. Altogether, the dark sector comprises 95% of the universe's current energy budget, impugning GR as the ultimate theory of gravity unless particle physics turns out to provide convincing explanations. It is therefore reasonable to look for alternatives on the gravitational side.

Coming to the smallest scales, the presence of singularities [29] and the renormalisation problem [30–35] limit our understanding of quantum gravity. In fact, GR serves as a low-energy effective field theory that requires an ultraviolet (UV) completion [36, 37]. String Theory (ST)

represents the arguably most celebrated such completion. At low energies, ST predicts effective actions that contain higher curvature corrections and couplings to fields with various spins, in addition to the Einstein–Hilbert term of GR [38]. Explicitly computing these effective actions in string perturbation theory is cumbersome, to say the least. Instead, we can seek alternatives to GR in a bottom–up approach and thereby chart the landscape of consistent low-energy effective theories. The latter is the approach that will be exploited in this thesis.

Modifying gravity at low energies is a rather difficult task as well. Almost any alteration of the Einstein–Hilbert action leads to formal inconsistencies, such as ghosts [39, 40]. Ghosts are additional propagating degrees of freedom (beyond the expected physical modes) and they possess a negative kinetic energy. Consequently, the presence of ghosts makes any theory mathematically ill-defined and unphysical. As such, ghostful theories must be ruled out. In addition, any modification must recover GR in its observationally tested limits; for example, in the solar system. Generically, modified gravity theories contain new degrees of freedom that also couple to matter. These couplings result in supplementary gravitational-strength fifth forces. Therefore, almost every viable modified gravity theory gives rise to a *screening mechanism*, which suppresses the said fifth force locally while maintaining its desired strength on cosmological scales. Finding viable alternatives to GR remains an ongoing important research program: it is capable of addressing the aforementioned open problems of modern cosmology and it contributes to finding a fundamental understanding of gravity.

From a field theoretic perspective, GR is the unique Lorentz-invariant theory describing a massless spin-2 field with nonlinear self-interactions [41–45]. Hence, a straightforward modification of Einstein's theory amounts to promoting its spin-2 field to be massive. Consistent field theories for massless and massive fields with spin up to 1 have been known for decades. The quest for finding a consistent theory for a massive spin-2 field dates back to Fierz and Pauli [46], who postulated a linearised theory. It was long thought that any nonlinear completion would unavoidably be plagued by ghost instabilities [47]. This fallacy has been overcome only rather recently, leading to the postulation of ghost-free nonlinear massive gravity [48–51] and its extension: bimetric theory (BT) [51, 52]. The latter theory describes a massive and a massless spin-2 fields, which are (self-)interacting fully nonlinearly.

BT is the basis for the analyses carried out in this thesis. By now, BT's theoretical consistency has been firmly established and thus we are naturally led to the thorough study of its phenomenological consequences. In the following, we present substantial progress on deciding whether BT is capable of addressing one or several of the aforementioned problems of modern cosmology. We are mostly concerned with the problem of dark energy. As a result, we will find that BT is not only theoretically consistent, but also withstands a long list of cosmological and local tests of gravity. Therefore, the self-accelerating bimetric models, which do not inherit any vacuum energy, stand out as particularly promising alternatives to the standard model.

Organisation of the thesis

In the remainder of this chapter, we provide more details on GR and we introduce the cosmological standard model. This serves as a basis for studying modified gravity theories and, in particular, cosmological solutions therein. We present more detailed theoretical and observational arguments against a cosmological constant, which serves as major motivation for seeking an alternative explanation for dark energy.

Chapter 2 discusses the usual challenges one must face when modifying gravity and provides an overview of some of their (potential) resolutions explored in the literature. We continue with a thorough introduction to theories of massive spin-2 fields, following the historical developments that ultimately led to the postulation of nonlinear ghost-free massive gravity. We finish with BT, for which we present the action and equations of motion, review its ghost freedom proof and discuss its coupling to matter.

In Chapter 3, we review the cosmological and the spherically symmetric solutions in the so-called singly-coupled version of BT. As we shall explain, these solutions are most relevant for assessing the phenomenological viability of the theory. This finishes the review of existing results.

In Chapter 4, we propose a new parametrisation for the solutions of BT. Our physical parametrisation provides the first unified framework to consistently study the phenomenology of BT. Moreover, it allows for the combination of the various theoretical and observational constraints that apply on the theory. Our detailed analyses set the basis for subsequent investigations of this promising theory.

As we will argue in due time, linear cosmological perturbations are unstable during early times in BT. Equipped with our physical parametrisation, in Chapter 5 we show that the early universe is screened by the Vainshtein mechanism. Our findings suggest that perturbations are nonlinearly stabilised. Consequently, we vouch for a substantial enlargement of the a priori consistent parameter space, compared to previous claims in the literature.

In Chapter 6, we confront the thus enlarged parameter space of BT with cosmological and local tests of gravity. We show that BT indeed withstands all these tests (just like GR), for large regions of its parameter space.

Leaving the realm of late-time cosmology, we study the implications of a massive spin-2 field during inflation in Chapter 7. We show that unitarity implies an upper limit on the derivative of the inflaton potential, which complements bounds from quantum gravity and the swampland.

Last but not least, in Chapter 8 we summarise our results, put them into context and provide a future outlook. For instance, we use our results to argue that BT has the potential to provide a unified explanation for the entire dark sector.

This thesis is based on the following publications:

- *Vainshtein Screening in Bimetric Cosmology*
  M. Lüben, J. Smirnov, A. Schmidt-May
  Phys.Rev.D 102 (2020) 123529 [1912.09449]

- *Physical parameter space of bimetric theory and SN1a constraints*
  M. Lüben, A. Schmidt-May, J. Weller
  JCAP 09 (2020) 024 [2003.03382]

- *Higuchi bound on slow-roll inflation and the swampland*
  M. Lüben, D. Lüst
  JHEP 09 (2020) 055 [2003.10494]

- *Combining cosmological and local bounds on bimetric theory*
  A. Caravano, M. Lüben, J. Weller
  — [2101.08791]

During the author's doctoral studies, also the following publications arose:

- *Ghost-Free Completion of An Effective Matter Coupling in Bimetric Theory*
  M. Lüben, A. Schmidt-May
  Fortsch.Phys. 66 (2018) 6, 1800031 [1804.04671]

- *Bimetric cosmology is compatible with local tests of gravity*
  M. Lüben, E. Mörtsell, A. Schmidt-May
  Class.Quant.Grav. 37 (2020) 4, 047001 [1812.08686]

- *Phase transitions in the early universe*
  M. B. Hindmarsh, M. Lüben, J. Lumma, M. Pauly
  SciPost Phys.Lect.Notes 24 (2021) 1 [2008.09136]

- *The Black Hole Entropy Distance Conjecture and Black Hole Evaporation*
  M. Lüben, D. Lüst, A. Ribes Metidieri
  Fortsch.Phys. 69 (2021) 3, 2000130 [2011.12331]

Notations and conventions

Throughout this thesis we work in natural units by setting the speed of light c and Planck's constant $\hbar$ to unity, $c = \hbar = 1$. We denote the reduced Planck mass as $M_{\rm P} = (8\pi G_{\rm N})^{-1/2}$ with $G_{\rm N} \simeq 6.674 \times 10^{-11}\,{\rm m}^3\,{\rm kg}^{-1}\,{\rm s}^{-2}$ Newton's gravitational constant. Occasionally we make use of the solar mass $M_\odot \simeq 2.0 \times 10^{30}\,{\rm kg}$ and the mass of the Earth $M_\oplus \simeq 6.0 \times 10^{24}\,{\rm kg}$.

For the metric we use the signature $(-,+,+,+)$. The flat Minkowski metric is denoted by $\eta_{\mu\nu}$. Spacetime indices are labeled by Greek letters $\mu, \nu, \cdots = 0, 1, 2, 3$, while spatial components are labeled by the Latin letters $i, j, \cdots = 1, 2, 3$. Symmetrisation on a pair of indices is denoted by parenthesis as $2S_{(\mu\nu)} = S_{\mu\nu} + S_{\nu\mu}$ for a generic tensor S. We denote the partial derivative by ∂ and the covariant derivative by ∇. Differentiation with respect to cosmic time t is denoted by a dot.

1.1 General Relativity

We start by providing a succinct overview of the theory that we we will later on modify: General Relativity. It is a geometrical theory, which relates the motion of matter to the curvature of spacetime. John A. Wheeler summarises the theory in the following way: "Spacetime tells matter how to move; matter tells spacetime how to curve" [53]. Here we will present the theoretical framework for that following standard textbooks [45, 54–59].

The first key concept we introduce is that of the *line element* ${\rm d}s$: the infinitesimal distance between two events in spacetime. Let $x := \{x^\mu\}$ be a coordinate system on a Lorentzian manifold. Then, the line element can be expressed as

$$ {\rm d}s^2 = g_{\mu\nu}{\rm d}x^\mu {\rm d}x^\nu \,. \tag{1.1} $$

The 4-dimensional symmetric metric tensor $g_{\mu\nu}$ generically depends on the spacetime coordinates and encodes the geometry of the Lorentzian manifold.

Another fundamental concept in GR is the principle of general covariance. It states that physics does not depend on the choice of coordinates x. This is implemented through the requirement that the physics of GR remains invariant under generic coordinate transformations $x \to \tilde{x}$ (or diffeomorphisms). Since the line interval must be invariant under the transformation, $\widetilde{{\rm d}s} = {\rm d}s$, the change of coordinates induces the following transformation on the metric tensor:

$$ g_{\mu\nu}(x) \;\longrightarrow\; \tilde{g}_{\mu\nu}(\tilde{x}) = \frac{\partial x^\alpha}{\partial \tilde{x}^\mu}\frac{\partial x^\beta}{\partial \tilde{x}^\nu} g_{\alpha\beta}(x)\,, \tag{1.2} $$

where $\tilde{g}_{\mu\nu}$ is the metric in the new coordinate system. In general, a (p,q)–tensor is defined to transform under a general coordinate transformations as

$$ T^{\mu_1\cdots\mu_p}_{\nu_1\cdots\nu_1} \;\longrightarrow\; \tilde{T}^{\mu_1\cdots\mu_p}_{\nu_1\cdots\nu_q} = \frac{\partial x^{\alpha_1}}{\partial \tilde{x}^{\nu_1}}\cdots\frac{\partial x^{\alpha_q}}{\partial \tilde{x}^{\nu_q}}\cdot\frac{\partial x^{\mu_1}}{\partial \tilde{x}^{\beta_1}}\cdots\frac{\partial x^{\mu_p}}{\partial \tilde{x}^{\beta_p}}\cdot T^{\beta_1\cdots\beta_q}_{\alpha_1\cdots\alpha_p}\,. \tag{1.3} $$

A tensor, which is vanishing in one coordinate system, is vanishing in every coordinate system (and vice versa). Therefore, tensors play a crucial role in defining physical observables.

Next, let us study derivatives of tensors. It can be shown that the partial derivative, schematically $\partial_\alpha T^{\mu_1\cdots}_{\nu_1\cdots}$, does not transform as a tensor. Instead, one introduces the covariant derivative, denoted by ∇_α, such that $\nabla_\alpha T^{\mu_1\cdots}_{\nu_1\cdots}$ transforms as a tensor. For the special case of a contravariant vector v^μ, the covariant derivative is explicitly given by

$$ \nabla_\alpha v^\mu = \partial_\alpha v^\mu + \Gamma^\mu_{\alpha\beta} v^\beta\,, \tag{1.4} $$

which generalises to (p,q)–tensors straightforwardly. The object $\Gamma^\mu_{\alpha\beta}$ is the *Levi–Civita connection*, which is chosen such that $\nabla_\alpha g_{\mu\nu} = 0$. The covariant derivative is then said to be metric compatible. It follows that

$$ \Gamma^\mu_{\alpha\beta} = \frac{1}{2} g^{\mu\nu}\left(\partial_\alpha g_{\nu\beta} + \partial_\beta g_{\alpha\nu} - \partial_\nu g_{\alpha\beta}\right)\,. \tag{1.5} $$

The covariant derivative allows to quantify the curvature of spacetime by means of the *Reimann curvature tensor*

$$R^{\alpha}{}_{\beta\mu\nu} = \partial_\mu \Gamma^{\alpha}_{\beta\nu} - \partial_\nu \Gamma^{\alpha}_{\mu\beta} + \Gamma^{\alpha}_{\mu\lambda}\Gamma^{\lambda}_{\beta\nu} - \Gamma^{\alpha}_{\nu\lambda}\Gamma^{\lambda}_{\mu\beta}\,, \tag{1.6}$$

which measures the relative shift of a vector after being parallelly transported around an infinitesimal closed curve. An important symmetry property of this tensor is the (differential) Bianchi identity

$$\nabla_\gamma R_{\mu\nu\alpha\beta} + \nabla_\alpha R_{\mu\nu\beta\gamma} + \nabla_\beta R_{\mu\nu\gamma\alpha} = 0\,. \tag{1.7}$$

We now have all the geometrical machinery to define Einstein's theory of gravitation.

In GR, the metric tensor $g_{\mu\nu}$ is a dynamical field. Its dynamics is captured by the renowned *Einstein–Hilbert action* [2–4, 60]

$$S_{\mathrm{EH}} = -\frac{M_{\mathrm{P}}^2}{2}\int \mathrm{d}^4x\sqrt{-g}\,(\mathcal{R} - 2\Lambda)\,, \tag{1.8}$$

where $\mathcal{R} = g^{\mu\nu}R_{\mu\nu}$ denotes the scalar curvature, with $R_{\mu\nu} = R^{\alpha}{}_{\mu\alpha\nu}$ the *Ricci tensor*. Notice that we have already included the cosmological constant Λ, although the theory was first presented without that term [2–4].

The Einstein–Hilbert action (1.8) encodes the dynamics of the metric tensor $g_{\mu\nu}$ in the presence of a cosmological constant, but without any matter fields yet. To couple the theory to matter, we introduce a generic matter Lagrangian $\mathcal{L}_{\mathrm{m}}$, which is determined by particle physics. Let us collectively denote all matter fields by Φ. The total action is then given by

$$S = -\frac{M_{\mathrm{P}}^2}{2}\int \mathrm{d}^4x\sqrt{-g}\,(\mathcal{R} - 2\Lambda) + \int \mathrm{d}^4x\sqrt{-g}\mathcal{L}_{\mathrm{m}}(g_{\mu\nu}, \Phi)\,. \tag{1.9}$$

The functional variation of the action (1.9) with respect to $g^{\mu\nu}$ leads to the equations of motion

$$G_{\mu\nu} + \Lambda g_{\mu\nu} = \frac{1}{M_{\mathrm{P}}^2}T_{\mu\nu}\,, \tag{1.10}$$

which are referred to as *Einstein equations*. The first term is the *Einstein tensor*, defined as $G_{\mu\nu} = R_{\mu\nu} - \frac{1}{2}g_{\mu\nu}\mathcal{R}$. The term on the right hand side is the *stress-energy tensor* of matter,

$$T_{\mu\nu} = -\frac{2}{\sqrt{-g}}\frac{\delta\left(\sqrt{-g}\mathcal{L}_{\mathrm{m}}\right)}{\delta g^{\mu\nu}}\,. \tag{1.11}$$

The Riemann curvature tensor fulfils the Bianchi identity (1.7), which is a geometrical property and hence independent of the field equations. It implies that the Einstein tensor is covariantly conserved:

$$\nabla^\mu G_{\mu\nu} = 0\,. \tag{1.12}$$

Note that here the spacetime indices can be freely raised and lowered with respect to $g_{\mu\nu}$, due to the metric compatibility of the covariant derivative. Applying the covariant derivative to the Einstein equations thus leads to

$$\nabla^\mu T_{\mu\nu} = 0\,. \tag{1.13}$$

This equation means that matter stress-energy is covariantly conserved as well.

After this brief mathematical introduction, let us jump to the phenomenological consequences of Einstein's theory of gravity in the context of cosmology.

1.2 The Standard Model of Cosmology

The main motivation for this thesis lies within cosmology, which is the study of the universe as a whole and as such concerned with the largest observable scales. The cosmological standard model, which will be introduced below, relies on GR as the gravitational theory and assumes the universe

to be filled with dark energy, non-relativistic matter, radiation and an inflaton field at very early times. Broadly speaking, cosmology falls into two categories: background and perturbations. We will be mostly concerned with the background level and will only briefly comment on the perturbative level in the context of bimetric theory. Our subsequent discussion closely follows standard textbooks, see e.g. [61–64].

The *cosmological principle* states that, on sufficiently large scales, the universe is homogenous and isotropic. This statement reflects that there is neither a preferred location nor a preferred direction in space. While isotropy is observationally confirmed to high significance [65], proving homogeneity is more involved [66]. Assuming the cosmological principle, the Friedmann–Lemaître–Robertson–Walker (FLRW) metric is the unique solution to Einstein's equations [67–74]. In spherical polar coordinates, the metric is given by

$$\mathrm{d}s^2 = -N(t)^2\mathrm{d}t^2 + a(t)^2\left(\frac{\mathrm{d}r^2}{1-kr^2} + r^2\mathrm{d}\Omega^2_{(2)}\right), \tag{1.14}$$

where $\mathrm{d}\Omega^2_{(2)} = \mathrm{d}\theta^2 + \sin^2\theta\mathrm{d}\phi^2$ is the metric on the unit 2-sphere. The spatial curvature is parametrised by k, and $k > 0$, $k = 0$, $k < 0$ describes an closed, flat, or open universe, respectively. The FLRW metric is defined in terms of the lapse function $N(t)$ and the scale factor $a(t)$. It is convenient to introduce the Hubble parameter H as

$$H(t) = \frac{\dot{a}(t)}{N(t)\,a(t)}, \tag{1.15}$$

where dot represents derivative with respect to time t.

By construction, GR allows to freely choose the coordinate system. On the level of the FLRW metric (1.14), this is reflected by the freedom to choose the lapse $N(t)$ to be an arbitrary function of time t. There are two commonly used choices in cosmology. Firstly, conformal time is defined by $N(t) = a(t)$ and usually denoted by τ. In this coordinate system, the FLRW metric is conformally related to the Minkowski metric if spatial curvature vanishes $k = 0$, i.e. $g_{\mu\nu} = a(\tau)^2\eta_{\mu\nu}$. Secondly, cosmic time t is defined by setting $N(t) = 1$ and has a direct physical interpretation: an observer comoving with the cosmic expansion measures cosmic time. In this thesis, we will always choose to work in cosmic time t unless stated otherwise. From now on, the explicit dependency on time t will be suppressed.

The scale factor a is the dynamical variable that determines the expansion of the universe. In our normalisation, it is related to the redshift as $a = (1+z)^{-1}$. Its time evolution is determined by Einstein's equations (1.10). In concordance with the cosmological principle, the matter content is modelled by a perfect fluid with stress-energy tensor given by

$$T^{\mu\nu} = (\rho + p)u^\mu u^\nu + pg^{\mu\nu}, \tag{1.16}$$

where u^μ is the velocity 4-vector of the fluid with energy density ρ and pressure p. Conservation of stress-energy (1.13) results in the continuity equation

$$\dot{\rho} + 3H(\rho + p) = 0. \tag{1.17}$$

To close the system of differential equations, one assumes an equation of state relating energy density and pressure as

$$\rho = wp. \tag{1.18}$$

Here, w is a constant and referred to as the equation-of-state parameter. Examples of perfect fluids that obey such an equation of state include non-relativistic matter (pressureless matter or dust) with $w_\mathrm{m} = 0$, relativistic matter (radiation) with $w_\mathrm{r} = 1/3$ and the cosmological constant with $w_\Lambda = -1$. Assuming the equation of state (1.18), the continuity equation (1.17) is solved by

$$\rho = \rho_0\, a^{-3(1+w)}. \tag{1.19}$$

Here, ρ_0 is a constant of integration, which corresponds to the energy density when $a = 1$. This instant is usually be taken to correspond to today. Note that, if the universe is filled with

multiple perfect fluids that are non-interacting, the continuity equation (1.17) holds for each fluid individually.

Upon the FLRW ansatz (1.14) with perfect fluid (1.16), the time-time component of the Einstein equation (1.10) becomes the *Friedmann equation*,

$$H^2 + \frac{k^2}{a^2} = \frac{\Lambda}{3} + \frac{\rho}{3M_{\rm P}^2}\,. \tag{1.20}$$

The spatial part, or more precisely the trace, of Einstein's equation (1.10) gives the acceleration equation

$$\dot{H} + H^2 = \frac{\Lambda}{3} - \frac{1}{2M_{\rm P}^2}\left(\rho + 3p\right)\,. \tag{1.21}$$

This equation can alternatively be obtained by taking the time derivative of Eq. (1.21) and using Eq. (1.17).

To bring Friedmann's equation (1.21) in a more compact form, we define effective energy densities for spatial curvature and the cosmological constant as

$$\frac{\rho_{\rm k}}{M_{\rm P}^2} = -\frac{k}{a^2}\,, \quad \frac{\rho_\Lambda}{M_{\rm P}^2} = \Lambda\,, \tag{1.22}$$

The effect of spatial curvature can be interpreted as the one of a perfect fluid with equation-of-state parameter $w_{\rm k} = -1/3$. The first Friedmann equation (1.21) can then be written in the convenient form

$$H^2 = \frac{1}{3M_{\rm P}^2}\left(\rho_\Lambda + \rho_{\rm k} + \rho_{\rm m} + \rho_{\rm r}\right)\,. \tag{1.23}$$

Let us discuss approximate solutions to this equation by assuming that only one of the cosmic fluids dominates. Then, the scale factor evolves with cosmic time as ($w \neq -1$)

$$a \sim t^{\frac{2}{3(1+w)}}\,, \tag{1.24}$$

where w denotes the equation-of-state parameter of the dominating energy component. For the special case of $w = -1$, we have instead

$$a \sim e^{Ht}\,, \tag{1.25}$$

where $H = \sqrt{\Lambda/3}$ is constant.

It is common to measure the the energy densities as ratios of the critical energy density $\rho_{\rm crit} = 3M_{\rm P}^2H^2$ by defining the density parameters

$$\Omega_i = \frac{\rho_i}{3M_{\rm P}^2H^2}\,, \tag{1.26}$$

where i stands for either radiation, non-relativistic matter, spatial curvature or the cosmological constant. In terms of these parameters, the Friedmann equation (1.21) becomes

$$1 = \Omega_{\rm r} + \Omega_{\rm m} + \Omega_{\rm k} + \Omega_\Lambda\,. \tag{1.27}$$

Latest observational data suggests the following approximate values for the energy density parameters [75],

$$\Omega_{\rm r0} \sim 10^{-4}\,, \quad \Omega_{\rm m0} \sim 0.3\,, \quad |\Omega_{\rm k0}| \lesssim 10^{-3}\,, \quad \Omega_{\Lambda 0} \sim 0.7\,, \tag{1.28}$$

where the subscript 0 means that the values correspond to present times. In particular that means that the universe is basically spatially flat. Further, the cosmological constant is dominating the energy budget of the universe at current times. Equipped with these parameter values, we can trace back the history of the Universe.

The time evolution of the scale factor is summarised in Table 1.1 for different types of dominating energy components. We first observe that, irrespective of which cosmic fluid is dominating, the scale factor increases with time. This allows to identify the following epochs of the cosmic expansion history:

dominating energy component	w	$\rho(a)$	$a(t)$
cosmological constant	-1	const	e^{Ht}
spatial curvature	$-1/3$	a^{-2}	t
dust	0	a^{-3}	$t^{2/3}$
radiation	$1/3$	a^{-4}	$t^{1/2}$

Table 1.1: Summary of the time evolution of the scale factor during different possible epochs in the cosmic expansion history.

- *Radiation domination.* Looking back in time, the energy density of radiation grows with $\rho_{\rm r} \sim a^{-4}$. Radiation is thus dominating the early stage of the universe.
- *Matter domination.* As the universe expands, the energy density of radiation drops faster than the one of dust. Therefore, after some time non-relativistic matter becomes the dominating energy component in the universe. The moment when the energy density of radiation equals the one of dust is referred to as matter-radiation-equality. Given the measured values (1.28), the equality corresponds to a redshift of $z \sim 3 \times 10^3$.
- *Dark energy domination.* Radiation, dust and spatial curvature dilute as time goes on and their energy densities decrease as $\rho \sim t^{-2}$. Contrarily, the energy density corresponding to the cosmological constant is non-evolving. Hence, given Eq. (1.28), at some point the cosmological constant will dominate the energy budget of the universe and cause the universe to expand exponentially. At present times, our universe transitions from the matter to the dark energy dominated era. The moment of equality occurred at redshift $z \sim 0.3$. Hence, the Universe currently enters a phase of accelerated expansion.

These different epochs of the cosmic expansion history are visualised in Fig. 1.1. To produce the figure, we used Eq. (1.26) along with the approximate values (1.28). The blue line corresponds to Ω_Λ, the yellow line to $\Omega_{\rm m}$, and the red line to $\Omega_{\rm r}$. As described above, the universe starts radiation dominated. It transitions into a matter dominated era at a redshift $z \sim 3 \times 10^{-3}$. At present times, the universe becomes dominated by dark energy.

Let us discuss a bit further what makes up the individual types of energy. The current accelerated expansion of the universe is modelled by the cosmological constant Λ, which will be discussed in more detail in the next Section 1.3.

Radiation mostly consists of photons, which were produced at the surface of last scattering and are observable as the CMB radiation. We denote the corresponding energy density parameter as Ω_γ. In addition, the neutrinos behave as radiation in the early universe, which contribute to the observed radiation density with Ω_ν.

Dark Matter

The components that enter $\Omega_{\rm m}$ deserve some more detail. Standard matter, such as electrons and atoms, are referred to as baryonic matter in cosmology. We denote the corresponding energy density parameter as $\Omega_{\rm b}$. Observations of various different physical systems show that there must be an additional type of non-relativistic matter, which is referred to as *dark matter*. Denoting the corresponding density parameter as $\Omega_{\rm c}$ so that $\Omega_{\rm m} = \Omega_{\rm b} + \Omega_{\rm c}$, observations suggest that [75]

$$\Omega_{\rm b0} h^2 \sim 0.022\,, \quad \Omega_{\rm c0} h^2 \sim 0.12\,, \tag{1.29}$$

where $h = H_0/\,100{\rm km\,s^{-1}\,Mpc^{-1}}$. So approximately 85% of non-relativistic matter is composed out of dark matter.

The first indications for dark matter on astrophysical scales were found by Zwicky [14,76], who measured the velocities of galaxies in clusters. Similar conclusions were inferred from astrophysical

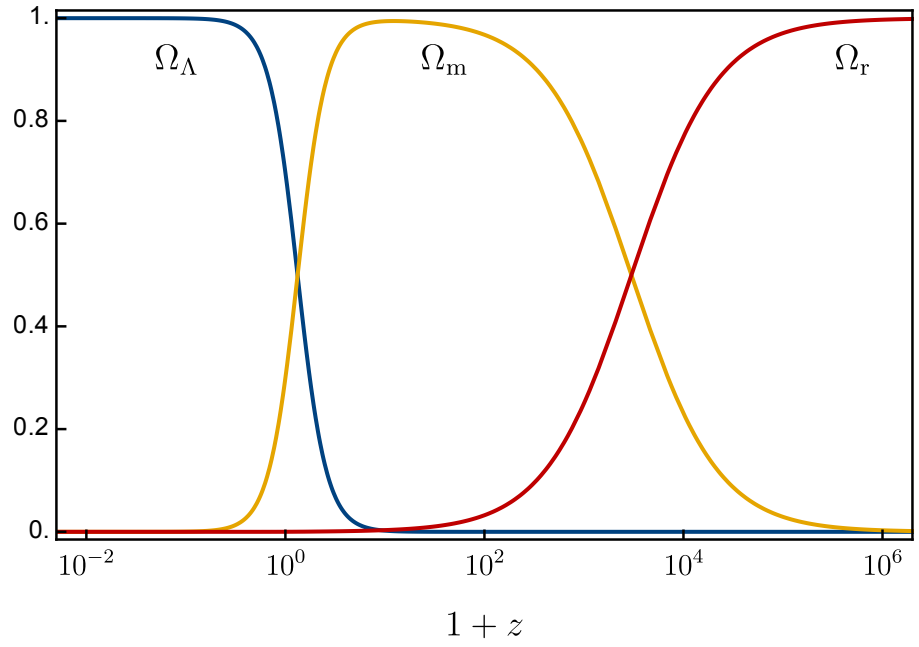

Figure 1.1: Visualisation of the radiation-, matter- and dark energy-dominated epochs of the universe. Spatial curvature is not included because it is always subdominant.

observations such as galaxy rotation curves [15, 16] and stellar velocity dispersions [77]. All these observations found that velocities were substantially higher than expected from estimates of the visible matter. Assuming GR, these high velocities can only be explained if a huge amount of unobservable gravitating matter is added, which forms a halo much larger in size than the cluster and galaxy, respectively.

The postulation of a dark matter component finds further support from measurements of the deflection of light due to a mass concentration. Remarkably, observations of the bullet cluster [78] show a relative spatial displacement of dark and baryonic matter.

Also measurements on cosmological scales require the aforementioned amount of dark matter such as Big Bang Nucleosynthesis (BBN) [79] and the anisotropies in the Cosmic Microwave Background (CMB) [75]. Going further, cosmic structure formation only works if there is a large amount of dark matter [80].

The nature of dark matter remains to be a major open puzzle in modern cosmology. If its origin lies within particle physics, we know that it interacts —if at all— with baryonic matter and photons only very weakly. Its motion is presumably non-relativistic, which is referred to as *cold* dark matter (CDM). This leaves a lot of room for theoretical models and the list of particle dark matter candidates is continually growing [81]

To date, all efforts to directly detect postulated dark matter particles produced experimental null results. This motivates the alternative interpretation that the phenomena attributed to dark matter are a manifestation of gravity itself. Within this point of view, Einstein's theory of gravity would not be appropriate to describe scales, on which a dark matter component needs to be introduced to match observations (see, e.g. [82]). This idea seeded the postulation of a plethora of proposals such as Modified Newtonian Dynamics (MOND) [83] (see [84] for a review and relativistic extensions). While these kind of theories require some sort of dark matter on cosmological scales, further investigations in the context of modified gravity are continuing. At the end of this thesis, we will come back to this point and discuss the problem of dark matter within bimetric theory.

1.3 The trouble with Λ

As anticipated, we discuss the presently dominating type of energy in some more detail. Within GR, the accelerated expansion of the universe at late times is modelled by a cosmological constant Λ or more generally by dark energy. Together with cold dark matter, these two dark components make up the Standard Model of Cosmology, the ΛCDM model.

As in the case of dark matter, the origin of dark energy is another major open problem in modern cosmology and the source of many ongoing investigations. In the remainder of this section, we will discuss some theoretical and observational shortcomings of a positive cosmological constant $\Lambda > 0$. Before doing so, we emphasise that these arguments do not strictly rule out a cosmological constant. Instead, we take these arguments as motivation to seek an alternative mechanism that accelerates the cosmic expansion at late times.

Cosmological constant problem

Previously, we noticed the lack of a fundamental description for a non-vanishing cosmological constant. In fact, Quantum Field Theory *predicts* a cosmological constant, to be understood as the energy density of the quantum vacuum. We move on to review this cornerstone idea, following [85].

The non-zero vacuum energy originates from the creation and subsequent annihilation of virtual particles. Let us denote the vacuum state in Quantum Field Theory by $|0\rangle$. The energy density of this state is given by

$$\langle 0|T_{\mu\nu}|0\rangle = -\rho_{\text{vac}}\, g_{\mu\nu}\,. \tag{1.30}$$

This term leads to an overall cosmological constant in Einstein's equation. Such observable cosmological constant Λ_{obs} is the sum of vacuum energy ρ_{vac} and the bare cosmological constant parameter Λ of GR,

$$\Lambda_{\text{obs}} = \Lambda + \frac{1}{M_{\text{P}}^2}\rho_{\text{vac}}\,. \tag{1.31}$$

In principle, we can set $\Lambda = 0$ and interpret the observed cosmological constant as pure vacuum energy.

Before doing so, let us approximate the value of the vacuum energy. It suffices to take a canonical scalar field with mass m and integrate over all modes, which leads to

$$\rho_{\text{vac}} \propto \int \mathrm{d}^3k\, \sqrt{k^2+m^2}\,, \tag{1.32}$$

which is obviously divergent in the UV. Regularising the integral leads to

$$\rho_{\text{vac}} \simeq \frac{m^4}{64\pi^2}\log\left(\frac{m^2}{\mu^2}\right)\,, \tag{1.33}$$

with μ the renormalisation scale. Taking the mass to correspond to the heaviest particle in the Standard Model of particle physics results in a vacuum energy that is 55 orders of magnitude larger than the observed value [85]. This constitutes "the worst theoretical prediction in the history of physics" [57]. So, to match Λ_{obs} to the observed value, the parameter Λ needs to be tuned to a non-zero number that almost cancels the large value of ρ_{vac}, but not exactly.

This, however, is not the end of the story. The dominant contribution to vacuum energy comes from the heaviest field in the theory. When going to higher energies, i.e. when raising the cutoff of the theory, the bare cosmological constant has to be tuned against every new particle that enters the effective field theory. Due to the high sensitivity of ρ_{vac} to the cutoff as in Eq. (1.33), this represents a dramatic change. This represents a *fine-tuning* that renders the cosmological constant *technically unnatural* in the sense of 't Hooft [86] (see [87] for a recent review on naturalness in the context of cosmology). When we take the cutoff of the theory to be given by the Planck scale, the mismatch between the theoretically predicted and observed value increases to 120 orders of magnitude. This fine-tuning constitutes the *cosmological constant problem* [20, 85, 88–99].

Quantum inconsistency of de Sitter

Beyond the observation that the cosmological constant is highly sensitive to the cutoff of the effective field theory employed for the matter Lagrangian, it has been argued that any $\Lambda > 0$ is quantum inconsistent.

We first present an argument from the swampland program [100], which aims at distinguishing those low-energy effective field theories that can be completed into quantum gravity from those that cannot (see [101, 102] for nice reviews). In String Theory, de Sitter is usually sourced by a scalar field ϕ, which sits at the extremum of a potential $V = V(\phi)$. In this case, the cosmological constant is given by the potential energy of the scalar field. However, it is conjectured that any such potential V must satisfy [24, 26, 27]

$$\frac{|V'|}{V} \geq \frac{c}{M_{\rm P}}\,, \quad \text{or} \quad \frac{V''}{V} \leq -\frac{c'}{M_{\rm P}^2}\,, \tag{1.34}$$

where $c, c' \sim \mathcal{O}(1)$ are universal constants (see [103] for some criticism). This combined bound forbids minima of scalar potentials with $V > 0$, but allows for metastable de Sitter vacua (extrema), which however are too short-lived in order to be relevant for our Universe. The bound clearly rules out a cosmological constant.

The de Sitter bound (1.34) can be related to more general arguments [25, 28, 104, 105]. The problem circles around the question of whether de Sitter, which represents a vacuum solution to Einstein's gravity with a positive cosmological constant, is a consistent vacuum state in a quantum field theoretical sense. The presence of an event horizon and the absence of a globally defined time in de Sitter spacetime make it impossible to define asymptotic in- and out-states and therefore the concept of a S-matrix is not well-defined [106]. To circumvent this issue, instead of a vacuum state, de Sitter could be viewed as a coherent state of N soft graviton quanta [21–23]. The soft gravitons are interacting with each other, such that the coherent state, which macroscopically admits a classical description, is destroyed after a finite amount of time. On time scales larger than this quantum break time, de Sitter dissolves into some quantum state, which cannot be described classically. The limit that makes the quantum break time infinite decouples gravity from matter. Therefore, the finite quantum break time of de Sitter in gravity signals a quantum inconsistency of any $\Lambda > 0$. As a consequence, a positive cosmological constant should be rejected already at the classical level.

Tension in the Hubble constant

Apart from theoretical arguments, observational data signal a slight disfavouring of a cosmological constant – under certain assumptions. A major source of discussion in recent times has been the apparent inconsistency between early-time and late-time observations in cosmology [107]. Local determinations of the Hubble constant H_0 lead to a value that is significantly larger than that inferred from early-universe physics. See [108] for a brief summary and [109] for a recent and thorough review including possible resolutions.

Local determinations of the Hubble constant do not depend on an assumed cosmological model (only assuming homogeneity and isotropy). Therefore, these allow to put model-independent constraints on the value H_0. The SH0ES collaboration estimates a value of $H_0 = (73.5 \pm 1.4)\,\frac{\rm km/s}{\rm Mpc}$ [110] using Cepheid variables and the H0LiCOW collaboration finds $H_0 = (73.3^{+1.7}_{-1.8})\,\frac{\rm km/s}{\rm Mpc}$ [111] using strong gravitational lensing of quasars. These values are consistent with a long list of other local determinations of the Hubble constant, see [108] and references therein.

Contrarily, constraints on H_0 inferred from early-universe physics heavily depend on the cosmological model. Assuming ΛCDM as base model, the Planck collaboration reports a value of $H_0 = (67.27 \pm 0.60)\,\frac{\rm km/s}{\rm Mpc}$ [75] from CMB data alone, which is consistent with ACT+WMAP [112] and other results. Averaging the late-Universe determinations of H_0, these are in conflict with the Planck result at 4.5σ to 6.3σ, depending on the details of the statistical method and averaging procedure employed [113]. This tension might hint towards an inconsistency in the Standard Model of Cosmology.

The inferred value by Planck depends on the entire cosmic expansion history and therefore on the assumed cosmological model. A plethora of alternatives to the ΛCDM-model has been proposed to solve, or at least alleviate, the H_0-tension. These can be divided into proposals modifying the early or the late universe. Here, we focus only on late-time modifications. For instance, dark energy with a phantom equation of state leads to an increased value of H_0. To see this, a common phenomenological ansatz is to promote the corresponding equation-of-state parameter to depend on redshift according to the Chevallier–Polarski–Linder (CPL) approximation [114, 115]:

$$w_{\mathrm{de}} = w_0 + w_a \frac{z}{1+z} \,. \tag{1.35}$$

The base ΛCDM-model corresponds to the point $w_0 = -1$ and $w_a = 0$. We emphasise that this is a purely phenomenological model without theoretical foundation.

A global analysis including the Planck results an local determinations leads to $w_0 = -0.83^{+0.29}_{-0.17}$ and $w_a < -1.05$ at 68% c.l. [116]. Such phantom dark energy removes the Hubble tension with a globally inferred value of $H_0 = (72.94 \pm 0.74)\,\frac{\mathrm{km/s}}{\mathrm{Mpc}}$. In particular, this excludes the ΛCDM scenario by more than 3σ. However, this analysis does not take into account measurements of Baryon Acoustic Oscillations (BAOs). Including these into the global analysis instead leads to $w_0 = -0.957 \pm 0.080$ and $w_a = -0.29^{+0.32}_{-0.26}$ at 68% c.l. and brings back the Hubble tension with $H_0 = 68.31 \pm 0.82\,\frac{\mathrm{km/s}}{\mathrm{Mpc}}$ [75].

The aforementioned results indicate that observations have a marginal preference for a time-dependent dark energy component instead of (only) a cosmological constant. In addition, data slightly favours a phantom equation-of-state parameter $w_{\mathrm{de}} < -1$. We take a mild point of view and regard the described mismatch as clear motivation to search for dark energy that does not arise from a cosmological constant. In Section 3.1.3 we will see that bimetric theory automatically leads to such phantom dark energy.

Chapter 2

Theory of massive and interacting spin-2 fields

The idea to give a mass to the graviton goes back to Fierz and Pauli, who presented a linear ghost-free theory of a massive graviton propagating in flat spacetime in 1939 [46]. However, their theory fails to pass even simple solar system tests due to the so-called van Dam–Veltman–Zakharov (vDVZ) discontinuity [117, 118]: the helicity-0 mode of the massive graviton couples to matter even in the massless limit. In 1972, Vainshtein argued that nonlinear self-interactions of the massive graviton remove the discontinuity rendering the nonlinear theory phenomenologically consistent [119]. Shortly after, Boulware and Deser presented a no-go theorem stating that nonlinear terms introduce a ghost mode, which is commonly referred to as the Boulware–Deser ghost [47]. This argument terminated with efforts to construct a consistent theory for a massive graviton for almost 30 years. The major breakthrough came in 2010/11, when de Rham, Gabadadze and Tolley identified a loophole in the argument of Boulware and Deser. This allowed the construction of the fully non-linear theory of massive gravity [48, 49, 120], which is indeed ghost-free [50]. Hassan and Rosen generalised massive gravity to ghost-free bimetric theory, which describes two nonlinearly interacting spin-2 fields, one massless and one massive [51, 52]. The latter theory is at the core of the present thesis.

In this chapter, we review the fundamental aspects of modified gravity theories. We first discuss some theoretical challenges that are related to Lovelock's [121, 122] and Ostrogradsky's [39] theorems and give a brief overview about modified gravity theories. We then revisit the aforementioned developments in the context of massive and interacting spin-2 fields and provide some technical details in the construction of the said theories. Reviews on massive gravity and bimetric theory can be found in [123–126], which we heavily use in the forthcoming discussion.

2.1 Modifying gravity

Einstein's General Relativity is the well accepted theory of gravity, not only due to its success to describe physical phenomena over a large range of scales, but also due its uniqueness. The latter property is a direct consequence of the following famous theorem.

> Lovelock's theorem [121, 122]: *In four dimensions, every rank-2 and divergence-free tensor, which depends only on the metric tensor and its first two derivatives, is a linear superposition of the Einstein and metric tensors.*

In particular, every such tensor is symmetric and is linear in the second derivatives of the metric tensor. In other words, the Einstein–Hilbert action (with a cosmological constant) is the only local diffeomorphism invariant action, which depends only on a metric and leads to second order equations of motion.

This last property is crucial for the theoretical consistency of General Relativity and also needs to be maintained by any theory of modified gravity. The reason lies within *Ostrogradsky's theorem* [39], which we briefly discuss following [127]. Consider a general Lagrangian density $\mathcal{L}(q, q^{(1)}, \dots, q^{(N)})$, which contains derivatives up to order N of the a priori independent variables: $q^{(n)}$, with $n = 1 \dots, N$. The Lagrangian is said to be non-degenerate iff the determinant of the Hessian is non-vanishing, i.e.

$$\det\left(\frac{\partial \mathcal{L}}{\partial q^{(N)} \partial q^{(N)}}\right) \neq 0\,. \tag{2.1}$$

Such Lagrangian always leads to equations of motion of order $2N$. Their full solution hence requires the specification of $4N$ initial conditions.

Ostrogradsky proved that for $N \geq 2$, the corresponding Hamiltonian is not bounded from below. The theory then propagates modes with negative energy in addition to the physically expected degrees of freedom, which are referred to as *(Ostrogradsky) ghosts*. In general, the theorem can be stated as:

> Ostrogradsky's theorem [39, 40]: *Any theory described by a non-degenerate Lagrangian that depends on the second or higher order derivatives of its variables necessarily propagates at least one ghost mode.*

The presence of a ghost mode has fatal consequences. If the theory is interacting[1], any state can decay into modes with positive and negative energy while respecting energy conservation. Since a highly excited state is entropically favoured, this leads to an almost instantaneous decay of, e.g. the vacuum state. Going further, it is not possible to define any stable state. A theory containing a ghost is therefore ill-defined and must be rejected.

The Einstein–Hilbert action (1.8) contains second derivatives of the metric tensor, which in principle would lead to fourth order equations of motion. One may then wonder why GR is not plagued by an Ostrogradsky ghost. It is Lovelock's theorem that tells us that *all* equations of motion are second order. This implies that GR admits reformulations that are manifestly first order in the derivatives of the a priori independent variables. A renowned first-order reformulation of GR is that of Palatini [128], where the metric and the connection are treated as a priori independent fields. These get related in the usual manner on-shell, by means of the equations of motion.

In fact, this is just a particular example of a more fundamental idea. Einstein's gravity violates Ostrogradsky's assumption of a non-degenerate Lagrangian density. A degenerate Lagrangian density is an intrinsic property of theories with (gauge-)symmetries[2]. The vanishing of the determinant of the Hessian signals that the theory is subject to constraints, i.e. field equations that contain only up to $(2N-1)$th order derivatives of its variables. The consistency condition that the constraints be preserved under time evolution is the starting point of the Dirac–Bergmann algorithm [129–131], which applies to theories with a manifestly first-order Lagrangian density and sets the ground for more involved algorithms capable of handling higher order Lagrangians. The question of ghosts is more involved and deeply connected to counting the number of propagating degrees of freedom, which necessitates the counting of (functionally independent) constraints, gauge identities and effective gauge parameters [132]. If this analysis unveils that a theory propagates more degrees of freedom than expected, these additional degrees of freedom are necessarily ghosts and the theory is ill-defined in the aforementioned sense. We refer to [133] for a review on the Hamiltonian constraint analysis in the context of GR, to [134] for a pedagogical introduction to the Lagrangian constraint analysis and to [127, 135] for more details on the problem of classical ghosts.

Since any meaningful theory must be devoid of (Ostrogradsky) ghosts, Lovelock's theorem severely restricts possible theories of gravitation. However, the theorem also provides a recipe on how to construct gravitational theories beyond GR. We can increase the number of spacetime dimensions, introduce non-local terms, change the number of degrees of freedom and/or add higher

[1] Every theory of the universe interacts at least gravitationally.

[2] The converse is not true. Namely, theories with no local symmetry can also be degenerate. The most well-known example is that of Proca electrodynamics.

derivative terms. When breaking any of these Lovelock's theorem entering assumptions to generate new gravitational theories, the absence of ghosts must be carefully inspected.

All the different possible directions to extend GR that are paved by Lovelock's theorem have been explored in the literature, as nicely reviewed in, e.g. [97,136–139]. The latter option of adding new degrees of freedom has become very popular and can be classified according to whether the new degrees of freedom are scalar, vectorial or tensorial. The addition of a new scalar degree of freedom while allowing for its nonminimal coupling to the metric tensor leads to the so-called Scalar–Tensor theories of gravity, which are most generally described by the Horndeski action [140, 141]. Horndeski's is the most general ghost-free action constructed from the metric and a scalar field such that the Lagrangian is second order and leads to second order equation of motions. Going further, it is claimed that even theories with higher-than-second order equations of motion are ghost-free, which led to the postulation of beyond Horndeski [142] and ultimately of the so-called degenerate higher order scalar-tensor (DHOST) theories [143,144]. Employing an analogous building principle as for Horndeski theory in the context of vector fields leads to the postulation of Generalised Proca or Vector Galileons theory [145–147], whose ghost-freedom and multi-vector extensions[3] are still under debate [148–154]. For a review on these class of theories, we recommend [155]. Coming to tensorial modifications, one can add a mass term for the graviton, which leads to dRGT massive gravity [48–50,120]. The extension of that theory to Hassan–Rosen bimetric theory [51,52] contains a massive tensor field in addition to the usual massless tensor field. For completeness, we also mention that the setup has been extended to multi-metric theories [156–165].

From a particle physics perspective, the Einstein field equations (1.10) are the unique Lorentz-invariant and nonlinear equations of motion for a massless spin-2 field [41–45]. This will be briefly demonstrated in the next section. Promoting the spin-2 field to be massive hence appears as a natural modification of GR.

Scalar–Tensor and Vector–Tensor theories generically modify the propagation speed $c_{\rm gw}$ of gravitational waves. However, the observation of gravitational wave signals together with their electromagnetic counterpart show that gravitational waves travel at the speed of light c, with the allowed deviations as small as $|c_{\rm gw}/c - 1| < 5 \times 10^{-16}$ [166]. This observational bound forces the Scalar–Tensor and Vector–Tensor theories of gravity into their simplest forms [167–170]. The finite graviton mass within massive gravity leads to a subluminal propagation speed and hence gravitational wave observations provide a strict upper limit on the graviton mass. This restriction, however, does not apply to bimetric theory, due to the presence of the massless spin-2 field in addition to the massive spin-2 field.

Summarising, the theoretical motivation and natural building principle together with the observational viability make bimetric theory a particularly appealing modified theory of gravitation. In the subsequent sections, we review the historical developments and theoretical challenges that ultimately led to the postulation of ghost-free bimetric theory.

2.2 Fierz-Pauli theory

Having outlined the technical challenges and possible courses to consistently extend GR, we focus on the theory that is at the core of the present thesis: bimetric theory. We begin with a historical recollection of the essential developments underlying bimetric theory, starting with the linear theory due to Fierz and Pauli. We discuss some of the technical issues as well as attempts for nonlinearly completing the Fierz–Pauli theory. This section closely follows [125].

2.2.1 Linearised gravity

General Relativity is the theory of a massless spin-2 field [41–45]. To see this, we go to flat spacetime[4], where there exist well-defined notions of mass and spin. We consider small perturbations

[3] The most general, ghost-free and first-order theory for an arbitrary number of vector fields has been constructed only in flat spacetime [148, 149].

[4] Mass and spin are intimately related to the Lorentz group, which describes the symmetries of Minkowski spacetime. The only other spacetimes to which the concept of mass and spin can be generalised are those with the

about the flat Minkowski background $\eta_{\mu\nu}$ of the form

$$g_{\mu\nu} = \eta_{\mu\nu} + h_{\mu\nu}\,. \tag{2.2}$$

with $h_{\mu\nu} \ll 1$. The linearisation of the Einstein-Hilbert action (1.8) leads to the Lagrangian of linearised gravity (here, we will always work in terms of Lagrangian densities instead of actions)

$$\mathcal{L} = -\frac{1}{4} h^{\mu\nu} \hat{\mathcal{E}}^{\alpha\beta}_{\mu\nu} h_{\alpha\beta}, \tag{2.3}$$

up to second order in $h_{\mu\nu}$. Here, we have introduced the Lichnerowicz operator

$$\hat{\mathcal{E}}^{\alpha\beta}_{\mu\nu} h_{\alpha\beta} = -\frac{1}{2}\left(\Box h_{\mu\nu} - 2\partial_{(\mu}\partial_\alpha h^\alpha_{\nu)} + \partial_\mu\partial_\nu h - \eta_{\mu\nu}(\Box h - \partial_\alpha\partial_\beta h^{\alpha\beta})\right)\,, \tag{2.4}$$

where $h = \eta^{\mu\nu} h_{\mu\nu}$ denotes the trace of the perturbation. The functional variation of the above with respect to $h_{\mu\nu}$ yields the following equations of motion:

$$\hat{\mathcal{E}}^{\alpha\beta}_{\mu\nu} h_{\alpha\beta} = 0. \tag{2.5}$$

The Lichnerowicz operator is dictated by requiring invariance of the theory under the following gauge transformation:

$$h_{\mu\nu} \longrightarrow h_{\mu\nu} + \partial_{(\mu}\xi_{\nu)}\,, \tag{2.6}$$

which correspond to linear diffeomorphisms. A deviation from the Lichnerowicz operator breaks linear diffeomorphism invariance and hence introduces additional, ghost degrees of freedom. The tensor field $h_{\mu\nu}$ has 10 a priori independent components. The gauge symmetry (2.6) removes $2 \times 4 = 8$ components. So in total, the theory propagates $10 - 8 = 2$ degrees of freedom. This is just the correct number for a massless spin-2 field.

The linear theory of gravity (2.3) is the basis for formulating the linear massive theory.

2.2.2 Fierz–Pauli Mass term

Next, we want to explore the implications of adding a mass term for the tensor field $h_{\mu\nu}$. The only Lorentz-invariant terms that can be constructed out of the fields at hand are $h^{\mu\nu}h_{\mu\nu}$ and h^2 at quadratic order. Both these terms can be used to give a mass to $h_{\mu\nu}$. So, in general, the kinetic term is to be supplemented by both these terms as

$$\mathcal{L} = -\frac{1}{4} h^{\mu\nu} \mathcal{E}^{\alpha\beta}_{\mu\nu} h_{\alpha\beta} - \frac{1}{8} m^2 \left(h^{\mu\nu}h_{\mu\nu} - a h^2\right)\,, \tag{2.7}$$

where m and a are free parameters of the theory. For convenience, we define the Lagrangian density only containing the mass term as

$$\mathcal{L}_{\text{mass}} = -\frac{1}{8} m^2 \left(h^{\mu\nu}h_{\mu\nu} - a h^2\right)\,. \tag{2.8}$$

This theory explicitly breaks linear diffeomorphism. To restore invariance under Eq. (2.6), we use the Stückelberg trick and split the tensor into a transverse $h^\perp_{\mu\nu}$ mode, which carries six components, and a vector field χ_μ, which carries four components, as

$$h_{\mu\nu} = h^\perp_{\mu\nu} + 2\partial_{(\mu}\chi_{\nu)}\,. \tag{2.9}$$

In terms of these variables, the mass term explicitly reads

$$\mathcal{L}_{\text{mass}} = -\frac{1}{8} m^2 \left((h^\perp_{\mu\nu} + 2\partial_{(\mu}\chi_{\nu)})^2 - a(h^\perp + 2\partial_\alpha\chi^\alpha)^2\right)\,, \tag{2.10}$$

same amount of symmetry. These are de Sitter and Anti-De Sitter. To keep the discussion as simple as possible, we stick to Minkowski backgrounds here. When studying the mass spectrum of bimetric theory later, we will also allow for a non-vanishing cosmological constant.

which is invariant under the simultaneous transformations:

$$h^{\perp}_{\mu\nu} \longrightarrow h^{\perp}_{\mu\nu} + \partial_{(\mu}\xi_{\nu)}\,, \quad \chi_\mu \longrightarrow \chi_\mu - \frac{1}{2}\xi_\mu\,. \tag{2.11}$$

Therefore, introducing the Stückelberg field χ_μ as in Eq. (2.9) restores linear diffeomorphism invariance.

The theory is stable only for a specific value of a, if it is to avoid Ostrogradsky instabilities. To see this, we note that the mass term includes a kinetic term for the Stückelberg field of the form

$$\mathcal{L}_{\rm mass} \supset \mathcal{L}^{\chi}_{\rm kin} = -\frac{1}{4}m^2\left((\partial_\mu\chi_\nu)^2 - a(\partial_\alpha\chi^\alpha)^2\right)\,, \tag{2.12}$$

after integration by parts. To restore the residual gauge freedom of the spin-1 field χ_μ, we introduce another Stückelberg field χ^0 as

$$\chi_\mu = \chi^{\perp}_\mu + \partial_\mu\chi^0\,. \tag{2.13}$$

Then, the kinetic term for χ_μ explicitly reads

$$\mathcal{L}^{\chi}_{\rm kin} = -\frac{1}{4}m^2\left((\partial_\mu\chi^{\perp}_\nu + \partial_\mu\partial_\nu\chi^0)^2 - a(\partial^\alpha\chi^{\perp}_\alpha + \Box\chi^0)^2\right)\,, \tag{2.14}$$

which is now invariant under the following simultaneous transformations:

$$\chi^{\perp}_\mu \longrightarrow \chi^{\perp}_\mu + \partial_\mu\xi^0\,, \quad \chi^0 \longrightarrow \chi^0 - \xi^0 \tag{2.15}$$

with ξ^0 a gauge parameter. The term $\mathcal{L}^{\chi}_{\rm kin}$ now contains a kinetic term for the scalar Stückelberg field χ^0 of the following form:

$$\mathcal{L}_{\rm mass} \supset \mathcal{L}^{\chi^0}_{\rm kin} = -\frac{1}{4}m^2\left((\partial_\mu\partial_\nu\chi^0)^2 - a(\Box\chi^0)^2\right) = -\frac{1}{4}m^2(1-a)(\Box\chi^0)^2\,, \tag{2.16}$$

where we integrated by parts for the second step. The kinetic term for χ^0 contains higher orders in time and space derivatives. To bring this kinetic term to a canonical form, we first introduce a Lagrange multiplier $\tilde{\chi}^0$ as

$$\mathcal{L}^{\chi^0}_{\rm kin} = -\frac{1}{4}m^2(1-a)(\tilde{\chi}^0\Box\chi^0 - \frac{1}{4}(\chi^0)^2)\,. \tag{2.17}$$

The functional variation of the above with respect to $\tilde{\chi}^0$ yields the equation of motion $\tilde{\chi}^0 = 2\Box\chi^0$. Plugging this back into the Lagrangian returns Eq. (2.16). The field redefinition $\phi_1 = \chi^0 + \tilde{\chi}^0$ and $\phi_2 = \chi^0 - \tilde{\chi}^0$ canonicalises the kinetic term as

$$\mathcal{L}^{\pi}_{\rm kin} = -\frac{1}{4}m^2(1-a)\left(\phi_1\Box\phi_1 - \phi_2\Box\phi_2 - \frac{1}{4}(\phi_1-\phi_2)^2\right)\,, \tag{2.18}$$

after integration by parts. These simple manipulations reveal that one of the scalar modes contained in the tensor field necessarily comes with a kinetic term with the wrong sign. Therefore, one of the scalar modes is a ghost. Only for the specific parameter choice $a = 1$, the higher derivative terms of the scalar mode are absent, which removes the Ostrogradsky instability we just spotted. This yields the stable theory for a massive graviton propagating on flat spacetime by Fierz and Pauli [46],

$$\mathcal{L}_{\rm FP} = -\frac{1}{4}h^{\mu\nu}\mathcal{E}^{\alpha\beta}_{\mu\nu}h_{\alpha\beta} - \frac{1}{8}m^2\left(h^{\mu\nu}h_{\mu\nu} - h^2\right) \tag{2.19}$$

to which we refer to as Fierz–Pauli theory.

As we will see now, the theory propagates 5 degrees of freedom as desired, with m the mass of the graviton. Functionally varying the Fierz-Pauli action in Eq. (2.19) with respect to $h_{\mu\nu}$ yields the equations of motion

$$\Box h_{\mu\nu} - 2\partial_\alpha\partial_{(\mu}h^{\alpha}_{\nu)} + \eta_{\mu\nu}(\partial_\alpha\partial_\beta h^{\alpha\beta} - \Box h) + \partial_\mu\partial_\nu h - m^2(h_{\mu\nu} - \eta_{\mu\nu}h) = 0\,. \tag{2.20}$$

Acting with ∂^μ on Eq. (2.20) yields $\partial^\mu h_{\mu\nu} = \partial_\nu h$ if $m \neq 0$. Upon using this constraint, Eq. (2.20) reduces to $\Box h_{\mu\nu} - \partial_\mu\partial_\nu h - m^2(h_{\mu\nu} - \eta_{\mu\nu}h) = 0$. Tracing this equation results in $h = 0$. Therefore, the equation of motion further simplifies to $(\Box - m^2)h_{\mu\nu} = 0$. Summarising, the equations of motion Eq. (2.20) are equivalent to the following set of equations:

$$\begin{aligned} &(\Box - m^2)h_{\mu\nu} = 0\,, \\ &\partial^\mu h_{\mu\nu} = 0\,, \quad h = 0\,. \end{aligned} \tag{2.21}$$

The first line represents the equations of motion, which are subject to the constraint equations stated in the second line. The tensor field $h_{\mu\nu}$ is symmetric and therefore has a priori 10 independent components. The constraint equations fix five components algebraically, thereby leaving 5 independent components in total. The theory therefore propagates 5 dynamical degrees of freedom as it is appropriate for a massive spin-2 field in 4 dimensions. The parameter m is the common mass of all modes of the massive field.

2.2.3 van Dam–Veltman–Zakharov discontinuity

Subsequently, we turn to the elucidation of the following key point: external sources not only excite the helicity-2 modes of the massive graviton, but also the helicity-0 mode. To make this apparent, we study the exchange amplitude of massive gravitons between two external sources $T_{\mu\nu}$ and $T'_{\mu\nu}$. The Fierz–Pauli Lagrangian in the presence of an external source $T_{\mu\nu}$ is given by

$$\mathcal{L}_{\text{FP}} = -\frac{1}{4}h^{\mu\nu}\hat{\mathcal{E}}^{\alpha\beta}_{\mu\nu}h_{\alpha\beta} - \frac{1}{8}m^2\left(h^{\mu\nu}h_{\mu\nu} - h^2\right) + \frac{1}{2M_{\text{P}}^2}h_{\mu\nu}T^{\mu\nu}\,. \tag{2.22}$$

The corresponding equations of motion are

$$\hat{\mathcal{E}}^{\alpha\beta}_{\mu\nu}h_{\alpha\beta} + \frac{m^2}{2}(h_{\mu\nu} - \eta_{\mu\nu}h) = \frac{1}{2M_{\text{P}}^2}T_{\mu\nu}\,. \tag{2.23}$$

As in the case without external sources, we can bring these equations into a more compact form. Taking the divergence of and tracing Eq. (2.23) yields the following constraints, respectively:

$$\begin{aligned} \partial^\mu h_{\mu\nu} - \partial_\nu h &= \frac{1}{m^2 M_{\text{P}}^2}\partial^\mu T_{\mu\nu}\,, \\ h &= -\frac{1}{3m^2M_{\text{P}}^2}\left(T + \frac{2}{m^2}\partial_\mu\partial_\nu T^{\mu\nu}\right)\,, \end{aligned} \tag{2.24}$$

where we have used the divergence of the first line to arrive at the second line.

To extract the vDVZ discontinuity, we insert the constraint (2.24) into Eq. (2.23) to obtain

$$(\Box - m^2)h_{\mu\nu} = \frac{1}{M_{\text{P}}^2}\left(\tilde{\eta}_{\mu(\alpha}\tilde{\eta}_{\beta)\nu} - \frac{1}{3}\tilde{\eta}_{\mu\nu}\tilde{\eta}_{\alpha\beta}\right)T^{\alpha\beta}\,, \tag{2.25}$$

where we introduced the tensor

$$\tilde{\eta}_{\mu\nu} = \eta_{\mu\nu} - \frac{1}{m^2}\partial_\mu\partial_\nu\,. \tag{2.26}$$

From here, we can read off the propagator of a massive graviton as

$$\Delta^{(m\neq0)}_{\mu\nu\alpha\beta}(x - x') = \frac{f^{(m\neq0)}_{\alpha\beta\mu\nu}}{\Box - m^2} \tag{2.27}$$

with the polarisation tensor $f^{(m\neq0)}_{\mu\nu\alpha\beta}$ given as

$$f^{(m\neq0)}_{\mu\nu\alpha\beta} = \tilde{\eta}_{\mu(\alpha}\tilde{\eta}_{\beta)\nu} - \frac{1}{3}\tilde{\eta}_{\mu\nu}\tilde{\eta}_{\alpha\beta}\,. \tag{2.28}$$

Therefore, the amplitude of exchanging massive gravitons between two external sources $T_{\mu\nu}$ and $T'_{\mu\nu}$ is given by

$$\mathcal{A}^{(m\neq 0)} = \int \mathrm{d}^4x\, h_{\mu\nu}T'^{\mu\nu} = \int \mathrm{d}^4x\, T'^{\mu\nu}\frac{f^{(m\neq 0)}_{\alpha\beta\mu\nu}}{\Box - m^2}T^{\alpha\beta}\,. \tag{2.29}$$

In the massless limit $m \to 0$, the external sources are conserved due to linear diffeomorphism invariance, $\partial_\mu T^{\mu\nu} = 0$. Hence, in the massless limit the amplitude simplifies to

$$\lim_{m\to 0}\mathcal{A}^{(m\neq 0)} = \int \mathrm{d}^4x\, T'^{\mu\nu}\frac{1}{\Box}\left(T_{\mu\nu} - \frac{1}{3}\eta_{\mu\nu}T\right)\,. \tag{2.30}$$

This amplitude needs to be compared to the amplitude due to the exchange of purely massless gravitons.

To compute the amplitude of massless gravitons, we first notice that the equations of motion are simply given by

$$\hat{\mathcal{E}}^{\alpha\beta}_{\mu\nu}h_{\alpha\beta} = \frac{1}{2M_{\mathrm{P}}^2}T_{\mu\nu}\,. \tag{2.31}$$

Since the massless theory is invariant under linear diffeomorphisms (2.6), we can pick a gauge. In the de Donder gauge $\partial^\mu h_{\mu\nu} - \frac{1}{2}\partial_\nu h = 0$, the equations of motion assume the simple form

$$\Box h_{\mu\nu} - \frac{1}{2}\eta_{\mu\nu}\Box h = \frac{1}{M_{\mathrm{P}}^2}T_{\mu\nu}\,. \tag{2.32}$$

The trace implies $\Box h = -\frac{1}{M_{\mathrm{P}}}T$, which can be plugged back into the equations of motion to yield

$$\Box h_{\mu\nu} = \frac{1}{M_{\mathrm{P}}^2}\left(T_{\mu\nu} - \frac{1}{2}\eta_{\mu\nu}T\right) = \frac{1}{M_{\mathrm{P}}^2}\left(\eta_{\mu(\alpha}\eta_{\beta)\nu} - \frac{1}{2}\eta_{\mu\nu}\eta_{\alpha\beta}\right)T^{\alpha\beta}. \tag{2.33}$$

Now we can read off the massless propagator as

$$\Delta^{(m=0)}_{\alpha\beta\mu\nu}(x-x') = \frac{f^{(m=0)}_{\alpha\beta\mu\nu}}{\Box}, \tag{2.34}$$

with the polarisation tensor $f^{(m=0)}_{\alpha\beta\mu\nu}$ given by

$$f^{(m=0)}_{\alpha\beta\mu\nu} = \eta_{\mu(\alpha}\eta_{\beta)\nu} - \frac{1}{2}\eta_{\mu\nu}\eta_{\alpha\beta}\,. \tag{2.35}$$

To compare with the massless limit of the massive case, we can compute the exchange amplitude of massless gravitons between two external sources $T_{\mu\nu}$ and $T'_{\mu\nu}$ as

$$\mathcal{A}^{(m=0)} = \int \mathrm{d}^4x\, h_{\mu\nu}T'^{\mu\nu} = \int \mathrm{d}^4x\, T'^{\mu\nu}\frac{1}{\Box}\left(T_{\mu\nu} - \frac{1}{2}\eta_{\mu\nu}T\right)\,. \tag{2.36}$$

Comparing the massless amplitude (2.36) to the massive amplitude in the massless limit (2.30), we find a mismatch of $\mathcal{O}(1)$. This discontinuity was independently discovered by van Dam and Veltman [117] and Zakharov [118] and henceforth referred to as vDVZ discontinuity (see also [171]). As a consequence, Fierz–Pauli theory is already ruled out by observations of the precession of Mercury's orbit.

Before moving on to the resolution of this (apparent) problem, we first demonstrate that it is the helicity-0 mode of the massive graviton that is responsible for the vDVZ discontinuity. We perform a flat space helicity decomposition of the tensor field $h_{\mu\nu}$ as

$$h_{\mu\nu} \longrightarrow h^{\perp}_{\mu\nu} + \frac{2}{m}\partial_{(\mu}A_{\nu)} + \frac{1}{m^2}\partial_\mu\partial_\nu\pi\,, \tag{2.37}$$

where the negative powers of m have been introduced for convenience. For better visibility, we simply write $h_{\mu\nu}$ in place of $h^{\perp}_{\mu\nu}$ in the following. The Fierz–Pauli action then takes the form

$$\begin{aligned}\mathcal{L}_{\rm FP} = &-\frac{1}{4}h^{\mu\nu}\hat{\mathcal{E}}^{\alpha\beta}_{\mu\nu}h_{\alpha\beta} - \frac{1}{2}h^{\mu\nu}\left(\Pi_{\mu\nu} - \eta_{\mu\nu}\Pi\right) - \frac{1}{8}F_{\mu\nu}F^{\mu\nu} \\ &-\frac{1}{8}m^2(h_{\mu\nu}h^{\mu\nu} - h^2) - \frac{1}{2}m(h^{\mu\nu} - \eta_{\mu\nu}h)\partial_{(\mu}A_{\nu)}\,,\end{aligned} \tag{2.38}$$

where $F_{\mu\nu} = \partial_\mu A_\nu - \partial_\nu A_\mu$ and $\Pi_{\mu\nu} = \partial_\mu\partial_\nu\chi$. The kinetic term for the helicity-0 mode π is not manifest yet, due to the mixing with $h_{\mu\nu}$. To diagonalise the action, we perform the field redefinition $h_{\mu\nu} = \tilde{h}_{\mu\nu} + \eta_{\mu\nu}\pi$, after which

$$\begin{aligned}\mathcal{L}_{\rm FP} = &-\frac{1}{4}\tilde{h}^{\mu\nu}\hat{\mathcal{E}}^{\alpha\beta}_{\mu\nu}\tilde{h}_{\alpha\beta} - \frac{3}{4}(\partial\pi)^2 - \frac{1}{8}F_{\mu\nu}F^{\mu\nu} \\ &-\frac{1}{8}m^2(\tilde{h}_{\mu\nu}\tilde{h}^{\mu\nu} - \tilde{h}^2) + \frac{3}{2}m^2\pi^2 + \frac{3}{2}m^2\pi\tilde{h} \\ &-\frac{1}{2}m(\tilde{h}^{\mu\nu} - \eta^{\mu\nu}\tilde{h})\partial_{(\mu}A_{\nu)} + 3m\pi\partial_\alpha A^\alpha\,.\end{aligned} \tag{2.39}$$

The first line contains the canonical kinetic terms for the fields, while the second and third lines contain the mass terms and interactions among the fields, respectively.

The field $\tilde{h}_{\mu\nu}$ is the pure helicity-2 mode, while π is the pure helicity-0 mode. External sources, however, couple to the combined mode $h_{\mu\nu}$ in the following way: $h_{\mu\nu}T^{\mu\nu} = \tilde{h}_{\mu\nu}T^{\mu\nu} + \pi T$. This unveils that the helicity-0 mode couples to the trace of the energy momentum tensor even in the massless limit, which in turn causes the vDVZ discontinuity. To render a theory of a single massive graviton observationally viable, we need a mechanism that unmixes the helicity-0 and helicity-2 mode within $h_{\mu\nu}$ in the massless limit.

2.2.4 Vainshtein mechanism

In 1972, Vainshtein conjectured that the vDVZ discontinuity is absent when equipping the theory with certain nonlinear terms [119]. Utilising an ad hoc ansatz for a nonlinearly completed Fierz–Pauli theory [172], he questioned the validity of perturbation theory in the massless limit. By solving the field equations in a power series in inverse powers of the mass m, he demonstrated for a static and spherically symmetric configuration that the theory indeed reduces to GR in the massless limit. This feature is commonly known as Vainshtein screening mechanism.

Here we discuss Vainshtein screening from a slightly different perspective, following [124]. For our purpose it suffices to assume that Fierz–Pauli theory admits a nonlinear completion. As we have seen before, the vDVZ discontinuity emerges from the interaction between the helicity-0 mode of the graviton and matter. To isolate the self-interactions of this helicity-0 mode, one usually studies the theory in the so-called decoupling limit, which is defined by the double-scaling limit

$$M_{\rm P}\to\infty\,,\quad m\to 0\,,\quad \Lambda_n = (M_{\rm P}m^{n-1})^{\frac{1}{n}} = \text{const.}\,,\quad \frac{T_{\mu\nu}}{M_{\rm P}} = \text{const.}\,. \tag{2.40}$$

This decoupling limit isolates the interactions of the helicity-0 mode π at the scale Λ_n. Therefore, it turns the fields $\tilde{h}_{\mu\nu}$ and A_μ free, while π is subject to nonlinear self-interacting by construction. As a result, the equations of motion can be recast as

$$\hat{\mathcal{E}}^{\alpha\beta}_{\mu\nu}\tilde{h}_{\alpha\beta} = \frac{1}{2M_{\rm P}}T_{\mu\nu}\,,\quad 3\Box\pi + \mathcal{F}^{\rm nl}_\pi = \frac{1}{M_{\rm P}}T\,, \tag{2.41}$$

where $\mathcal{F}^{\rm nl}_\pi$ captures the nonlinearities in π. For instance, within the proposals of nonlinear massive

gravity[5] of [47, 174], the derivative self-interactions of the helicity-0 mode are given by [124]

$$\mathcal{F}_\chi^{\rm nl} \sim \frac{1}{(\Lambda_5)^5}\left(3\Box(\Box\pi)^2 - \Box(\partial_\mu\partial_\nu\pi)^2 - 2\partial_\mu\partial_\nu(\Box\pi\partial^\mu\partial^\nu\pi)\right)\,, \tag{2.42}$$

up to an overall theory-dependent constant.

The above suffices to understand the Vainshtein mechanism. Away from the massless limit, schematically given by $k \ll m$ from a Fourier perspective, the nonlinear terms are suppressed by powers of (k/Λ_n). This implies that $\Box\chi \gg \mathcal{F}_\pi^{\rm nl}$ and the dynamical evolution of the helicity-0 mode is captured by the linear terms. Therefore, π is of the same order as $\tilde{h}_{\mu\nu}$ and the physical metric $h_{\mu\nu}$ receives $\mathcal{O}(1)$ corrections from the helicity-0 mode, $h_{\mu\nu} = \tilde{h}_{\mu\nu} + \eta_{\mu\nu}\pi$ as before. In the massless limit, i.e. when the mass is much smaller than all scales involved in the problem under consideration, schematically $k \gg m$, the nonlinear terms dominate in the scalar equation of motion, $\Box\pi \ll \mathcal{F}_\pi^{\rm nl}$. This implies that the scalar mode is subdominant, $\pi \ll \tilde{h}_{\mu\nu}$, and the physical metric fluctuation is composed solely out of the helicity-2 mode, $h_{\mu\nu} \sim \tilde{h}_{\mu\nu}$.

Summarising, the nonlinear self-interactions suppress the helicity-0 mode in the limit of small graviton mass, compared to the helicity-2 mode. This renders the metric fluctuations effectively massless so as to restore GR in that limit. Note that the Vainshtein mechanism kicks in at a finite graviton mass and hence at a finite scale. For spherically symmetric systems, this scale is referred to as Vainshtein radius $r_{\rm V}$ to be determined later.

An additional important requirement for the Vainshtein mechanism to work is that the close-to GR solution can be matched to an asymptotically flat solution [47, 175, 176]. This is indeed the case, as has been shown for certain massive gravity potentials [177–180]. In Section 3.2, we will demonstrate the concrete realisation of Vainshtein screening within bimetric theory and study the matching of solutions therein.

2.2.5 Towards a nonlinear massive theory

Given the metric $g_{\mu\nu}$, there are two Lorentz-invariant quantities that we can construct. The first quantity is the trace $[g] = 4$, which cannot be used to construct a mass term for $g_{\mu\nu}$. The second quantity is the determinant $g = \det(g_{\mu\nu})$ and functions thereof. As shown in [47], the only viable function of g is the one that gives a cosmological constant term. Hence, also the determinant cannot give rise to a mass term for $g_{\mu\nu}$.

The construction of a mass term at the nonlinear level necessitates the introduction of a reference metric, which we denote by $f_{\mu\nu}$. So far, we have taken the reference metric to be flat, $f_{\mu\nu} = \eta_{\mu\nu}$, and built the mass term at the linearised level out of the perturbation $h_{\mu\nu} = g_{\mu\nu} - f_{\mu\nu}$.

The Stückelberg trick has proven itself to be a powerful tool to make explicit the field content of the theory and thereby to address the ghost issue. The introduction of the reference metric allows for a nonlinear version of the Stückelberg trick. Instead of rewriting the perturbation field, we can rewrite the background as [174]

$$f_{\mu\nu} \longrightarrow \tilde{f}_{\mu\nu} = \partial_\mu\phi^a\partial_\nu\phi^b f_{ab}\,. \tag{2.43}$$

Here, ϕ^a stands for four Stückelberg fields for $a = 0, \ldots 3$. In the unitary gauge $\phi^a = \delta^a_\mu x^\mu$, we get $\tilde{f}_{\mu\nu} = f_{\mu\nu}$. When performing the Stückelberg trick, the field $h_{\mu\nu}$ gets promoted to the covariant tensor $H_{\mu\nu}$ as

$$h_{\mu\nu} = g_{\mu\nu} - f_{\mu\nu} \longrightarrow H_{\mu\nu} = g_{\mu\nu} - \tilde{f}_{\mu\nu}\,. \tag{2.44}$$

Performing a helicity decomposition of the Stückelberg fields amounts to writing

$$\phi^a = \delta^a_\mu x^\mu - \frac{1}{m}\eta^{a\mu}A_\mu - \frac{1}{m^2}\eta^{a\mu}\partial_\mu\pi\,, \tag{2.45}$$

[5] Note that these proposals contain an Ostrogradsky instability or Boulware–Deser ghost, which invalidates them as sensible physical theories. This point will be discussed in more detail in the next section. However, the same argument holds for ghost-free theories, as will be discussed in Section 2.3. For instance, in ghost-free massive gravity, the Λ_3 decoupling limit corresponds to the cubic Galileon [48, 49, 173]. There, the nonlinear self-interactions of the helicity-0 mode are given by $\mathcal{F}_\chi^{\rm nl} \sim \Lambda_3^{-3}\left((\Box\pi)^2 - (\partial_\mu\partial_\nu\pi)\right)^2$ [125].

where we associated the index a with a Lorentz index as suggested by the unitary gauge. Therefore, our new tensor field can be written as [125]

$$H_{\mu\nu} = h_{\mu\nu} + \frac{2}{m}\partial_{(\mu}A_{\nu)} - \frac{1}{m^2}\partial_\mu A_\alpha \partial_\nu A^\alpha + \frac{2}{m^2}\Pi_{\mu\nu} - \frac{1}{m^4}\Pi_{\mu\alpha}\Pi^\alpha{}_\nu - \frac{2}{m^3}\partial_\mu A_\alpha \Pi^\alpha{}_\nu \,. \tag{2.46}$$

This new framework serves as the basis for constructing a nonlinear mass term. We first observe that in the unitary gauge with a flat reference metric $f_{\mu\nu} = \eta_{\mu\nu}$, linearisation leads to $H_{\mu\nu} = h_{\mu\nu}$. Hence, the following ansatz for a nonlinear mass term [174]

$$\mathcal{L}_{\text{nl FP}} = -m^2 M_{\text{P}}^2 \sqrt{-g}\left([H^2] - [H]^2\right) \tag{2.47}$$

reduces to the Fierz–Pauli mass term (2.19) upon linearising in the above described sense. Here, $[\cdot]$ denotes the trace and indices are raised and lowered with respect to $g_{\mu\nu}$. However, this choice is not unique and other proposals have been presented in the literature, e.g. [47]. Expressing $H_{\mu\nu}$ in terms of the two metric tensors, all proposals can be collectively written as [124, 181]

$$\mathcal{L}_{\text{nl FP}} = -m^2 M_{\text{P}}^2 \sqrt{-g}\,\mathcal{U}\left(g^{-1}\tilde{f}\right) \,, \tag{2.48}$$

with $\mathcal{U}$ suitable scalar functions such that the theory is general covariant under diffeomorphisms, gives rise to flat solutions for $g_{\mu\nu}$ and reduces to the Fierz–Pauli mass term (2.19) upon linearising about flat spacetime $f_{\mu\nu} = \eta_{\mu\nu}$ in the unitary gauge.

2.2.6 Boulware–Deser ghost

Having proposals for nonlinear mass terms, Boulware and Deser argued that the Ostrogradsky instability, which at the linear level was avoided by choosing $a = 1$ in Eq. (2.8), generically reappears at the nonlinear level [47]. Their analysis relies on an ADM analysis (Arnowitt–Deser–Misner [182]) of a generic nonlinear theory as in Eq. (2.48). A thorough discussion of their proof is beyond the scope of the present review. Here, we will limit ourselves to simply demonstrating the occurrence of the nonlinear ghost mode, following [125].

We use the proposal Eq. (2.47) as a concrete example. Neglecting the helicity-2 and helicity-1 modes in the helicity decomposition of $H_{\mu\nu}$ (2.46) leads to

$$H_{\mu\nu} = \frac{2}{m^2}\Pi_{\mu\nu} - \frac{1}{m^4}\Pi_{\mu\alpha}\Pi^\alpha{}_\nu \,. \tag{2.49}$$

Plugging this decomposition into Eq. (2.47) unveils that the nonlinear mass term contains the following derivative terms of the helicity-0 mode [125],

$$\mathcal{L}_{\text{nl FP}} \supset -M_{\text{P}}^2\left(([\Pi^2] - [\Pi]^2) + \frac{4}{m^2}([\Pi^3] - [\Pi][\Pi^2]) + \frac{1}{m^6}([\Pi^4] - [\Pi^2]^2)\right). \tag{2.50}$$

The quadratic term turns out to be a total derivative after integrating by parts. This signals the special Fierz–Pauli tuning so as to remove the ghost mode. The cubic and quartic interaction terms, however, contain higher time derivatives of π, which do not combine into total derivatives. Therefore, the theory unavoidably propagates additional unphysical degrees of freedom, by Ostrogradsky's theorem.

Although our discussion focussed only on a particular example, the argument by Boulware and Deser applies to all nonlinear mass terms that are of the form Eq. (2.48) [47, 125]. It was therefore believed that *any* nonlinear completion of the Fierz–Pauli theory propagates a ghost mode, dubbed *Boulware–Deser ghost.* This conclusion was (erroneously) confirmed much later in [183], which used the framework of [174] as a starting point.

2.3 Ghost-free massive gravity

The question of a massive graviton became relevant again when brane-world scenarios were studied to explain the weakness of gravity and/or to solve the cosmological constant problem [184–192]. In particular, the Dvali–Gabadadze–Porrati (DGP) model [187,188] played a crucial role. Such brane induced gravity models gave rise to the appearance of massive spin-2 resonances on the brane, on which our Universe lives [193]. In particular, the method of imposing boundary conditions on an auxiliary extra dimension to generate mass terms [194–197] paved the road towards the construction of a ghost-free nonlinear theory of massive gravity.

Building upon the intuition developed over the last sections, we take the tensor $H_{\mu\nu}$ defined in Eq. (2.43) as a promising starting point. Keeping only the helicity-2 and helicity-0 modes while neglecting the helicity-1 mode in Eq. (2.46), the tensor is given by [48, 49]:

$$H_{\mu\nu} = h_{\mu\nu} + \frac{2}{m^2}\Pi_{\mu\nu} - \frac{1}{m^4}\eta^{\alpha\beta}\Pi_{\mu\alpha}\Pi_{\beta\nu}\,. \tag{2.51}$$

This suggests the definition of the following tensor [49]

$$\mathcal{K}^{\mu}{}_{\nu} = \delta^{\mu}{}_{\nu} - \sqrt{\delta^{\mu}{}_{\nu} - H^{\mu}{}_{\nu}}\,, \tag{2.52}$$

whose indices are raised and lowered with respect to $g_{\mu\nu}$. Defined in that way, the tensor reduces to $\mathcal{K}_{\mu\nu} = \Pi_{\mu\nu}$ when $h_{\mu\nu} = 0$.

The definition of $\mathcal{K}$ allows to covariantly extend the total derivative ($[\Pi]^2 - [\Pi^2]$), which we encountered in Eq. (2.50), in the following way [49]:

$$\mathcal{U}(g,H) = -\left((g^{\mu\nu}\mathcal{K}_{\mu\nu})^2 - g^{\mu\nu}g^{\alpha\beta}\mathcal{K}_{\mu\alpha}K_{\beta\nu}\right)\,. \tag{2.53}$$

Expressing the potential as an expansion in H, there exists a total derivative contribution at each order, wich is covariantised to [49]

$$\mathcal{U}(g,H;\alpha_n) = -\sum_{n\geq 2}\alpha_n\mathcal{L}^{(n)}_{\rm der}(\mathcal{K}), \tag{2.54}$$

with $\mathcal{L}^{(n)}_{\rm der}$ recursively defined as

$$\mathcal{L}^{(n)}_{\rm der}(\mathcal{K}) = -\sum_{m=1}^{n}(-1)^m\frac{(n-1)!}{(m-1)!}[\mathcal{K}^m]\mathcal{L}^{(n-m)}_{\rm der}(\mathcal{K})\,. \tag{2.55}$$

This is the de Rham–Gabadadze–Tolley mass term, which appears in the action of nonlinear massive gravity [48, 49],

$$S_{\rm dRGT} = \frac{M_{\rm P}^2}{2}\int {\rm d}^4x\sqrt{-g}\left(\mathcal{R} - m^2\,\mathcal{U}(g,H;\alpha_n)\right)\,. \tag{2.56}$$

The above action has been shown to be free of the Boulware–Deser ghost to all orders in nonlinearities in the decoupling limit, and up to quartic order away from the decoupling limit in [49].

Hassan and Rosen found that the infinite series in Eq. (2.54) actually terminates [120]. In addition, using the definition (2.43) of $H_{\mu\nu}$, from Eq. (2.52) we see that $\mathcal{K}^{\mu}{}_{\nu}$ can be rewritten as $\mathcal{K}^{\mu}{}_{\nu} = \delta^{\mu}{}_{\nu} - [\sqrt{g^{-1}f}]^{\mu}{}_{\nu}$. The potential (2.54) admits the physically equivalent rewriting [120]

$$\mathcal{U}(g,f;\beta_n) = \sum_{n=0}^{4}\beta_n e_{(n)}\left(\sqrt{g^{-1}f}\right)\,, \tag{2.57}$$

upon specialising to $f_{\mu\nu} = \eta_{\mu\nu}$. The potential is formulated in terms of the elementary symmetric polynomials $e_{(n)}$, which in four dimensions are given by

$$\begin{aligned} e_{(0)}(S) &= 1\,, \qquad e_{(1)}(S) = [S]\,, \qquad e_{(2)}(S) = \frac{1}{2!}\left([S]^2 - [S^2]\right)\,, \\ e_{(3)}(S) &= \frac{1}{3!}\left([S]^3 - 3[S][S^2] + 2[S^3]\right)\,, \\ e_{(4)}(S) &= \frac{1}{4!}\left([S]^4 - 6[S]^2[S^2] + 3[S^2]^2 + 8[S][S^3] - 6[S^4]\right) = \det(S)\,. \end{aligned} \tag{2.58}$$

All higher polynomials vanish in four dimensions: $e_{(n>4)} = 0$.

Further, Hassan and Rosen extended the ghost-free proof to the fully non-linear level, away from the decoupling limit in [50,51]. The ghost-proof was generalised to the case of an arbitrary reference metric $f_{\mu\nu}$ in [198] and confirmed in a series of studies utilising different approaches [199–209].

The modified Einstein equations stemming from S_{dRGT} are [120]

$$G_{\mu\nu} + V_{\mu\nu} = 0\,. \tag{2.59}$$

Here, $G_{\mu\nu}$ is the usual Einstein tensor of $g_{\mu\nu}$ and $V_{\mu\nu}$ arises from varying the potential (2.57) and is explicitly shown in Eq. (2.68). The Einstein tensor satisfies the Bianchi identity $\nabla^\mu G_{\mu\nu} = 0$. The equation of motion (2.59) therefore implies the Bianchi constraint

$$\nabla^\mu V_{\mu\nu} = 0\,. \tag{2.60}$$

Let us recap. More than 60 years after the first attempt by Fierz and Pauli, we finally arrived at a Lorentz-invariant, fully nonlinear and ghost-free theory of massive gravity. The construction of a consistent mass term for the metric $g_{\mu\nu}$ requires the introduction of a reference metric $f_{\mu\nu}$, which in dRGT massive gravity was fixed to $f_{\mu\nu} = \eta_{\mu\nu}$, together with a specific square-root structure to remove the Boulware–Deser ghost. The formulation by Hassan and Rosen makes manifest that the potential treats both metrics on an equal footing. In fact, the potential satisfies the identity

$$\sqrt{-g}\,\mathcal{U}(g, f; \beta_n) = \sqrt{-f}\,\mathcal{U}(f, g; \beta_{4-n})\,. \tag{2.61}$$

This identity results from the following property of the elementary symmetric polynomials:

$$e_{(n)}(S) = \frac{e_{(4-n)}(S)}{e_4(S)}\,. \tag{2.62}$$

The potential is thus invariant under the simultaneous transformations $g_{\mu\nu} \leftrightarrow f_{\mu\nu}$ and $\beta_n \leftrightarrow \beta_{4-n}$. The full action for massive gravity, however, does not reflect this symmetry because only $g_{\mu\nu}$ has a kinetic term. Consequently, a natural extension of massive gravity is obtained upon promoting $f_{\mu\nu}$ to a dynamical metric. In the following, we provide further arguments in favour of promoting the reference metric to a dynamical field, as will be done in Section 2.4.

The lowest order term ($n = 0$) in the potential (2.57) gives just the determinant of the dynamical metric $g_{\mu\nu}$. Therefore, the parameter β_0 represents a cosmological constant for the metric $g_{\mu\nu}$, just like the parameter Λ of GR. The highest order term ($n = 4$) can be written as $\sqrt{-g}\,e_{(4)}(\sqrt{g^{-1}f}) = \sqrt{-f}$ and is therefore not contributing to the dynamics, but would yield a cosmological constant, parametrised by β_4, for the metric $f_{\mu\nu}$. The remaining parameters β_1, β_2, and β_3 parametrise the nonlinear self-interactions of the massive spin-2 field.

We will not go into the phenomenological details of massive gravity, which are nicely reviewed in [125,210], but comment on one important aspect of cosmological solutions. On the flat FLRW ansatz (1.14) with scale factor a the Bianchi constraint (2.60) implies

$$\dot{a}\,(\beta_1 + 2a\beta_2 + a^2\beta_3) = 0, \tag{2.63}$$

with the only solution being $\dot{a} = 0$. Therefore, massive gravity does not give rise to flat FLRW solutions. In fact, the result even extends to closed FLRW solutions [211]. On the other hand,

open FLRW solutions do exist [212]. However, these are problematic at the perturbative level, due to strong coupling issues or instabilities [213–215].

The absence of physically relevant FLRW solutions motivates to generalise massive gravity. As mentioned before, a natural extension is to make the whole action invariant under the exchange symmetry of the potential (2.61) by giving dynamics to $f_{\mu\nu}$. This procedure leads us to ghost-free bimetric theory.

2.4 Ghost-free bimetric theory

After all previous preliminaries, we are finally in the position to introduce the bimetric theory of Hassan and Rosen. Here, the reference metric $f_{\mu\nu}$, which is fixed to a flat Minkowski metric in massive gravity, is promoted to a dynamical field. The following discussion closely follows [126].

2.4.1 Action and equations of motion

Ghost-free bimetric theory [52] considers the reference metric $f_{\mu\nu}$ to be a dynamical field. In practice, this means that the massive gravity action (2.56) with potential (2.57) is supplemented with an Einstein–Hilbert kinetic term for $f_{\mu\nu}$:

$$S_{\mathrm{HR}} = -\frac{M_{\mathrm{g}}^2}{2}\int \mathrm{d}^4x \left(\sqrt{-g}\mathcal{R}^{\mathrm{g}} + \alpha^2\sqrt{-f}\mathcal{R}^{\mathrm{f}} - m^2\sqrt{-g}\mathcal{U}(g,f;\beta_n)\right) . \tag{2.64}$$

Here, $\mathcal{R}^{\mathrm{g,f}}$ are the scalar curvatures of $g_{\mu\nu}$ and $f_{\mu\nu}$, respectively. Each Einstein–Hilbert term comes with its own Planck mass, M_{g} and M_{f}, in terms of which we introduced the Planck mass ratio

$$\alpha = \frac{M_{\mathrm{f}}}{M_{\mathrm{g}}} . \tag{2.65}$$

The potential $\mathcal{U}(g,f;\beta_n)$ is the same as in massive gravity and given by Eq. (2.57). Now that $f_{\mu\nu}$ is dynamical, the action (2.64) is invariant under the simultaneous transformations

$$g_{\mu\nu} \longleftrightarrow f_{\mu\nu} , \quad M_{\mathrm{g}} \longleftrightarrow M_{\mathrm{f}} , \quad \beta_n \longleftrightarrow \beta_{4-n} . \tag{2.66}$$

A natural question arises at this point: which metric, $g_{\mu\nu}$ or $f_{\mu\nu}$ is to be interpreted as the physical one? This issue will be addressed shortly, when discussing the couplings to matter.

The functional variation of the action (2.64) with respect to $g^{\mu\nu}$ and $f^{\mu\nu}$ leads to two sets of modified Einstein equations. These are given by [120, 216]

$$G^{\mathrm{g}}_{\mu\nu} + V^{\mathrm{g}}_{\mu\nu} = 0 , \quad \alpha^2 G^{\mathrm{f}}_{\mu\nu} + V^{\mathrm{f}}_{\mu\nu} = 0 , \tag{2.67}$$

where $G^{\mathrm{g,f}}_{\mu\nu}$ are the Einstein tensors of $g_{\mu\nu}$ and $f_{\mu\nu}$, respectively. The explicit form of the terms stemming from the potential are

$$V^{\mathrm{g}}_{\mu\nu} = g_{\mu\lambda}\sum_{n=0}^{3}(-1)^n\beta_n Y^{\lambda}_{(n)\nu}\left(\sqrt{g^{-1}f}\right) , \quad V^{\mathrm{f}}_{\mu\nu} = f_{\mu\lambda}\sum_{n=0}^{3}(-1)^n\beta_{4-n} Y^{\lambda}_{(n)\nu}\left(\sqrt{f^{-1}g}\right) . \tag{2.68}$$

The matrix functions $Y^{\lambda}_{(n)\nu}$ are of the form

$$Y^{\lambda}_{(n)\nu}(S) = \sum_{k=0}^{n}(-1)^k e_{(k)}(S)\,(S^{n-k})^{\lambda}{}_{\nu}, \tag{2.69}$$

with $S = \sqrt{g^{-1}f}$ and the elementary symmetric polynomials $e_{(n)}$ as defined in Eq. (2.58). The spacetime indices in the g-sector are raised and lowered with respect to $g_{\mu\nu}$ and in the f-sector with respect to $f_{\mu\nu}$.

Of course, each metric can be used to define a covariant derivative. Let us denote ${}^{(\mathrm{g})}\nabla_\mu$ the covariant derivative compatible with $g_{\mu\nu}$, i.e. ${}^{(\mathrm{g})}\nabla^\mu g_{\mu\nu} = 0$, and likewise ${}^{(\mathrm{f})}\nabla_\mu$ for $f_{\mu\nu}$, i.e. ${}^{(\mathrm{f})}\nabla^\mu f_{\mu\nu} = 0$. Quite obviously, the corresponding Einstein tensors satisfy the appropriate Bianchi identities:

$$ {}^{(\mathrm{g})}\nabla^\mu G^{\mathrm{g}}_{\mu\nu} = 0\,, \quad {}^{(\mathrm{f})}\nabla^\mu G^{\mathrm{f}}_{\mu\nu} = 0\,. \tag{2.70} $$

By virtue of the modified Einstein equations (2.67), the Bianchi identities imply the following Bianchi constraints on the potential terms:

$$ {}^{(\mathrm{g})}\nabla^\mu V^{\mathrm{g}}_{\mu\nu} = 0\,, \quad {}^{(\mathrm{f})}\nabla^\mu V^{\mathrm{f}}_{\mu\nu} = 0\,. \tag{2.71} $$

The interaction potential is covariant under simultaneous diffeomorphisms of both metrics, which implies that the Bianchi constraints are not independent, but related as [181]

$$ \sqrt{-g} g^{\mu\lambda}\, {}^{(\mathrm{g})}\nabla_\lambda V^{\mathrm{g}}_{\mu\nu} = -\sqrt{-f} f^{\mu\lambda}\, {}^{(\mathrm{f})}\nabla_\lambda V^{\mathrm{f}}_{\mu\nu}\,. \tag{2.72} $$

Note that this on-shell identity follows from covariance alone and is independent of the precise form of the potential $\mathcal{U}$.

2.4.2 Absence of Boulware–Deser ghost

Before moving on, we comment on the absence of the Boulware–Deser ghost instability. The full proof is technical and beyond the scope of the present review. For a pedagogical presentation of the proof, we refer to [126].

To understand how the ghost problem is avoided in bimetric theory, let us count the number of degrees of freedom we would naively expect [126]. We start with $2 \times 10 = 20$ a priori independent components in the two symmetric tensors. The interaction potential breaks the two diffeomorphism invariances of $g_{\mu\nu}$ and $f_{\mu\nu}$ down to the diagonal subgroup, under which both metrics are transformed simultaneously. This shared symmetry is to be gauge fixed, which determines $2 \times 4 = 8$ components of the 20 we started with. Next we notice that the previously obtained the Bianchi constraint (2.71) removes another 4 components. Thus, we are left with $20 - 8 - 4 = 8$ propagating degrees of freedom: two corresponding to the massless spin-2 field, five corresponding the the massive spin-2 field and one additional scalar mode. This latter mode is precisely the Boulware–Deser ghost. In order to remove that ghost and arrive at the desired 7 propagating degrees of freedom, one additional constraint is needed.

In fact, this additional constraint is present for the special form of the interaction potential (2.57). The original proof was performed in the ADM (Arnowitt–Deser–Misner [182]) language by Hassan and Rosen in [52] subsequently confirmed also in other approaches [202, 206, 209, 217–221]. Bimetric theory due to Hassan and Rosen is thus free of the Boulware–Deser ghost instability.

For completeness, we briefly mention that other types of inconsistencies can arise beyond the Bouldware–Deser ghost instability. A potential source of such inconsistency is that the definition of the square-root matrix $S = \sqrt{g^{-1}f}$ is not unique [222]. This renders the definition of bimetric theory ambiguous. Only if both metrics share a common time direction, the square-root matrix S is real-valued and bimetric theory can be defined unambiguously [222].

2.4.3 Linear mass spectrum

After having clarified the absence of the Boulware–Deser ghost instability, let us identify the propagating degrees of freedom of bimetric theory. As previously noted, the concept of mass (and also that of spin) is related to representations of the Lorentz group, which is the isometry group of Minkowski (M) spacetime. The notions can be meaningfully generalised to spacetimes with the same amount of symmetry, i.e. Anti-de Sitter (AdS) and de Sitter (dS) spacetimes. All M, AdS and dS are *maximally symmetric* spacetimes. Hence, in order to identify its linear mass spectrum, we need to study bimetric theory on a maximally symmetric background. This is the case when both metrics are proportional: $g_{\mu\nu} \propto f_{\mu\nu}$.

The class of proportional background solutions where both metric tensors are related by a conformal factor $c(x)$ as $\bar{g}_{\mu\nu} = c(x)^2 \bar{f}_{\mu\nu}$ was studied in [52, 223]. Upon employing the conformal ansatz, the Bianchi constraint (2.71) reduces to $\partial_\mu c = 0$, which forces c to be a constant. The most general proportional ansatz thus simplifies to

$$\bar{g}_{\mu\nu} = c^2 \bar{f}_{\mu\nu} \quad \text{with} \quad c = \text{const.} \tag{2.73}$$

The modified Einstein equations (2.67) become

$$G_{\mu\nu}(\bar{g}) + \Lambda_\text{g}\, \bar{g}_{\mu\nu} = 0\,, \qquad G_{\mu\nu}(\bar{g}) + \Lambda_\text{f}\, \bar{g}_{\mu\nu} = 0. \tag{2.74}$$

(Note that the Einstein tensor is conformally invariant, $G_{\mu\nu}(\bar{f}) = G_{\mu\nu}(\bar{g})$.) The effective cosmological constants are given by

$$\Lambda_\text{g} = m^2 \left(\beta_0 + 3c\beta_1 + 3c^2\beta_2 + c^3\beta_3\right)\,, \tag{2.75a}$$

$$\Lambda_\text{f} = \frac{m^2}{\alpha^2 c^2} \left(c\beta_1 + 3c^2\beta_2 + 3c^3\beta_3 + c^4\beta_4\right)\,. \tag{2.75b}$$

These are composed of both vacuum energy (as parametrised by β_0 and β_4) and interaction energy (as parametrised by β_1, β_2 and β_3). Combining both equations in (2.74) implies that $\Lambda \equiv \Lambda_\text{g} = \Lambda_\text{f}$, i.e. both metrics share the same effective cosmological constant. Proportional backgrounds are thus maximally symmetric and, depending on Λ, describe M or (A)dS spacetime.

Combining both Eq. (2.74) and using Eq. (2.75) leads to [223]

$$\alpha^2\beta_3 c^4 + (3\alpha^2\beta_2 - \beta_4)c^3 + 3(\alpha^2\beta_1 - \beta_3)c^2 + (\alpha^2\beta_0 - 3\beta_2)c - \beta_1 = 0\,, \tag{2.76}$$

which is a quartic polynomial in c and as such has up to four real-valued solutions. Each corresponds to a vacuum solution of bimetric theory, i.e. there is no source of stress-energy apart from the (self-)interactions of the spin-2 fields. Note already that these solutions are invariant under

$$c \longrightarrow -c \quad \beta_n \longrightarrow (-1)^n \beta_n\,. \tag{2.77}$$

We will discuss proportional solutions in more detail in Chapter 4.

After having identified the maximally symmetric spacetimes in bimetric theory, let us turn to the mass spectrum on such backgrounds. We introduce small perturbations about the proportional background and write the metrics as [52, 223]

$$g_{\mu\nu} = \bar{g}_{\mu\nu} + \frac{1}{M_\text{g}}\delta g_{\mu\nu}\,, \quad f_{\mu\nu} = c^2\bar{g}_{\mu\nu} + \frac{c}{M_\text{f}}\delta f_{\mu\nu}\,, \tag{2.78}$$

where $\delta g_{\mu\nu} \ll M_\text{g}$ and $\delta f_{\mu\nu} \ll c^{-1} M_\text{f}$. Here, the fluctuations are already canonically normalised. Linearising the Einstein equations (2.67) leads to [223]

$$\mathcal{E}^{\alpha\beta}_{\mu\nu}\delta g_{\alpha\beta} + \Lambda_\text{g}\delta g_{\mu\nu} - \frac{M_\text{g}\bar{\beta}}{2}\bar{g}_{\mu\alpha}\left(\delta S^\alpha{}_\nu - \delta^\alpha{}_\nu \delta S\right) = 0\,, \tag{2.79a}$$

$$\mathcal{E}^{\alpha\beta}_{\mu\nu}\delta f_{\alpha\beta} + \Lambda_\text{f}\delta f_{\mu\nu} + \frac{M_\text{g}\bar{\beta}}{2\alpha c}\bar{g}_{\mu\alpha}\left(\delta S^\alpha{}_\nu - \delta^\alpha{}_\nu \delta S\right) = 0\,. \tag{2.79b}$$

Here, we have introduced the short-hand notation $\bar{\beta} = c\beta_1 + 2c^2\beta_2 + c^3\beta_3$. The variation of the square-root matrix is given by [223]

$$\bar{g}_{\mu\alpha}\delta S^\alpha{}_\nu = \frac{c}{2M_\text{f}}(\delta f_{\mu\nu} - \alpha c\, \delta g_{\mu\nu}), \tag{2.80}$$

to linear order in fluctuations. To decouple the above system of equations, we introduce the new variables [223]

$$\delta G_{\mu\nu} = \frac{1}{\sqrt{1+\alpha^2 c^2}}\left(\delta g_{\mu\nu} - \alpha c\, \delta f_{\mu\nu}\right)\,, \quad \delta M_{\mu\nu} = \frac{1}{\sqrt{1+\alpha^2 c^2}}\left(\delta f_{\mu\nu} + \alpha c\, \delta g_{\mu\nu}\right)\,, \tag{2.81}$$

where the prefactors have been chosen for canonical normalisation. The equations of motion then assume the following form [223]:

$$\begin{aligned} 0 &= \mathcal{E}^{\alpha\beta}_{\mu\nu}\delta G_{\alpha\beta} + \Lambda\delta G_{\mu\nu}\,, \\ 0 &= \mathcal{E}^{\alpha\beta}_{\mu\nu}\delta M_{\alpha\beta} + \Lambda\delta M_{\mu\nu} + \frac{1}{2}m^2_{\mathrm{FP}}\left(\delta M_{\mu\nu} - \bar{g}_{\mu\nu}\delta M\right). \end{aligned} \tag{2.82}$$

Written in this manner, it is obvious that the field $\delta G_{\mu\nu}$ satisfies the equations of a massless spin-2 field, as in linearised GR (2.5), with a non-vanishing cosmological constant. Further, it is also clear that the field $\delta M_{\mu\nu}$ satisfies the equations of a massive spin-2 field with a Fierz–Pauli mass term (2.20). The mass is given by [223]

$$m^2_{\mathrm{FP}} = \left(1 + \frac{1}{\alpha^2 c^2}\right)\left(c\beta_1 + 2c^2\beta_2 + c^3\beta_3\right). \tag{2.83}$$

In contrast to the effective cosmological constant, the Fierz–Pauli mass only depends on the interaction parameters $\beta_{1,2,3}$. Summarising, this analysis reveals that bimetric theory describes a massless and a massive spin-2 fields at the linearised level.

Bimetric theory thus propagates the correct number of degrees of freedom, avoiding the fatal Boulware–Deser ghost. This however does not imply that the propagating modes are well-defined on any background. One important example is the *Higuchi ghost* [224, 225]. For a non-vanishing cosmological constant, the mass must not be arbitrarily small, but satisfy the Higuchi bound

$$3m^2_{\mathrm{FP}} > 2\Lambda\,. \tag{2.84}$$

If this bound is violated, the helicity-0 mode π of the massive spin-2 field has a kinetic term with the wrong sign. This mode is therefore tachyonic and commonly classified as a ghost. Therefore, solutions that give rise to violations of the Higuchi bound must be discarded as unphysical.

The original metric fluctuations in terms of the mass eigenstates are given by [223]

$$\delta g_{\mu\nu} = \frac{1}{\sqrt{1+\alpha^2c^2}}\left(\delta G_{\mu\nu} + \alpha c\,\delta M_{\mu\nu}\right), \quad \delta f_{\mu\nu} = \frac{1}{\sqrt{1+\alpha^2c^2}}\left(\delta M_{\mu\nu} - \alpha c\,\delta G_{\mu\nu}\right), \tag{2.85}$$

as follows directly from Eq. (2.81). This allows to identify two important parametric limits of bimetric theory [52, 223, 226, 227]. In the limit $\alpha c \ll 1$ or $\alpha c \gg 1$, the mixing of the mass eigenstates in the metric fluctuations disappears and the metric fluctuations precisely match the mass eigenstates. The phenomenological consequences of this unmixing will be discussed after having coupled the theory to matter.

2.4.4 Coupling to matter

We have not included matter fields yet. Since bimetric theory describes two dynamical metrics, the question arises, to which of them matter fields should couple. This question received a lot of attention in the literature and here we briefly summarise the possibilities that have been put forward.

Let us write the action of bimetric theory coupled to matter schematically as

$$S = S_{\mathrm{HR}} + S_{\mathrm{m}}\,, \tag{2.86}$$

where S_{HR} is the bimetric action (2.64) and S_{m} denotes a general matter action. In the following, we discuss the form of S_{m} that preserves the fundamental ghost-freedom feature of bimetric theory.

It was shown in [228, 229] that the Boulware–Deser ghost is excited whenever matter fields couple to both metrics at the same time[6]. In contrast, if two independent matter sectors Φ^{g} and Φ^{f} couple minimally to $g_{\mu\nu}$ and $f_{\mu\nu}$ respectively, the constraint structure of bimetric theory is

[6] Despite being plagued by Boulware–Deser ghosts, some phenomenological aspects of such setups were studied in [230, 231].

preserved and the Boulware–Deser ghost is absent [229]. The corresponding consistent matter action can be written as

$$S_{\mathrm{m}} = \int \mathrm{d}^4x \left(\sqrt{-g}\mathcal{L}^{\mathrm{g}}_{\mathrm{m}}(g, \Phi^{\mathrm{g}}) + \sqrt{-f}\mathcal{L}^{\mathrm{f}}_{\mathrm{m}}(f, \Phi^{\mathrm{f}}) \right) . \tag{2.87}$$

Notice that the two independent matter sectors are coupled to each other indirectly only, via the interactions between the two metric tensors. Therefore, the g-matter Φ^{g} lives in the geometry defined by $g_{\mu\nu}$, which in turn defines its geodesics (and likewise for the f-sector). So from the perspective of an observer composed out of Φ^{g}-matter, the metric $g_{\mu\nu}$ plays the role of the physical metric.

Since in the present thesis we are interested in minimally coupled matter, we present the equations of motion for this restrictive setup only. The functional variation of Eqs. (2.86) and (2.87) with respect to $g^{\mu\nu}$ and $f^{\mu\nu}$ leads to two sets of modified Einstein equations:

$$G^{\mathrm{g}}_{\mu\nu} + V^{\mathrm{g}}_{\mu\nu} = \frac{1}{M_{\mathrm{g}}^2} T^{\mathrm{g}}_{\mu\nu} , \qquad \alpha^2 G^{\mathrm{f}}_{\mu\nu} + V^{\mathrm{f}}_{\mu\nu} = \frac{1}{M_{\mathrm{g}}^2} T^{\mathrm{f}}_{\mu\nu} . \tag{2.88}$$

As before, $G^{\mathrm{g,f}}_{\mu\nu}$ denote the Einstein tensors and $V^{\mathrm{g,f}}_{\mu\nu}$ the potential terms of $g_{\mu\nu}$ and $f_{\mu\nu}$, respectively. In addition, the energy-momentum tensors of the two matter sectors are given by

$$T^{\mathrm{g}}_{\mu\nu} = -\frac{2}{\sqrt{-g}} \frac{\partial(\sqrt{-g}\mathcal{L}^{\mathrm{g}}_{\mathrm{m}})}{\partial g^{\mu\nu}} , \tag{2.89}$$

and similarly for $f_{\mu\nu}$. For matter actions that are invariant under the relevant diffeomorphisms, the stress-energy tensors are covariantly conserved: ${}^{(\mathrm{g})}\nabla^\mu T^{\mathrm{g}}_{\mu\nu} = {}^{(\mathrm{f})}\nabla^\mu T^{\mathrm{f}}_{\mu\nu} = 0$. Hence, the Bianchi constraint (2.71) applies also in the presence of matter fields. In this thesis, we will assume that there is no matter in the f-sector, $T^{\mathrm{f}}_{\mu\nu} = 0$, which leads to the so-called *singly-coupled bimetric theory*.

Alternatively, matter fields can couple minimally to an effective metric $g^{\mathrm{eff}}_{\mu\nu}$, which is composed out of both $g_{\mu\nu}$ and $f_{\mu\nu}$ in the following way [229]

$$g^{\mathrm{eff}}_{\mu\nu} = a^2 g_{\mu\nu} + 2ab\, g_{\mu\lambda} S^\lambda{}_\nu + b^2 f_{\mu\nu} . \tag{2.90}$$

Here, a and b are arbitrary constants. The matter action is then given by

$$S_{\mathrm{m}} = \int \mathrm{d}^4x \sqrt{-g^{\mathrm{eff}}} \mathcal{L}_{\mathrm{m}}(g^{\mathrm{eff}}, \Phi) . \tag{2.91}$$

It has been claimed that this is the unique non-minimal matter coupling possible within bimetric theory [232,233], although further ambiguities arise in the vielbein formulation [234]. An appealing feature of the above proposal is that the fluctuations of $g^{\mathrm{eff}}_{\mu\nu}$ are massless. Unfortunately, the Boulware–Deser ghost is found to reappear on nontrivial backgrounds, which lowers the cutoff of the theory. However, the effective matter coupling can be embedded into a trimetric setup with a single matter sector coupled to only one metric, which thereby serves as a ghost-free completion [235]. We will not further discuss the effective matter coupling in this thesis. For further information in this regard, the interested reader is referred to [236–252].

Chapter 3

Classical solutions in bimetric theory

The previous discussion set the theoretical foundations of Hassan–Rosen bimetric theory. In this chapter, we review two important classes of solutions to the bimetric field equations, which are relevant for confronting the theory with observations. These are cosmological solutions, which describe the dynamics of the universe, and spherically symmetric solutions, which are relevant to describe systems such as galaxies, stars, and planets as well as the solar system. Reviews on these classes of solutions can be found in, e.g. [126, 253, 254]

We focus on singly-coupled bimetric theory with only a single matter sector, which minimally couples to the metric $g_{\mu\nu}$. This singles out $g_{\mu\nu}$ as the physical metric, which defines the geometry in which matter fields, collectively denoted as Φ, live. Combining Eqs. (2.64) and (2.87), the action of singly-coupled bimetric theory explicitly reads

$$\begin{aligned} S = -\frac{M_{\rm g}^2}{2}\int \mathrm{d}^4x \left(\sqrt{-g}\mathcal{R}^{\rm g} + \alpha^2\sqrt{-f}\mathcal{R}^{\rm f} - m^2\sqrt{-g}\mathcal{U}(\sqrt{g^{-1}f};\beta_n)\right) \\ + \int \mathrm{d}^4x\sqrt{-g}\,\mathcal{L}(g,\Phi)\,. \end{aligned} \tag{3.1}$$

Consequently, the modified Einstein equations (2.88) in this case are given by

$$G^{\rm g}_{\mu\nu} + V^{\rm g}_{\mu\nu} = \frac{1}{M_{\rm g}^2}T^{\rm g}_{\mu\nu}\,, \quad \alpha^2 G^{\rm f}_{\mu\nu} + V^{\rm f}_{\mu\nu} = 0\,. \tag{3.2}$$

These serve as basis for the remainder of this thesis.

In the case of singly-coupled bimetric theory, it is possible to interpret the metric, to which matter minimally couples, as physical metric in the above-mentioned sense. It is therefore possible, to identify the parameter limits, in which bimetric theory approaches General Relativity (GR) or Massive Gravity (MG), by studying the dynamics of the physical metric. We denote the physical metric by $g_{\mu\nu}$ in Eq. (3.1). We denote the other metric by $f_{\mu\nu}$.

The GR- and MG-limits are most easily assessed from the mixing of the mass eigenstates in the metric fluctuations (2.85). In the limit $\bar{\alpha} \ll 1$, the massive mode is suppressed in the fluctuations of the physical metric and $\delta g_{\mu\nu}$ coincides with the massless mode. This limit hence brings bimetric theory arbitrarily close to GR [52, 226, 227, 255]. In the opposite limit characterised by $\bar{\alpha} \gg 1$, the physical metric fluctuations are aligned with the massive mode while the massless mode is suppressed. Therefore, bimetric theory is arbitrarily close to MG in this limit. To be precise, to arrive at the MG limit also some of the interaction parameters β_n as well as the matter sectors need to scale with $\bar{\alpha}$ in certain ways as discussed in [216, 223, 226, 256–259]. In addition, there are further parameter regions, where solutions of bimetric theory resemble GR solutions [227, 255, 260]. As a summary, bimetric theory extrapolates between the GR- and MG-limits controlled by the parameter $\bar{\alpha}$.

3.1 Cosmological solutions

One of the key motivations for bimetric theory lies within the context of cosmology. We are seeking a mechanism, which accelerates the cosmic expansion at late times without a cosmological constant. Such cosmologies are referred to as *self-accelerating*.

Within bimetric theory, the nonlinear interactions between the massive and massless spin-2 field give rise to *dynamical dark energy*, which can mimic the effect of a cosmological constant at late times. The bimetric potential explicitly breaks one set of diffeomoprhism invariance, which is restored in the limit[1] $m_{\mathrm{FP}} \to 0$. Therefore, the spin-2 mass and hence also the effective cosmological constant is protected against quantum corrections. A small value of the cosmological constant is thus technical natural in the sense of 't Hooft [86].

We will first discuss homogeneous and isotropic solutions in bimetric theory and derive the modified Friedmann equations. These give rise to several solutions, out of which only the so-called finite or expanding branch solution is physically meaningful. Next, we will discuss the phenomenological features of this solution in the context of the cosmic expansion history, phantom dark energy and technical naturalness. We finish with a brief summary of linear cosmological perturbations. Cosmological backgrounds in bimetric theory have first been studied in [216, 256, 257, 261–266]. Good reviews of bimetric cosmology can be found in [126, 254], of which we make substantial use in the following discussion.

3.1.1 Modified Friedmann equations and classification of solutions

According to the *cosmological principle* the Universe is homogenous and isotropic on sufficiently large scales. Within bimetric theory, both metrics can simultaneously be written in bidiagonal FLRW form as [216, 256, 257][2]

$$\mathrm{d}s_{\mathrm{g}}^2 = -X_{\mathrm{g}}^2 \mathrm{d}t^2 + a^2 \left(\frac{\mathrm{d}r^2}{1-kr^2} + r^2 \mathrm{d}\Omega_{(2)}^2 \right) , \tag{3.3}$$

$$\mathrm{d}s_{\mathrm{f}}^2 = -X_{\mathrm{f}}^2 \mathrm{d}t^2 + b^2 \left(\frac{\mathrm{d}r^2}{1-kr^2} + r^2 \mathrm{d}\Omega_{(2)}^2 \right) . \tag{3.4}$$

Here, $\mathrm{d}\Omega_{(2)}^2 = \mathrm{d}\theta^2 + \sin^2\theta \mathrm{d}\phi^2$ denotes the surface element of the two-sphere. In this section, we will fix the gauge as $X_{\mathrm{g}} = 1$ and work in cosmic time t. The remaining metric functions a, b and X_{f} depend on cosmic time t only. Finally, the spatial curvature is denoted by k, and $k > 0$, $k = 0$, $k < 0$ describes an closed, flat, or open universe, respectively. The spatial curvature must be common to both metrics [216, 256, 268].

The functions a and b are the scale factors of $g_{\mu\nu}$ and $f_{\mu\nu}$, while X is the lapse function of $f_{\mu\nu}$. To ease notation, let us introduce the Hubble parameters for both metrics

$$H = \frac{\dot{a}}{a} , \qquad H_{\mathrm{f}} = \frac{\dot{b}}{X_{\mathrm{f}} b} , \tag{3.5}$$

as well as the scale factor ratio

$$y = \frac{b}{a} . \tag{3.6}$$

As we will see, the latter quantity captures the dynamics of the background cosmology. In terms of these quantities, the square-root matrix assumes the simple form $S = \mathrm{diag}(X, y, y, y)$.

Upon this ansatz, the Bianchi constraint (2.71) simplifies to

$$\left(X\dot{a} - \dot{b} \right) \left(\beta_1 + 2y\beta_2 + y^2\beta_3 \right) = 0 . \tag{3.7}$$

[1] If the effective cosmological constant Λ is non-zero, we also need to take the appropriate limit $\Lambda \to 0$ to not hit the Higuchi bound.

[2] In fact, homogenous and isotropic solutions in bimetric theory do not have to be bidiagonal [256]. However, these solutions decouple the two metric sectors and the effect of the bimetric potential reduces to the one of a cosmological constant for $g_{\mu\nu}$. Other cosmological solutions without the assumption of isotropy and/or homogeneity were studied in [267–269].

This equation gives rise to two branches of solutions. The first one, referred to as *algebraic branch*, is obtained by requiring the term in the second parenthesis to vanish. This forces the scale factor ratio y to be a constant, determined by the interaction parameters[3] $\beta_{1,2,3}$. The effect of the bimetric potential reduces to an effective cosmological constant, such that the equations for $g_{\mu\nu}$ exactly coincide with GR [216]. On the perturbative level, however, the scalar and vector modes appear without kinetic term, which signals strong coupling [213, 270–272]. The tensor modes exhibit a late-time instability [273]. In addition, it was found that a non-perturbative ghost mode is excited on this branch [214]. Due to these pathologies, we will not take the algebraic branch into account as in most of the literature.

The other solution to Eq. (3.7) is obtained by setting the terms in the first parenthesis to zero, leading to the *dynamical branch*. The lapse X_f can be expressed as a function of the scale factors as $X_\mathrm{f} = \dot{b}/\dot{a}$, or written in terms of the Hubble functions

$$H = yH_\mathrm{f}\,. \tag{3.8}$$

This branch has a rich and viable phenomenology as will be explained in the remainder of this section.

We assume the matter sector to be composed out of a perfect fluid compatible with the cosmological principle. As for the cosmological standard model discussed in Section 1.2, the stress-energy tensor is given by Eq. (1.16). Energy density ρ and pressure p are related by the linear equation of state $w = p/\rho$ as in Eq. (1.18). The continuity equation is solved by $\rho = \rho_0 a^{-3(1+w)}$.

The tt-component of the modified Einstein equations (2.88) reduce to the following set of modified Friedmann equations:

$$3H^2 = \frac{1}{M_\mathrm{g}^2}\left(\rho_\mathrm{de} + \rho + \rho_\mathrm{k}\right)\,, \tag{3.9}$$

$$3y^2H_\mathrm{f}^2 = \frac{1}{\alpha^2 M_\mathrm{g}^2}\left(\rho_\mathrm{pot} + \rho_\mathrm{k}\right)\,. \tag{3.10}$$

Beyond the usual energy densities that contribute to the Hubble rate, here we introduced the dark energy component induced by the bimetric potential as

$$\frac{\rho_\mathrm{de}}{M_\mathrm{g}^2} = m^2\left(\beta_0 + 3y\beta_1 + 3y^2\beta_2 + y^3\beta_3\right)\,. \tag{3.11}$$

The modified Einstein equation of $f_{\mu\nu}$ is sourced solely by the bimetric interaction potential, which gives rise to the following energy density

$$\frac{\rho_\mathrm{pot}}{M_\mathrm{g}^2} = m^2\left(\frac{\beta_1}{y} + 3\beta_2 + 3y\beta_3 + y^2\beta_4\right)\,. \tag{3.12}$$

The modified Friedmann equations (3.9) together with the continuity equation (1.17) close the system of differential equations. For completeness, we also present the rr-component of the modified Einstein equations (2.88), which are given by

$$2\dot{H} + 3H^2 + \frac{k}{a^2} = -\frac{p_\mathrm{de}}{M_\mathrm{g}^2} - \frac{p_\mathrm{m}}{M_\mathrm{g}^2}\,, \tag{3.13}$$

$$2\frac{y^2}{X_\mathrm{f}}\dot{H}_\mathrm{f} + 3y^2H_\mathrm{f}^2 + \frac{k}{a^2} = -\frac{p_\mathrm{pot}}{M_\mathrm{g}^2}\,. \tag{3.14}$$

Here, we defined the pressure contribution arising from the bimetric potential as

$$-\frac{p_\mathrm{de}}{M_\mathrm{g}^2} = \beta_0 + 2y\beta_1 + y^2\beta_2 + X_\mathrm{f}\left(\beta_1 + 2y\beta_2 + y^2\beta_3\right)\,, \tag{3.15}$$

$$-\frac{p_\mathrm{pot}}{M_\mathrm{g}^2} = \beta_2 + 2y\beta_3 + y^2\beta_3 + \frac{1}{X_\mathrm{f}}\left(\beta_1 + 2y\beta_2 + y^2\beta_3\right)\,. \tag{3.16}$$

[3] Note that at least two of these interaction parameters must be non-vanishing in order to give rise to a solution with $y \neq 0$.

The lapse function X_f can be expressed in terms of the scale factor ratio as $X_\mathrm{f} = y + y'$ using the Bianchi constraint in Eq. (3.8), where prime denotes derivative with respect to e-folds $N = \ln a$, i.e. $y' = \dot{y}/H$. We can define a time-dependent equation-of-state parameter w_de for the dynamical dark energy component as

$$w_\mathrm{de} = \frac{p_\mathrm{de}}{\rho_\mathrm{de}} = -1 - \frac{\beta_1 + 2y\beta_2 + y^2\beta_3}{\beta_0 + 3y\beta_1 + 3y^2\beta_2 + y^3\beta_3} y' \,. \tag{3.17}$$

As we will see below, we can express y' in terms of y. The quantity w_de will be useful to discuss the phenomenological features of bimetric cosmology.

Combining both modified Friedmann equations (3.9) with the Bianchi constraint (3.8) results in

$$\alpha^2 y^4 \beta_3 + (3\alpha^2\beta_2 - \beta_4) y^3 + 3(\alpha^2\beta_1 - \beta_3) y^2 - \left(\alpha^2\beta_0 - \beta_2 + \alpha^2 \frac{\rho}{M_\mathrm{g}^2}\right) y - \beta_1 = 0 \,. \tag{3.18}$$

This equation represents a quartic polynomial in y and as such has up to four real-valued solutions. The solutions can be thought of as determining the time evolution of y in terms of ρ. Taking the time derivative of Eq. (3.18) yields [263]

$$y' = \frac{3\alpha^2 y^2 (1+w)\rho/M_\mathrm{g}^2}{\beta_1 - 3y^2\beta_3 - 2y^3\beta_4 + 3\alpha^2 y^2(\beta_1 + 2y\beta_2 + y^2\beta_3)} \,. \tag{3.19}$$

Since Eq. (3.18) can be used to eliminate ρ in terms of y, the phase space of bimetric theory is one-dimensional: y' depends only on y.

In Section 2.4.3 we noted that proportional solutions are invariant under Eq. (2.77). Similarly, the FLRW solutions are invariant under

$$y \longrightarrow -y \,, \quad \beta_n \longrightarrow (-1)^n \beta_n \,. \tag{3.20}$$

This implies that we can restrict ourselves to $y \geq 0$ without loss of generality as we will do from now on.

Another useful relation can be obtained for the energy density parameter of matter, which is defined as

$$\Omega = \frac{\rho}{3H^2 M_\mathrm{g}^2} \,. \tag{3.21}$$

Solving the $g_{\mu\nu}$–Friedmann equation (3.9) for Ω and replacing H by means of the $f_{\mu\nu}$–Friedmann equation (3.9) yields [265]

$$\Omega = 1 - \frac{\rho_\mathrm{de}}{\rho_\mathrm{pot}} = 1 - \frac{\beta_0 + 3y\beta_1 + 3y^2\beta_2 + y^3\beta_3}{\beta_1 + 3y\beta_2 + 3y^2\beta_3 + y^3\beta_4} y \,. \tag{3.22}$$

Let us discuss the different branches of solutions to Eq. (3.18) following [265]. These can be visualised easily in terms of the phase space as in Fig. 3.1, which is inspired by analogous figures given in [265, 274, 275]. From Eq. (3.19) we observe that $y' = 0$ iff $\rho = 0$ or $y = 0$. Therefore, the de Sitter points cannot be crossed dynamically and separate different branches from another as these necessarily have $y' = 0$. The point $y = 0$ is not a de Sitter point, but is characterised by a divergent matter energy density as can be seen from Eq. (3.18) (assuming $\beta_1 \neq 0$). The different branches can be identified by studying the early universe behaviour of y, i.e. when the matter energy density classically diverges:

- *Finite branch.* The first possibility is that y is small so as to cancel large values of ρ in Eq. (3.18). At early times, y can be approximated by

$$y \sim \frac{\beta_1}{\alpha^2} \left(\frac{\rho}{M_\mathrm{g}^2}\right)^{-1} \,. \tag{3.23}$$

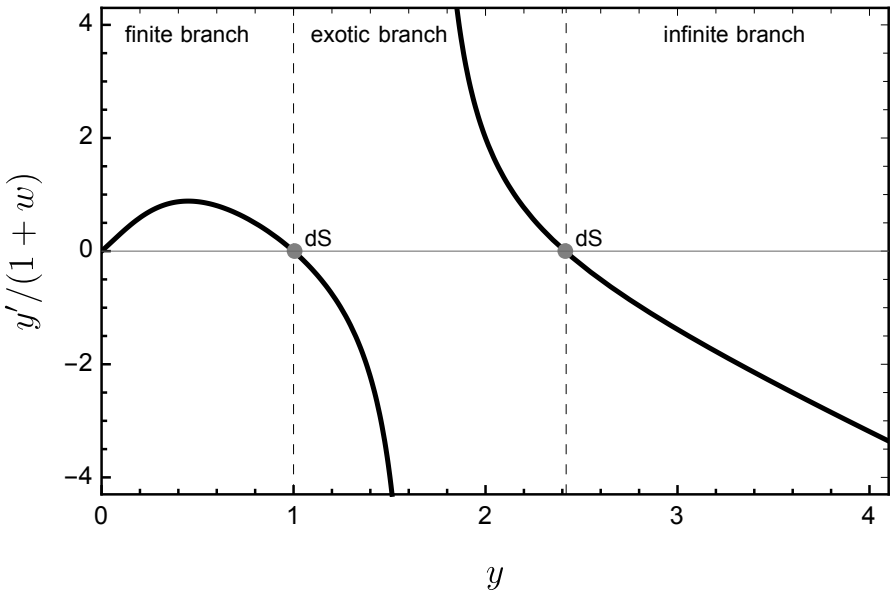

Figure 3.1: Phase space of the scale factor ratio y demonstrating the different branches of solutions. The grey dots represent the late-time de Sitter attractors. To produce the plot, the $\beta_0\beta_1\beta_4$-model with $\bar{\alpha} = 1$ and $m_{\mathrm{FP}}^2 = \Lambda$ is used as a concrete representative example.

The scale factor ratio monotonically increases with time, $y' > 0$, until the matter energy density vanishes in the asymptotic future and y approaches a constant value. This is the finite branch solution as depicted in the left part of Fig. 3.1. Existence of the finite branch imposes some restrictions on the bimetric parameters. To see this, we note that the $f_{\mu\nu}$–Friedmann equation (3.9) yields a real-valued and divergent Hubble parameter at early times only if $\beta_1 > 0$ [265]. In addition, this automatically leads to $\Omega = 1$ at early times as can be seen from Eq. (3.22) [265].

- *Infinite branch.* Alternatively, also the scale factor ratio diverges as ρ diverges, i.e. $y \gg 1$. The polynomial is then dominated by the highest order term and y can be approximated as

$$y \sim \left(-\frac{1}{\beta_3}\,\frac{\rho}{M_{\mathrm{g}}^2}\right)^{1/3} . \tag{3.24}$$

  The scale factor ratio evolves from $y = \infty$ at early times to a constant value in the asymptotic future, when the matter energy density vanishes. This is depicted in the right part of Fig. 3.1. The dark energy contribution to the Hubble parameter does not necessarily vanish during early times, which could in principle lead to substantial deviations from the standard model, such as early dark energy. From Eq. (3.22) we see that $\Omega = 1$ as $y \to \infty$ only if $\beta_4 > 0$ and $\beta_2 = \beta_3 = 0$ [265].

- *Exotic branches.* Eq. (3.18) represents a quartic polynomial in y, such that there are up to two more real-valued solutions for y in terms of ρ. These branches necessarily contain a pole in y' and usually describe bouncing cosmologies or a universe that is static in the asymptotic future or past [265, 275].

There are specific parameter values for which the exotic branches do not exist such that the finite and infinite branch have the same late-time de Sitter attractor. The discussion of the next section will reveal that the finite branch is physical, while the infinite branch is pathological.

3.1.2 Dynamical Higuchi bound

The Higuchi bound represents a lower limit on the allowed spin-2 mass in the presence of a non-vanishing cosmological constant $\Lambda = 3H^2$ of the form $m_{\mathrm{FP}}^2 \geq 2H^2$ [224, 225]. If the bound is violated, the helicity-0 mode of the massive spin-2 field has a kinetic term with the wrong sign rendering any vacuum unstable and the Hamiltonian to be unbounded from below. A sensible solution must therefore respect this bound to by physically meaningful. Despite the group-theoretic origin of the Higuchi bound, it can be generalised to FLRW space as done in [276]. By studying the minisuperspace action, the authors identified the kinetic term of the scalar mode of the massive graviton. The kinetic term has the correct sign only if the dynamical bound

$$m_{\mathrm{eff}}^2 - 2H^2 \geq 0 \tag{3.25}$$

in terms of the effective time-dependent mass parameter

$$m_{\mathrm{eff}}^2 = \left(1 + \frac{1}{\alpha^2 y^2}\right) y \left(\beta_1 + 2y\beta_2 + y^2\beta_3\right) \tag{3.26}$$

is satisfied. We will refer to this bound as *dynamical Higuchi bound*. The bound must be satisfied during the entire cosmic expansion history, otherwise the solution is not meaningful. In the limit of vanishing matter energy density, FLRW approaches dS and y approaches a constant, such that the usual Higuchi bound is recovered.

In terms of the variables appearing in the dynamical Higuchi bound, we can write Eq. (3.19) in the following compact form [277]:

$$\frac{y'}{y} = \frac{(1+w)\rho/M_{\mathrm{g}}^2}{m_{\mathrm{eff}}^2 - 2H^2} \tag{3.27}$$

(see also [266, 275, 278]). This equation immediately allows to rule out the aforementioned infinite branch solution. For positive energy densities of matter, $\rho > 0$, a decreasing scale factor ratio, i.e. $y' < 0$, implies the violation of the dynamical Higuchi bound. Contrarily, the scale factor ratio is increasing on the finite branch, $y' > 0$, and the dynamical Higuchi bound is consequently satisfied at all times for $\rho > 0$. This establishes that the finite branch solution is the unique FLRW solution in bimetric theory [275]. In the next section we will discuss the phenomenological features of the finite branch.

3.1.3 Features of bimetric cosmology

After having identified the finite branch as the unique FLRW solution in bimetric theory, let us now discuss its phenomenological features. In the expanding universe, the scale factor ratio y monotonically increases with time from zero in the asymptotic past, to a constant value in the asymptotic future. This is depicted in Fig. 3.2 for the $\beta_0\beta_1\beta_4$-model as representative concrete example, which is inspired by analogous figures from [260, 265].

The time evolution of the scale factor ratio y yields a dark energy component that evolves in time. The effect of the bimetric interaction potential is thus the one of dynamical dark energy, as in the sense of quintessence [279, 280]. Furthermore, the dynamical dark energy is growing as the universe expands. At late times, when y approaches a constant value, also the dark energy component approaches a constant value thus mimicking a cosmological constant. At early times, however, the dynamical dark energy component approaches the constant value $\rho_{\mathrm{de}}/M_{\mathrm{g}}^2 = \beta_0$, see Eq. (3.11). If $\beta_0 = 0$, there is no dark energy in the early universe. Going further, for $\beta_0 < 0$ the energy density of dark energy is negative during early times.

Such scenario is referred to as self-accelerating. For $\beta_0 = 0$, the accelerated expansion of the universe at late times is driven by the interaction between the two metric tensors. In the zero-mass limit $m_{\mathrm{FP}} \to 0$ the full diffeomorphism symmetry is recovered, which transforms both metrics separately. This symmetry protects the spin-2 mass scale and hence the interaction parameters $\beta_{1,2,3}$ from receiving large contributions from quantum corrections. This renders a small cosmological

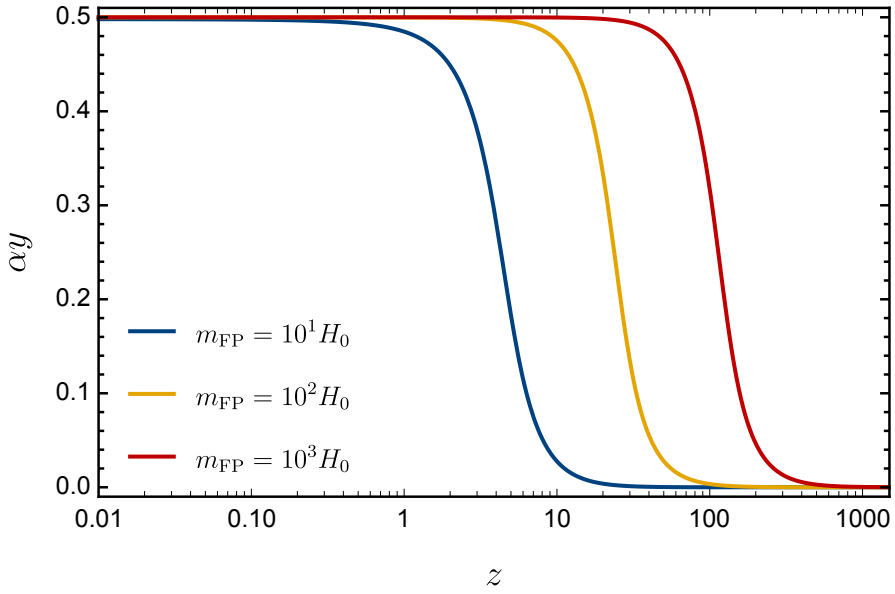

Figure 3.2: Evolution of the scale factor ratio $\bar{y} = \alpha y$ on the finite branch as a function of redshift z. To produce the figure, the $\beta_0\beta_1\beta_4$-model with $\bar{\alpha} = 0.5$ and $\Omega_\Lambda = 0.7$ is used for three different values of the spin-2 mass $m_{\rm FP}$.

constant Λ technically natural in the sense of 't Hooft [86], even if $m_{\rm FP}^2 \gg \Lambda$. The calculations performed in [242, 281–283] provide explicit confirmation of that last statement.

To demonstrate the dynamical growing of the dark energy component as the universe expands, we depict $\rho_{\rm de}$ as a function of redshift in Fig. 3.3. The left panel shows the evolution of $\rho_{\rm de}$ in the $\beta_0\beta_1\beta_4$-model for three different parameter values. The blue line has $\beta_0 > 0$, while the yellow and red lines have $\beta_0 < 0$. In the right panel the evolution of $\rho_{\rm de}$ for the $\beta_1\beta_2\beta_3$-model is depicted, i.e. we have $\beta_0 = 0$. Therefore, $\rho_{\rm de}$ vanishes at early times.

We see that the dynamical dark energy component $\rho_{\rm de}$ is monotonically increasing as the universe expands independent of the value β_0. This feature is usually referred to as phantom for positive energy densities [284]. Hence, if $\beta_0 \geq 0$ the interaction energy of the spin-2 fields yields *phantom dark energy*. For models with $\beta_0 < 0$, the dark energy density changes its sign at some redshift z_*. While dark energy is then negative at early times $z > z_*$, it is phantom at later times $z < z_*$. This feature can also be seen from the equation of state parameter $w_{\rm de}$. In terms of the effective mass parameter as defined in Eq. (3.26), we can write Eq. (3.17) as

$$w_{\rm de} = -1 - \frac{\alpha^2 y^2}{1+\alpha^2 y^2} \frac{m_{\rm eff}^2}{m_{\rm eff}^2 - 2H^2} \frac{(1+w)\rho}{\rho_{\rm de}}\,, \tag{3.28}$$

where we used Eq. (3.27) to eliminate y'. All quantities except $\rho_{\rm de}$ are manifestly positive on the finite branch. This implies that $w_{\rm de} < -1$ for $\rho_{\rm de} > 0$. Further, $w_{\rm de}$ diverges when $\rho_{\rm de}$ changes its sign and is larger than -1 for negative dark energy. Expanding the equation for early times, i.e. around $y = 0$, yields

$$\lim_{z\to\infty} w_{\rm de} = -1 - (1+w)\frac{3y\beta_1}{\beta_0 + 3y\beta_1}\,. \tag{3.29}$$

Therefore, the equation-of-state parameter assumes the value $w_{\rm de} = -2 - w_{\rm m}$ if $\beta_0 = 0$ and $w_{\rm de} = -1$ if $\beta_0 \neq 0$.

In Fig. 3.4 we depict the time evolution of $w_{\rm de}$ for the same models and parameter values as in Fig. 3.3. Analogous figures can be found in [260]. To produce the plot we set $w = 0$ so as to describe non-relativistic matter. In the left panel, the $\beta_0\beta_1\beta_4$-model is presented. As described

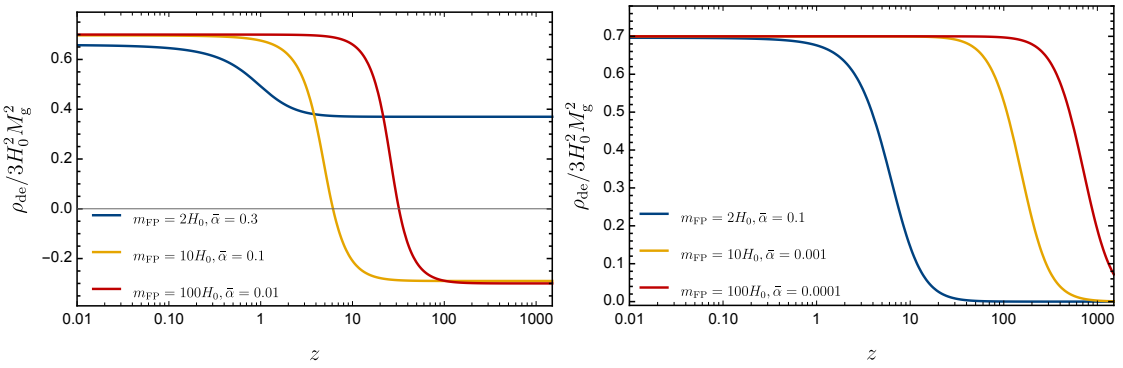

Figure 3.3: The time evolution on the finite branch of $\rho_{\rm m}$ normalised to $3H_0^2M_{\rm g}^2$ as function of redshift z for the $\beta_0\beta_1\beta_4$- (left) and $\beta_1\beta_2\beta_3$-model (right). All cases have $\Omega_\Lambda = 0.7$, which is approached in the asymptotic future. The past asymptotic value is set by β_0.

before, $w_{\rm de}$ approaches the value of -1 in the asymptotic past and future and exhibits a singularity if $\beta_0 < 0$. The right panel shows the $\beta_1\beta_2\beta_3$-model, for which $w_{\rm de}$ assumes the value of -2 in the asymptotic past. We have chosen these models as representative examples for the cases with $\beta_0 \neq 0$ and $\beta_0 = 0$, respectively. To summarise, for $\rho_{\rm de} > 0$ the dynamical dark energy is always phantom, $w_{\rm de} < -1$, with a time-evolving equation-of-state parameter.

Interestingly, cosmological observations allow and even seem to slightly favor dark energy to be phantom as we discussed in Section 1.3. Models of phantom dark energy that are based on scalar fields [284, 285] are plagued by inconsistencies such as ghosts or tachyons [286], but possible resolutions exist also in this context [287–289]. Contrarily, bimetric theory represents a theoretically derived and consistent model of phantom dark energy devoid of the aforementioned pathologies and without fine tuning[4]. In addition, models with a constant phantom equation of state yield a Big Rip, where the physical scale factor diverges after a finite time [284]. Since $w_{\rm de}$ dynamically evolves towards -1 as the universe expands, the Big Rip is avoided in bimetric theory [292]. It would be interesting to investigate, whether a little rip [293], pseudo-rip [294], or other types of future singularities [295] occur in bimetric cosmology.

To finish, we briefly comment on the observational status of bimetric cosmology on the background level. We already discussed that bimetric theory leads to self-accelerating solutions with a small Hubble scale being technically natural. Indeed, it was found that several models of bimetric theory fit measurements of the cosmic expansion such as Supernovae type 1a (SN1a), Baryon Acoustic Oscillations (BAOs) and the fluctuations in the Cosmic Microwave Background (CMB) as good as GR [216, 263, 265, 296–299]. We will discuss the observational viability in detail in Chapter 6.

3.1.4 On linear cosmological perturbations

The previous discussion concerned background cosmology. The real Universe, however, deviates from exact isotropy and homogeneity as our very existence indicates. One should thus study small deviations from the exact FLRW background. On the linear level, the tensor-, vector- and scalar modes are decoupled.

The scalar sector was studied in [226, 266, 270, 272, 274, 275, 300–305]. Instead of going through the technical and computationally lengthy steps, here we summarise the results inferred in these references. The two metric tensors up to linear order in fluctuations in the scalar sector can be

[4]Phantom dark energy violates the Null Energy Condition (NEC). This is true also in bimetric theory, where the energy-momentum arising from the bimetric potential violates the NEC [290]. This has interesting consequences in the context of wormhole solutions [291].

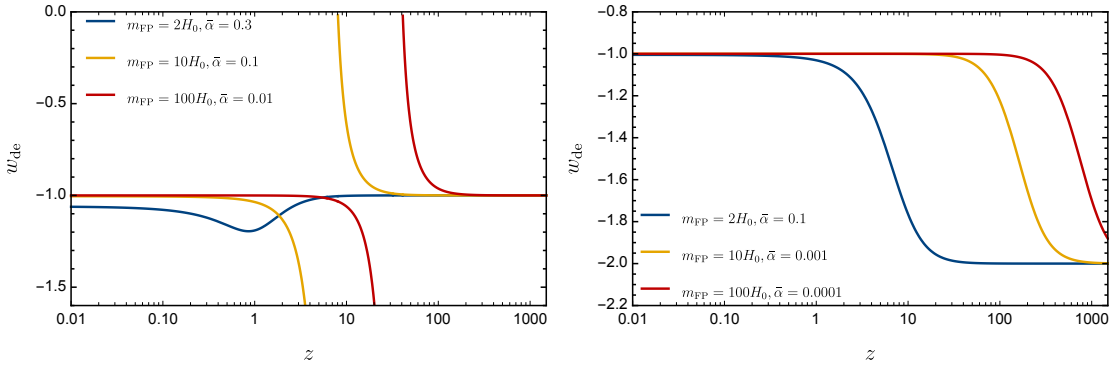

Figure 3.4: The equation-of-state parameter $w_{\rm de}$ as function of redshift z for the $\beta_0\beta_1\beta_4$- (left) and the $\beta_1\beta_2\beta_3$-model (right). This demonstrates the different early-time behavior and the phantom nature of the dynamical dark energy.

written as

$$\begin{aligned} \mathrm{d}s_{\rm g}^2 &= -(1+2\phi_{\rm g})\,\mathrm{d}t^2 + 2a\partial_i B_{\rm g}\,\mathrm{d}x^i\mathrm{d}t + a^2\Big[(1-2\psi_{\rm g})\delta_{ij} + 2\partial_i\partial_j E_{\rm g}\Big]\,\mathrm{d}x^i\mathrm{d}x^j\,, \\ \mathrm{d}s_{\rm f}^2 &= -X^2(1+2\phi_{\rm f})\,\mathrm{d}t^2 + 2Xb\partial_i B_{\rm f}\,\mathrm{d}x^i\mathrm{d}t + b^2\Big[(1-2\psi_{\rm f})\delta_{ij} + 2\partial_i\partial_j E_{\rm f}\Big]\,\mathrm{d}x^i\mathrm{d}x^j\,. \end{aligned} \tag{3.30}$$

As before, the functions a, b and X depend on cosmic time t. The perturbation fields $\phi_{\rm g,f}$, $\psi_{\rm g,f}$, $B_{\rm g,f}$ and $E_{\rm g,f}$ depend on time t and space x^i. To ease the presentation, we will suppress the explicit dependency in the following.

Matter is composed out of a perfect fluid with equation of state $p = w\rho$. We describe the perturbations in the matter sector by a single scalar field χ. The perturbed stress energy tensor coupled to the scalar perturbations in the metrics can be written as [305, 306]

$$\begin{aligned} \delta T^0{}_0 &= -(\rho+p)(3\psi_{\rm g} - \partial^2 E_{\rm g} - \partial^2\chi)\,, \\ \delta T^i{}_0 &= -(\rho+p)a\partial_i\dot{\chi}\,, \\ \delta T^0{}_i &= (\rho+p)(\partial_i B_{\rm g} + a\partial_i\dot{\chi})\,, \\ \delta T^i{}_j &= w(\rho+p)(3\psi_{\rm g} - 2\partial^2 E_{\rm g} - \partial^2\chi)\delta^i{}_j\,, \end{aligned} \tag{3.31}$$

where $\partial^2 = \partial^i\partial_i$.

The theory is invariant under simultaneous diffeomorphisms of the two metrics. The perturbation variables are thus gauge-dependent. This problem is usually addressed by defining a new set of gauge-invariant scalar fields. Alternatively, one can fix the gauge such that the remaining fields coincide with the gauge-invariant variables. It is particularly convenient to identify those variables with redundant equation of motion [307]. In our context, we can use the gauge to fix two perturbation variables. The appropriate candidates in our case are one of $(\psi_{\rm g}, \psi_{\rm f})$ and $(E_{\rm g}, E_{\rm f}, \chi)$ [305]. Fixing the gauge as $\psi_{\rm f} = \chi = 0$ yields that the fields $E_{\rm g}$ and $E_{\rm f}$ coincide with gauge-invariant variables in this gauge.

After fixing the gauge as above, the fields $B_{\rm g}$, $B_{\rm f}$, $\phi_{\rm g}$ and $\phi_{\rm f}$ appear without time derivatives in the linearised Einstein equations. Therefore, these are auxiliary variables that can be expressed in terms of $E_{\rm g}$, $E_{\rm f}$ and $\psi_{\rm g}$ algebraically. Replacing the auxiliary variables, all time derivatives of the variable $\psi_{\rm g}$ drop out of the equations of motion. Hence, also $\psi_{\rm g}$ is an auxiliary variable that can be expressed algebraically in terms of $E_{\rm g}$ and $E_{\rm f}$. Hence, there are only two scalar degrees of freedom present as it is appropriate in our case: one from the massive spin-2 field and one from the matter sector.

The final step is to solve the equations of motion and extract the time-evolution of the perturbation fields. In [305] it is found that both fields are decaying towards the same constant

value at late times (i.e. de Sitter) and also during early times on super-horizon scales, $k \ll aH$. On sub-horizon scales $k \gg aH$, however, the field $E_{\rm g}$ is oscillating, while $E_{\rm f}$ has an exponential instability. This is referred to as a *gradient instability*, as also identified in [274, 303]. Since $E_{\rm f}$ is exponentially growing in time, the perturbative assumption $E_{\rm f} \ll 1$ is violated at early times.

In [274] it was shown that in the subhorizon regime $k \ll aH$ the linearised Einstein equations admit a Wentzel–Kramers–Brillouin (WKB) solution (i.e. with $|\omega'/\omega^2| \ll 1$), which allows to write the perturbations as $E_{\rm g,f} \sim e^{i\omega N}$. Here, $N = \ln a$ describes e-folds and ω is the eigenfrequency. The eigenfrequencies can be solved for in terms of the bimetric parameters β_n and α as well as the scale-factor ratio y as [226]

$$\left(\frac{aH}{k}\right)^2 \omega^2 = 1 + \frac{(\beta_1 + 4y\beta_2 + 3y^2\beta_3)y'}{3y(\beta_1 + 2y\beta_2 + y^2\beta_3)} - \frac{(1+\alpha^2 y^2)(\beta_1 - y^2\beta_3)y'^2}{3\alpha^2 y^3(1+w_{\rm m})\rho_{\rm m}/M_{\rm g}^2} \tag{3.32}$$

If $\omega^2 < 0$, the gradient instability occurs rendering perturbation theory invalid.

A gradient instability, however, does not signal an inconsistency of the theory, but the breakdown of perturbation theory. Within bimetric theory, there are three ways to circumvent the gradient instability:

1. *Fine-tuned initial conditions.* The initial conditions can be finely tuned, schematically $E_{\rm f} \ll E_{\rm g}$ initially, such that $E_{\rm f}$ remains small during the entire observed cosmic expansion history. This scenario appears unfavored as it would remove the very motivation for introducing a massive spin-2 field in the first place. A mechanism to explain the initial fine-tuning would be required.

2. *GR-limit.* In [226] it was shown that the instance in time, before which the gradient instability is present, can be pushed to arbitrary early times by sending $\bar{\alpha} \to 0$. As an example, for $\bar{\alpha} \sim 10^{-55}$ the instability would occur before GUT-scale inflation [226]. This parametric limit brings bimetric theory arbitrarily close to GR, such that deviations are suppressed at all scales.

3. *Nonlinearities.* If $E_{\rm f} \gtrsim \mathcal{O}(1)$, nonlinear terms are as important as linear terms. Taking all nonlinearities into account might stabilise the perturbations in analogy to the Vainshtein mechanism [277, 308–310]. We will discuss this possibility in greater detail in Chapter 5.

Despite these possible resolutions, inferring phenomenological consequences on the perturbative level (such as cosmic structure formation) remains a difficult and yet unsolved task.

Going further, the vector sector was studied in [266, 305]. It was found that the vector perturbations are decaying and that their propagation speed is subluminal on the finite branch. The vector sector is thus not plagued by a gradient instability unlike the scalar sector. Since the vector modes are decaying, it is expected that these do not contribute to observable effects, just like in GR.

Finally let us summarise the tensor sector, i.e. gravitational waves. On the infinite branch solution, the tensor modes exhibit a power-law instability induced by violation of the Higuchi bound [266, 305, 311–314]. In addition, the tensor modes are plagued by instabilities on the algebraic branch [273]. As discussed before, these branches are not physical. Contrarily, on the finite branch the tensor modes are linearly stable with a decaying massive mode, with interesting consequences for the primordial gravitational wave power spectra and the CMB [266, 305, 313, 315–321]. Finally, the generation and propagation of gravitational waves were studied in [322–327], which found e.g. oscillations.

3.2 Spherically symmetric solutions

Gravitational interactions manifest themselves not only on cosmological scales, but also on smaller scales. On galaxy cluster and galactic scales, observations are in stark conflict with GR unless one introduces large portions of dark matter. On solar system scales and below, GR is confirmed with

remarkable precision. We should thus study deviations from GR implied by modified gravity to assess the observational viability of modified gravity.

To model the gravitational potential, in which a test body moves, one usually assumes staticity and spherical symmetry. In bimetric theory, solutions compatible with these assumptions were studied in [328–333]. We present the technical details of the derivation in Appendix A and discuss here the features of local solutions.

The most general, bidiagonal ansatz for spherically symmetric and static solutions is [331]

$$\mathrm{d}s_{\mathrm{g}}^2 = -e^{-\phi_{\mathrm{g}}}\mathrm{d}t^2 + e^{\psi_{\mathrm{g}}}\mathrm{d}r^2 + r^2\mathrm{d}\Omega_{(2)}^2\,, \tag{3.33}$$

$$\mathrm{d}s_{\mathrm{f}}^2 = c^2(-e^{-\phi_{\mathrm{f}}}\mathrm{d}t^2 + e^{\psi_{\mathrm{f}}}(r+r\mu)'^2\mathrm{d}r^2 + (r+r\mu)^2\mathrm{d}\Omega_{(2)}^2) \tag{3.34}$$

All field $\phi_{\mathrm{g,f}}$, $\psi_{\mathrm{g,f}}$ and μ depend on the radial coordinate r. The field μ parametrises the relative twist between the two coordinate systems and can thus be thought of as Stückelberg field that gets shifted by diffeomorphisms. For $\phi_{\mathrm{g}} = \phi_{\mathrm{f}}$, $\psi_{\mathrm{g}} = \psi_{\mathrm{f}}$, and $\mu = 0$ both metrics are proportional.

The equations of motion cannot be solved in general. Instead, we will consider to different regimes.

3.2.1 Linear regime

Let us assume that all metric fields as well as their derivatives are small, i.e. $\{\phi_{\mathrm{g,f}}, \psi_{\mathrm{g,f}}, \mu\} \ll 1$ and $\{r\phi'_{\mathrm{g,f}}, r\psi'_{\mathrm{g,f}}, r\mu'\} \ll 1$. As we present in Appendix A, the linearised Einstein equations are solved by [331,332,334]

$$\mu = -\frac{r_{\mathrm{S}}(1 + m_{\mathrm{FP}}r + m_{\mathrm{FP}}^2 r^2)e^{-m_{\mathrm{FP}}r}}{3(1+\bar{\alpha}^2)m_{\mathrm{FP}}^2 r^3}\,, \tag{3.35a}$$

$$\phi_{\mathrm{g}} = -\frac{\Lambda r^2}{3} - \frac{r_{\mathrm{S}}}{1+\bar{\alpha}^2}\left(\frac{1}{r} + \frac{4\bar{\alpha}^2}{3}\frac{e^{-m_{\mathrm{FP}}r}}{r}\right)\,, \tag{3.35b}$$

$$\phi_{\mathrm{f}} = -\frac{\Lambda r^2}{3} - \frac{r_{\mathrm{S}}}{1+\bar{\alpha}^2}\left(\frac{1}{r} - \frac{4\bar{\alpha}^2}{3}\frac{e^{-m_{\mathrm{FP}}r}}{r}\right)\,, \tag{3.35c}$$

$$\psi_{\mathrm{g}} = \frac{\Lambda r^2}{3} + \frac{r_{\mathrm{S}}}{1+\bar{\alpha}^2}\left(\frac{1}{r} + \frac{2\bar{\alpha}^2(1+m_{\mathrm{FP}}r)e^{-m_{\mathrm{FP}}r}}{3r}\right)\,, \tag{3.35d}$$

$$\psi_{\mathrm{f}} = \frac{\Lambda r^2}{3} + \frac{r_{\mathrm{S}}}{1+\bar{\alpha}^2}\left(\frac{1}{r} - \frac{2\bar{\alpha}^2(1+m_{\mathrm{FP}}r)e^{-m_{\mathrm{FP}}r}}{3r}\right)\,. \tag{3.35e}$$

In here, we have defined the Schwarzschild radius $r_{\mathrm{S}} = M/(4\pi\, M_{\mathrm{g}}^2)$ of a compact source of mass M. From here we can read off the effective Planck mass $M_{\mathrm{P}}^2 = (1+\bar{\alpha}^2)M_{\mathrm{g}}^2$. In the GR-limit $\bar{\alpha} \ll 1$, both Planck masses coincide.

Let us discuss these solutions. The function ϕ_{g} describes the gravitational field as felt by a massive test body. It consists of a part due to a non-vanishing cosmological constant Λ, which grows with distance as r^2 just like in GR. The gravitational potential induced by the compact object of mass M is composed out of two parts. Firstly, a term proportional to $1/r$ as in GR and secondly a Yukawa-like term, which receives an additional exponential suppression.

The additional Yukawa term represents a substantial deviation form GR. In the limit $\bar{\alpha} \to 0$ the deviations are suppressed on all length scales. This is expected because this parametric limit brings bimetric theory arbitrarily close to GR. On the other hand, on scales much larger than the Compton wavelength of the massive spin-2 field, $r \gg m_{\mathrm{FP}}^{-1}$, deviations are suppressed by the exponential term. Therefore, on these scales GR is approached even for finite $\bar{\alpha}$. On the other hand, deviations from GR are most important on length scales $r \lesssim m_{\mathrm{FP}}^{-1}$.

Let us discuss the validity of the linear approximation. In the presence of a non-vanishing cosmological constant, the assumption is valid inside the Hubble horizon, $r \ll \sqrt{3/\Lambda}$. Next, the fields $\phi_{\mathrm{g,f}}$ and $\psi_{\mathrm{g,f}}$ are small outside the Schwarzschild radius, i.e. for $r \gg r_{\mathrm{S}}$. This is analogous to GR. The Stückelberg field μ, however, becomes order unity at a different length scale already.

This is the Vainshtein radius $r_{\rm V}$, which can be read off from Eq. (3.35a) as

$$r_{\rm V} = \left(\frac{r_{\rm S}}{m_{\rm FP}^2}\right)^{1/3}, \tag{3.36}$$

where we have omitted an $\mathcal{O}(1)$ factor to follow standard notation [331]. The linear approximation is valid on scales $r \gg r_{\rm V}$. We thus need to seek an alternative set of solutions taking into account nonlinearities, which are valid inside the Vainshtein radius.

3.2.2 Nonlinear regime

As we have seen before, the fields $\phi_{\rm g,f}$ and $\psi_{\rm g,f}$ are linear also inside the Vainshtein radius. However, we now keep all nonlinearities in the Stückelberg field μ. Instead, we assume that we are far inside the Compton regime, i.e. $r \ll m_{\rm FP}^{-1}$.

To ease the presentation, we first define the parameters

$$\beta = \frac{c^2\beta_2 + c^3\beta_3}{c\beta_1 + 2c^2\beta_2 + c^3\beta_3}\,, \quad \gamma = \frac{c^3\beta_3}{c\beta_1 + 2c^2\beta_2 + c^3\beta_3}\,. \tag{3.37}$$

As we demonstrate in Appendix A, we can solve for all fields in terms of μ. Plugging the result into the Bianchi constraint results in a seventh order polynomial, which can schematically be written as

$$P(\mu) = 3\left(\frac{r_{\rm V}}{r}\right)^3 (1+\bar{\alpha}^2)(1+\mu)^2(1-\gamma\mu^2)\,, \tag{3.38}$$

Here, $P(\mu)$ is a polynomial in μ of seventh degree, which satisfies $P(0) = 0$ and is independent of r. The explicit expression can be found in Eq. (A.18). Let us classify the solutions, following [331]. In general, the polynomial has seven solutions, which can be real- or complex-valued. For $\gamma > 0$, there are three real and two complex conjugate solutions for all values of r. The remaining two solutions are real for small r and join together in a complex conjugate pair at some critical radius, which depends on the parameters $\bar{\alpha}$, β and γ. It is worth studying the two asymptotic limits of the three real solutions:

- *Large distance.* In the limit $r \gg r_{\rm V}$, the right hand side is small and Eq. (3.38) simplifies to $P(\mu) \ll 1$ asymptotically. The simplest solution is $\mu \ll 1$, which map to the linearised solution presented before. In the two remaining solutions, μ approaches constant values asymptotically, which depend on $\bar{\alpha}$, β and γ.

- *Small distance.* In the limit $r \ll r_{\rm V}$, there are three possibilities to cancel the large value of $(r_{\rm V}/r)^3$ on the right hand side. Either $\mu = -1$ or $\mu = \pm 1/\sqrt{\gamma}$. Alternatively, μ diverges as $r \to 0$, which does not correspond to one of the everywhere-real solutions.

See [331] for more details on the case $\gamma \leq 0$ and [329] for caveats regarding the case $\gamma = 0$.

In Fig. 3.5 we present the three everywhere real solutions for μ as a function of r. This figure is taken from [298] as inspired by [331]. From the figure we can easily assess the aforementioned asymptotic behavior of the real solutions. The green-dashed and red-dotted solutions have a asymptotically non-zero constant value for μ and connect to the solution $\mu = -1$ and $\mu = 1/\sqrt{\gamma}$, respectively. The solution represented by the black solid line realises the linear regime for large radii, $\mu \ll 1$, and connects to the solution $\mu = -1/\sqrt{\gamma}$ inside the Vainshtein radius.

The latter solution is referred to as *Vainshtein-Yukawa solution*. Since $\mu \ll 1$ outside the Vainshtein radius, the linear regime is described and the gravitational potential induced by a compact object is composed out of the standard $1/r$-term and the additional Yukawa-type potential. Plugging the result $\mu = -1/\sqrt{\gamma}$ into Eqs. (A.14) to (A.17), which are the expressions for the

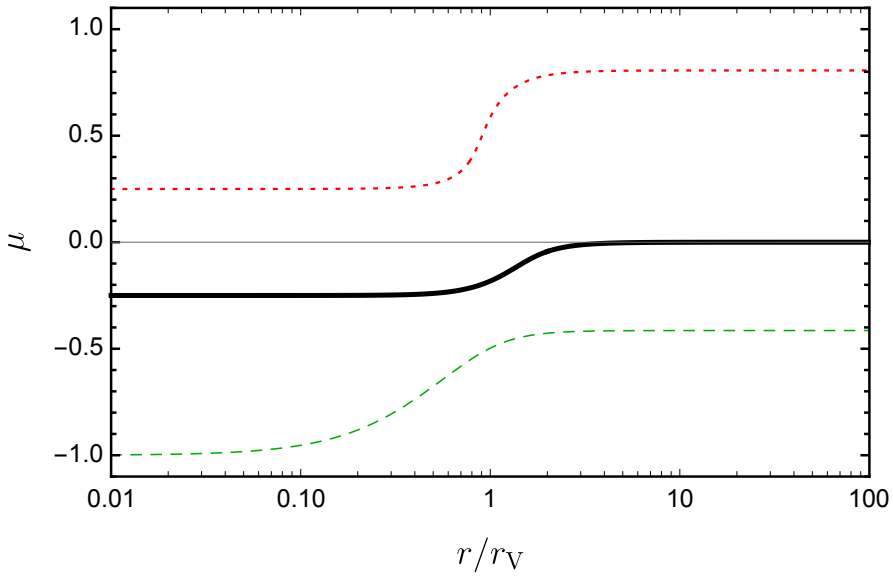

Figure 3.5: The three real solutions of μ as a function of r/r_V for the representative parameter choice $\bar{\alpha} = 1$, $\beta = 1$ and $\gamma = 16$. The black line corresponds to the Vainshtein-Yukawa solution, which realises the linear regime at large radii. This figure is taken from [298].

gravitational potentials valid inside the Vainshtein radius, yields

$$\phi_\mathrm{g} = -\frac{r_\mathrm{S}}{r} + \frac{\bar{\alpha}^2 m_\mathrm{FP}^2}{3(1+\bar{\alpha}^2)\sqrt{\gamma}} r^2 \tag{3.39}$$

$$\phi_\mathrm{f} = \frac{m_\mathrm{FP}^2 (1+\beta-3\sqrt{\gamma}+\gamma)}{3(1+\bar{\alpha}^2)\gamma(1-\sqrt{\gamma})} r^2 \,, \tag{3.40}$$

$$\psi_\mathrm{g} = \frac{r_\mathrm{S}}{r} - \frac{\bar{\alpha}^2 m_\mathrm{FP}^2 (4\sqrt{\gamma}-3\beta)}{3(1+\bar{\alpha}^2)\gamma} \,, \tag{3.41}$$

$$\psi_\mathrm{f} = -\frac{m_\mathrm{FP}^2 (4\gamma+(1+\beta)(1-3\sqrt{\gamma}))}{3(1+\bar{\alpha}^2)\gamma(1-\sqrt{\gamma})} r^2 \,. \tag{3.42}$$

In the limit $r \to 0$, the f-fields vanish identically, $\phi_\mathrm{f}, \psi_\mathrm{f} \to 0$. On the other hand, the g-fields are given by

$$\lim_{r\to 0} \phi_\mathrm{g} = -\lim_{r\to 0} \psi_\mathrm{g} = -\frac{r_\mathrm{S}}{r} \,, \tag{3.43}$$

in the limit. That means, inside the Vainshtein radius, the gravitational potentials are as in GR and solely composed out of the $1/r$-term. This explicitly demonstrates that the Vainshtein mechanism restores GR in spherically symmetric and static systems for $r \ll r_\mathrm{V}$.

For the Vainshtein mechanism to work, the Vainshtein-Yukawa solution must exist for every value of r without branch cuts. This is the case only if the bimetric parameters satisfy the following set of conditions [260, 331, 332]

$$\gamma > 1 \,, \tag{3.44a}$$

$$\beta < \sqrt{\gamma} \,, \tag{3.44b}$$

$$\beta > d_1/d_2 \qquad \text{if} \quad d_2 < 0 \,, \tag{3.44c}$$

with

$$d_1 = -1 + 6(1+\bar{\alpha}^2)\sqrt{\gamma}(1+\gamma) - (13+12\bar{\alpha}^2)\gamma \,,$$
$$d_2 = 1 + 3\bar{\alpha}^2 - 6(1+\bar{\alpha}^2)\sqrt{\gamma} + 3(1+\bar{\alpha}^2)\gamma \,.$$

The denominator in the definition (3.37) of the parameters β and γ also enters the expression for the Fierz–Pauli mass (2.83). Hence, the denominator is required to be positive to yield a positive value of the Fierz–Pauli mass. The first requirement (3.44a) then implies $\beta_3 > 0$. Next, defining the short-hand notation $\tilde{\beta} = c^2\beta_2/\bar{\beta}$, we can write the bound (3.44b) as

$$\tilde{\beta} < \sqrt{\gamma} - \gamma = \sqrt{\gamma}(1 - \sqrt{\gamma}) < 0 \tag{3.45}$$

due to Eq. (3.44a). This implies $\beta_2 < 0$. Summarising, a well-defined Yukawa–Vainshtein solution exists only for bimetric models that have $\beta_2 < 0$ and $\beta_3 > 0$.

These conditions will be useful when comparing bimetric theory to local tests of gravity in Section 6.2.

3.2.3 Comments on Vainshtein screening

The linear solutions are appropriate to describe scales $r \gg r_\mathrm{V}$. Below the Vainshtein scale, $r \ll r_\mathrm{V}$, the Stückelberg field is not small, $\mu \sim \mathcal{O}(1)$, rendering the linear approximation invalid. The nonlinearities are such that deviations from GR are suppressed. The resulting gravitational potential $\Phi = \phi_\mathrm{g}/r_\mathrm{S}$, valid far inside and outside the Vainshtein sphere can be written as

$$\Phi(r) = \begin{cases} \frac{1}{M_\mathrm{P}^2}\left(\frac{1}{r} + \frac{4\bar{\alpha}^2}{3}\frac{e^{-m_\mathrm{FP}\,r}}{r}\right) & , \quad r \gg r_\mathrm{V} \\ \frac{1}{M_\mathrm{g}^2}\frac{1}{r} & , \quad r \ll r_\mathrm{V} \end{cases} , \tag{3.46}$$

where we neglected the contribution from a non-vanishing cosmological constant. Both regimes are characterised by different effective Planck masses, which are related as $M_\mathrm{P}^2 = (1 + \bar{\alpha}^2)M_\mathrm{g}^2$. In the GR limit, $\bar{\alpha} \ll 1$, both Planck masses coincide. In this case, deviations form GR are suppressed on all scales.

This discussion demonstrates that the mechanism conjectured by Vainshtein [119] is indeed realised in bimetric theory. The screening works if the bimetric parameters satisfy the conditions (3.44). However, we point out that a working Vainshtein mechanism is not necessary for the observational viability of bimetric theory. The reason is that the free parameter $\bar{\alpha}$ can be adjusted to sufficiently suppress deviations from GR on all scales. In the limit $\bar{\alpha} \ll 1$, the Yukawa modification to the gravitational potential vanishes. On the other hand, the Vainshtein mechanism enlarges the parameter space of bimetric theory that is compatible with observations. This point will be discussed in more detail in Section 6.2.

Part II

Own results

Chapter 4

Physical parametrisation

In the previous chapter we discussed some of the phenomenological features of BT Among its virtues are phantom dark energy, which can cause the universe to exponentially expand at late times without vacuum energy, and the Vainshtein mechanism, which restores GR in the vicinity of massive objects. These qualitative considerations demonstrate that BT has the potential to overcome some of the shortcomings of the cosmological standard model. With this as a basis we need to take the next step and quantitatively confront BT with observations. We are particularly interested in those parameter combinations that are favoured by observational data. Importantly, we need to decide whether there are certain theoretically allowed parameter combinations that are compatible with all observational constraints.

Of course, the observational status of BT has sourced many investigations, which are summarised in, e.g. [335]. However, the inferred constraints on BT are plagued by some shortcomings as we elucidate now. In the context of cosmology, the theory has been confronted with observational data in [216, 263, 265, 274, 296, 297, 303, 309, 336, 337]. These studies consistently find that BT is indeed compatible with background cosmology for a large class of parameter combinations. However, some papers also included the infinite branch solution, which was later found to be plagued by the Higuchi ghost. In addition, explicit observational constraints were computed in terms of the interaction parameters β_n, which were a priori assumed to be of the order $\beta_n \sim H_0^2$.

In contrast, observational constraints from spherically symmetric systems [330, 332, 338, 339] and gravitational waves [324] were obtained in terms of the following parameters: the mass of the spin-2 field $m_{\rm FP}$ (or its Compton wavelength $m_{\rm FP}^{-1}$) and either the Planck mass ratio α or the conformal factor c. At the same time, either c or α was set to unity, respectively. In fact, these are the parameters that define the spherical gravitational potentials in Eqs. (3.35) and (3.39). We will come back to the explicit observational results in Chapter 6.

The different underlying assumptions and parametrisations, which enter the aforementioned investigations, prevent to consistently combine the various observational constraints. In addition, the parameters β_n get shifted by a rescaling transformation, which leaves the bimetric action (3.1) invariant [223, 301]. This point will be discussed in detail below. Hence, also the associated constraints depend on the rescaling. In summary, these earlier studies do not allow to assess whether BT is consistent with the various observational data simultaneously.

In this section, we present a unified framework to overcome the aforementioned drawbacks, which was developed in [340]. We propose a new parametrisation to bimetric solutions in terms of quantities, which are invariant under rescalings and have a direct physical meaning. Our commensurately baptised *physical parametrisation* is formulated in terms of the coupling $\bar{\alpha}$ of the massive spin-2 field to matter, its mass $m_{\rm FP}$, and the effective cosmological constant Λ. Our new parametrisation forms the basis for the remainder of this thesis.

In the following, we will first provide further details on the aforementioned rescaling transformation and define the physical parameters. As we will see, their unambiguous definition relies on the identification of the unique physical vacuum solution. We will proceed by explicitly working out the physical parametrisation for all bimetric models that fit into our framework; these

are models with up to three free interaction parameters β_n. At the same time, we will identify those regions of the physical parameter space that can consistently be described in terms of each corresponding model.

This chapter is based on our publication [340].

4.1 Rescaling invariance

A priori, the action of BT (2.86) is parametrised in terms of the seven independent parameters $\{M_\mathrm{g}, \alpha, \beta_n\}$. However, the action is invariant under the simultaneous transformation [223, 301]

$$f_{\mu\nu} \longrightarrow \tilde{f}_{\mu\nu} = \lambda^{-2} f_{\mu\nu}\,, \quad \alpha \longrightarrow \tilde{\alpha} = \lambda\alpha\,, \quad \beta_n \longrightarrow \tilde{\beta}_n = \alpha^n \beta_n\,, \tag{4.1}$$

while keeping the physical metric $g_{\mu\nu}$ fixed. This implies that one parameter is redundant and can be removed by fixing the redundancy. Going further, on the level of proportional background solutions $g_{\mu\nu} = c^2 f_{\mu\nu}$, the transformation of the metric $f_{\mu\nu}$ translates into a transformation of the conformal factor as

$$c \longrightarrow \tilde{c} = \lambda^{-1} c\,. \tag{4.2}$$

Therefore, out of the eight parameters $\{M_\mathrm{g}, \alpha, c, \beta_n\}$ of proportional background solutions, one parameter is redundant.

We focus on singly-coupled BT, where the physical metric $g_{\mu\nu}$ couples to matter. For this reason, we keep $g_{\mu\nu}$ fixed in Eq. (4.1) and hence also M_g. This implies that M_g is not a redundant parameter and hence cannot be removed by choosing an appropriate λ. Instead, M_g is fixed by Newton's constant G_N as $M_\mathrm{g}^2 = (8\pi G_\mathrm{N})^{-1}$. For this reason, we remove the parameter M_g from the list of free parameters. This leaves us with seven free parameters $\{\alpha, c, \beta_n\}$ on the level of proportional solutions, out of which one parameter is redundant.

In the literature, the rescaling invariance (4.1) and (4.2) has often been used to fix one parameter by choosing an appropriate λ to address the redundancy. The most common choices are either $\lambda = \alpha^{-1}$ leading to $\tilde{\alpha} = 1$ or $\lambda = c$ leading to $\tilde{c} = 1$. The transformed parameters, which we indicate here with a tilde, are usually henceforth used, and the redundancy is fixed. Let us denote the aforementioned way to remove the redundancy *rescaled parametrisation*. Choosing λ is ambiguous and so is the rescaled parametrisation.

The aforementioned procedure to remove the redundancy is perfectly consistent. However, naturalness arguments within the rescaled parametrisation might be misleading. To see that, let us identify the parameter regions where BT closely resembles GR. First, we assume that the interaction parameters are all of the same order as $\beta_n \sim \mathcal{O}(m^2)$ with m some mass scale. The GR-limit is arrived at by taking $\alpha \ll 1$ and keeping the β_n fixed [226,227,255]. That means that we need to adjust one parameter to arrive at the GR-limit. Next, we consider the rescaled parametrisation with $\lambda = \alpha^{-1}$. Therefore, the rescaled interaction parameters are given by $\tilde{\beta}_n \sim \alpha^{-n}\mathcal{O}(m^2)$. Hence, the parameters admit a huge hierarchy as $\tilde{\beta}_n \gg \tilde{\beta}_{n+1}$ among themselves within the GR-limit. Starting from the rescaled parametrisation, we need to tune all interaction parameters against each other in order to arrive in the GR-limit. Such tuned hierarchy among the parameters of the theory is usually perceived as unnatural. This apparent problem led to confusion in the past about the observational viability of BT [226].

In addition to the aforementioned limit, also the parametric limit $m_\mathrm{FP}^2 \gg \Lambda$ brings BT arbitrarily close to GR [227]. To be more precise, GR is recovered on energy scales much smaller than m_FP (or equivalently on length scales much larger than the Compton wavelength m_FP^{-1}). To achieve a spin-2 mass that is much larger than the cosmological constant requires a large amount of tuning among the rescaled interaction parameters $\tilde{\beta}_n$. As before, this tuning appears unnatural, but is another artefact of the rescaled parametrisation. To see this in greater detail, let us discuss how to achieve a large spin-2 mass in terms of the original parametrisation. The spin-2 mass and the cosmological constant are defined in terms of the conformal factor c, which is a root of the quartic polynomial in (2.76). The polynomial has up to four real-valued roots, which we can classify according to their scaling with α in the limit $\alpha \ll 1$ when keeping the interaction parameters β_n fixed:

- singular root: $c \sim \alpha^{-1}$
- constant root: $c \sim \text{const.}$

On both roots, $\alpha \ll 1$ automatically leads to a large spin-2 mass (unless one of the interaction parameters β_n are tuned accordingly), cf. Eq. (2.83). On a singular root also the cosmological constant is large, cf. Eq. (2.75a). That means that on a singular root the GR-limit is reached only if the interaction parameters β_n are tuned. Next, also on a constant root the limit $\alpha \ll 1$ leads to a large spin-2 mass, but the cosmological constant remains small. Therefore, $\alpha \ll 1$ automatically leads to $m_{\text{FP}}^2 \ll \Lambda$ on a constant root without further tuning of the interaction parameter. Of course, the hierarchy can be spoiled by appropriate tuning of the interaction parameters. Below, we explicitly demonstrate the above discussion for a representative example.

In fact, we will see that the parameters αc, m_{FP} and Λ are completely independent if one accepts tuning among the interaction parameters. To be precise, $m_{\text{FP}}^2 \ll \Lambda$ can be achieved even for finite α and, vice versa, $\alpha \ll 1$ can be achieved although $m_{\text{FP}}^2 \sim \Lambda$.

Example: Tuning of the interaction parameters

In the previous discussion we distinguished between singular and constant roots of the polynomial (2.76) and stated that the limit $\alpha \ll 1$ implies $m_{\text{FP}}^2 \gg \Lambda$ in the latter case, but not the former. Here, we demonstrate this explicitly for the $\beta_1\beta_2$-model as representative example, which is defined by setting $\beta_0 = \beta_3 = \beta_4 = 0$. The quartic polynomial (2.76) simplifies to

$$3\alpha^2 c^3 \beta_2 + 3\alpha^2 c^2 \beta_1 - 3c\beta_2 - \beta_1 = 0\,. \tag{4.3}$$

This is a polynomial in c of degree three and as such has up to three real-valued roots. Since the full expressions for the roots are lengthy, we here present the expressions only in the limit $\alpha \ll 1$. In that limit, the constant root is given by

$$c_{\text{c}} = -\frac{\beta_1}{3\beta_2} + \mathcal{O}(\alpha^2)\,. \tag{4.4}$$

The root is positive valued for $\beta_2 < 0$. The Fierz-Pauli mass (2.83) and the cosmological constant (2.75a) on the constant root are therefore given by

$$m_{\text{FP}}^2 = -\frac{\beta_2}{\alpha^2} + \mathcal{O}(\alpha^0)\,, \quad \Lambda = -\frac{2}{3}\frac{\beta_1^2}{\beta_2} + \mathcal{O}(\alpha^2)\,. \tag{4.5}$$

Both quantities are positive for $\beta_2 < 0$. This explicitly demonstrates that on a constant root, $\alpha \ll 1$ yields $m_{\text{FP}}^2 \gg \Lambda$ without further tuning. In particular, the hierarchy is controlled by α as $m_{\text{FP}}^2/\Lambda \sim \alpha^{-2}$.

The other two roots of (4.3) are the singular roots given by

$$c_{\text{s}\pm} = \pm\frac{1}{\alpha} - \frac{\beta_1}{3\beta_2} + \mathcal{O}(\alpha^2) \tag{4.6}$$

in the limit $\alpha \ll 1$. The Fierz-Pauli mass (2.83) and cosmological constant (2.75a) are given by

$$m_{\text{FP}}^2 = \frac{4\beta_2}{\alpha^2} + \mathcal{O}(\alpha^0)\,, \quad \Lambda = \frac{3\beta_2}{\alpha^2} + \mathcal{O}(\alpha^0) \tag{4.7}$$

on the singular root $c_{\text{s}\pm}$. Both quantities are positive valued only for $\beta_2 > 0$. Note that $\alpha \ll 1$ does not imply that the Fierz-Pauli mass is much larger than the cosmological constant. Instead, they are of the same order of magnitude with $m_{\text{FP}}^2/\Lambda \sim 4/3$, but still satisfy the Higuchi bound (2.84).

4.2 Definition of physical parameters

The discussion of the previous section unveils that the parameters $\{\alpha, c, \beta_n\}$ are no observables because they get shifted by the rescaling transformation in Eqs. (4.1) and (4.2), which leave the bimetric action (3.1) invariant. We further argued that the rescaled parametrisation, commonly used in the literature, is ambiguous and potentially misleading. In this section, we propose a new parametrisation that overcomes these aforementioned drawbacks.

We propose to parametrise the solutions of BT in terms of variables that are manifestly invariant under the rescaling (4.1). We further seek parameters, which enjoy a direct physical interpretation and make the relevant parametric limits manifest. The following set of parameters satisfies these criteria:

- coupling constant $\bar{\alpha} = \alpha c$,
- Fierz–Pauli mass m_{FP},
- cosmological constant Λ.

We refer to these variables as *physical parameters*.

The physical meaning of these parameters is straightforward. As we have seen in Section 3.2, the physical parameters define the gravitational potentials in spherically symmetric and static systems, both in the linear and nonlinear regime (to lowest order in r). The parameter $\bar{\alpha}$ paramtrises the coupling of the massive spin-2 field to matter and as such controls the Yukawa term in the gravitational potential (3.46). In addition, it parametrises the mixing of the massive and the massless mode within the fluctuation of the physical metric as in Eq. (2.85).

The physical parameters are defined on vacuum solutions c. However, since the c determining polynomial (2.76) is of degree four and as such has four roots, the definition of the physical parameters is a priori ambiguous. The ambiguity will be removed by identifying one of the vacuum solutions as the unique physical vacuum.

The identification of the unique physical vacuum is analytically possible only for models with up to three free interaction parameters. Therefore, our framework is suitable for all bimetric models with three interaction parameters β_n, or less. Recently, our framework was generalised in [260,299] to more general models by utilising the rescaling invariant parameters β and γ defined in Eq. (3.37) in addition to the physical parameters defined here.

After identifying the physical vacuum, we will provide a recipe, which yields the unambiguous relation between the parameters $\{\alpha, c, \beta_n\}$ and the physical parameters. To ease the notation, we also introduce the following parameters:

- rescaling invariant interaction parameters: $\bar{\beta}_n = \alpha^{-n}\beta_n$
- rescaling invariant scale factor ratio: $\bar{y} = \alpha y$.

These parameters will be used later to present some equations in a more compact way.

4.2.1 Unique vacuum solution

The physical parameters do not parameters the theory (the bimetric action depends on the parameters $\{\alpha, \beta_n\}$), but solutions to the bimetric field equations. In particular, the physical parameters are defined in terms of c. The conformal factor is determined by the quartic polynomial (2.76), which has up to four real-valued roots. Each root describes a vacuum solution of BT. In other words, there are up to four vacuum solutions $c_i = c_i(\alpha, \beta_n)$ for $i = 1, \ldots, 4$. Since the physical parameters are defined on top of vacuum solutions, there are up to four different sets of physical parameters $\{\bar{\alpha}, m_{\mathrm{FP}}, \Lambda\}$ for a given set of theory parameters $\{\alpha, \beta_n\}$. Therefore, defining physical parameters is ambiguous. To yield an unique set of physical parameters (for a given set of theory parameters $\{\alpha, \beta_n\}$), we need to identify the unique physical vacuum solution c_i. In this section, we define such unique physical vacuum solution.

The definition of the unique vacuum solution relies on consistency criteria. These allow to eliminate some of the roots c_i as consistent vacuum solution. In the following, we will discuss those criteria.

First, let us recall that proportional background solutions are invariant under[1] Eq. (2.77):

$$c \longrightarrow -c\,, \quad \beta_n \longrightarrow (-1)^n \beta_n\,. \tag{4.8}$$

Therefore, we can restrict ourselves to vacuum solutions with $c > 0$ for arbitrary interaction parameters β_n without loss of generality.

Next, the Fierz–Pauli mass must be positive $m_{\rm FP} > 0$ to avoid tachyonic instabilities. We further restrict ourselves to de Sitter vacua, $\Lambda > 0$. Then, the Fierz–Pauli mass and cosmological constant must satisfy the aforementioned Higuchi bound (2.84) [224, 225].

These requirements single out consistent vacuum solutions, but not an unique vacuum solution. For this we need to take into account the cosmic expansion history. As we explained in Section 3.1, out of the up to four solutions to Eq. (3.18) only the finite branch is physical. On the finite branch, the scale factor ratio y evolves from zero in the asymptotic past to a constant value in the asymptotic future. The constant corresponds to the lowest-lying strictly positive root of the vacuum polynomial (2.76). The consistent vacuum solution must correspond to the asymptotic future of the consistent cosmic expansion history. Hence, the lowest-lying, strictly positive root of Eq. (2.76) describes the consistent vacuum solution, which is unique. Recall, that the finite branch is well-defined iff $\beta_1 > 0$. Consequently, the consistent vacuum solution can only exist iff β_1 is positive.

The aforementioned requirements amount to define the physical vacuum solution of BT in the following way:

Definition (Physical vacuum solution): *The physical vacuum solution c of BT*

1. *satisfies*
$$c > 0\,, \quad m_{\rm FP} > 0\,, \quad \Lambda > 0\,, \quad 3m_{\rm FP}^2 > 2\Lambda\,, \tag{4.9}$$
2. *corresponds to the lowest-lying, strictly positive root of Eq. (2.76),*
3. *corresponds to the asymptotic future of the cosmic expansion history along the finite branch and thus exists iff $\beta_1 > 0$.*

By construction, the physical vacuum is unique. It therefore allows to define an unique set of physical parameters.

4.2.2 Recipe

In the previous section we discussed that an unique physical vacuum solution can be defined for a given set of theory parameters $\{\alpha, \beta_n\}$. In this section, we provide a recipe to identify the unique physical vacuum out of the four vacuum solutions and to express the interaction parameters in terms of physical parameters. The recipe goes as follows:

1. Replace two of the interaction parameters β_n in terms of the Fierz–Pauli mass and the cosmological constant using Eqs. (2.75) and (2.83).

2. Use step 1 to replace the two interaction parameters β_n in terms of the physical parameters $m_{\rm FP}$ and Λ in the quartic polynomial (2.76). Then solve the quartic polynomial (2.76) for the quantity $\bar{\alpha} = \alpha c$ in terms of the physical parameters and the remaining interaction parameter $\bar{\beta}_n$.

3. From the solutions of step 2 select those vacua $\bar{\alpha}$ that satisfy the criteria in Eq. (4.9). Pick the lowest-lying, strictly positive root for each set of parameters $\{m_{\rm FP}, \Lambda, \bar{\beta}_n\}$.

[1] Going further, also FLRW solutions admit the same symmetry. Here, the simultaneous transformation, under which FLRW solutions are invariant, is given by $y \to -y$ and $\beta_n \to (-1)^n \beta_n$.

4. For each lowest-lying, strictly positive root of the previous step solve the relation $\bar{\alpha} = \bar{\alpha}(m_{\rm FP}, \Lambda, \bar{\beta}_n)$ for the remaining interaction parameter $\bar{\beta}_n$. Eliminate that interaction parameter $\bar{\beta}_n$ in terms of the physical parameters $\bar{\alpha}$, $m_{\rm FP}$, and Λ in the other expressions.

5. Solve the requirement $\beta_1 > 0$ in terms of the physical parameters.

6. To ensure that the finite branch is non-singular, solve Eq. (3.18) for $\rho(y)$. Identify the parameter region in which $\lim_{\bar{y}\to\bar{\alpha}}(\rho(y)) \to 0$ is guaranteed.

For the one- and two-parameter models the recipe is correspondingly shorter.

This procedure replaces the interaction parameters β_n in terms of physical parameters. In addition, it yields theoretical constraints on the physical parameters, which ensure a consistent physical vacuum and cosmic expansion history.

For bimetric models with more than three free interaction parameters β_n, it is not possible to analytically solve the quartic polynomial (2.76) for $\bar{\alpha}$. Therefore, our framework is applicable to all bimetric models with three free interaction parameters, or less.

4.3 Parameter relations

In the previous sections we exposed our strategy on ow to identify the unique physical vacuum solution and how to define the physical parameters on top of that vacuum. In this section, we explicitly work out the physical parameterisation for all relevant bimetric models with up to three free interaction parameters. Since models with $\beta_1 = 0$ do not give rise to a viable finite branch solution, we focus on models with β_1 being among the free parameters. Therefore, our subsequent analysis builds up a dictionary between the $\{\alpha, c, \beta_n\}$ and the physical parameters. In addition, we identify regions of the physical parameter space that are consistent in the aforementioned sense.

4.3.1 One–parameter model

Let us start with the simplest case. There is only a single one-parameter model that can possibly give rise to a consistent cosmic expansion history: the β_1-model. It is defined by $\beta_0 = \beta_2 = \beta_3 = \beta_4 = 0$. The quartic polynomial (2.76) reduces to

$$\bar{\alpha}^2 = \frac{1}{3}\,, \tag{4.10}$$

out of which $\bar{\alpha} = +1/\sqrt{3}$ is the unique vacuum solution. This immediately implies that the β_1–model does not admit a GR-limit or MG-limit because $\bar{\alpha}$ is fixed by the equations of motion. The Eqs. (2.75) and (2.83) further imply that the Fierz–Pauli mass and the cosmological constant are related as

$$m_{\rm FP}^2 = \frac{4}{3}\Lambda\,, \tag{4.11}$$

which is not in conflict with the Higuchi bound.

There is only one independent physical parameter in the β_1–model. The model thus describes one point in the physical parameter space spanned by $\bar{\alpha}$ and $m_{\rm FP}^2/\Lambda$, as indicated by the grey dot in Fig. 4.1.

For the dictionary, the interaction parameter is given by

$$\alpha^{-1}\beta_1 = \frac{\sqrt{3}}{4}m_{\rm FP}^2 = \frac{1}{\sqrt{3}}\Lambda \tag{4.12}$$

in terms of the physical parameters. Therefore, the requirement $\beta_1 > 0$ is always satisfied for $m_{\rm FP} > 0$ or equivalently $\Lambda > 0$.

The other one-parameter models are characterised by $\beta_1 = 0$ and therefore do not give rise to a viable finite branch.

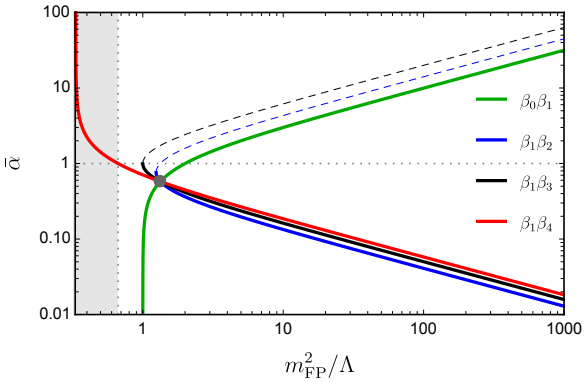

Figure 4.1: The relation between $\bar{\alpha}$ and $m^2_{\rm FP}/\Lambda$ for the two-parameter models on the consistent vacuum point. The grey dot corresponds to the β_1–model. The grey-shaded region violates the Higuchi bound. Figure taken from [340].

Model	GR limit	MG limit
β_1	–	–
$\beta_0\beta_1$	$m^2_{\rm FP} \simeq \Lambda$	$m^2_{\rm FP} \gg \Lambda$
$\beta_1\beta_2$	$m^2_{\rm FP} \gg \Lambda$	–
$\beta_1\beta_3$	$m^2_{\rm FP} \gg \Lambda$	–
$\beta_1\beta_4$	$m^2_{\rm FP} \gg \Lambda$	$(m^2_{\rm FP} = \Lambda/3)$

Table 4.1: Summary of the GR-limit and the MG-limit for one- and two-parameter models. The "–" indicates that the limit is not consistent.

4.3.2 Two–parameter models

After this warm-up, we move to those two-parameter models with β_1 being one of the free interaction parameters. In contrast to the one-parameter model, now two out of the three physical parameters are independent. For all models, we can express the coupling $\bar{\alpha}$ as function of $m^2_{\rm FP}/\Lambda$. This relation is visualised for all one- and two-parameter models in Fig. 4.1. The two-parameter models describe a line in the $\bar{\alpha}$–$m^2_{\rm FP}/\Lambda$–plane. The point, at which all the lines corresponding to two-parameter models cross, represents the β_1–model, as indicated by the grey dot.

In the following, we discuss all two-parameter models with β_1 as one of the free parameters individually.

$\beta_0\beta_1$–model

The $\beta_0\beta_1$–model is defined by setting $\beta_2 = \beta_3 = \beta_4 = 0$. Solving the background equations (2.75), (2.76), and (2.83) following our recipe leads to

$$\bar{\alpha}_\pm = \pm\sqrt{\frac{m^2_{\rm FP}}{\Lambda} - 1}\,, \tag{4.13a}$$

$$\beta_0 = -3m^2_{\rm FP} + 4\Lambda\,, \tag{4.13b}$$

$$\alpha^{-1}\beta_1 = \pm\sqrt{(m^2_{\rm FP} - \Lambda)\Lambda}\,. \tag{4.13c}$$

The vacuum point and the interaction parameter are real-valued only in the parameter range

$$m^2_{\rm FP} > \Lambda\,, \tag{4.14}$$

which is more restrictive than the Higuchi bound. Further, only the vacuum point $\bar{\alpha}_+$ is positive and we have to dismiss $\bar{\alpha}_-$. Therefore, $\bar{\alpha}_+$ is the unique de Sitter vacuum of the $\beta_0\beta_1$–model. On that root and for (4.14) we have $\beta_1 > 0$ as required.

At the point $4m^2_{\rm FP} = 3\Lambda$ we have $\beta_0 = 0$ and the model reduces to the β_1–model as expected. For $4m^2_{\rm FP} < 3\Lambda$ we have $\beta_0 > 0$ (i.e. the vacuum energy density is positive-valued) and for $4m^2_{\rm FP} > 3\Lambda$ the vacuum energy density is negative-valued with $\beta_0 < 0$.

From Eq. (4.13a) we see that the GR-limit $\bar{\alpha} \ll 1$ corresponds to the region where $m^2_{\rm FP} \simeq \Lambda$. On the other hand, the MG-limit $\bar{\alpha} \gg 1$ is arrived at by $m^2_{\rm FP} \gg \Lambda$. This is summarised in Table 4.1. The relation between the physical parameters defined on the consistent vacuum is depicted as the green line in Fig. 4.1

$\beta_1\beta_2$–model

Next, we set $\beta_0 = \beta_3 = \beta_4 = 0$ to arrive at the $\beta_1\beta_2$–model. Following our recipe by solving (2.75), (2.76), and (2.83) leads to the parameter relations:

$$\bar{\alpha}_\pm = \sqrt{\frac{3m_{\rm FP}^2 - 2\Lambda \pm \sqrt{9m_{\rm FP}^4 - 12m_{\rm FP}^2\Lambda + \Lambda^2}}{3\Lambda}}\,, \tag{4.15a}$$

$$\alpha^{-1}\beta_{1\pm} = \frac{\bar{\alpha}_\pm}{2}\left(3m_{\rm FP}^2 - 3\Lambda \mp \sqrt{9m_{\rm FP}^4 - 12m_{\rm FP}^2\Lambda + \Lambda^2}\right)\,, \tag{4.15b}$$

$$\alpha^{-2}\beta_{2\pm} = -\frac{1}{6}\left(3m_{\rm FP}^2 - 5\Lambda \mp \sqrt{9m_{\rm FP}^4 - 12m_{\rm FP}^2\Lambda + \Lambda^2}\right)\,. \tag{4.15c}$$

There are two more roots, which are given by $-\alpha_\pm$ and hence do not correspond to physical vacua. The vacuum points $\bar{\alpha}_\pm$ and the interaction parameters are real-valued only in the parameter region

$$m_{\rm FP}^2 > \frac{2+\sqrt{3}}{3}\Lambda\,, \tag{4.16}$$

which is more restrictive than the Higuchi bound. In that same region, both vacuum points are positive valued, $\bar{\alpha}_\pm > 0$, and they satisfy $\bar{\alpha}_- < \bar{\alpha}_+$. That means that $\bar{\alpha}_-$ corresponds to the lowest-lying strictly positive root of Eq. (2.76) and hence to the physical vacuum. In the parameter region (4.16) we automatically have $\beta_{1-} > 0$.

The relation between the physical parameters on the physical vacuum is shown as blue line in Fig. 4.1. We also present the relation between the physical parameters on the highest-lying, strictly positive root as a dashed line. The physical vacuum does not admit a MG-limit, i.e. $\bar{\alpha} \gg 1$ is inconsistent. Contrarily, the GR-limit $\bar{\alpha} \ll 1$ corresponds to the limit $m_{\rm FP}^2 \gg \Lambda$, as summarised in Table 4.1. In the GR-limit, the relation between the physical parameters can be approximated as

$$\bar{\alpha}^2 \simeq \frac{1}{6}\frac{\Lambda}{m_{\rm FP}^2}\,. \tag{4.17}$$

This relation follows from expanding Eq. (4.15a) for $m_{\rm FP}^2 \gg \Lambda$.

$\beta_1\beta_3$–model

We continue with the $\beta_1\beta_3$–model, which is defined by setting $\beta_0 = \beta_2 = \beta_4 = 0$. Following our recipe, Eqs. (2.75), (2.76) and (2.83) lead to

$$\bar{\alpha}_\pm = \sqrt{\frac{2m_{\rm FP}^2 - \Lambda \pm 2m_{\rm FP}\sqrt{m_{\rm FP}^2 - \Lambda}}{\Lambda}}\,, \tag{4.18a}$$

$$\alpha^{-1}\beta_{1\pm} = \frac{\bar{\alpha}_\pm}{4}\sqrt{3m_{\rm FP}^2 - 2\Lambda \mp 3m_{\rm FP}\sqrt{m_{\rm FP}^2 - \Lambda}}\,, \tag{4.18b}$$

$$\alpha^{-3}\beta_{3\pm} = -\bar{\alpha}_\pm\left(4m_{\rm FP}^4 - 7m_{\rm FP}^2\Lambda + 2\Lambda^2 \mp \sqrt{m_{\rm FP}^2 - \Lambda}(4m_{\rm FP}^2 - 5\Lambda)m_{\rm FP}\right)\,. \tag{4.18c}$$

The two other vacuum points are given by $-\bar{\alpha}_\pm$, which do not correspond to physical vacua. The vacuum points are real-valued in the parameter region

$$m_{\rm FP}^2 > \Lambda\,. \tag{4.19}$$

In that same region, also the interaction parameters β_{1-} and $\beta_{2\pm}$ are real-valued, while β_{1+} is real-valued only in the smaller region $\Lambda < m_{\rm FP}^2 < 4\Lambda/3$. In the region (4.19) both vacuum points are positive and satisfy $\bar{\alpha}_- < \bar{\alpha}_+$. This identifies $\bar{\alpha}_-$ as the unique physical vacuum of the $\beta_1\beta_3$–model, on which the interaction parameters are related to the physical parameters as given by β_{1-}

and β_{3-}. Hence, (4.19) describes the consistent parameter space. In that parameter region also $\beta_{1-} > 0$ is guaranteed.

The relation between the physical parameters, as defined by Eq. (4.18a), is visualised in Fig. 4.1. The black solid line corresponds to the relation on the physical vacuum. For completeness, we also show the parameter relation in the highest-lying root as dashed line. As for the previous case, the physical vacuum does not admit a MG-limit. The GR-limit $\bar{\alpha} \ll 1$ is arrived at by taking $m_{\mathrm{FP}}^2 \gg \Lambda$. In that limit, Eq. (4.18a) simplifies to

$$\bar{\alpha}^2 \simeq \frac{1}{4}\frac{\Lambda}{m_{\mathrm{FP}}^2}\,. \tag{4.20}$$

The limit is summarised in Table 4.1.

$\beta_1\beta_4$–model

Finally, we set $\beta_0 = \beta_2 = \beta_3 = 0$ to arrive at the $\beta_1\beta_4$–model. Solving Eqs. (2.75), (2.76) and (2.83) as described in Section 4.2.2 leads to the following parameter relations:

$$\bar{\alpha}_\pm = \pm\sqrt{\frac{\Lambda}{3m_{\mathrm{FP}}^2 - \Lambda}}\,, \tag{4.21a}$$

$$\alpha^{-1}\beta_{1\pm} = \frac{1}{3}\sqrt{(3m_{\mathrm{FP}}^2 - \Lambda)\Lambda}\,, \tag{4.21b}$$

$$\alpha^{-4}\beta_{4\pm} = -\frac{9m_{\mathrm{FP}}^4 - 15m_{\mathrm{FP}}^2\Lambda + 4\Lambda^2}{3\Lambda}\,. \tag{4.21c}$$

The vacuum points and interaction parameters are real valued in the parameter region $3m_{\mathrm{FP}}^2 > \Lambda$, which is less-restrictive than the Higuchi bound. The physical parameter region of the $\beta_1\beta_4$–model is therefore given by

$$m_{\mathrm{FP}}^2 > \frac{2}{3}\Lambda\,. \tag{4.22}$$

In this parameter regime we have $\alpha_- < 0$ and $\alpha_+ > 0$. Therefore, α_+ is the unique physical vacuum of the $\beta_1\beta_4$–model. On this root and within the parameter region (4.22) we also have $\beta_1 > 0$ as required.

Form Eq. (4.21a) it follows that the GR-limit $\bar{\alpha} \ll 1$ corresponds to the parameter region $m_{\mathrm{FP}}^2 \gg \Lambda$. In that limit, Eq. (4.21a) can be approximated by

$$\bar{\alpha}^2 \simeq \frac{1}{3}\frac{\Lambda}{m_{\mathrm{FP}}^2}\,. \tag{4.23}$$

The MG-limit $\bar{\alpha} \gg 1$ can in principle be arrived at by taking $m_{\mathrm{FP}}^2 = \Lambda/3$. This limit, however, violates the Higuchi bound and thus is inconsistent. The limits are summarised in Table 4.1. In addition, we visualise the relation between the physical parameters as red line in Fig. 4.1.

4.3.3 Three–parameter models

Let us move to models with three free interaction parameters β_n, one of which being β_1. Therefore, all physical parameters $\bar{\alpha}$, m_{FP}, and Λ are independent. Compared to the previous model, the parameter space, which can be consistently described by these models, enlarges to regions in the $\bar{\alpha}$–$m_{\mathrm{FP}}^2/\Lambda$–plane. We first discuss those models including β_0, i.e. with vacuum in the physical sector, and continue with models with $\beta_0 = 0$.

$\beta_0\beta_1\beta_2$–model

The $\beta_0\beta_1\beta_2$–model is defined by setting $\beta_3 = \beta_4 = 0$. Following our recipe, we trade β_0 and β_1 for the physical parameters. Then Eq. (2.76) has the following roots

$$\bar{\alpha}_\pm = \pm\sqrt{\frac{m_{\mathrm{FP}}^2 - \Lambda + \bar{\beta}_2}{\Lambda - \bar{\beta}_2}}\,. \tag{4.24}$$

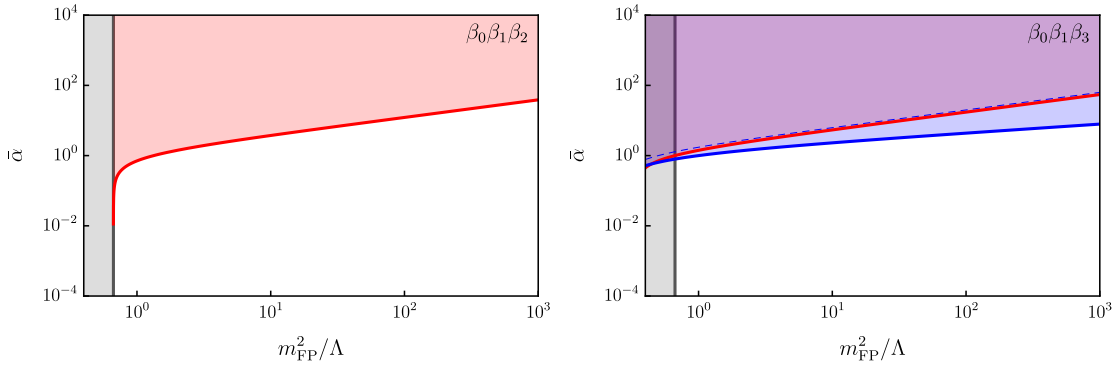

Figure 4.2: Exclusion plots taken from [340] obtained from theoretical consistency bounds for the $\beta_0\beta_1\beta_2$– (left) and the $\beta_0\beta_1\beta_3$–model (right). The red-shaded region yields $\beta_1 < 0$ and in the blue-shaded region the vacuum point is not well-defined. The grey-shaded region violates the Higuchi bound.

The roots are real-valued for $\Lambda - m^2_{\rm FP} < \bar{\beta}_2 < \Lambda$. In that parameter region we have $\bar{\alpha}_+ > 0$ and $\bar{\alpha}_- < 0$, such that $\bar{\alpha}_+$ corresponds to the unique physical vacuum solution in the $\beta_0\beta_1\beta_2$–model. Inverting Eq. (4.24) for $\bar{\beta}_2$ using on the root $\bar{\alpha}_+$ leads to the following relation between interaction and physical parameters:

$$\beta_0 = \frac{1}{1+\bar{\alpha}^2}\left(-6\bar{\alpha}^2 m^2_{\rm FP} + (1+4\bar{\alpha}^2+3\bar{\alpha}^4)\Lambda\right) , \tag{4.25a}$$

$$\alpha^{-1}\beta_1 = \bar{\alpha}\left(\frac{3m^2_{\rm FP}}{1+\bar{\alpha}^2} - 2\Lambda\right) , \tag{4.25b}$$

$$\alpha^{-2}\beta_2 = -\frac{m^2_{\rm FP}}{1+\bar{\alpha}^2} + \Lambda\,. \tag{4.25c}$$

From the parameter relations we can determine the viable physical parameter space. The condition on $\bar{\beta}_2$ is trivially satisfied for $\bar{\alpha} > 0$ and $m_{\rm FP} > 0$. The requirement $\beta_1 > 0$ translates into

$$3m^2_{\rm FP} > 2(1+\bar{\alpha}^2)\Lambda\,. \tag{4.26}$$

The resulting exclusion plot is given in the left panel of Fig. 4.2. The red-shaded region violates the bound in (4.26). The grey-shaded region violates the Higuchi bound. The remaining unshaded region is not excluded by our theoretical consistency requirements and might give rise to a viable cosmic expansion history.

$\beta_0\beta_1\beta_3$–model

Setting $\beta_2 = \beta_4 = 0$ leads to the $\beta_0\beta_1\beta_3$–model. Replacing β_1 and β_3 in terms of the physical parameters using Eqs. (2.75) and (2.83), the quartic polynomial (2.76) has the following roots:

$$\bar{\alpha}_\pm = \sqrt{\frac{4m^2_{\rm FP} - 2\Lambda + \beta_0 \pm \sqrt{(4m^2_{\rm FP}+\beta_0)^2 - 16m^2_{\rm FP}\Lambda}}{2\Lambda}}\,. \tag{4.27}$$

There are two more roots given by $-\bar{\alpha}_\pm$, which are always non-positive. The roots $\bar{\alpha}_\pm$ are real-valued if $\beta_0 > 4m_{\rm FP}(\sqrt{\Lambda} - m_{\rm FP})$. In addition, $\bar{\alpha}_+$ is real-valued only for $\beta_0 < \Lambda$. In that parameter region, the roots satisfy $\bar{\alpha}_- < \bar{\alpha}_+$. Therefore, $\bar{\alpha}_-$ corresponds to the physical vacuum

point. Solving Eq. (4.27) for β_0 using $\bar{\alpha}_-$ results in the following parameter relations:

$$\beta_0 = \frac{1}{1+\bar{\alpha}^2}\left(-4\bar{\alpha}^2 m_{\rm FP}^2 + (1+2\bar{\alpha}^2+\bar{\alpha}^4)\Lambda\right), \tag{4.28a}$$

$$\alpha^{-1}\beta_1 = -\frac{\bar{\alpha}}{2}\left(\frac{3m_{\rm FP}^2}{1+\bar{\alpha}^2} - \Lambda\right), \tag{4.28b}$$

$$\alpha^{-3}\beta_3 = -\frac{1}{2\bar{\alpha}}\left(\frac{m_{\rm FP}^2}{1+\bar{\alpha}^2} - \Lambda\right). \tag{4.28c}$$

Let us identify the theoretically consistent region of the physical parameter space as presented in the right panel of Fig. 4.2. The conditions on β_0 can be written in terms of physical parameters as

$$4m_{\rm FP}^2 > (1+\bar{\alpha}^2)\Lambda\,. \tag{4.29}$$

The boundary of this condition is represented by the blue dashed line and less constraining than the following bounds. The requirement $\beta_1 > 0$ translates into

$$3m_{\rm FP}^2 > (1+\bar{\alpha}^2)\Lambda\,, \tag{4.30}$$

which is violated within the red-shaded region. Finally, expanding $\rho(y)$ around $\bar{y} = \bar{\alpha}$ we find that the finite branch is non-singular only for

$$4m_{\rm FP}^2 > (1+\bar{\alpha}^2)^2\Lambda\,. \tag{4.31}$$

This bound corresponds to the most-stringent one in the region that satisfies the Higuchi bound, which in turn is indicated by the grey-shaded region. In the blue-shaded region, the bound (4.31) is violated. Summarising, the $\beta_0\beta_1\beta_3$–model is theoretically viable in the unshaded region of the right panel of Fig. 4.2.

$\beta_0\beta_1\beta_4$–model

The $\beta_0\beta_1\beta_4$–model is defined by setting $\beta_2 = \beta_3 = 0$ and contains vacuum energy in both sectors. Following our recipe, we use Eqs. (2.75) and (2.83) to replace β_1 and β_4 in terms of physical parameters. The roots of the quartic polynomial (2.76) are then given by

$$\bar{\alpha}_\pm = \pm\sqrt{\frac{\Lambda-\beta_0}{3m_{\rm FP}^2 - \Lambda + \beta_0}}\,. \tag{4.32}$$

The roots are real-valued in the parameter regime $\Lambda - 3m_{\rm FP}^2 < \beta_0 < \Lambda$. In that parameter region we have $\bar{\alpha}_- < 0$ and $\bar{\alpha}_+ > 0$, identifying $\bar{\alpha}_+$ as the unique physical vacuum of the $\beta_0\beta_1\beta_4$–model. Solving Eq. (4.32) for β_0 results in the the following parameter relations:

$$\beta_0 = -\frac{3\bar{\alpha}^2 m_{\rm FP}^2}{1+\bar{\alpha}^2} + \Lambda\,, \tag{4.33a}$$

$$\alpha^{-1}\beta_1 = \frac{\bar{\alpha} m_{\rm FP}^2}{1+\bar{\alpha}^2}\,, \tag{4.33b}$$

$$\alpha^{-4}\beta_4 = -\frac{1}{\bar{\alpha}^2}\left(\frac{m_{\rm FP}^2}{1+\bar{\alpha}^2} - \Lambda\right). \tag{4.33c}$$

The restriction on β_0 and the condition $\beta_1 > 0$ are automatically satisfied and the finite branch is non-singular in the entire parameter region that satisfies the Higuchi bound. The viable physical parameter region of the $\beta_0\beta_1\beta_4$–model therefore corresponds to $3m_{\rm FP}^2 > 2\Lambda$ without further restrictions.

$\beta_1\beta_2\beta_3$–model

Next, we move to the opposite model without vacuum energy by setting $\beta_0 = \beta_4 = 0$ resulting in the $\beta_1\beta_2\beta_3$–model. Replacing β_1 and β_3 by physical parameters using Eqs. (2.75) and (2.83), the roots of Eq. (2.76) are given by

$$\bar{\alpha}_\pm = \sqrt{\frac{2m_{\rm FP}^2 - \Lambda - \bar{\beta}_2 \pm \sqrt{(2m_{\rm FP}^2 - \bar{\beta}_2)^2 - 4m_{\rm FP}^2\Lambda}}{2\bar{\beta}_2 + \Lambda}}\,. \tag{4.34}$$

The two other roots are given by $-\bar{\alpha}_\pm$ and always non-positive. These roots are real-valued in the parameter region

$$\bar{\beta}_2 < 2m_{\rm FP}(m_{\rm FP} - \sqrt{\Lambda})\,. \tag{4.35}$$

The root $\bar{\alpha}_+$ is real-valued only in the smaller parameter region that also satisfied $\bar{\beta}_2 > -\Lambda/2$. In the parameter region, where both roots are real-valued, we find that $0 < \bar{\alpha}_- < \bar{\alpha}_+$. Therefore, $\bar{\alpha}_-$ is the unique physical vacuum of the $\beta_1\beta_2\beta_3$–model. Solving Eq. (4.34) for $\bar{\beta}_2$ on the root $\bar{\alpha}_-$ results in the following relations between interaction and physical parameters:

$$\alpha^{-1}\beta_1 = \frac{-6\bar{\alpha}^2 m_{\rm FP}^2 + (3 + 4\bar{\alpha}^2 + \bar{\alpha}^4)\Lambda}{4\bar{\alpha}(1+\bar{\alpha}^2)}\,, \tag{4.36a}$$

$$\alpha^{-2}\beta_2 = \frac{4\bar{\alpha}^2 m_{\rm FP}^2 - (1+\bar{\alpha}^2)^2\Lambda}{2\bar{\alpha}^2(1+\bar{\alpha}^2)}\,, \tag{4.36b}$$

$$\alpha^{-3}\beta_3 = \frac{-6\bar{\alpha}^2 m_{\rm FP}^2 + (1 + 4\bar{\alpha}^2 + 3\bar{\alpha}^4)\Lambda}{4\bar{\alpha}^3(1+\bar{\alpha}^2)}\,. \tag{4.36c}$$

For brevity, we already simplified the expression for β_1 and β_3 assuming that the physical parameters satisfy Eq. (4.37).

Let us identify the viable region of the physical parameter space, which we present in Fig. 4.3. The bound (4.35) on $\bar{\beta}_2$ in terms of physical parameters reads

$$4\bar{\alpha}^4 m_{\rm FP}^2 < (1+\bar{\alpha}^2)^2\Lambda\,. \tag{4.37}$$

This bound is violated in the blue-shaded region of Fig. 4.3. Next, the condition $\beta_1 > 0$ translates into

$$6\bar{\alpha}^2 m_{\rm FP}^2 < (3 + 4\bar{\alpha}^2 + \bar{\alpha}^4)\Lambda\,. \tag{4.38}$$

In the red-shaded region of Fig. 4.3, this bound is not satisfied. The grey-shaded region violates the Higuchi bound. Summarising, the $\beta_1\beta_2\beta_3$–model is theoretically viable in the unshaded region of Fig. 4.3.

$\beta_1\beta_2\beta_4$–model

The $\beta_1\beta_2\beta_4$–model is defined by setting $\beta_0 = \beta_3 = 0$. Following our recipe, we express the interaction parameters β_1 and β_4 in terms of physical parameters using Eqs. (2.75) and (2.83). The roots of Eq. (2.76) are then given by

$$\bar{\alpha}_\pm = \sqrt{\frac{3m_{\rm FP}^2 - \Lambda + 3\bar{\beta}_2 \pm \sqrt{(3m_{\rm FP}^2 - \Lambda - 3\bar{\beta}_2)^2 - 12\bar{\beta}_2\Lambda}}{6\bar{\beta}_2}}\,. \tag{4.39}$$

The two remaining roots are given by $-\bar{\alpha}_\pm$ and hence do not correspond to physical vacua. The roots are real-valued if the parameters satisfy

$$3\bar{\beta}_2 < 3m_{\rm FP}^2 - 2\sqrt{3}m_{\rm FP}\sqrt{\Lambda} + \Lambda\,. \tag{4.40}$$

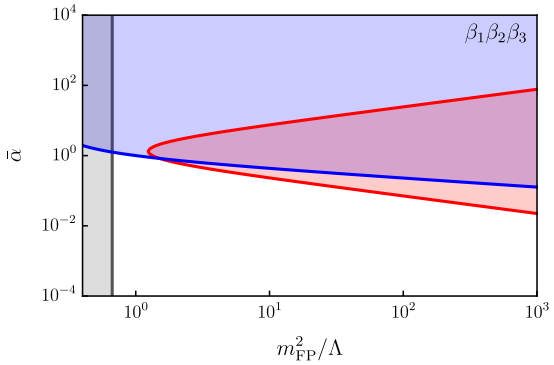

Figure 4.3: Exclusion plot taken from [340] obtained from theoretical consistency bounds for the $\beta_1\beta_2\beta_3$–model. The red-shaded region yields $\beta_1 < 0$ and in the blue-shaded region the vacuum point is not well-defined. The grey-shaded region violates the Higuchi bound.

The root $\bar{\alpha}_+$ is real-valued if additionally $\bar{\beta}_2 > 0$. The roots satisfy $\bar{\alpha}_- < \bar{\alpha}_+$ in the region, where both are real-valued, which identifies $\bar{\alpha}_-$ as the unique physical vacuum. Solving Eq. (4.39) for $\bar{\beta}_2$ on the root $\bar{\alpha}_-$ results in the following parameter relations:

$$\alpha^{-1}\beta_1 = \frac{-3\bar{\alpha}^2 m^2_{\rm FP} + 2(1+\bar{\alpha}^2)\Lambda}{2\bar{\alpha}(1+\bar{\alpha}^2)}\,, \tag{4.41a}$$

$$\alpha^{-2}\beta_2 = \frac{3\bar{\alpha}^2 m^2_{\rm FP} - (1+\bar{\alpha}^2)\Lambda}{3\bar{\alpha}^2(1+\bar{\alpha}^2)}\,, \tag{4.41b}$$

$$\alpha^{-4}\beta_4 = \frac{-6\bar{\alpha}^2 m^2_{\rm FP} + (1+4\bar{\alpha}^2+3\bar{\alpha}^4)\Lambda}{3\bar{\alpha}^4(1+\bar{\alpha}^2)}\,. \tag{4.41c}$$

Here, we already simplified the expressions assuming Eq. (4.43) to hold.

The viable region of the physical parameter space is presented in the left panel of Fig. 4.4 The bound on $\bar{\beta}_2$ is automatically satisfied. Requiring $\beta_1 > 0$ translates into

$$3\bar{\alpha}^2 m^2_{\rm FP} < 2(1+\bar{\alpha}^2)\Lambda\,. \tag{4.42}$$

The bound is violated in the red-shaded region. Expanding $\rho(y)$ around $\bar{y} = \bar{\alpha}$ unveils that the finite branch is non-singular only for

$$3\bar{\alpha}^4 m^2_{\rm FP} < (1+\bar{\alpha}^2)^2\Lambda\,. \tag{4.43}$$

This bound is violated in the blue-shaded region of the left panel of Fig. 4.4. As before, the grey-shaded region violates the Higuchi bound.

$\beta_1\beta_3\beta_4$–model

To complete the dictionary, we set $\beta_0 = \beta_2 = 0$ to arrive at the $\beta_1\beta_3\beta_4$–model. We use Eqs. (2.75) and (2.83) to replace β_3 and β_4 in terms of physical parameters. The polynomial (2.76) gives rise to three roots, out of which only

$$\bar{\alpha} = \frac{1}{6\bar{\beta}_1}\left(-m^2_{\rm FP} + \Lambda + \frac{-12\bar{\beta}_1^2 + (m^2_{\rm FP}-\Lambda)^2}{\mathcal{B}^{1/3}} + \mathcal{B}^{1/3}\right)\,, \tag{4.44}$$

is possibly real-valued. Here we defined the short-hand notation

$$\mathcal{B} = (\Lambda - m^2_{\rm FP})^3 + 18\bar{\beta}_1^2(m^2_{\rm FP}+2\Lambda) + 6\sqrt{3}\bar{\beta}_1\sqrt{16\bar{\beta}_1^4 - (m^2_{\rm FP}-\Lambda)^3\Lambda - \bar{\beta}_1^2(m^4_{\rm FP} - 20m^2_{\rm FP}\Lambda - 8\Lambda^2)}\,.$$

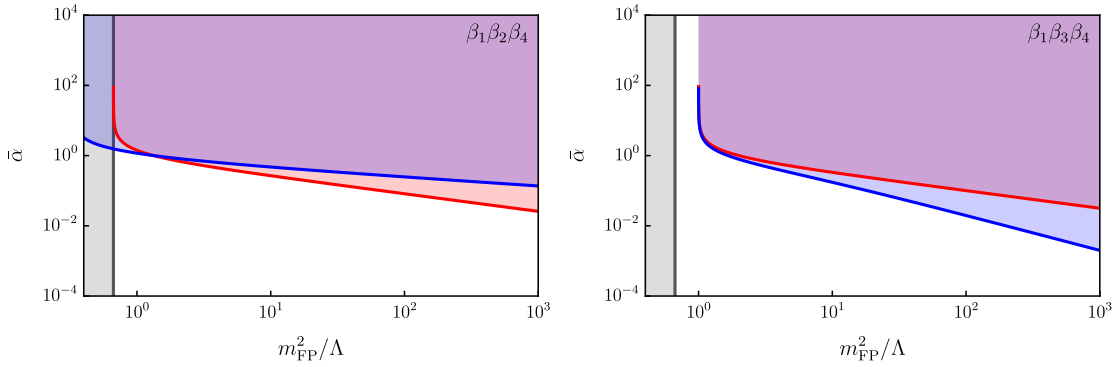

Figure 4.4: Exclusion plots taken from [340] obtained from theoretical consistency bounds for the $\beta_1\beta_2\beta_4$– (left) and the $\beta_1\beta_3\beta_4$–model (right). The red-shaded region yields $\beta_1 < 0$ and in the blue-shaded region the vacuum point is not well-defined. The grey-shaded region violates the Higuchi bound.

Employing analytical and numerical methods, we find that the root is real-valued if the parameters satisfy

$$\bar{\beta}_1 > \frac{\sqrt{m_{\rm FP}^4 - 8\Lambda^2 + m_{\rm FP}(m_{\rm FP}^2 + 8\Lambda)^{3/2}}}{4\sqrt{2}}\,, \tag{4.45}$$

which is non-trivial for $m^2_{\rm FP} > \Lambda$. Solving Eq. (4.44) for $\bar{\beta}_1$ results in the following relation between the parameters:

$$\alpha^{-1}\beta_1 = \frac{-\bar{\alpha}^2 m^2_{\rm FP} + (1+\bar{\alpha}^2)\Lambda}{2\bar{\alpha}(1+\bar{\alpha}^2)}\,, \tag{4.46a}$$

$$\alpha^{-3}\beta_3 = \frac{3\bar{\alpha}^2 m^2_{\rm FP} - (1+\bar{\alpha}^2)\Lambda}{2\bar{\alpha}^3(1+\bar{\alpha}^2)}\,, \tag{4.46b}$$

$$\alpha^{-4}\beta_4 = \frac{-4\bar{\alpha}^2 m^2_{\rm FP} + (1+\bar{\alpha}^2)^2\Lambda}{\bar{\alpha}^4(1+\bar{\alpha}^2)}\,. \tag{4.46c}$$

The bound (4.45) in terms of physical parameters reads

$$4(1+\bar{\alpha}^2)^3\Lambda^2 > \bar{\alpha}^2(m^2_{\rm FP} + 2(1+\bar{\alpha}^2)\Lambda)^2\,. \tag{4.47}$$

This condition is violated in the blue shaded region of the right panel of Fig. 4.4. The requirement $\beta_1 > 0$ translates onto the physical parameters as

$$\bar{\alpha}^2 m^2_{\rm FP} < (1+\bar{\alpha}^2)\Lambda\,. \tag{4.48}$$

The red-shaded region of the right panel of Fig. 4.4 violates this bound. Note that Eq. (4.47) represents the most-stringent bound. The Higuchi bound is violated in the gray-shaded region. Summarising, the $\beta_1\beta_3\beta_4$–model is viable in the unshaded region of Fig. 4.2. Note that the coupling $\bar{\alpha}$ is allowed to take arbitrary large values for $2\Lambda/3 < m^2_{\rm FP} < \Lambda$.

4.4 Discussion

On the one hand, cosmological solutions of BT are commonly parametrised in terms of the interaction parameters β_n or in terms of the rescaled parameters $\bar{\beta}_n$. As we have argued, the former are not invariant under the rescaling (4.1) rendering these parameters unphysical and the latter are ambiguous and have possibly misleading implications. On the other hand, spherically symmetric solutions are parametrised in terms of $m_{\rm FP}$ as well as either α or c, while the other constant is set

Model	Viable parameter space
β_1	$3\bar{\alpha}^2 = 1$ and $3m_{\rm FP}^2 = 4\Lambda$
$\beta_0\beta_1$	$m_{\rm FP}^2 = (1+\bar{\alpha}^2)\Lambda$
$\beta_1\beta_2$	$6\bar{\alpha}^2 m_{\rm FP}^2 \simeq \Lambda$
$\beta_1\beta_3$	$4\bar{\alpha}^2 m_{\rm FP}^2 \simeq \Lambda$
$\beta_1\beta_4$	$3\bar{\alpha}^2 m_{\rm FP}^2 = (1+\bar{\alpha}^2)\Lambda$
$\beta_0\beta_1\beta_2$	$3m_{\rm FP}^2 > 2(1+\bar{\alpha}^2)\Lambda$
$\beta_0\beta_1\beta_3$	$4m_{\rm FP}^2 > 2(1+\bar{\alpha}^2)^2\Lambda$
$\beta_0\beta_1\beta_4$	
$\beta_1\beta_2\beta_3$	$4\bar{\alpha}^4 m_{\rm FP}^2 < (1+\bar{\alpha}^2)^2\Lambda$ and $6\bar{\alpha}^2 m_{\rm FP}^2 < (3+4\bar{\alpha}^2+\bar{\alpha}^4)\Lambda$
$\beta_1\beta_2\beta_4$	$3\bar{\alpha}^2 m_{\rm FP}^2 < 2(1+\bar{\alpha}^2)\Lambda$ and $3\bar{\alpha}^4 m_{\rm FP}^2 < (1+\bar{\alpha}^2)^2\Lambda$
$\beta_1\beta_3\beta_4$	$\bar{\alpha}^2 m_{\rm FP}^2 < (1+\bar{\alpha}^2)\Lambda$

Table 4.2: Summary of the parameter space regions that are consistently described by the one-, two- and three-parameter models. Note that we only give the approximate parameter relations for the $\beta_1\beta_2$– and $\beta_1\beta_3$–models for brevity. In addition, the parameters must satisfy the Higuchi bound (2.84) in all cases.

to unity. This limits the comparability and interpretability of the hitherto obtained observational constraints on these parameters.

To circumvent the associated drawbacks, we proposed a new parametrisation of bimetric solutions. Our strategy is to formulate solutions in terms of the following rescaling-invariant physical parameters: the coupling strength of the massive spin-2 field to ordinary matter $\bar{\alpha}$, its mass $m_{\rm FP}$, and the effective cosmological constant Λ. Their unambiguous definition requires the identification of the unique vacuum solution.

In this chapter, we worked out the unique relations between the theory parameters $\{\alpha, \beta_n\}$ and the physical parameters $\{\bar{\alpha}, m_{\rm FP}, \Lambda\}$ for all models that fit into our framework. These are the models with three free interaction parameters being free, or less. Recently, our setup was generalised to four- and five-parameter models in [260, 299].

Our method of identifying the unique physical vacuum also yields theoretical consistency conditions on the physical parameters, which ensure a viable (i.e. real-valued, non-singular and devoid of the Higuchi ghost) cosmic expansion history. We explicitly worked out these conditions for all bimetric models with up to three free interaction parameters as summarised in Table 4.2. In addition, all models are subject to the Higuchi bound (2.84) of de Sitter.

Our results unveil that the bimetric models are able to consistently describe only certain subregions of the parameter space spanned by the physical parameters. The one-parameter model corresponds to a point in the plane spanned by $\bar{\alpha}$ and $m_{\rm FP}^2/\Lambda$. The two-parameter models describe lines and the three-parameter models entire regions in that plane.

Having thoroughly established the physical parametrisation, we are now in the position to overcome the aforementioned shortcomings of prior investigations and to consistently revisit the phenomenological consequences of BT. Our new parametrisation forms the basis for the remainder of this thesis.

Chapter 5

Vainshtein screening in bimetric cosmology

The previously proposed physical parametrisation enables us to consistently explore the entire parameter space of BT. At the same time, the required identification of the unique vacuum solution as well as consistency of the cosmic expansion history yielded theoretical constraints on the physical parameters. Going beyond, the consistency of the perturbative level of bimetric cosmology might impose further restrictions on the parameters. In fact, the gradient instability [226, 266, 270, 272, 274,275,300–305] discussed in Section 3.1.4 generally questioned the viability of bimetric cosmology on the perturbative level.

However, this is not the end of the story. As we have argued in Section 3.1.4, there are three ways to circumvent the instability: fine-tuning the initial conditions, going to the GR-limit $\bar{\alpha} \ll 1$ [226], or taking nonlinearities into account [277]. The first option is less appealing due to the lack of a mechanism that would generate such tuning. The second option excludes most of the phenomenologically interesting regions of the parameter space. Instead, this chapter explores the third option and as such demonstrates the validity of BT also away from the GR-limit.

It is a challenging task to study nonlinear perturbations on top of a FLRW background. To make progress nonetheless, we take inspiration from static systems with spherical symmetry [119, 124, 331, 332], which we reviewed in Section 3.2. The gravitational potentials can be viewed as perturbations about flat spacetime[1]. When approaching the source, or equivalently in the massless limit of the theory, nonlinear effects in the perturbations become relevant and render the linear approximation invalid. This is the well-known Vainshtein screening mechanism [119] that restores GR in spacetime regions where the energy density is large (compared to the spin-2 mass). In this chapter, we apply this logic to the FLRW solutions.

We will give a physical argument for the cosmological version of the Vainshtein mechanism. We will show that the spin-2 mass sets the energy scale at which Vainshtein screening sets in. In the context of background cosmology, the will see that the energy density due to the bimetric interactions is screened away precisely above this energy scale. This can be understood from the decoupling of the nonlinear massless and massive modes in this regime. We therefore expect linear perturbation theory to break down at this energy scale. As we will demonstrate that this is indeed the case.

Our results agree with similar arguments within Galileon cosmology [341, 342]. Here, the dynamics in the early universe are governed by nonlinear self-interactions of the Galileon field. These render the Galileon strongly coupled and suppress its energy density compared to matter and radiation.

This chapter is based on our publication [277].

[1] In case of a non-vanishing effective cosmological constant $\Lambda > 0$, the gravitational potentials can be viewed as perturbations about de Sitter spacetime.

5.1 Vainshtein screening

We discussed Vainshtein screening [119, 124] in detail in Section 3.2 and Appendix A. In this section, we first briefly summarise and rephrase the standard Vainshtein mechanism in a manner suitable for our discussion in the context of cosmology. We proceed by applying our insights to a spatially extended matter distribution.

5.1.1 The standard Vainshtein mechanism

The Vainshtein mechanism introduces a new scale into the system. For a spherically symmetric and static configuration, this scale is given as the Vainshtein radius, which we defined in Eq. (3.36) and is given by [331, 332],

$$r_{\mathrm{V}} = \left(\frac{r_{\mathrm{S}}}{m_{\mathrm{FP}}^2}\right)^{1/3} , \tag{5.1}$$

where $r_{\mathrm{S}} = M/(4\pi\, M_{\mathrm{g}}^2)$ denotes the Schwarzschild radius of the source of mass M. On length scales larger than the Vainshtein radius, $r \gg r_{\mathrm{V}}$, the gravitational fields are small and can be treated perturbatively. This means that the field equations can be linearised in this regime. As a result, the gravitational potential is modified compared to GR due to an additional Yukawa-like contribution, which arises from the propagating massive degrees of freedom. On length scales larger than the Compton wavelength, $r \gg m_{\mathrm{FP}}^{-1}$, the Yukawa-like modification is exponentially suppressed, which recovers GR with effective Planck mass $M_{\mathrm{P}} = \sqrt{1+\bar{\alpha}^2}M_{\mathrm{g}}$.

On smaller length scales, $r \ll r_{\mathrm{V}}$, the perturbative ansatz is not applicable and the linear approximation breaks down. That means that all nonlinearities need to be taken into account. The nonlinearities suppress deviations from and thus restore on these length scales. In this case, the parameter M_{g} serves as effective Planck mass. Therefore, spherical configurations give rise to two different GR-regimes, both characterised by different effective Planck masses. In the GR-limit of the theory $\bar{\alpha} \ll 1$, both Planck masses coincide.

On the technical level, the Stückelberg field $\mu(r)$ leads to the breakdown of the linear approximation. Inside the Vainshtein sphere, the function is of order unity, and quickly drops off outside the Vainshtein sphere. A visual depiction can be found in Fig. 3.5. Taking all nonlinearities in $\mu(r)$ into account restores GR. In the following we will see, that the Stückelberg field in the context of FLRW backgrounds gives rise to a similar behaviour.

For a source of finite size, the radius, in which the matter is concentrated, must be smaller than its own Vainshtein radius for the screening mechanism to work. Therefore, the Vainshtein mechanism restores GR only if the energy density of the source is above a certain minimal density. In the next section, we will elaborate on this observation and apply its logic to cosmology.

5.1.2 The Vainshtein mechanism in cosmology

As anticipated, we will now study the Vainshtein mechanism in the case of an extended and constant matter distribution in more detail. This setup is appropriate to describe our homogeneous and isotropic universe. In particular, we want to find the critical energy density ρ_{cr} of a homogeneous mass distribution, for which the entire mass lies inside its own Vainshtein radius.

We start with a spherical and constant energy distribution of size R, such that the energy density is given by

$$\rho(r) = \begin{cases} \bar{\rho}\,, & r \leq R\,, \\ 0\,, & r > R \end{cases} . \tag{5.2}$$

The size of the energy distribution is not relevant for the following discussion and can be infinitely extended to $R = \infty$. The mass $M(r)$, which is enclosed within a radius $r < R$, is given by

$$M(r) = 4\pi \int_0^r \mathrm{d}r'\, r'^2 \rho(r') = \frac{4\pi}{3} r^3 \bar{\rho}\,. \tag{5.3}$$

The Schwarzschild radius corresponding to this enclosed mass is

$$r_{\mathrm{S}} = \frac{M(r)}{4\pi\, M_{\mathrm{g}}^2} = \frac{r^3 \bar{\rho}}{3M_{\mathrm{g}}^2}\,. \tag{5.4}$$

The Vainshtein radius (5.1) corresponding to the mass $M(r)$ enclosed within a sphere of radius r is

$$r_{\mathrm{V}} = \left(\frac{\bar{\rho}}{3M_{\mathrm{g}}^2 m_{\mathrm{FP}}^2}\right)^{1/3} r\,. \tag{5.5}$$

So for a source with constant density, the Vainshtein radius linearly increases with the radius r defining the enclosed mass $M(r)$.

The enclosed mass fits precisely inside its own Vainshtein radius if $r = r_{\mathrm{V}}$. The critical density is therefore given by

$$\bar{\rho}_{\mathrm{V}} = 3M_{\mathrm{g}}^2 m_{\mathrm{FP}}^2\,. \tag{5.6}$$

If the density of the matter distribution is smaller, $\bar{\rho} < \bar{\rho}_{\mathrm{V}}$, the Vainshtein radius is always smaller than the radius that encloses its corresponding mass. In this case, the Vainshtein mechanism does not restore GR on small scales. On the other hand, if the density is higher, $\bar{\rho} > \bar{\rho}_{\mathrm{V}}$, the mass enclosed by a radius r lies entirely inside its own Vainshtein radius. Since $\bar{\rho}_{\mathrm{V}}$ is independent of r, the entire spacetime region enclosed by R is screened in that case.

Next, we apply this result to cosmology, assuming that the arguments are not invalidated by the time evolution. Let $\bar{\rho}(t)$ denote the total energy density of the universe. At the background level, the energy density is homogeneous and isotropic and decreases with time t. Therefore, at a critical moment during the cosmic expansion, the energy density passes the value $\bar{\rho}_{\mathrm{V}}$. From the modified Friedmann equation (3.9), we find that the corresponding critical Hubble rate is given by $H_{\mathrm{V}} = \bar{\rho}_{\mathrm{V}}/3M_{\mathrm{g}}^2$. Plugging this into Eq. (5.6) leads to the following expression for the critical Hubble rate:

$$H_{\mathrm{V}} = m_{\mathrm{FP}}\,. \tag{5.7}$$

If $H > H_{\mathrm{V}}$, i.e. at early times, the energy density of the universe is larger than the critical value implying that the universe is screened. At later times, $H < H_{\mathrm{V}}$, the energy density is below the critical value and hence unscreened.

The Vainshtein radius for a constant, homogeneous matter distribution scales linearly with radius, $r_{\mathrm{V}} \sim r$. If the energy density is below the critical value, i.e. if the Hubble parameter is small $H < m_{\mathrm{FP}}$, each Hubble patch is larger than its own Vainshtein radius. On the other hand, for energy densities above the critical value, i.e. for $H > m_{\mathrm{FP}}$, each Hubble patch is smaller than its Vainshtein radius and hence entirely screened. Although we started from a spherically symmetric setup, which we applied to cosmology, our result does not single out a preferred direction or point in space. Our analogy does not spoil the cosmological principle.

Our analogy instead allows for a different, rather curious interpretation. Let us treat the Big Bang singularity as central source, from where the distance r is measured by the inverse Hubble scale, $r \sim H^{-1}$. The modified Friedmann equation (3.9) leads to a density profile of the form $\rho \sim H^2 \sim r^{-2}$. The corresponding Schwarzschild radius is $r_{\mathrm{S}} = H^{-1}$, which leads to the Vainshtein radius (5.1)

$$r_{\mathrm{V}} = \left(m_{\mathrm{FP}}^2 H\right)^{-1/3}\,. \tag{5.8}$$

The critical time is defined as the moment, when the size of the Hubble patch equals its own Vainshtein sphere, i.e. $r_{\mathrm{V}} = H_{\mathrm{V}}^{-1}$. This leads to the same expression for the critical Hubble rate H_{V} is in Eq. (5.7).

In Fig. 5.1, we compare the time evolution of the size of a Hubble patch with the cosmological Vainshtein radius. To produce the figure, we choose a spin-2 mass of $m_{\mathrm{FP}} = 1\,\mathrm{GeV}$. We use the Hubble scale H as time parameter. The blue line represents the size of the Hubble patch, which is scales as $\sim H^{-1}$. The yellow line shows the cosmological Vainshtein radius corresponding to each Hubble patch, which scales as $H^{-1/3}$ according to Eq. (5.8). Hence, each Hubble patch grows

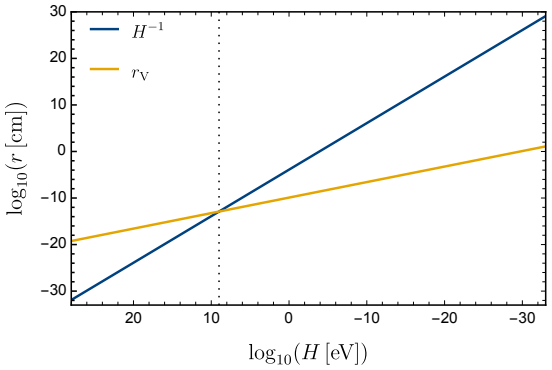

Figure 5.1: Time evolution of the size of each Hubble patch (blue) and the corresponding Vainshtein radius (yellow). The dashed vertical line indicates the critical time when $H = m_{\mathrm{FP}}$. To produce the figure, we set $m_{\mathrm{FP}} = 1\,\mathrm{GeV}$.

faster than the corresponding Vainshtein sphere. At the critical scale $H = m_{\mathrm{FP}}$, the Hubble patch becomes larger than its Vainshtein sphere and the universe leaves the screened regime.

Our analogy with spherically symmetric systems shows that the universe is smaller than its own vainshtein sphere for $H > m_{\mathrm{FP}}$ and larger otherwise. This suggests that the early universe is screened such that GR is restored by means of nonlinearities. In particular, we expect that linearisation is applicable only as long as $H < m_{\mathrm{FP}}$. We emphasise that our results only give a rough estimate for the critical Hubble rate due to our simplifying assumptions. However, we will see in the next sections that our expectation is indeed quantitatively confirmed on the level of both cosmological background and perturbative level.

5.2 The spin-2 mass in cosmology

In the previous section we have identified the critical Hubble rate $H_{\mathrm{V}} = m_{\mathrm{FP}}$, at which the universe transitions from a Vainshtein screened to an unscreened phase. In this section, we analyse how cosmological solutions to bimetric theory behave in the two regimes. We will remain completely general, but occasionally specialise to the $\beta_0\beta_1\beta_4$–model to provide explicit examples. This model is particularly simple on a mathematical level and still captures all the relevant features discussed here.

We discussed cosmological solutions in bimetric theory in Section 3.1. This serves as basis for the present discussion. Previously, we have worked in cosmic time t by setting the lapse of $g_{\mu\nu}$ to $X_{\mathrm{g}} = 1$. For convenience, here we will work in conformal time τ by setting the lapse of $g_{\mu\nu}$ to $X_{\mathrm{g}} = a$. In addition, we write the $f_{\mu\nu}$ lapse function as $X_{\mathrm{f}} = b(1+\mu)$. We will discuss the meaning of the function μ in greater detail later. Further specialising to spatial flatness $k = 0$, the metrics assume the conformal FLRW form,

$$\mathrm{d}s_{\mathrm{g}}^2 = a^2\left(-\mathrm{d}\tau^2 + \mathrm{d}r^2 + r^2\mathrm{d}\Omega_{(2)}^2\right) \tag{5.9a}$$

$$\mathrm{d}s_{\mathrm{f}}^2 = b^2\left(-(1+\mu)^2\mathrm{d}\tau^2 + \mathrm{d}r^2 + r^2\mathrm{d}\Omega_{(2)}^2\right). \tag{5.9b}$$

All metric functions a, b, and μ depend on conformal time τ. On the dynamical branch solution of the Bianchi constraint (3.7), the field μ is related to the scale factor ratio as

$$\mu = \frac{y'}{y}. \tag{5.10}$$

Recall that a prime denotes derivative with respect to e-folds $N = \ln a$.

For $\mu = 0$, both metrics are conformally related, $g_{\mu\nu} = y^2 f_{\mu\nu}$. Therefore, the field μ measures the deviation from proportionality and hence the relative twist between the coordinate systems of

the two metrics. In this sense, the field is similar to a Stückelberg field since it would be shifted by time reparametrisations of the metric $f_{\mu\nu}$. As such, the field $\mu(\tau)$ in our FLRW ansatz is analogous to the field $\mu(r)$ of the static, spherically symmetric solutions of Section 3.2. Hence, we would expect that for $|\mu| \ll 1$ linear perturbation theory is valid and the universe is governed by the bimetric equations of motion. In the opposite case, $|\mu| \sim \mathcal{O}(1)$, nonlinearities have to be taken into account, activating the Vainshtein screening. In the following, we make this intuition quantitatively robust.

5.2.1 Vainshtein screening of background cosmology

We start with a discussion at the level of background cosmology, using the modified Friedmann equations (3.9). The scale factor ratio $\bar{y}$ evolves on the finite branch from zero at early times to a constant value in the asymptotic future, which is determined by the vacuum polynomial Eq. (2.76). A detailed discussion is given in Section 3.1.

Focussing on early times, the energy density of matter is large, $\rho/M_{\rm g}^2 \gg \beta_n$, which allows to expand the quartic polynomial (3.18) and solve for $\bar{y}$. This results in

$$\bar{y} = \bar{\beta}_1 \left(\frac{\rho}{M_{\rm g}^2}\right)^{-1} + \mathcal{O}\left(\frac{\rho}{M_{\rm g}^2}\right)^{-2} . \tag{5.11}$$

Plugging this into (3.11) yields the energy density of dark energy during early times as

$$\frac{\rho_{\rm de}}{M_{\rm g}^2} = \beta_0 + \frac{3\bar{\beta}_1^2 M_{\rm g}^2}{\rho} + \mathcal{O}\left(\frac{\rho}{M_{\rm g}^2}\right)^{-2} . \tag{5.12}$$

The parameter β_0 is a constant. Since $\rho_{\rm de}$ linearly scales with ρ^{-1} to first order, we find that $\rho_{\rm de} \ll \rho$ during early times. That means that the bimetric interaction energy density does not contribute to the cosmic expansion during early times. This effect was first pointed out in [216].

The energy density arising from the bimetric potential is suppressed during early times. This represents a screening in close analogy to Galileon cosmology [341] on the level of background cosmology and implies that the expansion history resembles the one of GR during early times. Next, we are interested in the time scale at which this cosmological screening sets in.

The screening sets in when the scale factor ratio transitions from its late time value $\bar{y} \simeq \bar{\alpha}$ to its early-time value $\bar{y} \simeq 0$. For this, we use the time when $\bar{y}$ changes most quickly, i.e. when $\bar{y}'$ is at its maximum value, as a bookkeeper. We therefore have to solve for $\bar{y}'' = 0$. Taking the time derivative of Eq. (3.19) and using Eq. (1.17) together with Eq. (3.18) yields $\bar{y}''$ as a function of $\bar{y}$ as

$$\bar{y}'' = 3(1+w)\frac{D_{(1)}}{D_{(2)}^2} \tag{5.13}$$

with

$$\begin{aligned} D_{(1)} =& (1 - 12\bar{y}^2 - 9\bar{y}^4)\bar{\beta}_1^2 + 2\bar{y}\bar{\beta}_1\Big[\bar{y}^2(4+3\bar{y}^2)\bar{\beta}_4 + 2\bar{y}(3+\bar{y}^2)\bar{\beta}_3 + 3(1-4\bar{y}^2-3\bar{y}^3)\bar{\beta}_2 - \beta_0\Big] \\ & - \bar{y}^4\Big[18(1+\bar{y}^2)\bar{\beta}_2^2 + 3(3+\bar{y}^4)\bar{\beta}_3^2 + 2(\beta_0 + \bar{y}^2\bar{\beta}_4)\bar{\beta}_4 - 6(\beta_0 + (1+2\bar{y}^2)\bar{\beta}_4 - 2\bar{y}^3\bar{\beta}_3)\bar{\beta}_2 \\ & + 2\bar{y}((3-2\bar{y}^2)\bar{\beta}_4 - 3\beta_0)\bar{\beta}_3\Big] , \\ D_{(2)} =& \bar{\beta}_1(1+3\bar{y}^2) + \bar{y}^2(6\bar{y}\bar{\beta}_2 + 3(\bar{y}^2-1)\bar{\beta}_3 - 2\bar{y}\bar{\beta}_4) . \end{aligned}$$

In general, the equation $\bar{y}'' = 0$ represents a polynomial in $\bar{y}$ of degree eight, which in general cannot be solved analytically for $\bar{y}$. Let us denote the roots as $\bar{y}_*$ and the resulting critical Hubble rate as $H_* = H(\bar{y}_*)$. Next, we estimate the value of H_* in two different simplifying ways.

As anticipated, we specialise to the $\beta_0\beta_1\beta_4$–model by setting $\beta_2 = \beta_3 = 0$ and solve for H_* numerically. In the left panel of Fig. 5.2 we plot the numerically determined H_* in units of $m_{\rm FP}$ as function of $m_{\rm FP}^2/\Lambda$ for different values of $\bar{\alpha}$. We see that $H_*/m_{\rm FP}$ is approximately independent

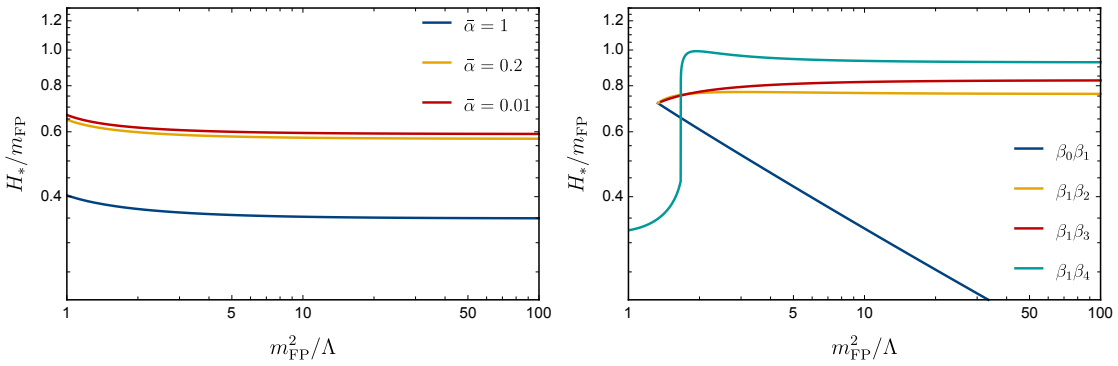

Figure 5.2: The critical Hubble rate H_* in units of the spin-2 mass $m_{\rm FP}$ for the $\beta_0\beta_1\beta_4$-model (left) and the two-parameter models (right) for different parameter values.

of $m^2_{\rm FP}/\Lambda$ and becomes independent of $\bar{\alpha}$ in the limit $\bar{\alpha} \ll 1$. Remarkably, in that parameter limit the critical Hubble rate is given by

$$H_* \simeq m_{\rm FP} \tag{5.14}$$

up to an $\mathcal{O}(1)$ constant. For parameter values $\bar{\alpha} \gtrsim \mathcal{O}(1)$, the critical Hubble rate H_* is suppressed by inverse powers of $\bar{\alpha}$ compared to the scale $m_{\rm FP}$. Note that this parameter region is inconsistent for models with $\beta_0 = 0$.

To gain further intuition, we specialise to the two-parameter models $\beta_0\beta_1$ and $\beta_1\beta_4$ (the remaining two-parameter models will be discussed in the next section). Now we can solve the polynomial $\bar{y}'' = 0$ analytically and compute the resulting critical Hubble rate H_*. The results in both cases are lengthy, but in the limit $\bar{\alpha} \ll 1$ we again get the remarkably simple result $H_* \simeq m_{\rm FP}$. Since the physical parameters are related within the two-parameter models, the limit $\bar{\alpha} \ll 1$ corresponds to $m^2_{\rm FP} \sim \Lambda$ in the case of the $\beta_0\beta_1$–model, and to $m^2_{\rm FP} \gg \Lambda$ in the case of the $\beta_1\beta_4$–model. On the other hand, the limit $m^2_{\rm FP} \gg \Lambda$ corresponds to $\bar{\alpha} \gg 1$ in the case of the $\beta_0\beta_1$–model. In this limit, the critical Hubble rate is given by $H_* \sim (m_{\rm FP}\Lambda)^{1/3}$.

This asymptotic behaviour can also be inferred from the right panel of Fig. 5.2. Here, H_* in units of $m_{\rm FP}$ is plotted as a function of $m^2_{\rm FP}/\Lambda$ for all two-parameter models. For the $\beta_1\beta_4$-model, the critical Hubble rate is of the order of the spin-2 mass for any value of $m_{\rm FP}$ or equivalently $\bar{\alpha}$. In the case of the $\beta_0\beta_1$-model, the critical Hubble rate is suppressed by inverse powers of $\bar{\alpha}$ in the limit $\bar{\alpha} \gtrsim \mathcal{O}(1)$.

Our previous results show that cosmological screening sets in when $\bar{y} \lesssim \bar{y}_*$. Let us provide some further physical interpretation for the parameter $\bar{y}$. We make use of the mass eigenstates, which we discussed at the linearised level in Section 2.4.3. The mass eigenstates are well-defined only for proportional backgrounds, i.e. in vacuum. The FLRW background, however, significantly differs form proportionality as measured by μ. Nonetheless, nonlinear massless and massive fields can be designed by requiring that these reduce to the linear mass eigenstates upon linearising [223]. The resulting candidate nonlinear massless $G_{\mu\nu}$ and massive $M_{\mu\nu}$ fields are not unique, but can be selected by employing simplicity arguments. The simplest nonlinear massless field is given by [223]

$$G_{\mu\nu} = g_{\mu\nu} + \alpha^2 f_{\mu\nu}\,. \tag{5.15}$$

We now specialise to the FLRW background (5.9). The spatial components are given by $G_{ij} = a^2(1+\bar{y}^2)\delta_{ij}$. In the limit $\bar{y} \ll 1$ the nonlinear massless mode is aligned with the physical metric (5.9a) as $G_{ij} \simeq g_{ij}$ and independent of the reference metric $f_{\mu\nu}$. This implies that the nonlinear massless and massive modes are decoupled. This observation is consistent with the decoupling of the linear massless and massive mode in the limit $\bar{\alpha} \ll 1$ [226, 335]. The decoupling renders the physical metric massless so as to restore GR. We conclude that $\bar{y}$ parametrises the mixing of the nonlinear massless and massive field on top of an FLRW background and that these decouple exactly when $\bar{y} \simeq \bar{y}_*$.

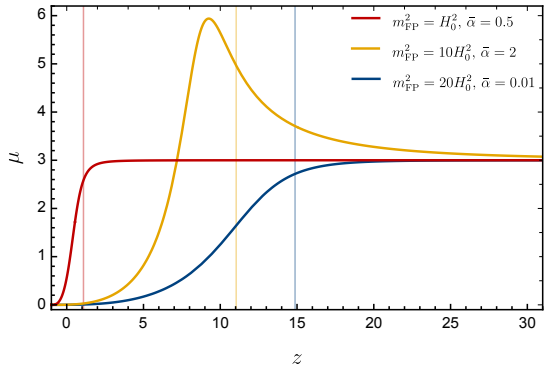

Figure 5.3: Time evolution of the Stückelberg field μ for different parameter values in the $\beta_0\beta_1\beta_4$-model. In each case, the parameters $\Omega_{\rm m0} = 0.3$ and $\Omega_\Lambda = 0.7$ are chosen. Figure taken from [277].

The temporal component of the nonlinear massless mode is given by $G_{00} = -a^2(1+\bar{y}^2(1+\mu)^2)$, which is not only controlled by $\bar{y}$, but also by the Stückelberg field μ. In the following, we study the time evolution of μ in more detail. At late times, the Stückelberg field vanishes because $\bar{y}'$ vanishes, see Eq. (3.27). During early times, μ approaches a constant value, because both $\bar{y}$ and $\bar{y}'$ vanish. To be precise and to summarise, the Stückelberg field assumes the following asymptotic values:

$$\lim_{\tau\to+\infty} \mu(\tau) = 0\ , \qquad \lim_{\tau\to-\infty} \mu(\tau) = 3(1+w)\,. \tag{5.16}$$

Note that these asymptotic values are common to all bimetric models. We see that the Stückelberg field transitions from an $\mathcal{O}(1)$ value during early times to zero at late times. This behaviour does not spoil the decoupling of the nonlinear massless and massive modes. Instead, the evolution is analogous to the spherically symmetric configuration as reviewed in Section 5.1.1, where μ approaches a constant $\mathcal{O}(1)$ value close to the source [331].

To see the time scale at which the Stückelberg field transitions from the early-time to the late-time constant values, we plot μ as a function of redshift z in Fig. 5.3. To produce the figure, we use the $\beta_0\beta_1\beta_4$–model for different couplings $\bar{\alpha}$ and spin-2 masses $m_{\rm FP}$. The vertical lines indicate the redshift, at which the Hubble rate equals the critical Hubble rate, i.e. $H = m_{\rm FP}$. Qualitatively, the plot unveils that the Stückelberg field starts to deviate from the early-time $\mathcal{O}(1)$ value when $H \simeq m_{\rm FP}$. We confirmed this observation quantitatively for various examples[2]. We conclude that the Stückelberg field μ transitions from the nonlinear to the linear regime at the critical time scale $H \simeq m_{\rm FP}$, as identified in Eq. (5.14).

Let us summarise. Our analysis on the level of background cosmology confirms our expectation that the early universe is screened and GR is restored. Remarkably, in the limit $\bar{\alpha} \ll 1$ we identified the same critical Hubble value as before, above which the universe is screened. Away from the limit, the ratio H_* is of the order of $m_{\rm FP}$, but also depends on $\bar{\alpha}$.

5.2.2 Linear perturbations

Our previous results show that the universe is screened for $H > m_{\rm FP}$, while at the same time the nonlinear mass eigenstates decouple and the Stückelberg field μ assumes a value of order unity. We therefore expect that linear perturbation theory breaks down exactly at the previously identified critical scale $H \simeq m_{\rm FP}$.

Indeed, the scalar sector of the cosmological perturbations are plagued by a gradient instability during early times on the linearised level, as discussed in Section 3.1.4. Here, we want to identify the time at which the gradient instability sets in.

[2]The yellow line indicates that μ has a maximum for certain parameter values. Indeed, the peak occurs only if $\beta_0 < 0$. That means that for self-accelerating models, μ does not develop a peak, for which the red and blue lines serve as representative examples.

The time evolution of the perturbation fields can be parametrised in term of the eigenfrequencies ω given by Eq. (3.32) as $E_{\mathrm{g,f}} \sim e^{i\omega N}$. For $\omega^2 > 0$, the perturbation fields are oscillating. For $\omega^2 < 0$, there is one mode that exponentially decays and one mode that exponentially grows. The exponential growth signals a gradient instability and invalidates linear perturbation theory. The stability requirement $\omega^2 > 0$ is equivalent to the following dynamical bound [275]:

$$y'' < \frac{y'}{2y}\frac{2Hy'(y'-3wy) - 3(1+2)(1+2w)\rho y^2}{(1+w)\rho y + H^2 y'} \,. \tag{5.17}$$

For the special models with $\beta_2 = \beta_3 = 0$, the bound reduces to the simple relation $y'' < 0$ [275]. This equation serves as basis to infer the energy scale at which the gradient instability sets in. We denote the critical scale factor ratio, at which the bound is violated, as y_* and the corresponding Hubble rate as $H_* = H(y_*)$.

Estimating H_* for the $\beta_0\beta_1\beta_4$–model and its two-parameter submodels $\beta_0\beta_1$ and $\beta_1\beta_4$ is particularly simple. In fact, we already solved $y'' = 0$ and inferred H_* for these models in the previous section.

For completeness, we compute the critical time at which linear perturbations become unstable also for the remaining two-parameter models. So for the case of the $\beta_1\beta_2$– and the $\beta_1\beta_3$–model, we determine the critical Hubble rate at which the dynamical bound (5.17) is violated[3]. Since the explicit results are too lengthy, we visualise them in the right panel of Fig. 5.2. The yellow line corresponds to the $\beta_1\beta_2$- and red lines to the $\beta_1\beta_3$–model. As for the other models, the critical Hubble rate at which linear perturbation theory breaks down is given by $H_* \simeq m_{\mathrm{FP}}$ up to $\mathcal{O}(1)$ constants. The figure unveils that H_*/m_{FP} is indeed approximately independent of $\bar{\alpha}$ and $m_{\mathrm{FP}}^2/\Lambda$.

Summarising, the gradient instability of linear cosmological perturbations sets in precisely at the energy scale when we expect nonlinear terms to become dominant. Our Vainshtein analogy suggests that GR is restores also on the perturbative level when all nonlinearities are taken into account.

This conclusion is supported by earlier results as we discuss now. The consequences of the gradient instability on structure formation were studied in [309] under the assumption that the onset of the local Vainshtein mechanisms restores GR and terminates the instability. This analysis constrains the redshift below which the instability is observationally ruled out. If the gradient instability is unobservable if it occurs above that redshift. Next, spherically symmetric scalar perturbations including all nonlinearities in the Stückelberg field were studied in [308]. Their analysis is based on BT with two independent matter sectors, which allows for FLRW solutions with proportional metrics, vastly simplifying computations. They indeed find that the perturbations are dominated by nonlinearities during early times, which restores GR. However, it remains to identify whether a nonlinear solution exists, which smoothly connects to the usual perturbative solution without branch cuts. Finally, the bimetric field equations were analytically for a homogenous overdensity in [310]. Depending on the bimetric parameters, the density contrast is indeed enhanced with respect to GR, but the solutions are well-behaved and devoid of physical instabilities.

5.3 Discussion

Equipped with the physical parametrisation, we revisited the problem of linear scalar perturbations in bimetric cosmology. We approached the problem in three ways.

Firstly, we established an analogy between the Vainshtein mechanism in spherically symmetric systems and in the universe by identifying the minimal density required such that the entire mass distribution lies within its own Vainshtein radius. This established $H_{\mathrm{V}} = m_{\mathrm{FP}}$ as the critical Hubble rate. During earlier times, i.e. for $H > m_{\mathrm{FP}}$, the universe is smaller than its own Vainshtein sphere. We therefore expect the early universe to be screened by the Vainshtein mechanism, such

[3]The critical Hubble rate H_* for the $\beta_1\beta_2$–model was previously computed in [226]. Due to the lack of the physical parameterisation, the authors did not interpret their result as the spin-2 mass.

that GR is restored by means of nonlinearities. In particular, we expect that linear perturbation theory breaks down during such early times.

Secondly, we demonstrated that the early universe is screened and GR is restored on the level of background cosmology. This can be understood from the decoupling of the nonlinear massless and massive mode as controlled by $\bar{y}$, which happens for $H > m_{\rm FP}$. At the same time, the Stückelberg field μ assumes a value of order unity. When the Hubble rate falls below the critical value $m_{\rm FP}$, the value of the Stückelberg field quickly drops to $|\mu| \ll 1$, the mixing of the nonlinear mass eigenstates becomes $\bar{y} \simeq \bar{\alpha}$ and the metrics become proportional $f_{\mu\nu} \sim y^2 g_{\mu\nu}$.

Thirdly, we addressed the stability of linear cosmological perturbations. We indeed find that the gradient instability occurs exactly when the Hubble rat exceeds the critical value, i.e. for $H > m_{\rm FP}$. This invalidates linear perturbation theory during these early times and necessitates taking into account all nonlinearities. Combined with our Vainshtein analogy and with the results obtained in [308–310], we expect that the nonlinearities remove the instability and restore GR also on the perturbative level.

For the remainder of this thesis we will use our here discussed results as clear indication that the early universe is screened by the Vainshtein mechanism. Our working assumption is that GR is restored during early times also on the perturbative level. This assumption enables us to use early universe observables such as the CMB to constrain BT.

Most importantly, our results indicate that the finite branch solution of bimetric cosmology is a priori viable both on the background and perturbative level despite the gradient instability. In particular, we are not forced to push the onset of the instability to arbitrary early times as in [226], which would forbid a small spin-2 mass. For instance, pushing the instability to times before BBN requires a large spin-2 mass of $m_{\rm FP} > 10^{-16}\,\text{eV}$. Instead, the cosmological Vainshtein mechanism enlarges the viable parameter space to arbitrarily small spin-2 masses (only limited by the Higuchi bound).

Next, we will confront the entire thus consistent parameter space of BT with observations. In the context of cosmology we have to limit ourselves to background observables because the nonlinearities prevent the usage of standard perturbative techniques. It remains an important task to constrain BT also on the perturbative level.

Chapter 6

Constraining bimetric theory

The previous chapters set the basis for thoroughly testing BT with observed data. In particular, our proposed physical parametrisation enables us to confront BT with various observational and theoretical constraints simultaneously within a unified framework. Moreover, it straightforwardly allows us to study the entire theoretically consistent parameter space of BT.

Previous studies in the context of background cosmology were limited to the parameter regime where $m_{\rm FP} \sim H_0$ [216, 263, 265, 296, 297, 337], which was found to give a good fit to observational data. Contrarily, the gradient instability at the perturbative level was believed to rule out bimetric cosmology. It was argued that the perturbative level is consistent if the gradient instability is pushed to arbitrary early times [226]. The discussion of our previous discussion elucidates that this requires $m_{\rm FP} \gg H_0$[1]. Comparing these parameter regimes with each other, it follows that bimetric cosmology cannot be consistent on the background and perturbative level simultaneously.

This conclusion is overcome by our discussion in the previous chapter. The Vainshtein mechanism removes the requirement to push the gradient instability to arbitrary early times [277, 308–310]. Hence, also the parameter regime $m_{\rm FP} \sim H_0$ is a priori consistent at the perturbative level. Since standard perturbative techniques are not applicable in the context of BT due to Vainshtein screening, we are still lacking observational constraints from the perturbative level.

In this chapter we will first revisit the background level of bimetric cosmology. In particular, we will show that the parameter regime $m_{\rm FP} \gg H_0$ gives an equally good fit to data as the previously studied region of the parameter space as well. We therefore overcome the aforementioned erroneous conclusion twice: firstly, the small mass region is a priori consistent at the perturbative level, and secondly, the large mass region is in fact consistent at the cosmological background level. This explicitly demonstrates for the first time that the entire parameter space of BT leads to an interesting and viable phenomenology[2].

To be more precise, we test BT with observations of Supernovae type 1a (SNe 1a), Baryon Acoustic Oscillations (BAOs), and the Cosmic Microwave Background (CMB) in a statistical analysis using Markov Chain Monte Carlo (MCMC) sampling. In addition to the aforementioned considerations regarding the bimetric parameters, we also analyse the usual cosmological parameters. For example, since we study the enlarged bimetric parameter space, we revisit the question of spatial curvature within BT. In agreement with earlier results, we find that the cosmological parameters take values very close to the standard values [216, 263, 265, 296, 337], including the preference for a spatially flat universe [297]

We go another step further in the second part of this chapter and confront BT with local tests of gravity. By this we mean tests of the gravitational potential and tests of the scalar curvature, which probe scales from laboratory to extragalactic scales. These tests have a long history and provide

[1] The physical parametrisation unveils that this parametric limit corresponds to $\bar{\alpha} \ll 1$ in the context of two-parameter models with $\beta_0 = 0$ [340]. In fact, [226] argued that the gradient instability is pushed to arbitrary early times for $\bar{\alpha} \ll 1$.

[2] The theoretically consistent parameter space is further subjected by cosmological constraints. In particular, the coupling $\bar{\alpha}$ must be sufficiently small if the spin-2 field is heavy, as will become clear from the subsequent analysis.

stringent constraints on modifications of the gravitational interactions [343–348]. Here we apply the existing results as obtained within the Yukawa parametrisation to the bimetric parameters $\bar{\alpha}$ and $m_{\rm FP}$. In particular, we consistently implement the Vainshtein screening mechanism. Building upon some earlier work [330,332,338,339], we provide the first thorough confrontation of BT with a plethora of local tests of gravity.

We finally compare the local and cosmological constraints to each other. Our combined analysis explicitly demonstrates that large regions of the bimetric parameter space withstand both classes of tests. In addition, our herein obtained constraints are to date the most stringent ones.

This chapter is based on our publications [298, 340].

6.1 Cosmological tests

We constrain bimetric theory with cosmological background observations. In particular, we use measurements of SN1a, BAOs, and the CMB. Of course, bimetric theory has been confronted with these observations before [216, 263, 265, 296, 297, 337], which we will review at the end of this section. However, these earlier papers constrained the β_n–parameters, studied only a specific region of the parameter space[3], or did not distinguish between the finite and the infinite branch.

In our analysis, we use the physical parametrisation to overcome the aforementioned problems. We directly constrain the physical parameters, which allows to unambiguously study the entire parameter space and implement the theoretical consistency conditions. Constraints on the physical parameters from SN1a observations were computed in [340]. In the present section, we present our more general work [298], where we in addition included constraints from BAOs and the CMB.

6.1.1 Parametrisation

As in standard cosmology, we introduce the energy density parameters Ω_i as in Eq. (1.26), explicitly

$$\Omega_i = \frac{\rho_i}{3M_{\rm g}^2H^2}\,, \tag{6.1}$$

where the index i stands for radiation ($i = {\rm r}$), matter ($i = {\rm m}$), spatial curvature ($i = {\rm k}$), and dynamical dark energy ($i = {\rm de}$). To ease the notation, we also introduce the following constant parameters

$$B_n = \frac{\alpha^{-n}\beta_n}{3M_{\rm g}^2H_0^2}\,, \quad \Omega_{\rm FP} = \frac{m_{\rm FP}^2}{3M_{\rm g}^2H_0^2}\,, \quad \Omega_\Lambda = \frac{\Lambda}{3M_{\rm g}^2H_0^2}\,, \tag{6.2}$$

inspired by the energy density parameters. The modified Friedmann equation of $g_{\mu\nu}$ reads

$$1 = \Omega_{\rm de} + \Omega_{\rm k} + \Omega_{\rm m} + \Omega_{\rm r}\,. \tag{6.3}$$

Note the difference between the parameter Ω_Λ and the energy density parameter of dynamical dark energy, $\Omega_{\rm de}$. The energy density parameter associated to dynamical dark energy depends on the bimetric parameters as

$$E^2\Omega_{\rm de} = B_0 + 3\bar{y}B_1 + 3\bar{y}^2B_2 + \bar{y}^2B_3\,, \tag{6.4}$$

according to Eq. (3.11), where we defined the dimensionless Hubble parameter

$$E = H/H_0\,, \tag{6.5}$$

which at present times is given by $E = 1$.

[3] In some papers, the rescaling invariance is used to set $\alpha = 1$, which brings the theory into a very specific region of the parameter space. Other papers assumed that $\beta_n \sim H_0^2$, which again represents only a certain region of the parameter space.

Evaluating the modified Friedmann equation (6.3) today yields a relation among the energy density parameters as

$$1 = \Omega_{\mathrm{de0}} + \Omega_{\mathrm{k0}} + \Omega_{\mathrm{m0}} + \Omega_{\mathrm{r0}} \,, \tag{6.6}$$

where the subscript 0 refers to the corresponding value of the energy density today, i.e. at redshift $z = 0$. This allows to eliminate one of the energy density parameters in terms of the others. In our analysis, we choose to eliminate Ω_{m0}.

To fix the values of the energy density parameters at present times, we need to determine Ω_{de0}. To do this, we use the Friedmann equation of $f_{\mu\nu}$ (3.10) evaluated at present times, which explicitly reads

$$0 = B_1 + (3B_2 + \Omega_{\mathrm{k0}} - 1)\bar{y}_0 + 3\bar{y}_0^2 B_3 + \bar{y}_0^3 B_4 \,. \tag{6.7}$$

This equation represents a cubic polynomial for $\bar{y}_0$. Here, $\bar{y}_0$ stands for the rescaled scale factor ratio $\bar{y}$ at present times. From Eq. (6.7), we pick the lowest-lying, strictly positive solution and impose $\bar{y}_0 < \bar{\alpha}$ to ensure that we are on the finite branch. With this result, we can compute Ω_{de0} via evaluating Eq. (6.4) today.

Next, we need to determine Ω_{de} as a function of redshift z to determine $H(z)$, which requires determining $\bar{y}$ as a function of z. One possibility is to solve the differential equation (3.19) [263]. However, we found that this strategy leads to numerical instabilities, in particular in the parametric limits $\bar{\alpha} \ll 1$ or $m_{\mathrm{FP}}^2 \gg \Lambda$. To avoid these numerical instabilities, we instead solve the quartic polynomial (3.18), explicitly given by

$$B_3\bar{y}^4 + (3B_2 - B_4)\bar{y}^3 + 3(B_1 - B_3)\bar{y}^2 + (B_0 - 3B_2 + E^2\Omega_{\mathrm{m}} + E^2\Omega_{\mathrm{r}})\bar{y} - B_1 = 0 \,, \tag{6.8}$$

for each redshift z. Picking the lowest-lying, strictly positive root and ensuring $\bar{y} < \bar{\alpha}$ yields a cosmic expansion on the finite branch.

6.1.2 Statistical analysis

We want to confront our cosmological model with observational data to identify those parameter combinations, which best fit the cosmological observations. For this purpose, we take the Bayesian perspective, which has become standard in cosmology for parameter estimation (for reviews, see [349–353]). Let x be a vector containing the data, and θ containing the parameters of the cosmological model. We need to compute the probability that the set of parameters θ given the observational data x are the true parameters. This probability is denoted by $p(\theta|x)$ and referred to as posterior distribution function (PDF). By Bayes' theorem, the posterior distribution function can be computed as [354]

$$p(\theta|x) = \frac{p(x|\theta)p(\theta)}{p(x)} \,, \tag{6.9}$$

with $p \in [0, 1]$ denoting probability. Let us discuss the terms appearing on the right hand side.

The term $p(x)$ is the probability for the observational data to occur, which in cosmology is referred to as the evidence. The evidence is independent of the parameters of the cosmological model and hence appears as overall normalisation. Therefore, we can ignore the evidence in our analysis.

The likelihood, denoted by $\mathcal{L}(\theta) = p(x|\theta)$, describes the probability that the observational data x occurs given the parameters of the model θ. The likelihood can be computed by a χ^2-analysis as

$$\mathcal{L}(\theta) = e^{-\chi^2/2} \,. \tag{6.10}$$

Let $X = x - x_{\mathrm{th}}(\theta)$ the vector describing the difference between the observed data x and the theoretical prediction x_{th} of the model given the parameters θ. Then, the χ^2 is given by

$$\chi^2 = X^{\mathrm{T}} C^{-1} X \,, \tag{6.11}$$

with C the covariance matrix of the data set.

To compute the likelihood, one would need to compute the χ^2 for every set of model parameters θ. In practice, the simplest possibility to estimate the likelihood is to discretise the parameter space of the cosmological model and to compute the likelihood on every point of the grid. This method however, is computationally demanding, in particular if the dimension of the parameter space is large. In our analysis we instead utilise the Monte Carlo Markov Chain (MCMC) sampling method with the Metropolis–Hastings algorithm [355,356], whose usage for cosmology is described in [357,358]. This method explores those regions of the parameter space in great detail, where the likelihood is large. The likelihood function is approximated by the point frequencies of the chains. Therefore, the accuracy of the approximation increases with the length of the chains.

As final step, we need to choose priors $p(\theta)$, which describe the probability distributions of the model parameters. Here we use our previous knowledge about the parameters from theoretical considerations or earlier statistical analyses. In the following we detail our choice of priors.

In our case, we scan over the following set of model parameters[4]:

$$\left(\log_{10}(\bar{\alpha}), \log_{10}(\Omega_{\mathrm{FP}}), \Omega_\Lambda, \Omega_{\mathrm{k0}}, \Omega_{\mathrm{b0}}h^2, H_0\right) . \tag{6.12}$$

Let us first discuss priors on the standard cosmological parameters. We choose the following flat priors

$$p(\theta) = \begin{cases} 1 & \text{if} \quad \begin{cases} 45\,\frac{\mathrm{km/s}}{\mathrm{Mpc}} \leq H_0 \leq 85\,\frac{\mathrm{km/s}}{\mathrm{Mpc}}\,, \\ 0 \leq \Omega_{\mathrm{b0}}h^2 \leq 1\,, \\ -1 \leq \Omega_{\mathrm{k0}} \leq 1\,, \\ 0 \leq \Omega_\Lambda \leq 1\,, \end{cases} \\ 0 & \text{else} \end{cases} , \tag{6.13}$$

to ensure that the bimetric cosmological models do not differ substantially from the standard cosmological model.

The two remaining parameters, $\bar{\alpha}$ and m_{FP}, are subject to theoretical constraints. The spin-2 mass m_{FP} mus satisfy the Higuchi bound (2.84). In addition, the spin-2 mass is limited by the cutoff of the effective theory. Otherwise, the low-energy effective theory is not meaningful. The cutoff depends on the spin-2 mass, but is limited from above by the Planck mass M_{g}. Therefore, we choose the following flat prior on the spin-2 mass:

$$p(\theta) = \begin{cases} 1\,, & \text{if} \quad 2\Lambda/3 < m_{\mathrm{FP}}^2 < M_{\mathrm{g}}^2 \\ 0\,, & \text{else} \end{cases} . \tag{6.14}$$

In terms of the energy density parameter, the upper limit reads $\Omega_{\mathrm{FP}} \lesssim 10^{122}$. The coupling $\bar{\alpha}$ is not restricted by theoretical bound, but can take values from $0 \leq \bar{\alpha} \leq \infty$. To ensure numerical stability, we choose the following flat priors:

$$p(\theta) = \begin{cases} 1\,, & \text{if} \quad -100 < \log_{10}(\bar{\alpha}) < 100 \\ 0\,, & \text{else} \end{cases} . \tag{6.15}$$

The upper limit is justified because we do not expect the massive gravity limit to be cosmologically consistent [210]. In the parameter region $\bar{\alpha} \ll 1$, bimetric theory is arbitrarily close to GR. Therefore, at the lower limit on $\bar{\alpha}$ our cosmological model is indistinguishable from the standard model in any practical sense.

In addition to these limiting values, the physical parameters are subject to the theoretical consistency conditions, which we computed in Chapter 4 and summarised in Table 4.2. We set the priors such that $p(\theta) = 0$ if the physical parameters in θ violate the consistency conditions and $p(\theta) = 1$ if the conditions are satisfied.

[4]For some bimetric models and data sets, the parameter vector is shorter. The β_1–model does not contain the parameters $\log_{10}(\bar{\alpha})$ and $\log_{10}(\Omega_{\mathrm{FP}})$. The two–parameter models do not contain the parameter $\log_{10}(\bar{\alpha})$. In addition, the parameters $\Omega_{\mathrm{b0}}h^2$ and H_0 are irrelevant in the context of SN1a.

From these parameters, we can obtain the value of Ω_{m0} following the procedure outlined in the previous section. We implement the required positivity of this quantity as additional prior in the following way

$$p(\theta) = \begin{cases} 1\,, & \text{if} \quad \Omega_{\mathrm{m0}} > 0 \\ 0\,, & \text{else} \end{cases} \,. \tag{6.16}$$

This completes our list of priors.

As a final step, we discuss a possibility to compare the different cosmological models. We use the Bayesian Information Criterion (BIC) [359]

$$\mathrm{BIC} = \chi^2 + k \ln N \,, \tag{6.17}$$

where $\chi^2 = -2 \ln \mathcal{L}$ is evaluated at maximum likelihood. The parameter k describes the number of independent model parameters and N the number of data points. The combined data set SN+BAO+CMB has $N = 740 + 3 + 10 = 753$ data points, as will be explained in the next section. From Eq. (6.12) it follows that the number of independent model parameters is given by $k = 3 + \hat{k}$, where $\hat{k}$ describes the number of free physical parameters. So the one-parameter model has $\hat{k} = 1$, the two-parameter models have $\hat{k} = 2$, and the three-parameter models have $\hat{k} = 3$. For model comparison, we use the ΛCDM model as reference. The difference in the BIC, which we denote as ΔBIC, allows to assess wether a model is statistically preferred over the ΛCDM model according to [297, 360]: strong support ($\Delta\mathrm{BIC} < -12$), favourable ($\Delta\mathrm{BIC} < -6$), inconclusive ($\Delta\mathrm{BIC} < 6$), disfavoured ($\Delta\mathrm{BIC} < 12$), strongly disfavoured ($\Delta\mathrm{BIC} \geq 12$).

6.1.3 Data sets

Due to the gradient instability, we are limited to probes of the cosmic expansion history. These rely on measuring certain distance scales and redshifts in the universe. In the following, we provide a succinct summary required for implementing the data sets. More details can be found in the standard textbooks on cosmology such as [61–64].

The co-moving distance as a function of redshift is given by

$$d_{\mathrm{c}}(z) = \int_0^z \frac{\mathrm{d}z'}{H(z')} \,. \tag{6.18}$$

For convenience, we also define the dimensionless co-moving distance as

$$D_{\mathrm{c}}(z) = H_0 d_{\mathrm{c}}(z) = \int_0^z \frac{\mathrm{d}z'}{E(z')} \,. \tag{6.19}$$

Taking into account spatial curvature k amounts to define the following quantity:

$$\mathcal{I}_k(D_{\mathrm{c}}(z)) = \begin{cases} \sqrt{\Omega_{\mathrm{k0}}}^{-1} \sinh\left(\sqrt{\Omega_{\mathrm{k0}}}\, D_{\mathrm{c}}(z)\right) \,, & k < 0 \\ D_{\mathrm{c}}(z) \,, & k = 0 \\ \sqrt{\Omega_{\mathrm{k0}}}^{-1} \sin\left(\sqrt{\Omega_{\mathrm{k0}}}\, D_{\mathrm{c}}(z)\right) \,, & k > 0 \end{cases} \tag{6.20}$$

From these quantities we can define various distance indicators, which are relevant in cosmology. The luminosity distance d_{L} and the angular diameter distance d_{A} are given by

$$d_{\mathrm{L}}(z) = \frac{1}{H_0}(1+z)\,\mathcal{I}_k(D_{\mathrm{c}}(z)) \,, \quad d_{\mathrm{A}}(z) = \frac{1}{H_0}(1+z)^{-1}\mathcal{I}_k(D_{\mathrm{c}}(z)) \,. \tag{6.21}$$

We can define the corresponding dimensionless distances as $D_{\mathrm{L}} = H_0 d_{\mathrm{L}}$ and $D_{\mathrm{A}} = H_0 d_{\mathrm{A}}$. These distance indicators are the basis for the cosmological data sets, which we introduce in the following.

As will be detailed later, these measured distances are to be compared to the co-moving sound horizon $r_{\mathrm{s}}(z)$ at different redshifts z. It is given by the formula

$$r_{\mathrm{s}}(z) = \frac{1}{\sqrt{3}} \int_z^\infty \frac{\mathrm{d}z'}{H(z')\sqrt{1 + (3\Omega_{\mathrm{b0}}/4\Omega_{\gamma 0})/(1+z')}} \,, \tag{6.22}$$

where $\Omega_{\rm b0}$ and $\Omega_{\gamma 0}$ are the current energy densities of baryons and photons, respectively. We treat $\Omega_{\rm b0}h^2$ as fitting parameter in our statistical analysis. The energy density of photons is fixed by the CMB temperature $T_{\rm CMB} = 2.7255\,{\rm K}$ [361] as

$$\frac{3}{4\Omega_{\gamma 0}h^2} = 3.15 \times 10^4 \times \left(T_{\rm CMB}/2.7\,{\rm K}\right)^{-4} . \tag{6.23}$$

Going further, determining the sound horizon $r_{\rm s}(z)$ relies on $H(z)$, which in turn depends on the energy density of all radiation $\Omega_{\rm r}$. Since neutrinos are relativistic during these early times, they contribute to radiation. The relation between the photon and radiation energy densities can be written as

$$\Omega_{\rm r0} = (1 + 0.2271 N_{\rm eff})\Omega_{\gamma 0} . \tag{6.24}$$

The numerical prefactor captures the relative temperatures of the neutrino and photon backgrounds as well as the relative amount of free energy per fermionic and bosonic degree of freedom. The parameter $N_{\rm eff}$ denotes the effective number of relativistic neutrino species [362, 363]. In our analysis we use the standard value of $N_{\rm eff} = 3.046$ obtained from particle physics [364–366]. Note that this value is slightly larger than 3 due to radiative corrections.

Supernovae type 1a

It is believed that the (properly calibrated) luminosities of Supernovae type 1a (SNe 1a) are independent of redshift, which allows to calibrate cosmological distances. In 1998, their observation showed that our Universe currently enters a phase of accelerated expansion and therefore provided the first robust evidence for dark energy [17, 18].

The apparent magnitude m and the absolute magnitude M of a SN1a are related to the luminosity distance as

$$m = \mathcal{M} + 5\log_{10} D_{\rm L} , \tag{6.25}$$

with $\mathcal{M} = 25 + M - 5\log_{10}(H_0)$. The parameters M and H_0 are degenerate because both appear as additive parameters in the above equation.

In our analysis, we use the catalogue of the Joint–Lightcurve–Analysis (JLA) containing 740 SN1a events [367]. As mentioned before, we need to calibrate the observed apparent magnitude $m_{\rm obs}$ in the following way:

$$m = m_{\rm obs} - \Delta_{\rm M} + \alpha X_1 - \beta C , \tag{6.26}$$

where X_1 and C are measured light-curve parameters of each SN1a. For the fiiting parameters α, β and $\Delta_{\rm M}$ we use the best-fit values of $\alpha = 0.140 \pm .006$ and $\beta = 3.139 \pm 0.072$ as obtained in [367]. The parameter $\Delta_{\rm M}$ is a correction to the absolute magnitude, which depends on the stellar mass M_* of the host galaxy of the supernova. Using a simple step-function, the best fit-value is given by

$$\Delta_{\rm M} = \begin{cases} -0.060 \pm 0.012 , & \text{if } M_* < 10^{10} M_\odot \\ 0 , & \text{else} \end{cases} , \tag{6.27}$$

with $M_\odot$ the solar mass.

With these ingredients we can construct the likelihood $\mathcal{L}_{\rm SN1a}$. The parameter $\mathcal{M}$ appears as a nuisance parameter. Analytically marginalising over $\mathcal{M}$ yields

$$-2\log\mathcal{L}_{\rm SN1a}(\theta) = S_2 - \frac{S_1^2}{S_0} \tag{6.28}$$

where

$$S_0 = \sum_{ij}(C^{-1}_{\rm SN1a})_{ij} , \quad S_1 = \sum_{ij}(C^{-1}_{\rm SN1a})_{ij} X_i , \quad S_2 = \sum_{ij}(C^{-1}_{\rm SN1a})_{ij} X_i X_j \tag{6.29}$$

in terms of the vector $X = m - 5\log_{10} D_{\rm L}$. The components of the covariance matrix $C_{\rm SN1a}$ are given in [367], to which we add the errors on α, β, and $\Delta_{\rm M}$ in quadrature.

Cosmic Microwave Background

Despite the importance of SN1a data, they are not very restrictive for cosmological models that allow for non-zero spatial curvature and that include dark energy with a time-varying equation-of-state parameter $w_{\rm de}$. Including the distance scale from the Cosmic Microwave Background (CMB) as additional information strengthens the constraints. Instead of analysing the full CMB power spectrum, it is a common approach to cast this information in the form of two distance scale ratios [368–374]. For an introduction to CMB physics, see [375].

The first ratio is related to the first peak in the CMB power spectrum and given by [368]

$$\ell_{\rm A} = (1+z_*)\frac{\pi d_{\rm A}(z_*)}{r_{\rm s}(z_*)}\,. \tag{6.30}$$

It measures the ratio between the angular diameter distance of the first peak $d_{\rm A}(z_*)$ and the sound horizon $r_{\rm s}(z_*)$, both evaluated at photon decoupling z_*.

The second parameter measures the ratio between the angular diameter distance and the Hubble horizon at decoupling and is implemented by the shift-parameter[5] [369]

$$\mathcal{R} = \frac{d_{\rm A}(z_*)H(z_*)}{\sqrt{1+z_*}} \simeq H_0\sqrt{\Omega_{\rm m0}}(1+z_*)d_{\rm A}(z_*)\,. \tag{6.31}$$

It is assumed that the universe is dominated by matter during photon decoupling.

At the epoch of recombination, the ionised material in the cosmic plasma combines into neutral atoms. During this epoch, the photons decouple and the universe becomes transparent for photons. The redshift of photon decoupling z_* can be obtained from the fitting function [368]:

$$z_* = 1048\left[1+0.00124\,(\Omega_{\rm b0}h^2)^{-0.738}\right]\left[1+g_1(\Omega_{\rm m0}h^2)^{g_2}\right], \tag{6.32}$$

$$g_1 = \frac{0.0783\,(\Omega_{\rm b0}h^2)^{-0.238}}{1+39.5\,(\Omega_{\rm b0}h^2)^{0.763}}\,, \quad g_2 = \frac{0.560}{1+21.1\,(\Omega_{\rm b0}h^2)^{1.81}}\,. \tag{6.33}$$

For our analysis, we assume that the early-universe is not modified as compared to the standard model. This assumption is justified because the dark energy density is subdominant compared to the other energy densities on the finite branch, as we discussed in Section 3.1. In addition, we expect the Vainshtein screening mechanism to be active in the early universe as discussed in Chapter 5. We also assume inflation to work as in the standard model. For a critical discussion of the usage of the shift parameters in the context of non-standard cosmological models, see e.g. [299, 373].

We follow the procedure of [374] and implement the CMB information in the three variables $(\ell_{\rm A},\,\mathcal{R},\,\Omega_{\rm b0}h^2)$. From the Planck 2018 data release [75], the best-fit values for these parameters are [376]

$$\ell_{\rm A} = 301.471^{+0.089}_{-0.090}\,, \quad \mathcal{R} = 1.7502 \pm 0.0046\,, \quad \Omega_{\rm b0}h^2 = 0.02236 \pm 0.00015\,. \tag{6.34}$$

In our analysis, we use the full covariance matrix $C_{\rm CMB}$, which can be found in [376]. Defining the vector

$$X_{\rm CMB} = \begin{pmatrix} \ell_{\rm A} - 301.471 \\ \mathcal{R} - 1.7502 \\ \Omega_{\rm b0}h^2 - 0.02236 \end{pmatrix} \tag{6.35}$$

amounts to writing the likelihood as

$$-2\log\mathcal{L}_{\rm CMB} = X_{\rm CMB}^{\rm T} C_{\rm CMB}^{-1} X_{\rm CMB}\,. \tag{6.36}$$

[5] The here defined shift-parameter $\mathcal{R}$ is not to be confused with the scalar curvature, which appears in the Einstein–Hilbert term of the actions.

Data set	$z_{\rm eff}$	Distance measure
6dFGS [377]	0.106	$d_{\rm V}/r_{\rm d} = 2.976 \pm 0.133$
SDSS MGS [378]	0.15	$d_{\rm V}/r_{\rm d} = 4.466 \pm 0.168$
BOSS DR12 [379]	0.38	$d_{\rm M}/r_{\rm d} = 0.27 \pm 0.15$
	0.51	$d_{\rm M}/r_{\rm d} = 13.38 \pm 0.18$
	0.61	$d_{\rm M}/r_{\rm d} = 15.45 \pm 0.22$
BOSS DR14 [380]	0.72	$d_{\rm V}/r_{\rm d} = 16.08 \pm 0.41$
eBOSS QSO [381]	0.978	$d_{\rm A}/r_{\rm d} = 10.7 \pm 1.9$
	1.23	$d_{\rm A}/r_{\rm d} = 12.0 \pm 1.1$
	1.526	$d_{\rm A}/r_{\rm d} = 11.97 \pm 0.65$
	1.944	$d_{\rm A}/r_{\rm d} = 12.23 \pm 0.99$

Table 6.1: The BAO data sets that we used in our analysis. Here $r_{\rm d} = r_{\rm s}(z_{\rm d})$. The covariance matrices can be found in the original references.

Baryonic Acoustic Oscillations

The CMB anisotropies are imprinted in the distribution of matter at low redshifts. The Baryonic Acoustic Oscillations (BAOs) measure the ratio between certain angular diameter distances (the precise relation to $d_{\rm A}$ depends on the data set) to the sound horizon $r_{\rm s}(z_{\rm d})$ at the drag epoch $z_{\rm d}$. BAOs serve as standard rulers, which have become a powerful tool for constraining cosmological models.

Before the epoch of recombination, the radiation pressure drives baryonic material away from potential wells. At recombination, the ionised material combines such that baryons and photons decouple. After recombination, the motion of the baryonic material still continues for a short while due to its momentum, until the so-called drag epoch, at which time the acoustic oscillations of the baryonic material are frozen in. The scale of BAOs is hence related to the sound horizon $r_{\rm s}(z_{\rm d})$ at the drag epoch $z_{\rm d}$. The redshift of the drag epoch $z_{\rm d}$ can be obtained from the fitting formula [368]

$$\begin{aligned} z_{\rm d} &= \frac{1351\,(\Omega_{\rm m0}h^2)^{0.251}}{1+0.659\,(\Omega_{\rm m0}h^2)^{0.828}}\big[1+b_1(\Omega_{\rm b0}h^2)^{b_2}\big]\,, \\ b_1 &= 0.313\,(\Omega_{\rm m0}h^2)^{-0.419}\big[1+0.607\,(\Omega_{\rm m0}h^2)^{0.674}\big]\,, \quad b_2 = 0.238\,(\Omega_{\rm m0}h^2)^{0.223}\,. \end{aligned} \tag{6.37}$$

As in the case of the CMB anisotropies, also in the context of BAOs distances related to the angular diameter at a given redshift are measured. Depending on the data set, the volume averaged distance $d_{\rm V}$ or the redshift-weighted co-moving distance $d_{\rm M}$ are constrained, which are related to the angular diameter distance $d_{\rm A}$ as

$$d_{\rm V}(z) = \Big[\frac{z}{H(z)}(1+z)^2 d_{\rm A}^2(z)\Big]^{1/3}\,, \quad d_{\rm M}(z) = (1+z)d_{\rm A}(z)\,, \tag{6.38}$$

respectively. As before, we also define the dimensionless analogues $D_{\rm V} = H_0 d_{\rm V}$ and $D_{\rm M} = H_0 d_{\rm M}$.

We use several data sets in the context of BAOs with 10 data points in total, which we summarise in Table 6.1. The likelihood associated to BAO measurements is the product of the likelihoods obtained from the individual data sets, i.e.

$$-2\log\mathcal{L}_{\rm BAO} = \sum_a \chi_a^2\,, \tag{6.39}$$

Model	β_0 (ΛCDM)	β_1	$\beta_0\beta_1$	$\beta_1\beta_{2,3,4}$
$\bar{\alpha}$	–	$3^{-1/2}$	< 0.2	< 0.016
$m_{\rm FP}$ $[10^{-32}\text{eV}]$	–	1.82 ± 0.02	1.33 ± 0.02	> 42.4
Λ $[10^{-64}\text{eV}^2]$	1.76 ± 0.05	2.5 ± 0.1	1.8 ± 0.1	$1.76^{+0.1}_{-0.09}$
H_0 $[\frac{\text{km/s}}{\text{Mpc}}]$	$68.8^{+1.4}_{-1.2}$	$73.1^{+1.6}_{-1.4}$	68.8 ± 0.2	69.0 ± 1.0
Ω_Λ	0.69 ± 0.01	0.86 ± 0.01	$0.69^{+0.03}_{-0.02}$	0.69 ± 0.01
$\Omega_{\rm m0}$	0.31 ± 0.01	0.27 ± 0.01	0.31 ± 0.02	0.31 ± 0.01
$\Omega_{\rm de0}$	0.69 ± 0.01	0.73 ± 0.01	0.69 ± 0.02	0.69 ± 0.01
$\Omega_{\rm k0}$	$0.002^{+0.004}_{-0.003}$	$-0.007^{+0.004}_{-0.003}$	$0.002^{+0.005}_{-0.001}$	0.002 ± 0.004
$\Omega_{\rm b0}h^2$	0.0224 ± 0.0001	0.0223 ± 0.0003	0.0224 ± 0.0004	0.0224 ± 0.0003
χ^2	694.7	726.0	694.7	694.7
ΔBIC	(721)	+31	+6.6	+6.6

Table 6.2: The best-fit values and errors at 68% c.l. from SN+CMB+BAO for the one- and two-parameter models.

where the index a runs over the individual data sets: 6dFGS [377], SDSS MGS [378], BOSS DR12 [379], BOSS DR14 [380], and eBOSS QSO [381]. The individual χ^2_a are computed in the usual way as in Eq. (6.11), with errors and covariance matrices given in the original references.

6.1.4 Numerical implementation

To perform the statistical analysis, we wrote a new computer code in `Python`, which we plan to make publicly available soon. For a given set of parameters the code computes the prior probability. If the prior probability is non-zero, the code numerically constructs the Hubble rate upon a list of redshifts as described in Section 6.1.1, from where the various distance indicators are computed. The result together with the aforementioned observational data is used to compute the value of χ^2 for the given set of parameters.

The resulting value of χ^2 is used to construct the Monte Carlo Markov Chains. To initialise the chains, we randomly choose a set of fitting parameters. For each data set, we run several chains in parallel, each with a length of $\mathcal{O}(10^4 \dots 10^5)$, depending on the model and data set.

Before analysing the results, we assess the compatibility of the individual chains and remove $\mathcal{O}(10^3)$ steps as burn-in. For the analysis we acknowledge the intensive use of the `Getdist` package [382], which we also used to produce most of the subsequent figures.

6.1.5 Results

Let us present and discuss the results of the statistical analysis separately for each bimetric model. The standard ΛCDM model serves as a reference, to which we compare the bimetric models and from which we assess the robustness of our statistical analysis.

The best-fit values for all models are summarised in Tables 6.2 to 6.4. The parameters $m_{\rm FP}$ and Λ are derived from $\Omega_{\rm FP}$ and Ω_Λ using the values of H_0 in the chains.

ΛCDM reference model

Let us start with the ΛCDM model as reference, which corresponds to the β_0–model from the bimetric perspective. The one- and two-dimensional posterior distributions are presented in Fig. 6.1a. For this model, dark energy is solely composed out of vacuum energy, i.e. $\Omega_{\rm de0} = \Omega_\Lambda$.

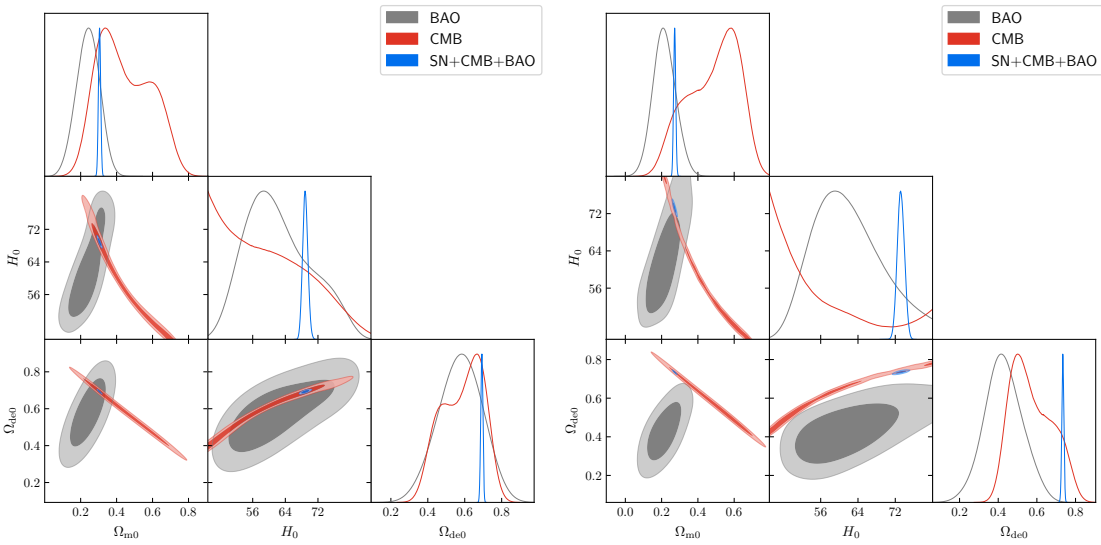

(a) The standard ΛCDM model as reference

(b) The β_1–model

Figure 6.1: The one- and two-dimensional posterior distributions with contours corresponding to 68% and 95% c.l. for the one-parameter models taken from [298].

The Fig. 6.1a suggests that the data sets do not constrain the cosmological parameters individually. While SN1a do not constrain the Hubble parameter H_0 as explained earlier, also CMB and BAO data alone are not constraining when allowing for non-zero spatial curvature. The degeneracy is broken when combining all three data sets. We then get a spatially flat universe within 68% c.l. in agreement with earlier results [75]. The Hubble parameter is stabilised to a value of $H_0 = (68.9^{+1.4}_{-1.2})\,\frac{\mathrm{km/s}}{\mathrm{Mpc}}$. This value is slightly but not significantly larger than the reported value in [75], which can be understood as an artefact of using the distance scale ratios instead of the full CMB likelihood [376]. Since our analysis reproduces the standard results without significant deviations, we conclude that our analysis is robust.

As mentioned in Table 6.2, the maximum likelihood leads to BIC = 721 given the number of data points and free parameters. This value serves as reference, to which we compare the bimetric models.

β_1–model

The only bimetric one-parameter model with a possibly viable cosmic expansion history is the β_1–model. The marginalised one- and two-dimensional distributions are presented in Fig. 6.1b and the best-fit values are summarised in Table 6.2.

As in the case of the standard model, CMB and BAO data alone are not able to stabilise the values of H_0 and Ω_{k0}. In addition, the data sets appear to be incompatible in the following sense. The best-fit values with respect to one data set are in conflict with the other data sets by several standard deviations. Quantitatively, this is reflected by the rather small likelihood with $\chi^2 \simeq 726$, when combining all three data sets, which leads to a substantially larger BIC with $\Delta\mathrm{BIC} \simeq +31$. Therefore, the β_1–model is statistically strongly disfavoured by cosmological data.

Despite this inconsistency, we combine all three data sets to compute the global constraints on the parameters within this model. Data then prefers positive spatial curvature, with a spatially flat universe included at 95% c.l.

The Hubble parameter is stabilised at the remarkably high value of $H_0 = (73.1^{+1.6}_{-1.4})\,\frac{\mathrm{km/s}}{\mathrm{Mpc}}$, which is in agreement within 68% c.l. with local determinations of H_0 as reviewed in Section 1.3. In other words, the Hubble-tension is absent in the β_1–model. Note that we did not use any

local prior in our analysis. Nonetheless, the β_1–model does not solve the H_0–tension because the cosmological data sets are in disagreement.

The β_1–model does not have a smooth GR-limit because the coupling constant is fixed by the equations of motion as $\bar{\alpha} = 1/\sqrt{3}$. This is also reflected in the cosmological parameters. The current dark energy fraction $\Omega_{\rm de0} = 0.73 \pm 0.01$ is significantly smaller than the effective cosmological constant $\Omega_\Lambda = 0.86 \pm 0.01$. Note that the β_1–model is self-accelerating. This leads to a smaller matter fraction $\Omega_{\rm m0} = 0.27 \pm 0.01$ as compared to the standard model value.

Finally, the combined data sets lead to a preferred spin-2 mass of $m_{\rm FP} = (1.82 \pm 0.02) \times 10^{-32}\,\text{eV}$, which lies close to the Higuchi bound. Since the value of the coupling is theoretically predicted to be $\bar{\alpha} = 1/\sqrt{3}$, we can easily compare these results to constraints from local tests of gravity.

$\beta_0\beta_1$–model

Moving to two-parameter models, we start with the $\beta_0\beta_1$–model, which allows for non-zero vacuum energy. The GR-limit $\bar{\alpha} \ll 1$ corresponds to $m_{\rm FP}^2 \simeq \Lambda$ in contrast to the other two-parameter models, which leads to substantially different observational constraints on the parameters. The best-fit values obtained from the combined data sets SN+BAO+CMB are summarised in Table 6.2. Selected one- and two-dimensional posterior distributions are presented in Fig. 6.2.

In contrast to the previous model, the data sets are compatible because the contour regions are overlapping. Quantitatively, this is reflected by a likelihood with $\chi^2 \simeq 694.7$ that coincides with the value in the ΛCDM model. That means that the model fits the cosmological data as good as the standard model. However, the higher number of free parameters is penalised by a higher BIC with $\Delta\text{BIC} = +6.6$ statistically disfavouring the $\beta_0\beta_1$–model. Nonetheless in the following we discuss the results on the cosmological parameters.

While the individual data sets are not constraining, the combined data sets stabilise the parameter values. The universe is spatially flat within 95% c.l. and the Hubble parameter is favoured to be $H_0 = (68.8 \pm 0.2)\frac{\text{km/s}}{\text{Mpc}}$. The current dark energy fraction coincides with the effective cosmological constant, $\Omega_{\rm de0} \simeq \Omega_\Lambda$, such that the model is already in its de Sitter phase at present times. Summarising, all parameter values agree with the standard values implying that the $\beta_0\beta_1$–model is close to its GR-limit.

In the case of the $\beta_0\beta_1$–model, only two out of the three physical parameters are independent. The value of the effective cosmological constant is stabilised as described above, such that only one parameter remains. The spin-2 mass is constrained to be $m_{\rm FP} = (1.33 \pm 0.02) \times 10^{-32}\,\text{eV}$, which implies a value for the coupling of $\bar{\alpha} \lesssim 0.2$ given the value of Λ.

$\beta_1\beta_n$–models

The remaining two-parameter models share the property that the GR-limit $\bar{\alpha} \ll 1$ corresponds to the parametric limit $m_{\rm FP}^2 \gg \Lambda$. This allows to discuss the $\beta_1\beta_n$–models with $n = 2, 3, 4$ together. The constraints on the parameters are very similar as summarised in Table 6.2. Selected one- and two-dimensional posteriors are presented in Fig. 6.2b.

The models fit the cosmological data as well as the standard model because all models have the same maximal likelihood with $\chi^2 = 694.7$. The $\beta_1\beta_n$–model have one additional free parameter as compared to the standard model, which is reflected by the higher BIC value with $\Delta\text{BIC} \simeq +6.6$. Hence, these models are statistically disfavoured. This, however, is not the end of the story because these models are self–accelerating and hence theoretically favoured over the standard model.

The combined data sets constrain the values of the cosmological parameters to be very close to the standard model values as is summarised in Table 6.2.

As before these models have two free physical parameters. The effective cosmological constant is stabilised to $\Omega_\Lambda = 0.69 \pm 0.1$ such that only one parameter remains. The spin-2 mass is bounded only from below with $m_{\rm FP} \gtrsim 4.24 \times 10^{-32}\,\text{eV}$, which corresponds to an upper bound on the coupling of $\bar{\alpha} \lesssim 0.016$. Apart from these limiting values, the physical parameters are approximately related

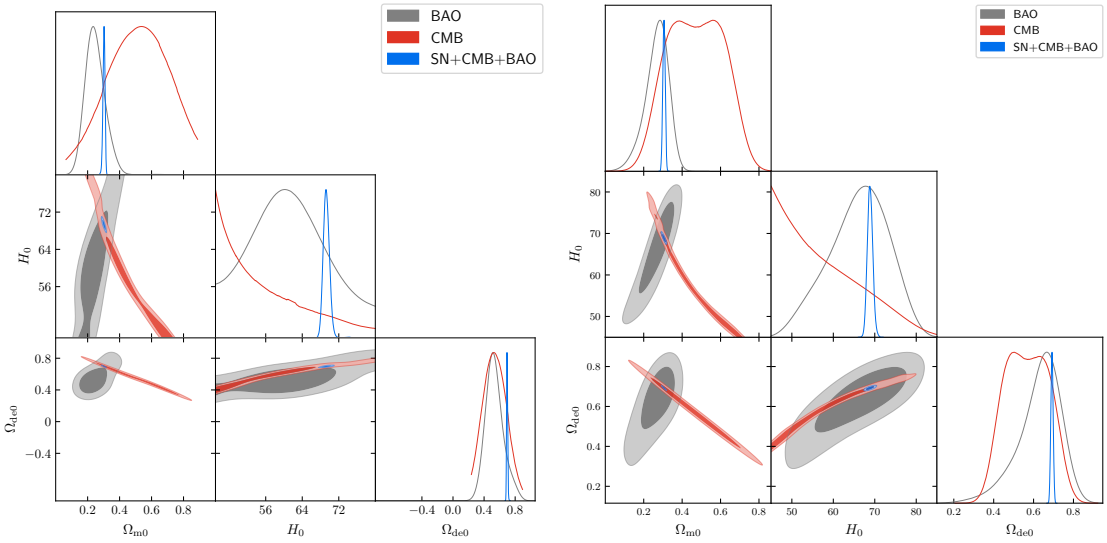

(a) The $\beta_0\beta_1$–model (b) The $\beta_1\beta_n$–models.

Figure 6.2: The one- and two-dimensional posterior distributions with contours corresponding to 68% and 95% c.l. for the two-parameter models taken from [298].

according to

$$\bar{\alpha}^2 \simeq \frac{12}{n}\frac{\Lambda}{m_{\rm FP}^2}\,, \tag{6.40}$$

in the limit $m_{\rm FP}^2 \gg \Lambda$ for the $\beta_1\beta_n$–models, which follows from combining Eqs. (4.15a), (4.18a) and (4.21a). All these models are therefore approaching their GR-limits.

$\beta_0\beta_1\beta_n$–models

We move on to the three-parameter models and start with those models that allow for non-vanishing vacuum energy, i.e. models that include the parameter β_0. Since the resulting constraints are very similar, we discuss all three models together. The best-fit values are summarised in Table 6.3.

The data sets are compatible for all the $\beta_0\beta_1\beta_n$–models with $n = 2, 3, 4$ as can be seen from Figs. 6.3a, 6.3b and 6.4a. The maximum likelihood is the same as for the standard model with $\chi^2 = 694.7$. That means that these models fit the cosmological data as good as the standard model. The two additional free parameters of these models are penalised by a higher BIC with $\Delta\text{BIC} \simeq +11.6$. These models are therefore statistically disfavoured compared to the standard model.

At the point of maximum likelihood, the cosmological parameters assume the same values as for the standard model. In particular we have $\Omega_{\rm de0} \simeq \Omega_\Lambda$ at the level of the errors. Therefore, the effect of dynamical dark energy reduces to a cosmological constant at present times.

In contrast to the previous models, all three physical parameters are independent. In the first three panels of Fig. 6.6 the two-dimensional posterior distributions at 95% c.l. are presented for the physical parameters $\bar{\alpha}$ and $m_{\rm FP}$. The figures indicate that a large portion of the physical parameter space is consistent with cosmological observations. In particular, for small values of the coupling $\bar{\alpha}$, the spin-2 mass $m_{\rm FP}$ is allowed to take large values.

The upper right region is excluded by our statistical analysis. To understand the reason, we study the value of β_0 in that region. The relations between the physical parameters and β_0, as

Model	$\beta_0\beta_1\beta_4$	$\beta_0\beta_1\beta_3$	$\beta_0\beta_1\beta_2$
$\bar{\alpha}$	< 0.14	< 0.03	< 0.06
$m_{\rm FP}$ [eV]	$> 1.01 \times 10^{-32}$	$> 1.17 \times 10^{-32}$	$> 1.08 \times 10^{-32}$
$\Lambda\,[10^{-64}\mathrm{eV}^2]$	$1.77^{+0.10}_{-0.09}$	1.77 ± 0.09	$1.77^{+0.10}_{-0.09}$
H_0 $[\frac{\mathrm{km/s}}{\mathrm{Mpc}}]$	$68.8^{+1.5}_{-1.3}$	$68.9^{+1.4}_{-1.3}$	$68.9^{+1.4}_{-1.3}$
Ω_Λ	$0.69^{+0.02}_{-0.01}$	$0.69^{+0.02}_{-0.01}$	$0.69^{+0.03}_{-0.01}$
$\Omega_{\rm m0}$	0.31 ± 0.01	0.30 ± 0.01	0.31 ± 0.01
$\Omega_{\rm de0}$	0.69 ± 0.01	0.69 ± 0.01	0.69 ± 0.01
$\Omega_{\rm k0}$	0.002 ± 0.004	$0.002^{+0.004}_{-0.003}$	$0.002^{+0.006}_{-0.001}$
$\Omega_{\rm b0}h^2$	0.0224 ± 0.0003	0.0224 ± 0.0003	0.0224 ± 0.0003
χ^2	694.7	694.7	694.7
ΔBIC	+11.6	+11.6	+11.6

Table 6.3: The best-fit values and errors at 68% c.l. from SN+CMB+BAO for the three-parameter models that allow for non-zero vacuum energy in the physical sector.

Model	$\beta_1\beta_2\beta_3$	$\beta_1\beta_2\beta_4$	$\beta_1\beta_3\beta_4$
$\bar{\alpha}$	< 0.004	< 0.01	< 0.002
$m_{\rm FP}$ [eV]	$> 1.10 \times 10^{-32}$	$> 1.15 \times 10^{-32}$	$> 1.10 \times 10^{-32}$
$\Lambda\,[10^{-64}\mathrm{eV}^2]$	$1.78^{+0.09}_{-0.1}$	1.77 ± 0.09	$1.77^{+0.10}_{-0.09}$
H_0 $[\frac{\mathrm{km/s}}{\mathrm{Mpc}}]$	$68.9^{+1.4}_{-1.3}$	$69.0^{+1.3}_{-1.2}$	$68.9^{+1.4}_{-1.3}$
Ω_Λ	0.69 ± 0.01	0.69 ± 0.01	0.69 ± 0.01
$\Omega_{\rm m0}$	0.31 ± 0.01	0.30 ± 0.01	0.31 ± 0.01
$\Omega_{\rm de0}$	0.69 ± 0.01	0.69 ± 0.01	0.69 ± 0.01
$\Omega_{\rm k0}$	0.002 ± 0.004	$0.0023^{+0.0003}_{-0.004}$	0.002 ± 0.003
$\Omega_{\rm b0}h^2$	0.0224 ± 0.0003	0.0224 ± 0.0003	0.0224 ± 0.0003
χ^2	694.7	694.7	694.7
ΔBIC	+11.6	+11.6	+11.6

Table 6.4: The best-fit values and errors at 68% c.l. from SN+CMB+BAO for the self-accelerating three-parameter models.

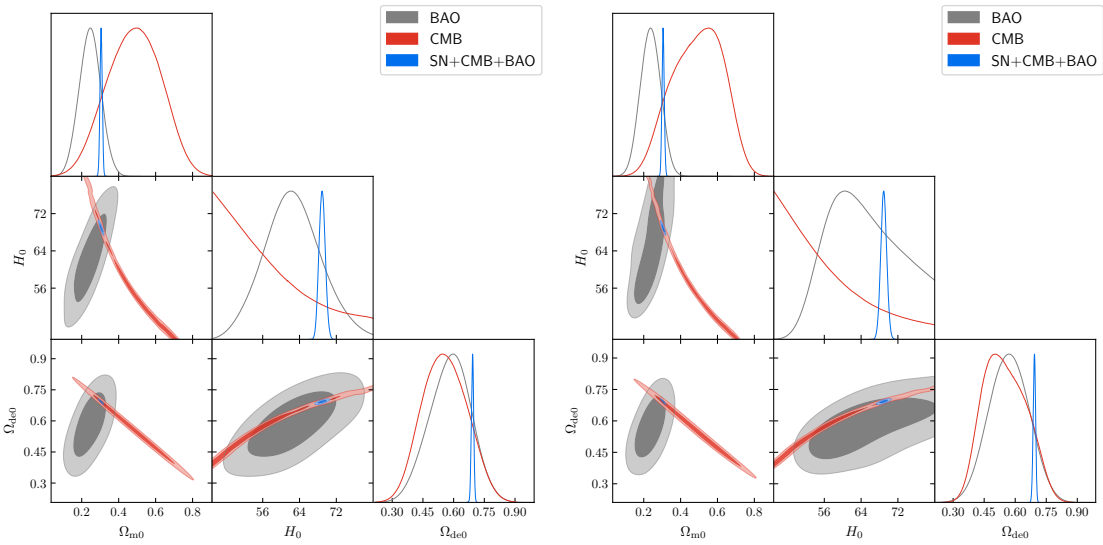

(a) $\beta_0\beta_1\beta_2$–model (b) $\beta_0\beta_1\beta_3$–model

Figure 6.3: Selected one- and two-dimensional posteriors corresponding to 68% and 95% c.l. for the three-parameter models taken from [298].

presented in Section 4.3.3, can be summarised as

$$\beta_0 = -\frac{12}{n}\frac{\bar{\alpha}^2}{1+\bar{\alpha}^2}m_{\rm FP}^2 + \left[1+(2^{4-n}-1)\bar{\alpha}^2\right]\Lambda \tag{6.41}$$

for the $\beta_0\beta_1\beta_n$–model. So for a spin-2 mass sufficiently larger than the cosmological constant, we have that $\beta_0 < 0$. That means, data does not accept large negative values of β_0. In other words, $\rho_{\rm de}$ is allowed to change its sign only at sufficiently large redshifts. For a large spin-2 mass this can be achieved by a correspondingly small value of $\bar{\alpha}$.

The shape of the contour corresponding to 95% c.l. can be cast into two regimes. For small spin-2 masses, the constraint on the coupling becomes independent of the spin-2 mass. Here, the coupling is constrained to be $\bar{\alpha} \lesssim \mathcal{O}(0.01-0.1)$, see Table 6.3 for the exact values for each model. For larger spin-2 masses, the coupling $\bar{\alpha}$ must be sufficiently small. To quantify the relation, we perform a polynomial fit to the contour line of the form

$$\bar{\alpha}^{c_1} m_{\rm FP} = 10^{-c_2}\,{\rm eV}\,. \tag{6.42}$$

The results on the constants c_1 and c_2 for the three-parameter models can be found in Table 6.5.

$\beta_1\beta_2\beta_3$– and $\beta_1\beta_n\beta_4$–models

We finish with the results for the self-accelerating three-parameter models. The constraints on the parameters are very similar among these models and summarised in Table 6.4.

From Figs. 6.4b, 6.5a and 6.5b we can infer that the cosmological data sets are compatible for all three models. The maximum likelihoods with a value of $\chi^2 = 694.7$ indicate that these models fit the data as good as the standard model. Nonetheless, these models are statistically disfavoured due to the additional free parameters, as reflected by the higher BIC with $\Delta{\rm BIC} \simeq +11.6$. However, these models are theoretically preferred because these accomodate late-time acceleration without vacuum energy.

The cosmological parameters are preferred to take values very close to the standard values as summarised in Table 6.4. In particular we have $\Omega_{\rm de0} \simeq \Omega_\Lambda$. This implies that the effect of dynamical dark energy reduces to a cosmological constant at present times.

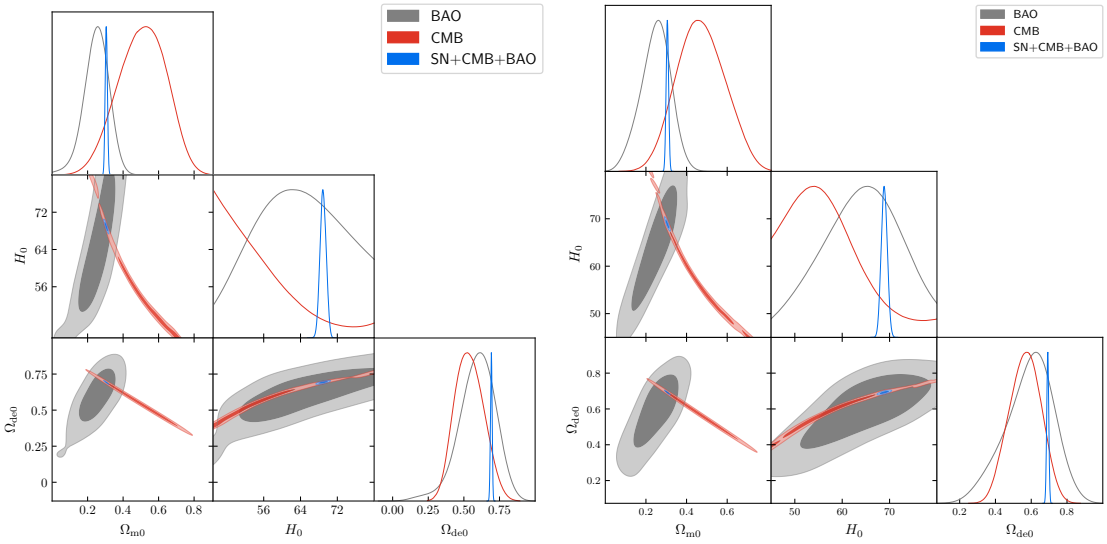

(a) $\beta_0\beta_1\beta_4$–model (b) $\beta_1\beta_2\beta_3$–model

Figure 6.4: Selected one- and two-dimensional posteriors corresponding to 68% and 95% c.l. for the three-parameter models taken from [298].

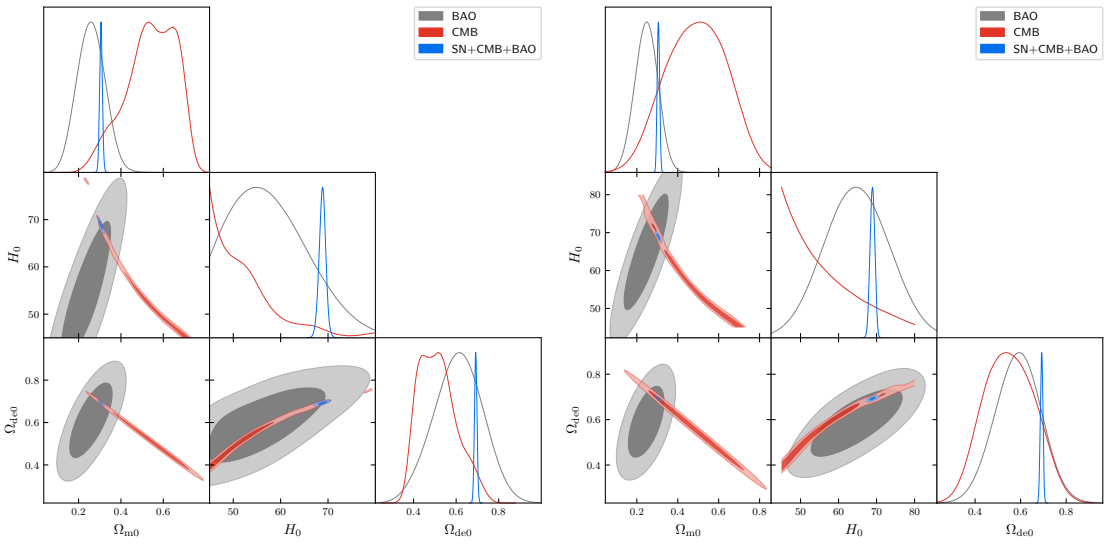

(a) $\beta_1\beta_2\beta_4$–model (b) $\beta_1\beta_3\beta_4$–model

Figure 6.5: Selected one- and two-dimensional posteriors corresponding to 68% and 95% c.l. for the three-parameter models taken from [298].

Model	c_1	c_2
$\beta_0\beta_1\beta_2$	0.964 ± 0.006	24.6 ± 0.2
$\beta_0\beta_1\beta_3$	1.117 ± 0.006	32.9 ± 0.2
$\beta_0\beta_1\beta_4$	0.97 ± 0.01	23.6 ± 0.4
$\beta_1\beta_2\beta_3$	1.047 ± 0.007	35.5 ± 0.2
$\beta_1\beta_2\beta_4$	1.021 ± 0.006	32.7 ± 0.2
$\beta_1\beta_3\beta_4$	0.959 ± 0.008	32.7 ± 0.3

Table 6.5: The best-fit values and errors corresponding to 68% c.l. of the coefficients appearing in the fitting formula (6.42).

The constraints at 95% c.l. on the physical parameters $\bar{\alpha}$ and $m_{\rm FP}$ are visualised in the last three panels of Fig. 6.6, which unveil that a large portion of the physical parameter space is compatible with cosmological observations. In particular, even a large spin-2 mass is consistent with data, if the coupling $\bar{\alpha}$ is sufficiently small. As before, the upper right region is excluded. The reason in the case of the self-accelerating models are the theoretical consistency conditions, which we discussed in Section 4.3.3 and used as theoretical priors in our statistical analysis.

The contour lines corresponding to 95% c.l. in the $\bar{\alpha} - m_{\rm FP}$-plane has a similar shape as for the previous three-parameter models. To quantify the constraints on the physical parameters, we perform a polynomial fit as in Eq. (6.42). The results on the parameters are presented in Table 6.5.

Summary

We confronted all submodels of bimetric theory with up to three free interaction parameters β_n with cosmological observations. Utilising the physical parametrisation, which we introduced in Chapter 4, we computed constraints on the physical parameters $\bar{\alpha}$ and $m_{\rm FP}$ from cosmological data for the first time.

All models (except the β_1–model) fit the data as good as the standard ΛCDM model. The cosmological parameters are preferred to take values that coincide with the standard model values given the current precision. In particular, data favours a spatially flat universe also within bimetric cosmology. In contrast to the two- and three-parameter models, the data sets appear to be inconsistent for the β_1–model, which is reflected by a larger value of χ^2 at the best-fit point when combining the data sets. This statistically rules out the β_1–model.

The constraints on the physical parameters $\bar{\alpha}$ and $m_{\rm FP}$ depend on the bimetric model. As a summary, the coupling is forced to be sufficiently small, $\bar{\alpha} \ll \mathcal{O}(0.1)$, which means that data pushes the models towards their GR limits, but not entirely. The spin-2 mass $m_{\rm FP}$ is allowed to take arbitrarily large values, if the coupling is sufficiently small. Only for the $\beta_0\beta_1$–model, the spin-2 mass is constrained to be of the order of H_0.

As we review now, our results are in agreement with earlier results, whenever comparable. In [216] two classes of bimetric models were tested against cosmological observations: a model with $\beta_1 = 0$ for $\bar{\alpha} = 1$ and for $\bar{\alpha} = 3$ as well as a general model with $c = 1$ and the additional a priori assumption $\Omega_\Lambda = 0$. The former model does not give rise to a viable finite branch and is hence excluded from our analysis. The latter model is devoid of an effective cosmological constant and hence excluded by our analysis by many standard deviations. Unfortunately, the goodness of fit is not discussed in [216], so a comparison to our results and to the ΛCDM model is not possible.

Next, all bimetric models were tested with cosmological data in [263] in the parameter region where $\beta_n \sim H_0^2$ and assuming $\Omega_{\rm k0} = 0$. The resulting preferred values for the cosmological parameters are close the standard values given the level of accuracy. Since this reference took into account both the finite and infinite branch solution, it is not clear to which branch the best-fit point corresponds.

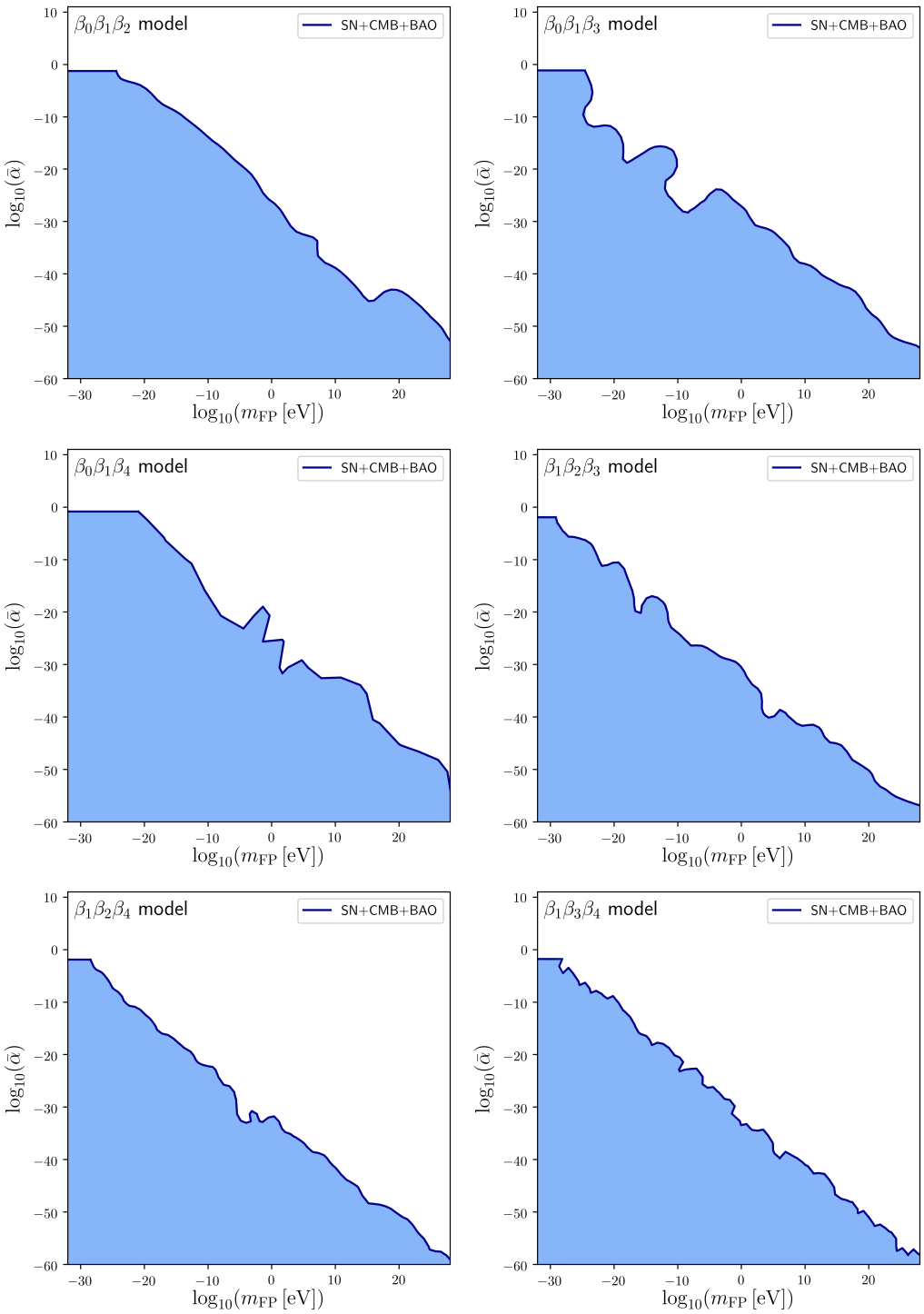

Figure 6.6: 95% c.l. inclusion plots for the three-parameter models from SN+CMB+BAO.

One- and two-parameter models, rescaled so that $\alpha = 1$, were tested against SN1a data in [265], distinguishing between the finite and infinite branch solution. On the finite branch solutions the statistically favoured values of the energy density parameters are close to the standard values given the accuracy, while the interaction parameters are of the order $\beta_n \sim H_0^2$.

Next, [337] tested the β_1– and the $\beta_1\beta_2$–models. They also find that the β_1–model fits the cosmological data poorly, while the $\beta_1\beta_2$–model is driven into its GR-limit, resulting in statistically favoured values of the cosmological parameters close to the standard value. The $\beta_0\beta_1$– and again the $\beta_1\beta_2$–model were tested in [296] with an emphasise on the Hubble tension. They find that both models are driven into their GR-limits. Both these studies allow for arbitrary values of the interaction parameters, but the resulting constraints on the physical parameters are not straightforward.

Finally, [297] tested the $\beta_1\beta_2\beta_3$–model against cosmological data[6] under the assumption of $\beta_n \sim H_0^2$. They allowed for non-zero spatial curvature for the first time in the context of bimetric cosmology. In agreement with our results, they find a clear preference for a spatially flat universe. Also the other cosmological parameters are favoured to take standard values on the level of present accuracy. Under the aforementioned assumption, also the corresponding observational constraints on the spin-2 mass are inferred.

While the aforementioned investigations and results are certainly consistent and interesting, the constraints on the bimetric parameters lack comparability. Our analysis does not only provide such comparability, but also represents the hitherto most comprehensive observational test of bimetric background cosmology of models with up to three parameters because we test the entire parameter space. In particular, our results represent the first thorough cosmological constraints on the spin-2 mass $m_{\rm FP}$ and its coupling constant $\bar{\alpha}$. This explicitly demonstrates that the entire theoretically consistent physical parameter space yields a good fit to the observed data, even if the spin-2 field is very heavy.

As next step, we derive constraints from local tests of gravity on these physical parameters. In Section 6.3 we will combine the various observational and theoretical constraints on the physical parameters.

6.2 Local tests

Modifications of the gravitational interactions are also manifest on other than cosmological scales. In this section, we put the observational limits inferred from local tests of gravity in the framework of bimetric theory. By local tests of gravity we mean tests of the gravitational interactions from laboratory and solar system scales to galactic and galaxy cluster scales. In our analysis, we use constraints from tests of the gravitational potential and from tests of the scalar curvature, which we discuss individually in the following. Reviews on current constraints and experimental methodologies can be found in [343–348], which form the basis of the following review.

6.2.1 Tests of the gravitational potential

We start with tests of the gravitational potential as felt by massive test bodies. Modifications are easiest understood for a spherically symmetric potential, as induced by the Sun or the Earth as central object. We provide some detail on how to obtain the constraint lines for the individual tests later.

In GR, the gravitational force is mediated by massless gravitons. This leads to the following gravitational potential

$$\Phi_{\rm GR}(r) = -\frac{1}{M_{\rm P}^2}\frac{1}{r} \tag{6.43}$$

induced by a point-like source and felt by a massive test body.

Modified gravity generically gives rise to a fifth force, which modifies the gravitational potential. These lead to an additional Yukawa-type contribution to the gravitational potential, if the

[6] In addition to SN1a, BAOs, and CMB they also included quasar data.

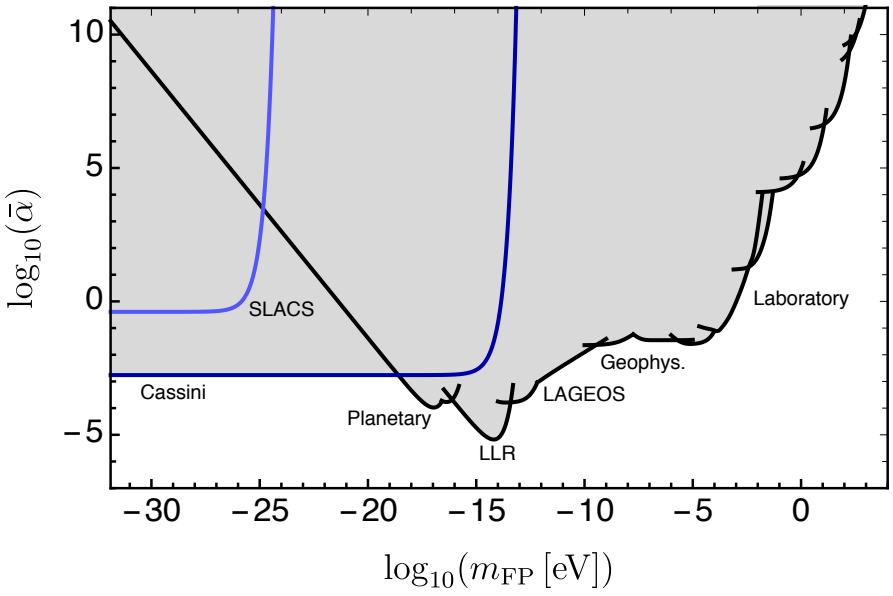

Figure 6.7: Exclusion plot at 95% c.l. from local tests of gravity as reviewed in the current section taken from [298]. Tests of the gravitational potential lead to the black lines and tests of the scalar curvature lead to the blue lines.

additional gravitational degrees of freedom are massive. The effect of the fifth force can then be parametrised as

$$\Phi_{\rm Y}(r) = -\frac{1}{M_{\rm P}^2}\left(\frac{1}{r} + \xi\frac{e^{-r/\lambda}}{r}\right), \tag{6.44}$$

which is known as *Yukawa parametrisation*. Here, ξ parametrises the coupling of the fifth force mediator to matter with Compton wavelength λ. Since bimetric theory gives rise to additional massive degrees of freedom, this parametrisation is appropriate here. Comparing the modified gravitational potential in the Yukawa parametrisation (6.44) to the linearised gravitational potential in bimetric theory (3.46) unveils the following parameter relation:

$$\xi = 4\bar{\alpha}^2/3\,, \quad \lambda = 1/m_{\rm FP}\,. \tag{6.45}$$

Current constraints on the Yukawa parameters, or equivalently on $\bar{\alpha}$ and $m_{\rm FP}$ are summarised in Fig. 6.7. In the following, we discuss how to obtain the individual constraint lines. Note that the constraints are valid only without Vainshtein screening. In Section 6.2.3 we will implement the Vainshtein mechanism.

Planetary constraints

The most stringent planetary constraints are derived from measurements of the precession of the orbit of the planets moving around the Sun. The contribution to the precession induced by the Yukawa potential is given by [343]

$$\delta\phi_P \simeq \pi\xi\,(a_P/\lambda)^2\,e^{-a_P/\lambda}\,, \tag{6.46}$$

where a_P is the semi-major axis of the orbit of planet P. In Fig. 6.7, the limits on $\bar{\alpha}$ are present for Mercury $P = \mathrm{☿}$ and Mars $P = \mathrm{♂}$, where the observational data is [383]

$$\begin{aligned} \delta\phi_{\mathrm{☿}} &= (-80 \pm 210)\times 10^{-9}\,, \quad a_{\mathrm{☿}} = 5.79\times 10^{12}\,\mathrm{cm}\,, \\ \delta\phi_{\mathrm{♂}} &= (-130 \pm 180)\times 10^{-9}\,, \quad a_{\mathrm{♂}} = 2.28\times 10^{13}\,\mathrm{cm}\,, \end{aligned} \tag{6.47}$$

respectively.

Constraints from Lunar-Laser-Ranging

The most stringent constraint comes from measurements of the anomalous precession $\delta\phi_{\rm L}$ of the Moon's orbit about the Earth. So we can use the same formula (6.46) for the parameters of the Moon's orbit [344]

$$\delta\phi_{\rm L} < 1.6 \times 10^{11}\,, \quad a_{\rm L} = 3.844 \times 10^{10}\,{\rm cm}\,. \tag{6.48}$$

This observational data leads to the LLR curve in Fig. 6.7.

Constraints from the LAGEOS satellite

Another important class of constraints comes form measurements of the gravitational potential at the hight of the LAGEOS satellite, which orbits the Earth [384]. Let $g_{\rm terr}(r)$ and $g_{\rm sat}(r)$ denote the gravitational acceleration induced by the Earth at the distance r, extrapolated from measurements at the surface of the Earth and at the hight of the LAGEOS satellite, respectively. We introduce the quantity

$$\eta_\oplus = \frac{g_{\rm terr}(R_\oplus) - g_{\rm sat}(R_\oplus)}{g_{\rm terr}(R_\oplus)}\,, \tag{6.49}$$

which measures the mismatch between both extrapolations when evaluated at the Earth's radius $R_\oplus$. The observational data is [384]

$$\begin{aligned} \eta_\oplus &= (-2 \pm 5) \times 10^{-7}\,, \\ R_\oplus &= (6.3781362 \pm 0.0000001) \times 10^8\,{\rm cm}\,, \\ r_{\rm sat} &= 1.2271 \times 10^9\,{\rm cm}\,, \\ R_\oplus^2 g_{\rm sat}(R_\oplus) &= (3.98600436 \pm 0.00000002) \times 10^{14}\,{\rm m^3\,s^{-2}} \end{aligned} \tag{6.50}$$

where $r_{\rm sat}$ is the averaged distance between the Earth and the satellite.

Assuming the Yukawa parametrisation for the gravitational potential, the theoretical prediction for $\eta_\oplus$ can be computed to be [343]

$$\eta_\oplus = \xi \frac{R_\oplus^2 \mathcal{F}_\oplus(R_\oplus,\lambda) - r_{\rm sat}^2 \mathcal{F}_\oplus(r_{\rm sat},\lambda)}{R_\oplus^2 g_{\rm sat}(R_\oplus)}\,, \tag{6.51}$$

The gravitational force is given by [343]

$$\mathcal{F}_\oplus(r,\lambda) = \frac{M_\oplus}{8\pi M_{\rm P}^2}(1 + r/\lambda)\frac{e^{-r/\lambda}}{r^2}\Phi_{\rm s}(R_\oplus/\lambda)\,, \tag{6.52}$$

where the form factor

$$\Phi_{\rm s}(x) = 3[(x\cosh(x) - \sinh(x)]/x^3\,, \tag{6.53}$$

takes into account that the Earth is an extended, approximately spherical object.

Another constraint can be obtained by comparing the gravitational potential as measured at the location of the LAGEOS satellite with the gravitational potential as measured at the location of the Moon. In this case, we introduce the quantity

$$\eta_{\rm L} = \frac{R_\oplus^2 g_{\rm sat}(R_\oplus) - r_{\rm L}^2 g_{\rm moon}(r_{\rm L})}{[R_\oplus^2 g_{\rm sat}(R_\oplus) + r_{\rm L}^2 g_{\rm moon}(r_{\rm L})]/2}\,, \tag{6.54}$$

which turns out to be independent of the Earth's mass. Here, $r_{\rm L}^2 g_{\rm moon}(r_{\rm L})$ is related to the gravitational acceleration measured at the distance of the Moon's orbit $r_{\rm L}$. Note that the quantity $r^2 g(r)$ is independent of radius r in GR. The measured data is given by [384, 385]

$$\eta_{\rm L} = (-1.8 \pm 1.6) \times 10^{-8}\,, \quad r_{\rm L} \simeq (3.88401 \pm 0.0001) \times 10^{10}\,{\rm cm}\,. \tag{6.55}$$

Starting from the Yukawa parametrisation of the gravitational potential, the theoretical prediction can be obtained to be [343]

$$\eta_{\rm L} = \xi \frac{(1+\frac{r_{\rm sat}}{\lambda})\Phi_{\rm s}(\frac{R_\oplus}{\lambda})e^{-\frac{r_{\rm sat}}{\lambda}} - (1+\frac{r_{\rm L}}{\lambda})\Phi_{\rm s}(\frac{R_\oplus}{\lambda})\Phi_{\rm s}(\frac{R_{\rm L}}{\lambda})e^{-\frac{r_{\rm L}}{\lambda}}}{1-\xi\left[(1+\frac{r_{\rm sat}}{\lambda})\Phi_{\rm s}(\frac{R_\oplus}{\lambda})e^{-\frac{r_{\rm sat}}{\lambda}} + (1+\frac{r_{\rm L}}{\lambda})\Phi_{\rm s}(\frac{R_\oplus}{\lambda})\Phi_{\rm s}(\frac{R_{\rm L}}{\lambda})e^{-\frac{r_{\rm L}}{\lambda}}\right]}\,, \tag{6.56}$$

where $R_{\rm L} \simeq 1.738 \times 10^8\,\mathrm{cm}$ denotes the Moon's averaged radius and the form factor $\Phi_{\rm s}(R_{\rm L}/\lambda)$ takes into account that the Moon has finite size.

Confronting the theoretical predictions Eqs. (6.51) and (6.56) with the observational data Eqs. (6.50) and (6.55) defines the two LAGEOS constraint lines in Fig. 6.7.

Geophysical constraints

Putting precise geophysical constraints is more involved because the composition of the Earth and the shape of the surface play substantial roles. Here, we use the constraints implied by two different experiments at geophysical scales.

Tower gravity experiments measure the gravitational acceleration $g(z)$ as a function of height z up a tall tower. One measures the gravitational acceleration g_0 around the bottom of the tower, which allows to extrapolate to the gravitational potential at the height z. This result is to be compared with the gravitational acceleration measured at the top of the tower g_t, which can be extrapolated to the height z. Given the Yukawa parametrisation, the difference between both accelerations evaluated at height z is given by [343]

$$\delta g(z) \equiv g_0(z) - g_t(z) = 2\pi\rho G\xi\lambda(e^{-z/\lambda} - 1) \tag{6.57}$$

for a spherical, non-rotating Earth. Here, $\rho = 2670\,\mathrm{kg\,m^{-3}}$ is the mean terrain density and $G = 6.67408 \times 10^{-11}\,\mathrm{m^3\,kg^{-1}\,s^{-2}}$ the measured gravitational constant at the Earth's surface. The most-stringent constraint was obtained at the BREN tower at Jackass Flats, Nevada [386, 387]. At the maximum height of $z = 454.86\,\mathrm{m}$ the anomalous acceleration was constrained as $\delta g(z) = (-60 \pm 95) \times 10^{-8}\,\mathrm{m\,s^{-2}}$.

The next constraint that we use comes from lake experiments, where the change in gravity due to the changing water levels is measured. Given, the Yukawa parametrisation, the effective gravitational constant at distance r can be written as

$$G(r) = G_\infty\left[1 + \xi(1 + r/\lambda)e^{-r/\lambda}\right], \tag{6.58}$$

Here, G_∞ is the effective gravitational constant at infinite distance, i.e. in the context of bimetric theory $G_\infty = 1/(8\pi M_{\rm P}^2)$. Let $\beta = G(r_2)/G(r_1)$ the ratio between the measured gravitational constant at the two effective interaction distances r_2 and r_1. The associated constraint line can be written as [388]

$$\xi(\lambda) = \frac{\beta - 1}{(1 + r_2/\lambda)e^{-r_2/\lambda} - \beta(1 + r_1/\lambda)e^{-r_1/\lambda}}\,. \tag{6.59}$$

We use the result from the experiment at the Gigerwald lake [389, 390]. At an effective interaction distance of $r_2 = 88\,\mathrm{m}$, the value $G(r_2) = (6.678 \pm 0.007) \times 10^{-11}\,\mathrm{m^3\,kg^{-1}\,s^{-2}}$ was obtained. This result is compared to the laboratory value $G(r_1) = (6.6726 \pm 0.0005) \times 10^{-11}\,\mathrm{m^3\,kg^{-1}\,s^{-2}}$, which was obtained at an effective distance of $r_1 = 5\,\mathrm{cm}$ [391].

The resulting constraints on the parameters $\bar{\alpha}$ and $m_{\rm FP}$ are depicted in Fig. 6.7, as indicated by the geophysical lines.

Laboratory constraints

Finally, we present constraints from experiments in the laboratory. Here, the experimental setups are much more involved as compared to the previous tests and beyond the scope of the present discussion. Therefore, we limit our presentation to quoting the constraints defining functions.

$\lambda\,(\mu\mathrm{m})$	upper limit on ξ
4	1.5×10^8
6	2.0×10^6
10	5.1×10^4
18	3.7×10^3
34	8.4×10^2
66	4.4×10^2
130	3.6×10^2
258	3.3×10^2

Table 6.6: Upper limit on the Yukawa parameter ξ corresponding to 95% c.l. for different interaction scales λ from the Stanford experiment.

We start with the torsion balance experiment of Hoskins et al. [392]. The limit on the Yukawa parameter ξ is given by

$$\xi(\lambda) = \frac{\delta_{\mathrm{Hoskins}}}{\beta(r_5/\lambda)(1+\delta_{\mathrm{Hoskins}}) - \beta(r_{105}/\lambda)}\,, \tag{6.60}$$

where $\delta_{\mathrm{Hoskins}} = (1.2 \pm 7 \times 10^{-4})$ is determined experimentally and the distances $r_5 = (4.7901 \pm 0.0004)\,\mathrm{cm}$ and $r_{105} = (105.016 \pm 0.008)\,\mathrm{cm}$ are characteristic to the experimental setup. The function appearing in the constraint equation is given by $\beta(x) = (1+x)e^{-x}$.

Next, we mention the constraints from the Stanford experiment [393], which provides the most stringent constraints on the Yukawa parameters at the $\mathcal{O}(\mu\mathrm{m})$ scale. The experimental bounds are presented in Table 6.6 as reported in [393]. We extrapolate between the individual data points to produce the constraint line in Fig. 6.7.

For laboratory experiments on even smaller length scales, the constraint lines can be obtained using an approximate framework, which suffices for our purposes. The upper limit on the Yukawa coupling can approximately be written as [348]

$$\xi(\lambda) = \xi_{\mathrm{exp}}\, e^{r_{\mathrm{exp}}/\lambda}\,, \tag{6.61}$$

where ξ_{exp} is the measured upper limit on the Yukawa coupling at the experimental length scale r_{exp}. In Table 6.7, we present the approximate experimental data for several torsion balance and Casimir experiments at $\mathcal{O}(\mathrm{nm} - \mathrm{mm})$ scales as summarised in [348].

All these laboratory constraints are visualised in Fig. 6.7, for which we transformed from the Yukawa parameters ξ and λ to the physical parameters $\bar{\alpha}$ and m_{FP} according to Eq. (6.45).

Let us point towards the recently obtained limits on the Yukawa parameters obtained by the MICROSCOPE experiment [404]. The most stringent bound on the Yukawa coupling is of the order $\xi \lesssim 10^4 \cdot 10^6$ for a mass range $10^{-6}\,\mathrm{eV} \lesssim m_{\mathrm{FP}} \lesssim 10^{-2}\,\mathrm{eV}$. While this constraint is many orders of magnitude weaker than the aforementioned ones, it demonstrates the ongoing efforts to test gravity on laboratory scales.

6.2.2 Tests of the scalar curvature

The aforementioned bounds on the gravitational potential are not restrictive in the region of small spin-2 mass m_{FP}. However, deviations from Newtonian gravity are strongly constrained also in this parameter region by tests of the scalar curvature. Since the scalar curvature dictates the motion of massless test bodies, it can be tested by measurements of the deflection and time delay of light rays passing by a massive object.

Experiment	$r_{\rm exp}$	$\xi_{\rm exp}$
Eöt–Wash [394]	0.5 mm	2×10^{-3}
Lamoreaux [395]	5 μm	2×10^{8}
Sushkov [396]	1 μm	2×10^{9}
Decca [397, 398]	100 nm	10^{13}
Ederth [399, 400]	20 nm	5×10^{17}
Mohideen [401]	10 nm	10^{19}
van der Waals [402, 403]	1 nm	10^{30}

Table 6.7: Approximate constraints on Yukawa parameters from torsion balance and Casimir experiments at $\mathcal{O}(10^{-4} \dots 10^{-9})$ m scales.

It is common to introduce the gravitational slip parameter γ, which measures the ratio between the gravitational potentials as felt by massive and massless particles. In GR, the parameter is exactly unity. In bimetric theory, the gravitational slip parameter is given by [338]

$$\gamma = \frac{3 + 2\bar{\alpha}^2 e^{-m_{\rm FP}\, r}}{3 + 4\bar{\alpha}^2 e^{-m_{\rm FP}\, r}} \tag{6.62}$$

obtained utilising the Parameterised–Post–Newtonian (PPN) formalism [405] such that the expression is valid outside the Vainshtein radius. A review on experimental bounds on γ can be found, e.g. in [406].

The gravitational slip parameter can obtained from the deflection of light rays passing by a massive object. Here, we use a constraint obtained on galactic scales. Gravitational lensing data due to elliptical galaxies as presented by the Sloan Lens ACS (SLACS) [407–409] allows to constrain the gravitational slip parameter as $\gamma - 1 = -0.02 \pm 0.07$ at 68% c.l. [410]. To compute an approximate constraint line, we use that the deflected light rays effectively probe scales similar to the galactic radii of $r \simeq 5\,\text{kpc} \simeq 1.54 \times 10^{20}\,\text{m}$. These values lead to the blue line labeled SLACS in Fig. 6.7, which is in agreement with the more detailed results of [330], which were obtained in the context of BT.

The most stringent bound is obtained from measurements of the time delay of light signals, which were sent by the Cassini spacecraft to the Earth and closely passed by the Sun. The gravitational slip parameter was constrained to be $\gamma - 1 = (2.1 \pm 2.3) \times 10^{-5}$ [411]. The light rays passed by the Sun at a distance of ~ 1.6 solar radii, so the effective interaction distance is $r \simeq 1.11 \times 10^{9}\,\text{m}$. With these values, we obtain the blue Cassini constraint line in Fig. 6.7.

6.2.3 Implementing Vainshtein screening

All the previously discussed observational constraints apply to the gravitational potential in the Yukawa parametrisation, which in terms of the bimetric parameters is given by

$$\Phi(r) = -\frac{1}{M_{\rm P}^2}\left(\frac{1}{r} + \frac{4\bar{\alpha}^2}{3}\frac{e^{-m_{\rm FP}\, r}}{r}\right), \tag{6.63}$$

see also Eq. (3.35). In bimetric theory, this expression describes the gravitational potential induced by a compact object outside the Vainshtein radius, where the linear approximation is well-defined. Therefore, the aforementioned observational constraints are not applicable in regimes where the Vainshtein screening is active. In this section, we take into account the Vainshtein mechanism.

We discussed the Vainshtein mechanism in detail in Section 3.2. We found that the linear approximation is valid on scales larger than the Vainshtein radius given by $r_{\rm V} = (r_{\rm S}/m_{\rm FP}^2)^{1/3}$. On smaller scales $r \ll r_{\rm V}$, deviations from GR are suppressed, such that the observational constraints

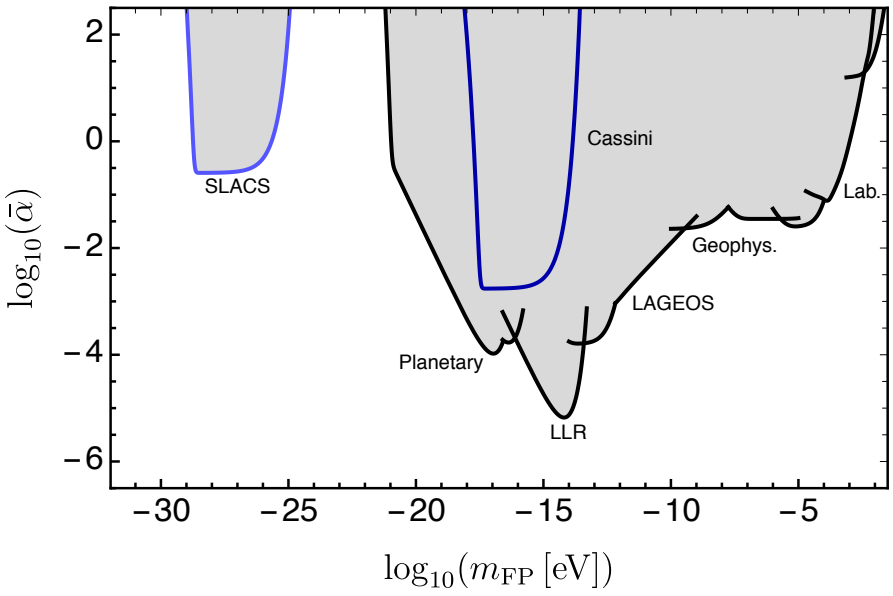

Figure 6.8: Exclusion plot from tests of the gravitational potential and scalar curvature at 95% c.l. phenomenologically taking into account the Vainshtein mechanism. It is assumed that screening is active in the entire parameter space.

on the parameters $\bar{\alpha}$ and $m_{\rm FP}$ are weaker. To quantify the effect of Vainshtein screening on the observational constraints, we make a phenomenological ansatz inspired by [339] and replace the coupling $\bar{\alpha}$ by the distance-dependent function

$$\bar{\alpha}_{\rm eff}(r) = \frac{\bar{\alpha}}{2}\left[1 + \tanh\left(\frac{r - r_{\rm V}}{\Delta r}\right)\right]. \tag{6.64}$$

The function is chosen such that $\bar{\alpha}_{\rm eff}(r \gg r_{\rm V}) \simeq \bar{\alpha}$ and $\bar{\alpha}_{\rm eff}(r \ll r_{\rm V}) \simeq 0$. The parameter Δr quantifies the length scale of transition from the linear to the nonlinear regime. Using this phenomenological ansatz, we can write the gravitational potential (3.46) valid inside and outside the Vainshtein sphere in the following approximative way

$$\Phi(r) = -\frac{1}{(1+\bar{\alpha}_{\rm eff}^2)M_{\rm g}^2}\left(\frac{1}{r} + \frac{4\bar{\alpha}_{\rm eff}^2}{3}\frac{e^{-m_{\rm FP}\,r}}{r}\right). \tag{6.65}$$

The gravitational slip parameter (6.62) valid inside and outside the Vainshtein sphere can be approximated as

$$\gamma = \frac{3 + 2\bar{\alpha}_{\rm eff}^2 e^{-m_{\rm FP}\,r}}{3 + 4\bar{\alpha}_{\rm eff}^2 e^{-m_{\rm FP}\,r}} \tag{6.66}$$

We emphasise that this parametrisation is a vast simplification compared to solving the full non-linear equations of motion. However, this approximation is sufficient for our current discussion.

In Fig. 6.8, we present the constraints on the parameter $\bar{\alpha}$ and $m_{\rm FP}$ using the phenomenological ansätze in Eqs. (6.65) and (6.66) to implement Vainshtein screening and assuming that Vainshtein screening is active in the entire parameter space. To compute the Vainshtein radii corresponding to each experiment, we use the mass of the central object inducing the gravitational potential and scalar curvature. For the SLACS constraint, we use that the typical mass of an elliptical galaxy is $\sim 10^{11} M_\odot$. For the Cassini and planetary constraints, the Sun is the central object with mass $M_\odot$. The Earth with mass $M_\oplus$ serves as central object in case of the LLR, LAGEOS and geophysical constrains. In all cases, we assume $\Delta r = 0.1 r_{\rm V}$ for the transition length scale.

The Vainshtein mechanism is most important for small spin-2 masses, which is also reflected in Fig. 6.8. The constraints on $\bar{\alpha}$ are substantially weaker or even absent for small spin-2 masses.

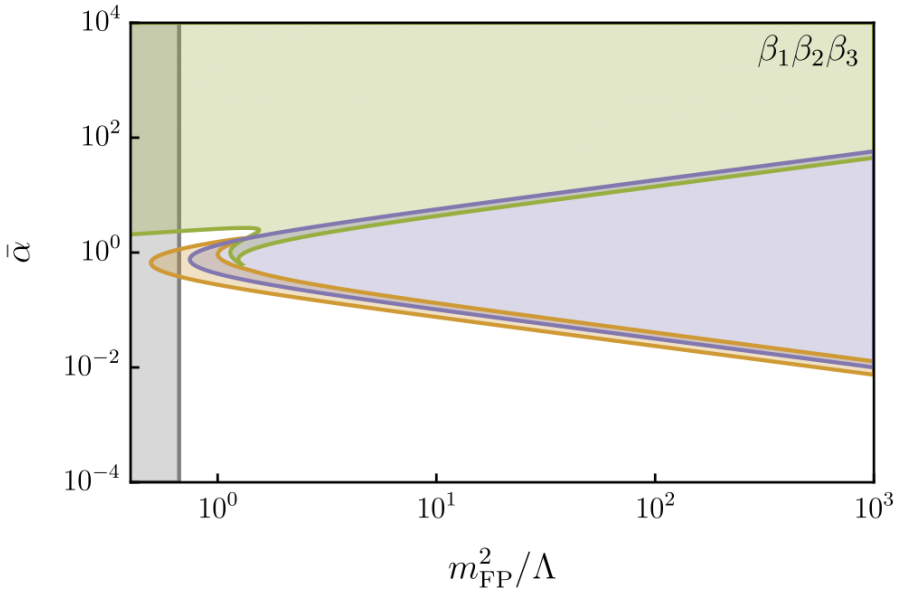

Figure 6.9: Exclusion plot from the theoretical conditions ensuring a working Vainshtein mechanism in the $\beta_1\beta_2\beta_3$–model taken from [298]. The conditions are violated in the shaded regions. Vainshtein screening is active in the region left white.

Further, the Vainshtein mechanism is most efficient if the mass of the central object is large. On the other hand, the constraints coming from experiments, where the Earth is the central object, are unaffected by Vainshtein screening. To provide a numerical example, we compute the critical spin-2 mass at which the Earth's Vainshtein radius equals the Earth's radius, i.e. $r_{\rm V} = R_\oplus$. Using the expression for the Vainshtein radius (3.36), we obtain the critical value of

$$m_{\rm FP} = \left(\frac{M}{M_{\rm g}^2 R_\oplus^2}\right)^{1/2} \simeq 1.28 \times 10^{-17}\,{\rm eV}\,. \tag{6.67}$$

So for larger spin-2 masses $m_{\rm FP} \gtrsim 1.28 \times 10^{-17}\,{\rm eV}$, the Earth's Vainshtein radius is smaller than its own radius. Therefore, the LAGEOS and geophysical constraints are not affected by Vainshtein screening, as can be seen in Fig. 6.8.

In addition, we did not take into account Vainshtein screening for laboratory constraints in Fig. 6.8 for the following reason. The experimental setups are not spherically symmetric, but have less amount of symmetry. In the context of Galileons, it has been found that Vainshtein screening is weaker around cylindrical objects and completely absent for planar sources [412]. We expect a similar shape dependence also within bimetric theory, although the explicit demonstration is still pending.

As we discussed in Section 3.2, Vainshtein screening is active only if the conditions (3.44) are satisfied. In particular, these conditions require the interaction parameters to satisfy $\beta_2 < 0$ and $\beta_3 > 0$. Therefore, the $\beta_1\beta_2\beta_3$–model is the only bimetric model with three or less free interaction parameters β_n that can support Vainshtein screening and gives rise to a viable finite branch solution. The other three-parameter models and all one- and two-parameter models do not give rise to Vainshtein screening. That means that the observational constraints presented in Fig. 6.7 apply to these models.

In case of the $\beta_1\beta_2\beta_3$–model, we need to identify the region of the physical parameter space, which satisfies the conditions (3.44). In order to do so, we use our physical parametrisation (4.36) to express the interaction parameters β_n in terms of the physical parameters $\bar{\alpha}$ and $m_{\rm FP}$. This procedure results in lengthy analytic expressions, which are not very illuminating.

Instead of presenting the analytic expressions, we visualise the corresponding constraints

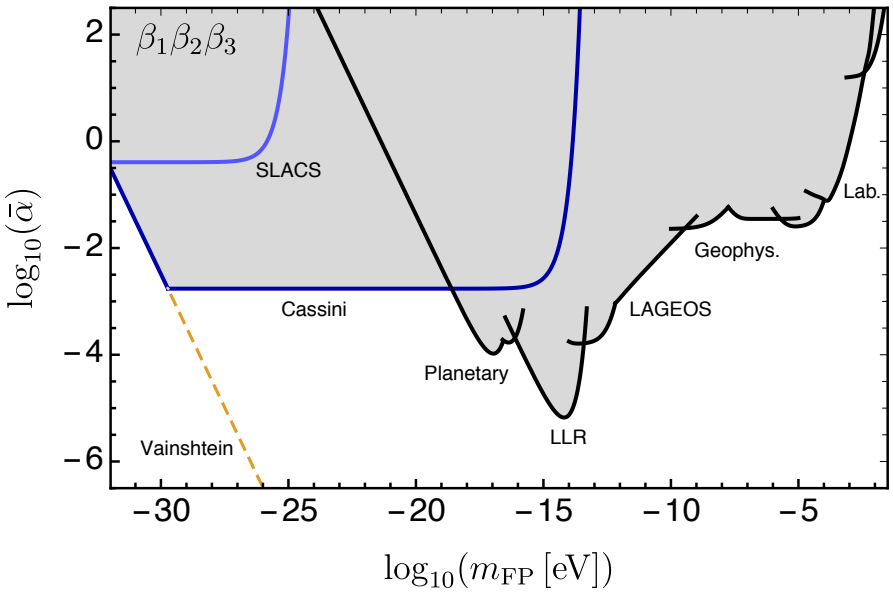

Figure 6.10: Exclusion plot from local constraints for the $\beta_1\beta_2\beta_3$-model including the Vainshtein mechanism. The grey shaded region is excluded at 95% c.l. The region below the yellow dashed line supports Vainshtein screening, weakening the Cassini constraint.

in Fig. 6.9. The coloured regions violate the bounds presented in Eq. (3.44). In particular, the bound (3.44a) is violated in the purple shaded region, the bound (3.44b) is violated in the green shaded region, and the bound (3.44c) is violated in the yellow shaded region. The grey shaded region violates the Higuchi bound. Summarising, only the region of the parameter space that is left unshaded supports Vainshtein screening.

The most stringent constraint is represented by the yellow shaded region. Its lower boundary can be well approximated by

$$\bar{\alpha}^2 < \frac{\Lambda}{16 m_{\rm FP}^2}\,, \tag{6.68}$$

except close to the Higuchi bound.

We have identified the region of the physical parameter space of the $\beta_1\beta_2\beta_3$–model that gives rise to a working Vainshtein mechanism. As next step, we compare the theoretical conditions ensuring Vainshtein screening with with the observational constraints from local tests of gravity. To do so, we use the phenomenological ansatz (6.64) to compute the constraints on $\bar{\alpha}$ and $m_{\rm FP}$ from the observational data in those regions of the physical parameter space, which support Vainshtein screening. In the regions without Vainshtein screening, the observational constraints are obtained as before.

This procedure leads to the exclusion plot presented in Fig. 6.10, where the grey shaded region is excluded at 95% c.l. The boundary of the region, which gives rise to a working Vainshtein mechanism, is indicated by the yellow dashed line. The Vainshtein mechanism is active in the entire region below that line. The region above that line does not give rise to Vainshtein screening. So compared to the constraints on the other models, the Vainshtein mechanism enlarges the observationally consistent parameters space. In particular for spin-2 masses close to the Higuchi bound, the coupling is allowed to take values as large as $\mathcal{O}(0.1)$.

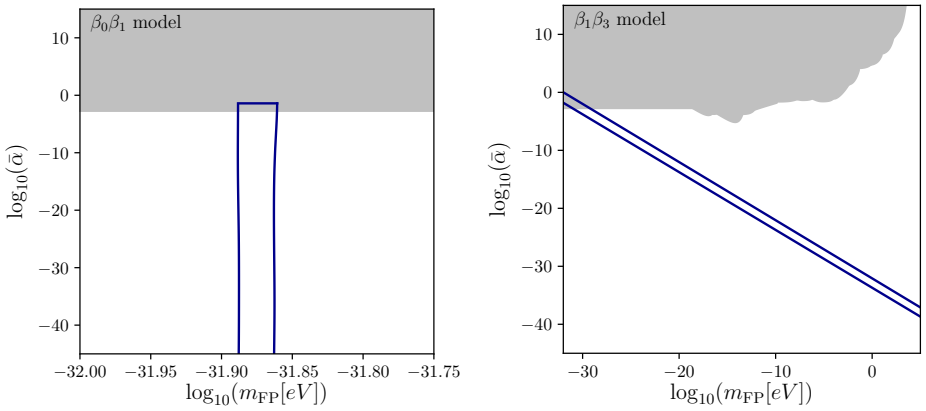

Figure 6.11: Exclusion plot for the two-parameter models combining the 95% c.l. constraints from local tests of gravity (grey shaded region) and cosmological observations (region not enclosed by blue line) taken from [298].

6.3 Combining cosmological and local constraints

In the previous sections, we identified the regions of the parameter space in terms of $\bar{\alpha}$ and m_{FP} that are either compatible with cosmological observations or compatible with local tests of gravity, also taking into account Vainshtein screening. Now we identify those regions of the parameter space that are compatible with both local and cosmological bounds. Note that in contrast to Section 6.1.5, in this section we present the constraints on the physical parameters as *ex*clusion plots. In addition, we zoom into a subregion of the full physical parameter space for better visibility.

We start with the β_1–model as the simplest example, although this model is statistically strongly disfavoured by cosmological observations alone. Cosmological data constrains the spin-2 mass to $m_{\mathrm{FP}} = (1.82 \pm 0.02) \times 10^{-32}\,\mathrm{eV}$. The coupling is not a free parameter, but fixed by the equations of motion (4.10) as $\bar{\alpha} = 1/\sqrt{3} \simeq 0.58$. In this parameter region, the most stringent local bound comes from the Cassini satellite, which constrains the coupling as $\bar{\alpha} < 1.73 \times 10^{-3}$ at 95% c.l., as follows from Eq. (6.62). This bound is in conflict with the theoretical prediction by many standard deviations. So combining local and cosmological bounds statistically disfavours the β_1–model even further.

In the context of the $\beta_0\beta_1$–model, the spin-2 mass is constrained as $m_{\mathrm{FP}} = (1.33 \pm 0.02) \times 10^{-32}\,\mathrm{eV}$ by cosmological data. This leads to an upper limit on the coupling of $\bar{\alpha} < 0.2$ at 68% c.l. In the same parameter region, the most stringent local bound comes from the Cassini spacecraft, which constrains the coupling to $\bar{\alpha} < 1.73 \times 10^{-3}$ at 95% c.l., which is a stronger bound than the one inferred from cosmological data. The combined constraints are presented in the left panel of Fig. 6.11. The grey shaded region is excluded by local tests of gravity and the region not enclosed by the blue contour line is excluded by cosmological observations, both at 95% c.l. Summarising, the bound on m_{FP} is unaltered, while local tests strengthen the bound on $\bar{\alpha}$ as compared to cosmological tests.

Moving on to the $\beta_1\beta_n$–models with $n = 2, 3, 4$, we present the local and cosmological constraints on the physical parameters in the right panel of Fig. 6.11 for the representative $\beta_1\beta_3$–model. As before, the grey shaded region is excluded by local tests of gravity and the region not enclosed by the blue contour line is excluded by cosmological data. The constraints are exactly the same for the other two-parameter models $\beta_1\beta_2$ and $\beta_1\beta_4$ at the level of current accuracy. For most parts of the parameter space, the cosmological constraints are the most stringent ones. For small spin-2 masses m_{FP}, the aforementioned constraint from the Cassini spacecraft is relevant, which forces the coupling to be $\bar{\alpha} < 1.73 \times 10^{-3}$ at 95% c.l. This bound translates into a stronger lower limit on the spin-2 mass due to the parameter relations Eqs. (4.15a), (4.18a) and (4.21a)

of $m_{\rm FP} > 1.85 \times 10^{-30}\,\text{eV}$ at 95% c.l. With these limiting values and given the best-fit value for the cosmological constant Λ, the parameters are approximately related as $\bar{\alpha}^2 m_{\rm FP}^2 \simeq (12/n)\Lambda$, see Eq. (6.40).

Coming to three-parameter models, we first discuss those models which allow for non-vanishing vacuum energy as parametrised by β_0. The combined exclusion plots are presented in the first three panels of Fig. 6.12. The grey shaded region is excluded due to local tests of gravity and the red shaded region is excluded due to the theoretical consistency conditions. In addition, the region above the blue contour line is excluded by cosmological observations.

First, we observe that local tests of gravity have more constraining power than the theoretical consistency conditions for all three models. For small spin-2 masses, the constraint due to Cassini is stronger than the cosmological constraints on $\bar{\alpha}$. For larger spin-2 masses, i.e. where the cosmological constraints on $\bar{\alpha}$ and $m_{\rm FP}$ can be approximated as in Eq. (6.42), the cosmological constraints are stronger than the local ones. Summarising, large regions of the physical parameter space are consistent with both local and cosmological tests of gravity. In particular, the cosmologically relevant parameter region automatically passes the most stringent local constraints, which comes from LLR. The coupling is bounded from above as $\bar{\alpha} < 1.73 \times 10^{-3}$ at 95% c.l due to the Cassini experiment.

We move to the self-accelerating three-parameter models, which have $\beta_0 = 0$. The exclusion plots according to the combined constraints are presented in the last three panels of Fig. 6.12. As before, the grey shaded region is excluded by local tests of gravity. The red shaded region is theoretically inconsistent. The region above the blue contour line is excluded by cosmological observations. For the $\beta_1\beta_2\beta_3$–model, the region that gives rise to Vainshtein screening is indicated by the hatching.

Compared to the previous three-parameter models, the constraints from theoretical consistency are much stronger than constrains from local tests in the case of self-accelerating models. Except for a small region when the spin-2 mass is small, the parameter region excluded by local tests is excluded by the much stronger theoretical consistency conditions. Except for a few wiggles, the contour lines corresponding to 95% c.l. from cosmological tests coincide with the theoretical lines. We used the theoretical consistency conditions as priors in our cosmological data analysis. So the prior and posterior distributions are almost the same. This means that the cosmological data does not substantially constrain the parameter $\bar{\alpha}$ and $m_{\rm FP}$ beyond the prior knowledge. Only for small spin-2 masses, the bound on $\bar{\alpha}$ from the statistical analysis is significantly stronger than the priors. Here, the cosmological and local constraints on $\bar{\alpha}$ are of the same order. For the $\beta_1\beta_2\beta_3$–model, the Vainshtein mechanism weakens the local constraints on $\bar{\alpha}$ for small spin-2 masses. In this case, the cosmological constraint is significantly stronger.

6.4 Discussion

Our proposed physical parametrisation enabled us to consistently confront BT with various theoretical and observational constraints for the first time in a unified framework. We surpassed both prior fallacies that a viable background cosmology would require $m_{\rm FP} \sim H_0$ and a viable perturbative level would require $m_{\rm FP} \gg H_0$. As such, we tested the entire theoretically consistent parameter space against observed data, generalising the previous analyses [216, 263, 265, 296, 297, 337], but limiting to models with up to three free parameters. As we will summarise now, our obtained constraints are the to date most stringent ones.

On the cosmological side, we tested BT against observed data from SN1a, BAOs, and the CMB. The simple β_1–model gives a poor fit to the observed data such that our statistical analysis strongly disfavours this model. Contrarily, all two- and three-parameter models fit the observed data as good as the standard cosmological model. The additional free parameter leads to a slight disfavouring of the bimetric models compared to the cosmological standard model. However, the self-accelerating models, which are characterised by $\beta_0 = 0$ and are devoid of vacuum energy, have a clear preference from a theoretical perspective. Therefore, the self-accelerating models of BT are promising alternatives to the cosmological standard model.

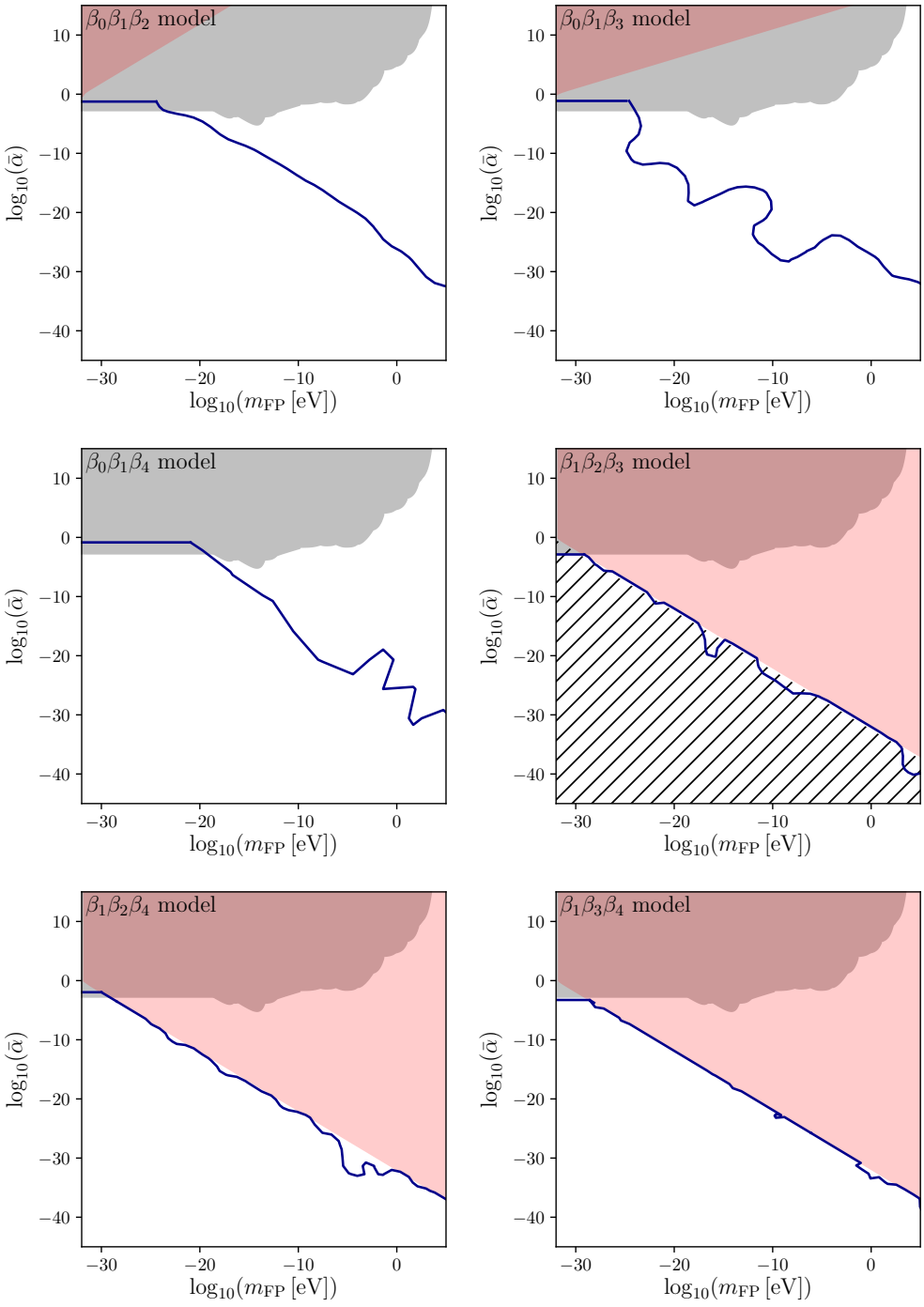

Figure 6.12: Exclusion plots for the three-parameter models combining the 95% c.l. constraints from local tests of gravity (grey shaded region), theoretical conditions (red shaded region), and cosmological observations (region above blue line) taken from [298]. The hatched region for the $\beta_1\beta_2\beta_3$–model indicates where Vainshtein screening is active.

We identified the cosmologically relevant parameter space in terms of $\bar{\alpha}$ and m_{FP}. We demonstrated that also a heavy spin-2 field is cosmologically consistent. In this case the coupling $\bar{\alpha}$ must be sufficiently small.

On the local side, we confronted BT with measurements of the gravitational potential and the scalar curvature. These range from laboratory to extragalactic scales. Importantly, we also implemented Vainshtein screening, which is relevant for the $\beta_1\beta_2\beta_3$–model.

Without Vainshtein screening, the Yukawa parameters $\bar{\alpha}$ and m_{FP} are already tightly constrained. Assuming Vainshtein screening to be active within the entire bimetric parameter space substantially enlarges the observationally consistent parameter space in the region of small spin-2 mass. However, the Vainshtein mechanism works only within a subregion of the parameter space of the $\beta_1\beta_2\beta_3$–model.

The most stringent bounds come from cosmological tests for a large region of the parameter space. Only for small spin-2 mass the local constraint on $\bar{\alpha}$ from Cassini is more restrictive than the cosmological constraints. In summary we conclude that all these models are pushed towards their GR-limits because the maximum allowed value for the coupling is $\bar{\alpha} < 1.73 \times 10^{-3}$ at 95% c.l. Nonetheless, large regions of the physical parameter space pass both cosmological and local tests of gravity. In addition, even the region of small coupling is phenomenologically interesting, as we will discuss in Chapter 8.

There is but one exception from this conclusion: the $\beta_1\beta_2\beta_3$–model. The Vainshtein mechanism partly removes the Cassini constraint on $\bar{\alpha}$ for small spin-2 mass. As we would like to argue now, also the significantly stronger cosmological constraint might in fact be weakened. The reason is that we expect this region to be fairly prior dominated. In fact, this region of the parameter space was studied in greater detail in [299], where $\bar{\alpha} \lesssim 0.4$ at 90% c.l. was found as the upper limit on the coupling. Therefore, we expect that the $\beta_1\beta_2\beta_3$–model is not forced into its GR-limit, but that the coupling can be as large as $\bar{\alpha} \sim \mathcal{O}(0.1)$ if the mass is of the order $m_{\mathrm{FP}} \sim H_0$.

In fact, this is exactly the region of the parameter space, where the effect of phantom dark energy on background cosmology is most prominent. As shown in [277], the Hubble tension is alleviated for such parameter combinations.

Finally, let us review other existing constraints on the bimetric parameters. In the context of gravitational waves, the aforementioned oscillations allow to constrain the parameters of the massive spin-2 mode. Analysing the observed data from the two gravitational wave events [166] leads to an upper limit on the coupling of $\bar{\alpha} \lesssim 0.4$ in the mass range $m_{\mathrm{FP}} \sim 10^{-22} \ldots 10^{-21}\,\mathrm{eV}$ [324]. Outside this range, the coupling is not constrained at all.

Also observed data from galaxy rotation curves have been analysed in the context of BT implementing in [339]. For a mass of the order $m_{\mathrm{FP}} \sim 10^{-30} \ldots 10^{-20}\,\mathrm{eV}$, their analysis excludes values for the coupling $\bar{\alpha}$ much larger than unity

In summary, our combined analysis using observed data from cosmological and local tests of gravity provides the to date most stringent constraints. Only the $\beta_1\beta_2\beta_3$–model is not pushed into its GR-limit and as such stands out as the most promising alternative to the standard cosmological model. Next, we will leave the realm of late-time cosmology and study the effect of a massive spin-2 field during early times.

Chapter 7

Higuchi bound on slow-roll inflation and the swampland

The precedent analysis demonstrates that ghost-free bimetric theory provides a model of dark energy and is observationally consistent for large parameter ranges. In particular, the spin-2 mass is allowed to take values within the range only confined by the Higuchi bound and the cutoff of the effective theory. In other words, the mass can range from the Hubble all the way up to the Planck scale as long as the coupling $\bar{\alpha}$ is sufficiently small for the theory to be observationally and theoretically viable. We should therefore study implications of the presence of a massive spin-2 field, e.g. also during inflation.

More generally, higher spin states both massless and massive are a genuine prediction of String Theory and Quantum Gravity [38]. From this perspective we generally expect that such states are present on, e.g. inflationary spacetimes. Hence, these higher spin states and their interactions should be included in the effective field theory description. This will be done in the present chapter for the simplest non-trivial case of spin $s = 2$, for which BT serves as the consistent low-energy effective field theory.

Theoretical consistency highly constrains the effective field theory of higher spin fields. For instance, the Higuchi bound [224, 225] forbids the mass m to be arbitrarily small in de Sitter spacetime. For a massive bosonic field with spin s, the bound is given by

$$m^2 \geq s(s-1)H^2\,, \tag{7.1}$$

where $1/H$ is the de Sitter radius. If the bound is violated, the higher spin field contains helicity modes with negative norm, which spoils unitarity. The simplest nontrivial example of the bound is for a massive spin-2 field, i.e. for $s = 2$. As we encountered in Eq. (2.84), in that case the bound becomes

$$m_{\rm FP}^2 \geq 2H^2 \tag{7.2}$$

with $m_{\rm FP}$ the Fierz-Pauli.

To model inflation, one usually uses a scalar field ϕ moving in an effective potential V [413]. The potential energy of the scalar field acts as a cosmological constant, which drives the accelerated expansion of the universe. For the expansion to be exponential, the scalar field has to slowly roll down the potential. On the level of Friedmann's equation that means that the condition $\dot{H} \ll H^2$ must be maintained. In the presence of a massive spin-2 field of mass $m_{\rm FP}$, the usual Higuchi bound (7.2) immediately implies the following restriction on the scalar potential:

$$V \leq \frac{3}{2} m_{\rm FP}^2 \tag{7.3}$$

In the present chapter, we will go one step further by considering slight deviations from exact de Sitter spacetime to derive a bound on the derivative of the scalar potential. We therefore use the

generalisation of the Higuchi bound to FLRW spacetime [276], which we reviewed in Section 3.1.2. Let us recall that unitarity requires the dynamical bound (3.25)

$$m_{\text{eff}}^2 \geq 2H^2 \tag{7.4}$$

to be satisfied. Here, m_{eff} is the effective, time-varying mass parameter as defined in (3.26).

Our present discussion should be viewed within the larger context of the swampland program [100], which we already mentioned in Section 1.3. The effective potential of scalar fields in effective gravitational theories is severely constrained by quantum gravity considerations [21–28]. These constraints have profound implications on the evolution of the universe, in particular on inflationary scenarios and on dark energy models [26, 103, 414, 415]. In addition, recently some implications from the Higuchi bound on massive higher spin states in String Theory and on the scale of inflation were discussed in [416–418]. Furthermore, for some work about BT in relation to the swampland and String Theory realisations see [419–424].

This chapter is based on our publication [425].

7.1 Setup

We use BT to describe inflationary spacetime in the presence of massive spin-2 fields. We reviewed cosmological solutions in Section 3.1. Here, we specialise to a spatially flat universe with $k = 0$ consistent with the inflationary paradigm [426, 427]. In this section, we rephrase some aspects of bimetric cosmology necessary for the current purpose.

In our setup, we assume that the accelerated expansion is driven by potential energy V of a slowly rolling scalar field ϕ (instead of the interaction energy of the massless and massive spin-2 field). Inflationary spacetime corresponds to a de Sitter background, which implies that both metrics are (approximately) proportional, $f_{\mu\nu} = c^2 g_{\mu\nu}$. We discussed proportional background solutions already in Section 2.4.3. In that previous discussion, we assumed an empty matter sector. In our case, the matter sector consists of a slowly rolling scalar field. The pure cosmological constant β_0 is hence shifted by potential energy V. To account for the potential energy, we make the following replacement: $\beta_0 \to \beta_0 + V$. The effective cosmological constant during inflation is therefore given by

$$\begin{aligned}\Lambda &= V + \beta_0 + 3c\beta_1 + 3c^2\beta_2 + c^3\beta_3 \\ &= \frac{1}{\alpha^2 c^2}(c\beta_1 + 3c^2\beta_2 + 3c^3\beta_3 + c^4\beta_4)\,,\end{aligned} \tag{7.5}$$

cf. Eq. (2.75). As before, equality of the first and second line determines the conformal factor c. Let us denote the contribution to the overall cosmological constant, which does not originate from the scalar potential, as $\Lambda_{\text{g}} = \beta_0 + 3c\beta_1 + 3c^2\beta_2 + c^3\beta_3$. Later we will assume that $V \gg \Lambda_{\text{g}}$[1].

In Section 3.1 we did not further specify the constituents of the matter sector. Since in this context we are now interested in the effective scalar potential, let us specify the matter Lagrangian. We assume that the matter sector consists of a real scalar field ϕ with Lagrangian

$$\mathcal{L}_{\text{m}} = -\frac{1}{2}g^{\mu\nu}\partial_\mu\phi\partial_\nu\phi - V(\phi) \tag{7.6}$$

and scalar potential $V(\phi)$. According to the cosmological principle, the scalar field can only depend on time t. From Eqs. (1.11) and (1.16), it follows that the energy density and pressure are given by

$$\frac{\rho_\phi}{M_{\text{g}}^2} = \frac{1}{2}\dot{\phi}^2 + V\,, \quad \frac{p_\phi}{M_{\text{g}}^2} = \frac{1}{2}\dot{\phi}^2 - V \tag{7.7}$$

[1] In fact, vacuum energy parameter β_0 is degenerate with an unspecified potential V. In our setup, however, the parameter V serves as an input parameter breaking the degeneracy. In other words, we will express the interaction parameters β_n (including β_0) as functions of the physical parameters of our setup. These are V, m_{FP}, and $\bar{\alpha}$. For these reasons we treat V and β_0 as independent parameters.

Varying the full bimetric action (2.86) with matter sector (7.6) with respect to the scalar field ϕ leads to the equation of motion

$$\ddot{\phi} + 3H\dot{\phi} + V' = 0\,. \tag{7.8}$$

As last ingredient, we write the modified Friedmann equation in a more compact way, adopting the notation of [318]. The physical Friedmann equation, i.e. the equation of motion of $g_{\mu\nu}$, can be written as

$$3H^2 = \frac{\rho_\phi}{M_{\rm eff}^2} \tag{7.9}$$

in terms of the time-varying effective Planck mass

$$M_{\rm eff}^2 = \frac{1+\alpha^2 y^2}{1+U/\rho_\phi} M_{\rm g}^2\,. \tag{7.10}$$

The function U depends on the parameters of the bimetric potential as

$$U = M_{\rm g}^2\left(\beta_0 + 4y\beta_1 + 6y^2\beta_2 + 4y^3\beta_3 + y^4\beta_4\right)\,. \tag{7.11}$$

The scale factor ratio is determined by the quartic polynomial (3.18), which in terms of U can be written as

$$\rho_\phi = \frac{1+\alpha^2 y^2}{4\alpha^2 y} U' - U \tag{7.12}$$

where $U' = \mathrm{d}U/\mathrm{d}y$.

7.2 Constraint on the derivative of the scalar potential

After these preliminaries, we study the generalised Higuchi bound (3.25) in the context of slow-roll inflation. We assume that the scale of inflation is set by the potential energy of the scalar field, $\Lambda \simeq V$. In other words, we assume that vacuum energy and interaction energy of the spin-2 fields is subdominant, $V \gg \Lambda_{\rm g}$. We further assume that the Higuchi bound is not saturated, i.e. we exclude the partially-massless case [428, 429], in order to avoid devision by zero.

We aim at expressing the quantities appearing in the dynamical Higuchi bound in terms of the scalar potential V and its derivative $V' = \mathrm{d}V/\mathrm{d}\phi$. It is convenient to work in terms of the slow-roll parameter

$$\epsilon = \frac{M_{\rm eff}^2}{2}\left(\frac{V'}{V}\right)^2\,. \tag{7.13}$$

We assume slow-roll, i.e. $\epsilon \ll 1$ and $\ddot{\phi} \ll H\dot{\phi}$. Then, the equation of motion (7.8) for ϕ can be rearranged to

$$\dot{\phi} = -\frac{V'}{3H} = -\frac{\sqrt{2\epsilon}\,V}{3M_{\rm eff}H}\,. \tag{7.14}$$

Using this expression to eliminate H from Friedmann's equation (7.9) and replacing the scalar energy density with (7.7) yields

$$\left(\frac{1}{2}\dot{\phi}^2 + V\right)\dot{\phi}^2 = \frac{2\epsilon}{3}V^2\,. \tag{7.15}$$

Solving this expression for $\dot{\phi}$ yields the two solutions $\dot{\phi}^2 = -V(1 \pm \sqrt{1+4\epsilon/3})$. We pick the branch with the lower sign, which leads to $\dot{\phi} = 0$ for $\epsilon = 0$ as desired. With this solution, we can express the energy density (7.7) in terms of the potential and its derivative as

$$\frac{\rho_\phi}{M_{\rm g}^2} = V\left(1 + \frac{\epsilon}{3}\right) \tag{7.16}$$

up to first order in slow-roll. This result allows to write the Friedmann equation (7.9) as

$$3H^2 = \frac{\rho_\phi}{M_{\rm eff}^2} = V\left(1 + \frac{\epsilon}{3}\right)\,, \tag{7.17}$$

where we used that $M_{\rm eff}/M_{\rm g} \sim \mathcal{O}(1)$ during slow-roll. This expression determined the Hubble rate H in terms of the scalar potential and its derivative.

The second quantity, which we need to relate to the slow-roll parameter ϵ, is the generalised spin-2 mass $m_{\rm eff}$ as defined in Eq. (3.26). To do so, we plug Eq. (7.16) into the quartic polynomial (7.12) and perturbatively solve for y, which leads to

$$y = c\left(1 - \frac{V}{3m_{\rm FP}^2 - 2V}\frac{\epsilon}{3}\right) \tag{7.18}$$

up to first order in slow-roll. The parameter c is the conformal factor determined by Eq. (7.5), i.e. for $\epsilon = 0$, with Fierz–Pauli mass $m_{\rm FP}$ as defined in Eq. (2.83). With this solution, we can write the dynamical mass parameter (3.26) as

$$m_{\rm eff}^2 = m_{\rm FP}^2 + \mathcal{M}\,\frac{\epsilon}{3} \tag{7.19}$$

up to first order in slow-roll. We defined the quantity $\mathcal{M}$ as short–hand notation, which depends on the bimetric parameters and scalar potential as

$$\mathcal{M} = -\frac{c\,V}{3m_{\rm FP}^2 - 2V}\left(\frac{c^2\beta_3 - \beta_1}{\alpha^2 c^2} + \beta_1 + 4c\beta_2 + 3c^2\beta_3\right).$$

We now have all the ingredients to write the generalised Higuchi bound to first order in slow-roll. Plugging Eqs. (7.17) and (7.19) into Eq. (3.26) leads to

$$0 \leq 3m_{\rm FP}^2 - 2V + \left(\mathcal{M} - \frac{2}{3}V\right)\epsilon\,. \tag{7.20}$$

This expression reduces to the usual Higuchi bound of de Sitter if $\epsilon = 0$, as expected. For $\epsilon > 0$ we can distinguish two cases depending on the sign of its prefactor. For $\mathcal{M} \geq 2V/3$ the bound on ϵ is trivial because the slow-roll parameter is a genuinely positive quantity. However, in the opposite case $\mathcal{M} < 2V/3$, we find the following non-trivial bound on ϵ:

$$\epsilon \leq 3\frac{3m_{\rm FP}^2 - 2V}{2V - 3\mathcal{M}}\,. \tag{7.21}$$

Note that this bound is well-defined only if the de Sitter Higuchi bound (7.3) is satisfied. In Section 7.2.1 we evaluate the right hand side of Eq. (7.21) for various simplified models and different regions of the parameter space.

To be explicit, let us rewrite the bound (7.21) in terms of the scalar potential and its derivative by using the definition (7.13) as

$$\frac{|V'|}{V} \lesssim \frac{\sqrt{6}}{M_{\rm g}}\sqrt{\frac{3m_{\rm FP}^2 - 2V}{2V - 3F}}\,, \tag{7.22}$$

where we used that $M_{\rm eff}/M_{\rm g} \sim \mathcal{O}(1)$ during slow-roll. This bound represents an upper limit on the absolute value of the derivative of the scalar potential. Close to the Higuchi bound, this bound is most restrictive. In our derivation we assumed that the Higuchi bound is not saturated, which excludes the case that the right hand side vanishes.

7.2.1 Model-specific considerations

In this section, we study the typical values of the right hand side of Eq. (7.21). To do so, we use the physical parametrisation developed in Chapter 4 to replace the interaction parameters β_n in terms of the physical parameters $\bar{\alpha}$, $m_{\rm FP}$ and V, where we assume that the effective cosmological constant is dominated by scalar potential energy, $V \gg \Lambda_{\rm g}$. Compared to the parameter relations

presented in Chapter 4, we make the replacement $\beta_0 \to \beta_0 + V$. We will study several representative bimetric models and regions of the parameter space. To ease notation, we define

$$\epsilon_{\max} = \frac{3(3m_{\mathrm{FP}}^2 - 2V)}{2V - 3\mathcal{M}}\,, \tag{7.23}$$

which is the maximum value of ϵ, see Eq. (7.21). The generalised Higuchi bound thus reads $\epsilon < \epsilon_{\max}$ to first order in slow-roll.

First, we compute $\epsilon_{\max}$ for the two-parameter models. For the $\beta_0\beta_1$–model, Eq. (7.23) is given in terms of physical parameters by

$$\epsilon_{\max}^{01} = \frac{3(3m_{\mathrm{FP}}^2 - 2V)^2}{(3m_{\mathrm{FP}}^2 - 4V)V}\,. \tag{7.24}$$

This model is well-defined only if $m_{\mathrm{FP}}^2 > V$ is satisfied, which is more restrictive than the Higuchi bound. Small spin-2 masses in the range $V < m_{\mathrm{FP}}^2 < 4V/3$ lead to a negative upper value, $\epsilon_{\max}^{01} < 0$, such that the bound trivialises. For large spin-2 masses $m_{\mathrm{FP}}^2 \gg V$, the upper limit can be approximated by $\epsilon_{\max}^{01} \simeq 9m_{\mathrm{FP}}^2/V$. For the $\beta_1\beta_4$–model, the expression for the upper limit is the same as in the $\beta_0\beta_1$–model, i.e. $\epsilon_{\max}^{14} = \epsilon_{\max}^{01}$. Moving to the $\beta_1\beta_2$-model, the upper limit is given by

$$\epsilon_{\max}^{12} = \frac{3(3m_{\mathrm{FP}}^2 - V)^2}{(15m_{\mathrm{FP}}^2 - 7V)V}\,. \tag{7.25}$$

Expanding this expression for $m_{\mathrm{FP}}^2 \gg V$ leads to $\epsilon_{\max}^{12} \simeq 9m_{\mathrm{FP}}^2/(5V)$. In case of the $\beta_1\beta_3$–model, Eq. (7.23) in terms of physical parameters is given by

$$\epsilon_{\max}^{13} = \frac{3(3m_{\mathrm{FP}}^2 - 2V)^2}{16(3m_{\mathrm{FP}}^2 - V)m_{\mathrm{FP}}^2}\,. \tag{7.26}$$

For large spin-2 mass $m_{\mathrm{FP}}^2 \gg V$, this expression can be approximated by $\epsilon_{\max}^{13} \simeq 9/16$, which is independent of m_{FP}^2/V in contrast to the previous models.

Summarising the two-parameter models, the upper limit on the slow-roll parameter can be approximated by $\epsilon_{\max} \simeq m_{\mathrm{FP}}^2/V$ up to $\mathcal{O}(1)$ constants. The $\beta_1\beta_3$–model is an exception with the upper limit approximately given by $\epsilon_{\max} \leq 9/16$.

Let us move on to selected three-parameter models. We study the $\beta_1\beta_2\beta_3$-model without vacuum energy and the $\beta_0\beta_1\beta_4$-model with vacuum energy in both metric sectors. In case of the $\beta_0\beta_1\beta_4$–model, setting $\beta_2 = \beta_3 = 0$, solving Eqs. (2.83) and (7.5) for β_0, β_1 and β_4 and plugging the result into Eq. (7.23), leads to the same expression as in the case of the $\beta_0\beta_1$– and $\beta_1\beta_4$–models, i.e. $\epsilon_{\max}^{014} = \epsilon_{\max}^{01}$. We already discussed the typical values of this quantity. Setting $\beta_0 = \beta_4 = 0$ leads to the $\beta_1\beta_2\beta_3$–model, for which the upper limit on ϵ is given by

$$\epsilon_{\max}^{123} = \frac{6(3m_{\mathrm{FP}}^2 - 2V)^2}{(12m_{\mathrm{FP}}^2 - (5 - 3\bar{\alpha}^2)V)V}\,. \tag{7.27}$$

This expression not only depends on m_{FP} and V, but also on the coupling $\bar{\alpha}$.

We plot $\epsilon_{\max}^{123}$ normalised to m_{FP}^2/V as a function of m_{FP}^2/V for different values of $\bar{\alpha}$ in Fig. 7.1. If the coupling is small, $\bar{\alpha} \lesssim 1$, $\epsilon_{\max}^{123}$ becomes independent of $\bar{\alpha}$ and can be approximated by $9m_{\mathrm{FP}}^2/(2V)$ for sufficiently large spin-2 mass. This also follows from expanding Eq. (7.27) for $m_{\mathrm{FP}}^2 \gg V$ and $\bar{\alpha} \ll 1$. For large couplings $\bar{\alpha} \gtrsim \mathcal{O}(1)$, the upper limit on ϵ is suppressed by inverse powers of $\bar{\alpha}$. Expanding Eq. (7.27) for $\bar{\alpha} \gg 1$ leads to $\epsilon_{\max}^{123} \simeq 2(9m_{\mathrm{FP}}^4/V^2 - 12m_{\mathrm{FP}}^2/V + 4)/\bar{\alpha}^2$. However, this parameter region of large coupling is theoretically inconsistent as discussed in Section 4.3.3.

Summarising, within the theoretically consistent regions of the parameter space, the upper limit on ϵ is of the order of m_{FP}^2/V up to $\mathcal{O}(1)$ factors. We thus identified the same scale as for the two-parameter models. Instead of discussing also the other three-parameter models, we next study the full bimetric model with five free interaction parameters β_n.

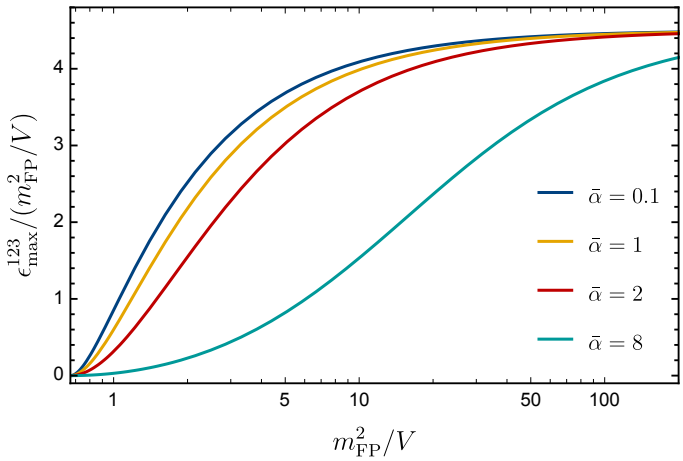

Figure 7.1: The upper limit on ϵ normalised to $m^2_{\rm FP}/V$ as a function of $m^2_{\rm FP}/V$ for the $\beta_1\beta_2\beta_3$-model for different values of $\bar{\alpha}$.

We solve the background Eqs. (2.83) and (7.5) without specifying to a restricted model for the rescaling invariant interaction parameters $\bar{\beta}_1$, $\bar{\beta}_2$, and $\bar{\beta}_3$ in terms of the physical parameters $\bar{\alpha}$, $m_{\rm FP}$, and V. Plugging the results into Eq. (7.23) yields

$$\epsilon_{\max} = \frac{6\bar{\alpha}^2(3m^2_{\rm FP} - 2V)^2}{(3\beta_0 + \bar{\alpha}^2(12m^2_{\rm FP} - 5V + 3\beta_0) + 3\bar{\alpha}^4(V - \bar{\beta}_4) - 3\bar{\alpha}^6\bar{\beta}_4)V}\,, \tag{7.28}$$

as upper limit on ϵ. To assess the order of magnitude, we expand this expression for large spin-2 mass $m^2_{\rm FP} \gg V$, which results in

$$\epsilon_{\max} \simeq \frac{9}{2}\frac{m^2_{\rm FP}}{V}\,. \tag{7.29}$$

The expression is independent of $\bar{\alpha}$ and the order of magnitude is set by $m^2_{\rm FP}/V$ up to an $\mathcal{O}(1)$ factor.

Let us summarise. The bound on ϵ is trivial in some regions of the parameter space because either $\epsilon_{\max} \gg 1$ or $\epsilon_{\max} < 0$. In the remaining regions of the parameter space we found that the order of magnitude of the upper limit is given by $\epsilon_{\max} = \mathcal{O}(m^2_{\rm FP}/V)$. That means that the dynamical Higuchi bound is guaranteed to be satisfied if $\epsilon \lesssim m^2_{\rm FP}/V$.

7.3 Summary and discussion

Ghost-free bimetric theory serves as the low-energy effective field theory to describe FLRW spacetime in the presence of interacting massless and massive spin-2 fields. These fields are subject to the Higuchi bound, which can be generalised to FLRW spacetime by demanding unitarity. Specialising to inflationary spacetime, we assumed that the matter sector consists of a slowly rolling scalar field with effective potential V. In the presence of a massive spin-2 field, the generalised Higuchi bound leads to Eq. (7.21) as upper bound on the slow-roll parameter, which can be summarised as

$$\epsilon \leq c^2\,\frac{m^2_{\rm FP}}{V}\,, \tag{7.30}$$

where $c \sim \mathcal{O}(1)$ a constant[2]. This implies an upper bound on the derivative of the scalar potential upon using Eq. (7.13) of the form

$$\frac{|V'|}{V} \leq \frac{c}{M_{\rm g}}\sqrt{\frac{m^2_{\rm FP}}{V}}\,. \tag{7.31}$$

[2]This constant is not to be confused with the conformal factor, which relates the two metrics on proportional backgrounds.

To arrive at this bound, we assumed that the potential energy of the scalar field dominates the effective cosmological constant, $V \gg \Lambda_{\rm g}$.

The derivation relies on the slow-roll approximation, for which $\epsilon \ll 1$ serves as perturbative parameter. In the parameter regime where $\epsilon \gg 1$, our bound should be treated with caution because the derivation is strictly speaking not trustworthy. This parameter regime corresponds to large spin-2 masses $m_{\rm FP}^2 \gg V$. If the mass of the spin-2 field is close to the Higuchi bound, the bound is trustworthy and most stringent. In addition, there are certain regions of the parameter space, where the generalised Higuchi bound does not imply (7.31). On the other hand, if the scalar potential satisfies the bound (7.31), the generalised Higuchi bound is guaranteed to be satisfied. The various $\mathcal{O}(1)$ factors, which we encountered in the previous section, are collectively captured by the $\mathcal{O}(1)$ parameter c.

The de Sitter swampland conjectures [24, 26, 27] also lead to a bound on the scalar potential, to which we compare our Higuchi bound (7.31). As anticipated in Section 1.3, it is conjectured that the scalar potential must satisfy

$$\frac{|V'|}{V} \geq \frac{c'}{M_{\rm g}} \qquad \text{or} \qquad V'' \leq -\frac{c''}{M_{\rm g}^2} V \,, \tag{7.32}$$

with $c', c'' \sim \mathcal{O}(1)$ universal constants, for the effective theory to not lie on the swampland.

Combining the lower bound from the de Sitter swampland conjecture (7.32) with the upper bound from the generalised Higuchi bound (7.31) in BT restricts the derivative of the scalar potential into the parametric window

$$\frac{c'}{M_{\rm g}} \leq \frac{|V'|}{V} \leq \frac{c}{M_{\rm g}} \sqrt{\frac{m_{\rm FP}^2}{V}} \,. \tag{7.33}$$

If the spin-2 mass is close to the de Sitter Higuchi bound, the parametric window is small and in the derivative has to be of the order $|V'|/V \simeq 1/M_{\rm g}$. The window does not close completely due to the de Sitter Higuchi bound (7.3).

Since we discuss our bound in the context of the swampland, let us connect our setup to String Theory. It is natural to assume that the spin-2 mass $m_{\rm FP}$ is related to higher spin string excitations [420]. This allows to identify the spin-2 mass with the string scale $m_{\rm FP} \sim M_{\rm s}$. Assuming that our bound holds generally, Eq. (7.31) becomes

$$\frac{|V'|}{V} \leq c \frac{M_{\rm s}}{M_{\rm g}} \sqrt{\frac{1}{V}} \,. \tag{7.34}$$

As derived in [416], the string scale must satisfy the lower bound $M_{\rm s} > \sqrt{H M_{\rm g}}$, which follows from requiring that the entire string Regge trajectory satisfies the Higuchi bound. Trading the Hubble parameter for the scalar potential at $\epsilon = 0$ leads to

$$M_{\rm s}^2 \geq \sqrt{\frac{V}{3}} M_{\rm g} \,. \tag{7.35}$$

Therefore, our condition (7.34) is always satisfied if the stronger bound

$$\frac{|V'|}{V} \leq \frac{c}{M_{\rm g}} \sqrt{\frac{M_{\rm g}}{(V/3)^{1/2}}} \tag{7.36}$$

is satisfied.

To summarise, we utilised the physical parametrisation of Chapter 4 to single out the following implication of the presence of a massive spin-2 field during slow-roll inflation. From the generalised Higuchi bound, we derived an upper bound on the derivative of the scalar potential, which is complementary to the lower bound obtained from string theoretic considerations [24–28]. The derivative is therefore forced to lie in the parametric window (7.33) for quantum consistency.

It would be interesting to study whether the upper bound on V' is a generic implication of unitarity when massive spin-2 fields propagate on FLRW spacetime. This requires a treatment beyond slow-roll. Further, it would be interesting to check, whether this combined bound is satisfied, e.g. in concrete String Theory settings. Finally, inflationary spacetimes in the presence of spin-2 fields were studied in [313–316, 318–321]. It would be interesting to confront our formal bound with the phenomenological constraints of these references.

Chapter 8

Summary and outlook

Einstein's General Relativity (GR) is the widely celebrated theory of gravity. However, while it describes laboratory to solar system scales to very high precision, its viability on larger scales has been challenged in recent times. For the cosmological standard model to be compatible with observations and simulations, the universe is required to be filled with dark energy and dark matter, which together comprise 95% of the current energy budget of the universe, but for which we lack a fundamental description. This thesis is part of the ongoing efforts to furtherance our understanding of the dark sector.

Dark energy is modelled by a cosmological constant within GR, which is added to the Einstein–Hilbert term as in Eq. (1.8). Nevertheless, the validity of a positive cosmological constant *per se* has been questioned. The huge mismatch between its observed value and the value predicted by robust theories of particle physics represents a fine-tuning problem in the sense of 't Hooft [86]. The noted discrepancy theoretically disfavours the observed tiny value of the cosmological constant. Besides, very general results from the swampland program [24, 26, 27] and the quantum breaking of de Sitter [21–23, 25, 28] strongly hint at a true theoretical inconsistency for *any* value larger than zero of the cosmological constant at the fundamental level. Moreover, the latest available observational data has a slight preference for dark energy that dynamically evolves in time, as opposed to (only) a cosmological constant [75, 109, 430, 431]; a conclusion that is drawn utilising a purely phenomenological model.

All the above motivates us to seek for alternatives to a cosmological constant when it comes to a fundamental explanation for dark energy. Indeed, the given considerations suggest that GR with a cosmological constant might not be the appropriate gravitational theory on cosmological scales. Therefore, we are naturally drawn to the study of modifications of the said gravitational theory on large scales and/or to replacements of its cosmological constant by some other form of dark energy, both directions being related [432].

The ongoing pursuit for novel mechanisms that lead to an accelerated expansion of the universe at late times has resulted in the postulation of a plethora of modified gravity theories. Here, we focus on the particular subset of such theories that entertain the simple and appealing idea of giving a mass to the graviton. The implementation of this idea turned out to be mathematically challenging, due to the appearance of ghost instabilities [39, 40, 47]. The postulation of ghost-free massive gravity and bimetric theory (BT) [48–52, 209] not only solved this longstanding problem, but also filled the gap in the list of effective theories for massless and massive fields with spin up to 2[1]

By now, the theoretical viability of BT has been firmly established and its potential to address the aforementioned problems in modern cosmology has been convincingly argued for. Among the virtues of BT are self-accelerating cosmological models with a technically natural effective cosmological constant [216, 256, 257, 262–265, 329], its ability to alleviate the Hubble tension [277,

[1]The consideration of higher than 2 spin fields requires an infinite tower of higher spin fields for the internal consistency of the theory. We do not consider such scenarios in this thesis.

296], the Vainshtein screening mechanism, which restores GR on small scales [329, 331, 332], and the massive spin-2 field as a dark matter candidate [227, 255, 433]. However, these features have been analysed within different parametrisations and under different assumptions. Such variety prevents the comparison between related constraints. For this reason, it is not yet clear which of these features can be realised simultaneously while being consistent with all observational data.

This thesis overcomes the aforementioned shortcomings of the previous analyses. To do so, we first developed a new unified framework, which allows to consistently study the phenomenology of BT and compare the relevant constraints among themselves. Building upon our new framework, we thoroughly revisited the phenomenological consequences of BT on length scales ranging from the laboratory to cosmology. In the following, we elaborate on our said results.

Summary of original results and contextualisation

This thesis is concerned with the phenomenological consequences of nonlinear ghost-free bimetric theory (BT) [51, 52, 209]. The bimetric action (3.1) has a priori six independent free parameters $\{\alpha, \beta_n\}$ with $n = 0, \ldots, 4$. One of these parameters is redundant due to the theory's invariance under the rescaling transformation (4.1) [223, 301]. The final five independent free parameters of BT span a huge parameter space, which is challenging to handle[2].

To deal with the large free parameter space, the aforementioned rescaling invariance has been commonly used to set $\alpha = 1$ in the literature. However, such choices to fix the rescaling are ambiguous. To avoid this ambiguity, we require a parametrisation of the bimetric solutions, which are invariant under the said rescaling.

In addition, cosmological data has been used to compute constraints on the remaining interaction parameters $\{\beta_n\}$. However, these parameters are not observables themselves, because they get shifted under the rescaling transformation (4.1). Hence, also their associated constraints depend on the chosen rescaling. We thus need an alternative parametrisation to consistently constrain BT with cosmological observations.

The first main goal of this thesis has been to overcome the shortcomings of the previous analyses, with an emphasis on the bimetric phenomenology. To begin with, in Chapter 4 we proposed a new parametrisation of solutions of BT in terms of quantities that are manifestly invariant under the aforementioned rescaling and that enjoy a direct physical interpretation. We chose the following three apposite physical parameters: the coupling strength $\bar{\alpha}$ of the massive spin-2 field to standard matter, its mass $m_{\rm FP}$ and the effective cosmological constant Λ [340]. Our framework is suited for all bimetric models with up to three free interaction parameters. The value and potential of our proposed parametrisation has been acknowledged by the community and recently it has been extended to even more general bimetric models [260].

Our unoriginally baptised *physical parametrisation* has several advantages. Firstly, the parameters are rescaling invariant and hence observable by construction. Secondly, it provides the unified framework to comprehensively study the phenomenological implications of BT. As such, it forms the basis to combine the various existing and future theoretical and observational constraints on BT and thus identify the consistent regions of its parameter space. Thirdly, the parameter values are very intuitive, due to their direct physical meaning. For instance, our parametrisation vastly simplifies choosing priors in a statistical analysis.

We explicitly worked out the physical parametrisation for all models with up to three free interaction parameters [340]. We built up a dictionary between the parameters $\{\alpha, \beta_n\}$ and $\{\bar{\alpha}, m_{\rm FP}, \Lambda\}$ for all such models, which can immediately be used for future investigations. Further, we computed the theoretical consistency constraints on the physical parameters to ensure a viable cosmic expansion history, i.e. real-valued, non-singular, and devoid of the Higuchi ghost. These can directly be used as theoretical priors and be compared to other constraints coming from other theoretical and observational considerations. Our results set the basis to thoroughly study the phenomenological consequences of BT.

[2]Note that GR has only a single free parameter, the cosmological constant Λ. In general, also the Planck mass is a free parameter of both GR and BT, which however is already tightly constrained by observations. Therefore, we exclude it from our discussion on the free parameters.

Equipped with the physical parametrisation, we reinvestigated the problem of cosmological perturbations in Chapter 5. As we reviewed, the gradient instability challenges the viability of bimetric cosmology at the perturbative level [226, 266, 270, 272, 274, 275, 300–305]. The problem can be avoided by pushing the gradient instability to arbitrarily early times. This is achieved in the parametric limit $m_{\rm FP} \gg H_0$ [226, 277]. However, in the context of background cosmology, it is usually assumed that $m_{\rm FP} \sim H_0$. Put together, these considerations would naively imply that bimetric cosmology cannot be viable at the background and perturbative levels simultaneously. We invalidated this hasty conclusion in two distinct ways.

In Chapter 5, we investigated the Vainshtein screening in the context of cosmology. Drawing inspiration from spherically symmetric systems, we showed that the universe is smaller than its own corresponding Vainshtein radius during early times, precisely when $H > m_{\rm FP}$. We therefore expect linear perturbation theory to break down during such early times. We verified that deviations form GR are indeed screened away on the level of background cosmology and that the gradient instability occurs precisely when the Hubble rate exceeds the spin-2 mass. Combined with the results of [308–310], our results indicate that perturbations are nonlinearly stabilised by means of the Vainshtein mechanism. This implies that also the parameter region with $m_{\rm FP} \sim H_0$ is a priori viable on the perturbative level, thus reviving bimetric cosmology.

These considerations show that the entire theoretically allowed parameter space is a priori consistent. However, many of the previous studies assumed $m_{\rm FP} \sim H_0$ in the context of background cosmology. As a first step, we demonstrated that this region is potentially consistent also on the level of cosmological perturbations. As the next step, we explicitly demonstrated that $m_{\rm FP} \gg H_0$ is consistent at the level of background cosmology. Our physical parametrisation serves as the basis to straightforwardly study the thus enlarged parameter space.

In Chapter 6, we compared the entire bimetric parameter space to cosmological observations. Specifically, we performed a statistical analysis using data from measurements of Supernovae type 1a, Baryon Acoustic Oscillations and the Cosmic Microwave Background, as it has become standard in parameter estimation for cosmological models. As expected, all our bimetric models fit the observed data as good as the standard cosmological model, which is in agreement with earlier results in the appropriate limits [216, 263, 265, 296, 297, 337]. The preferred values of the cosmological parameters are indistinguishable from the standard values at the level of current precision. For instance, we find that a spatially flat universe is always preferred, consenting with [297]. Therefore, the self-accelerating bimetric models, which are characterised by $\beta_0 = 0$ and thus devoid of a cosmological constant, stand out as promising competitors to the standard cosmological model.

There is but one exception from the previous conclusion. The special β_1–model of BT leads to a cosmic expansion history significantly different from the standard one. Nonetheless, our statistical analysis strongly disfavours this model. Combining the cosmological with the later discussed local constraints further disfavours this model by many standard deviations. Therefore, we concluded that this model is statistically ruled out and we will exclude it from our subsequent discussions.

Moreover, our results constitute the first ever cosmological constraining of the physical parameters of BT theory [298, 340]. We showed that the coupling is constrained to be small $\bar{\alpha} \lesssim \mathcal{O}(0.1)$ for all models. This means that deviations from GR must be sufficiently suppressed, but not entirely. The spin-2 mass is constrained to be rather small $m_{\rm FP} \sim H_0$ only for the special $\beta_0\beta_1$–model. For the remaining models, the spin-2 mass is limited only by the Higuchi bound (2.84) and the cutoff of the effective theory, i.e. $2\Lambda/3 \lesssim m_{\rm FP}^2 \lesssim M_{\rm g}^2$. Notwithstanding, our results show that large spin-2 masses require the coupling $\bar{\alpha}$ to be sufficiently small at the same time for consistency. We explicitly quantified the combined restriction on the physical parameters. The constraints are depicted in Fig. 6.6 for the three-parameter models. In summary, our results are the first demonstration that BT provides a good fit to the observed cosmological data even if the spin-2 field is heavy.

Moving beyond cosmology, modifications of the gravitational interactions are tightly constrained by local tests of gravity. We are here referring to the gravitational potential and the scalar curvature as felt by massive and massless test bodies, respectively. These probe scales mostly within the solar system, but also galactic and extragalactic scales. In Chapter 6, we re-

lated the existing constraints [343, 344, 346–348] on modifications of the gravitational interaction within the Yukawa parametrisation to the physical parameters $\bar{\alpha}$ and m_{FP} of BT [298]. The results are graphically summarised in Fig. 6.7. The most stringent bound comes from Lunar-Laser-Ranging, which leads to $\bar{\alpha} \lesssim 8.9 \times 10^{-6}$ at the mass scale $m_{\mathrm{FP}} \sim 6.5 \times 10^{-15}\,\mathrm{eV}$. For small spin-2 masses, Cassini provides the most stringent bound $\bar{\alpha} \lesssim 1.7 \times 10^{-3}$. The coupling is essentially unconstrained for large masses $m_{\mathrm{FP}} \gtrsim 10^{-2}\,\mathrm{eV}$. Thanks to our physical parametrisation, these constraints can be straightforwardly compared to our previously obtained cosmological constraints.

Our said conclusions are valid only without the Vainshtein screening. In fact, the Vainshtein mechanism suppresses modifications from GR in spacetime regions close to massive sources, which potentially removes the associated observational constraints. We also took this effect into account, which turned out to be relevant only for the $\beta_1\beta_2\beta_3$–model. For this model, the Vainshtein screening alleviates the Cassini constraint on the coupling for small spin-2 mass as $\bar{\alpha} \leq \mathcal{O}(0.1)$. The constraints, when taking the Vainshtein screening into account, are portrayed in Fig. 6.10. Building upon some earlier work [330, 332, 338], our results conform the first thorough constraining of BT from local tests of gravity [298].

As mentioned before, one of the key motivations for our proposed physical parametrisation is to confront the various observational and theoretical bounds with each other, in order to assess the ultimate phenomenological viability of BT. In this thesis, we have also accomplished this final step [298]. Indeed, we identified those parameter combinations that are consistent with all aforementioned constraints. For most of the bimetric parameter space, the cosmological constraints are more stringent than the local constraints. Although we found that all models are perfectly consistent, models that do not give rise to Vainshtein screening are essentially driven into their GR-limits, since the coupling is bounded from above as $\bar{\alpha} \lesssim 1.3 \times 10^{-3}$. The Vainshtein mechanism alleviates this bound for the $\beta_1\beta_2\beta_3$–model to $\bar{\alpha} \leq \mathcal{O}(0.1)$. In short, this thesis comprises the hitherto most thorough and stringent constraining of BT because we consistently studied the entire available parameter space, we imposed our derived theoretical consistency constraints, we utilised a plethora of cosmological and local tests of gravity and we implemented the Vainshtein screening.

Last but not least, we went beyond observational considerations and utilised the physical parametrisation in the context of slow-roll inflation. Since higher spin states, both massless and massive, are a generic prediction of quantum gravity, these should be included in the effective field theory describing, e.g. inflation. However, these states are subject to severe consistency restrictions, such as the Higuchi bound. In Chapter 7, we analysed the simplest non-trivial case of a massive spin-2 field in addition to the usual massless spin-2 field. We showed that the generalisation of the Higuchi bound implies an upper limit on the derivative of the inflaton potential, which is complementary to the de Sitter swampland [24, 26, 27] and quantum breaking [28] bounds. Future investigations in the context of inflation and the CMB within BT should certainly take our unveiled bound into account.

Further contextualisation and outlook

Our comprehensive study simultaneously confronted BT with theoretical constraints ensuring a viable cosmic expansion history and with observational constraints from cosmological and local tests of gravity. In this manner, we have placed the most stringent constraints on BT to date. In particular, our results are more constraining than galactic [339] and gravitational waves [324] measurements. Our analysis shows that large regions of the bimetric parameter space remain consistent.

The obvious next step based on our physical parameterisation is to confront BT with further constraints. On the observational side, we want to highlight the next generation of surveys such as DES [434], DESI [435], Euclid [436], SKA [437] and VRO [438], which will provide data at various redshifts and to high precision, already relevant for background cosmology. For instance, these surveys will yield new BAO data, which in turn will allow to accurately trace back the dark energy equation-of-state. A null detection of phantom dark energy would imply a stricter upper

limit on $\bar{\alpha}$ or a stricter lower limit on $m_{\rm FP}$. If these surveys instead provide further evidence supporting phantom dark energy, BT will be statistically favoured over GR. As we have discussed, such slight preference already exists, but it is statistically insignificant at the level of current uncertainties. Hence, once these new data are available, bimetric background cosmology will need to be revisited. The methodology presented in this thesis provides a solid basis for such essential future investigations.

Staying in the realm of cosmology, the surveys aiming at mapping out the anisotropies and in particular the polarisation patterns in the CMB such as CMB-S4 [439] and LiteBIRD [440] are very promising for testing BT. A main reason is that the Vainshtein screening is active in the scalar sector, but not in the tensor sector. Therefore, primordial gravitational waves are an excellent playground for further constraining BT. In particular, since $\bar{\alpha}$ quantifies the mixing between the massless and massive mode in the original metric fluctuation, and since the massive mode quickly decays [313, 315, 318], these measurements will provide an upper limit on $\bar{\alpha}$. Hence, expected constraints implied by these future surveys should be compared to the results presented in this thesis, once the new data are available.

As already mentioned, the Vainshtein screening mechanism —if active— makes it extremely difficult to find distinct signatures of BT, for example, in the solar system. A possible way around this is to study systems with less than spherical symmetry. In the context of Galileons, it was found that the Vainshtein screening is weaker or even completely absent in systems with cylindrical or planar symmetry, respectively [412]. Although the explicit confirmation is still pending, we expect a similar behaviour also for BT. To make use of this effect, one possible direction are laboratory tests of gravity [441, 442]. However, due to the involved scales, we expect that these would mostly be able to probe the mass range $m_{\rm FP} \gtrsim 10^{-5}\,\mathrm{eV}$, where it will be extremely challenging for laboratory constraints on $\bar{\alpha}$ to compete with our stringent cosmological constraints.

Alternatively, astrophysical objects and the cosmic web might help to constrain screened modified gravity, because of the reduced amount of symmetry or as a result of the multiple scales involved. See [443–456] for work regarding the Vainshtein screening, among others, and [457, 458] for reviews. However, all these studies are based on modified gravity theories other than BT (e.g. Galileons or DGP), which incorporate the Vainshtein screening as well. It would be an interesting task to carry out similar investigations and compare the resulting constraints to the ones presented in this thesis.

Leaving aside the observational realm, BT can also be subjected to further theoretical constraints. Just like GR, BT serves as a low-energy effective theory. Requiring a local, unitary, analytic and Lorentz-invariant UV-completion imposes so-called *positivity bounds* on the parameters of the low-energy effective theory [459]. These have already been studied in the context of spin-2 fields [460–466]. For instance, positivity bounds turned out to have strong constraining power in the context of Scalar–Tensor theories [467]. It would be interesting to apply this methodology to BT and elucidate the obtained positivity bounds by means of our physical parametrisation.

The question of a consistent UV-completion is also closely related to the swampland program [421, 422]. The ultimate goal is arguably to explicitly embed BT into String Theory. See [419, 420, 423, 424] for first studies into this promising direction. This program would also identify the quantum consistent parameter combinations, which would then need to be complemented by our observational constraints.

Probably the most pressing next step regards cosmological perturbations. As we discussed in Section 3.1.4 and Chapter 5, the scalar sector is plagued by an early-time gradient instability rendering linear perturbation theory invalid. Our results the cosmological perturbations are non-linearly stabilised due to the Vainshtein screening. First results into this direction exist [308–310], but there is clearly more work required to fully understand the perturbative level in BT. This will open up the possibility to apply the plethora of perturbative constraints on BT. In particular, it will allow to understand the formation of structure in the universe. Interestingly, this might shed new light on the required dark matter abundance within BT, due to the enhanced gravitational strength on scales between Vainshtein and Compton.

One way to tackle cosmic structure formation is via simulations. This problem has been solved in the context of Galileons, which also exhibit the Vainshtein screening [468–472]. There

is progress regarding simulations also within BT, mostly in the context of spherical collapse [473–480]. However, technical difficulties related to finding stable (well-posed) equations of motion still prevent long-termed simulations. Clearly, being able to handle numerical simulations will open up many new possibilities to assess the viability of BT.

At last, let us direct our attention to the second constituent of the dark sector. In fact, BT contains the massive spin-2 particle as an ideal dark matter candidate. It interacts with matter exclusively gravitationally with universal coupling $\bar{\alpha}$ [227, 255, 433]. Depending on the production mechanism, the mass must be of the order $m_{\mathrm{FP}} \sim 1 \ldots 100\,\mathrm{TeV}$ [227] or below, down to $m_{\mathrm{FP}} \sim 10\,\mathrm{MeV}$ [481]. Within BT, the phenomena ascribed to dark matter are but a manifestation of gravity itself. Since our previous discussions explicitly showed that this mass region is observationally consistent in the context of dark energy as well, BT has the potential to provide an unified explanation for the whole dark sector.

This appealing idea requires further investigation. In more detail, computational control over the aforementioned dark matter scenario requires the perturbative bound $\bar{\alpha} M_{\mathrm{P}} \geq m_{\mathrm{FP}}$ to be satisfied [227], which implies a lower limit on the coupling. The weakest bound is realised for the lowest spin-2 mass possible, leading to $\bar{\alpha} \gtrsim 10^{-21}$ [481]. Unfortunately, this bound is in conflict with our upper bound from cosmology by many standard deviations (see Eq. (6.42) and Fig. 6.6). The conflict seems to persist even in more general bimetric models [299].

One possible, but presumably rather challenging, way out is to study the dark matter phenomenology by means of non-perturbative techniques to avoid the aforementioned perturbative bound. Alternatively, the implied strong constraints can be alleviated by considering smaller spin-2 masses, as in the context of ultra light dark matter [482]. Some phenomenological consequences of this scenario have been explored in [483–489]. It remains an open question whether BT can incorporate both phenomena ascribed to the dark sector in this mass region. Our proposed physical parametrisation and the herein obtained parameter constraints serve as excellent basis to make substantial progress into this exciting direction.

Finally, these previous studies implicitly assume that the dark matter abundance required to match observations is the same as in standard cosmology. This might not be the case within BT, due to the fifth force and the Vainshtein screening. Such interesting direction has been pursued in [339], in the context of galaxy cluster lensing and galaxy rotation curves. Indeed, it is found that the required dark matter abundance on these scales is lowered with respect to GR for certain values of the spin-2 mass. More generally, the effect of a Yukawa-type fifth force on galaxy rotation curves in the presence of dark matter has been explored in [490, 491], which indeed shows a preference for a non-zero Yukawa modification to the Newtonian potential. In addition, less dark matter might be required for cosmic structure formation to work for the same reasons mentioned above. These considerations might affect the spin-2 dark matter scenario notably. Although their quantification is a topic beyond this thesis, we here set the basis for consistently constraining such spin-2 dark matter scenario and, going even further, such unified dark sector scenario.

* * * * *

Within the ongoing pursuit to give a fundamental explanation for the Universe's dark sector, BT is a particularly appealing and promising alternative to GR. The theory proposes to supplement the usual massless spin-2 field with an additional massive spin-2 field, both of which (self-)interact fully nonlinearly. The interaction energy can cause the Universe to exponentially expand at late cosmic times. The massive spin-2 field serves as a dark matter candidate. In this thesis, we proposed a new unified framework to assess the phenomenological consequences of BT. With this as a basis, we thoroughly constrained the properties of such massive spin-2 field by means of various cosmological and local tests of gravity for the first time. Our results indicate that BT has the potential to provide an unified explanation for the entire dark sector, which calls for additional research efforts building on that idea. Going beyond, our methodology and results set the basis for further constraining BT by means of theoretical and observational considerations. Such future investigations will help addressing the aforementioned open and pressing problems of our current

understanding of the Universe. Exciting years lie ahead for modern cosmology, as exemplified by the many ongoing and pending research directions here mentioned. This thesis constitutes an important step forward in their consecution.

Appendix A

Details on static, spherically symmetric solutions

In this appendix, we present the derivation of static and spherically symmetric solutions as presented in [298] and as summarised in Section 3.2. These solutions were first studied in [328–333]. We follow the derivation of [331, 332], but allow for a non-vanishing effective cosmological constant [334]. This allows to match the local solutions to cosmological solutions asymptotically and compare the corresponding observational constraints. In the limit of vanishing cosmological constant, our results reduce straightforwardly to the ones obtained in [331, 332].

As starting point, we assume spacetime to be static and spherically symmetric. The appropriate ansatz for the the metrics $g_{\mu\nu}$ and $f_{\mu\nu}$ in the bidiagonal case is [331]

$$\begin{aligned} \mathrm{d}s_{\mathrm{g}}^2 &= -e^{-\phi_{\mathrm{g}}}\mathrm{d}t^2 + e^{\psi_{\mathrm{g}}}\mathrm{d}r^2 + r^2\mathrm{d}\Omega^2\,, \\ \mathrm{d}s_{\mathrm{f}}^2 &= c^2\left(-e^{-\phi_{\mathrm{f}}}\mathrm{d}t^2 + e^{\psi_{\mathrm{f}}}(r+r\mu)'^2\mathrm{d}r^2 + (r+r\mu)^2\mathrm{d}\Omega^2\right)\,, \end{aligned} \tag{A.1}$$

where all functions $\phi_{\mathrm{g,f}}$, $\psi_{\mathrm{g,f}}$, and μ depend only on the radius r. The field μ can be associated with a Stückelberg field, which restores diffeomorphisms in the r-dimension [177]. In the limit where $\phi_{\mathrm{g}} = \phi_{\mathrm{f}}$ and $\psi_{\mathrm{g}} = \psi_{\mathrm{f}}$, as well as $\mu = 0$, both metrics are proportional $f_{\mu\nu} = c^2 g_{\mu\nu}$.

We want to compute the gravitational potentials outside a compact object like a star or planet. In this case, we can write the matter energy-momentum tensor as $T^{\mu}_{\ \nu} = \mathrm{diag}(M, 0, 0, 0)$. The Schwarzschild radius r_{S} of a compact object of mass M is given by

$$r_{\mathrm{S}} = \frac{M}{4\pi M_{\mathrm{g}}^2}\,. \tag{A.2}$$

Following [331], we linearise the equations of motion in the gravitational fields $\phi_{\mathrm{g,f}}$ and $\psi_{\mathrm{g,f}}$, but we keep all nonlinearities in μ. Technically, we assume $\{|\psi_{\mathrm{g,f}}|, |\phi_{\mathrm{g,f}}|\} \ll 1$ and $\{|r\psi'_{\mathrm{g,f}}|, |r\phi'_{\mathrm{g,f}}|\} \ll 1$. Under these approximations, the tt-, rr, and $\theta\theta$-components of the $g_{\mu\nu}$–Einstein equation (3.2) simplify to

$$\begin{aligned} \frac{(r\psi_{\mathrm{g}})'}{r^2} &= \Lambda + \frac{\rho(r)}{m_{\mathrm{g}}^2} + \frac{\bar{\alpha}^2 m_{\mathrm{FP}}^2}{1+\bar{\alpha}^2}\left(\frac{1}{2}(\psi_{\mathrm{f}} - \psi_{\mathrm{g}}) + \frac{1}{r^2}\Big[r^3\left(\mu + \beta\mu^2 + \frac{\gamma}{3}\mu^3\right)\Big]'\right) \\ \frac{\psi_{\mathrm{g}}}{r^2} - \frac{\phi'_{\mathrm{g}}}{r} &= \Lambda + \frac{\bar{\alpha}^2 m_{\mathrm{FP}}^2}{1+\bar{\alpha}^2}\left(\frac{1}{2}(\phi_{\mathrm{f}} - \phi_{\mathrm{g}}) + 2\mu + \beta\mu^2\right)\,, \\ -\frac{\psi'_{\mathrm{g}}}{2r} + \frac{(r\phi'_{\mathrm{g}})'}{2r} &= \Lambda + \frac{\bar{\alpha}^2 m_{\mathrm{FP}}^2}{1+\bar{\alpha}^2}\left(\frac{1}{2}(\psi_{\mathrm{f}} - \psi_{\mathrm{g}} + \phi_{\mathrm{f}} - \phi_{\mathrm{g}}) + \frac{1}{r}\Big[r^2\left(\mu + \frac{\beta}{2}\mu^2\right)\Big]'\right)\,, \end{aligned} \tag{A.3}$$

respectively. The parameters β and γ are defined in Eq. (3.37). The same components of the

$f_{\mu\nu}$–Einstein equations (3.2) can be brought into the form

$$\begin{aligned}
\frac{((r+r\mu)\psi_{\rm f})'}{r^2} &= \Lambda - \frac{m_{\rm FP}^2}{1+\bar{\alpha}^2}\left(\frac{1}{2}(\psi_{\rm f}-\psi_{\rm g}) + \frac{1}{r^2}\Big[r^3\Big(\mu + (1+\beta)\mu^2 + \frac{1+\beta+\gamma}{3}\mu^3\Big)\Big]'\right),\\
(r+r\mu)'\frac{\psi_{\rm f}}{r^2} - (1+\mu)\frac{\phi_{\rm f}'}{r} &= \Lambda - \frac{m_{\rm FP}^2}{1+\bar{\alpha}^2}\Big(\frac{1}{2}(\phi_{\rm f}-\phi_{\rm g}) + 2\mu + (1+\beta)\mu^2\Big)(r+r\mu)',\\
\frac{\psi_{\rm f}}{2r} - \frac{1}{2r}\left(\frac{(r+r\mu)\phi_{\rm f}'}{(r+r\mu)'}\right)' &= \Lambda - \frac{m_{\rm FP}^2}{1+\bar{\alpha}^2}\left(\frac{1}{2}(\psi_{\rm f}-\psi_{\rm g}-\phi_{\rm f}-\phi_{\rm g}) + + \frac{1}{r}\Big[r^2\left(\mu + \frac{1+\beta}{2}\mu^2\right)\Big]'\right),
\end{aligned} \tag{A.4}$$

respectively. The $\phi\phi$-components coincide with the $\theta\theta$-components in both cases due to the assumed spherical symmetry. Finally, the Bianchi constraint (2.71) is given by

$$\frac{(r+r\mu)'}{r}(1+\beta\mu)(\psi_{\rm f}-\psi_{\rm g}) - \frac{1}{2}(1+2\beta\mu+\gamma\mu^2)(\phi_{\rm f}' - (r+r\mu)'\phi_{\rm g}') = 0\,. \tag{A.5}$$

The equations do not admit an analytic solution. Instead of solving the equations numerically, we go to two different regimes that lead to further simplifications, which give rise to analytical solutions. We focus on scales much smaller than the de Sitter horizon, i.e. $r \ll 3/\sqrt{\Lambda}$. Firstly, we assume that also μ is a small, which allows further linearisation. Secondly, we take into account all nonlinearities in μ, but assume that we are on scales much smaller than the Compton wavelength of the massive spin-2 field, $r \ll m_{\rm FP}^{-1}$. Thirdly, we match both solutions to each other on scales, where both are well-defined.

Linear regime

As mentioned above, we first assume that all functions are small, including μ. In the technical level, we expand Eqs. (A.3) to (A.5) also for $|\mu| \ll 1$ and $|r\mu'| \ll 1$. To ease the notation, we define the auxiliary fields

$$\psi_\pm = \psi_{\rm f} \pm \psi_{\rm g}\,,\ \phi_\pm = \phi_{\rm f} \pm \phi_{\rm g}\,. \tag{A.6}$$

The fully linearised Bianchi constraint (A.5) becomes independent of the +-fields and is given by

$$2\psi_- = r\phi_-'\,. \tag{A.7}$$

The fully linearised Einstein equations for $g_{\mu\nu}$ and $f_{\mu\nu}$ can be combined so that the +-fields drop out of the expressions. This results in

$$0 = 2r\psi_-' + \left(2 + m_{\rm FP}^2 r^2\right)\psi_- + 2m_{\rm FP}^2 r^2(3\mu + r\mu')\,, \tag{A.8a}$$

$$0 = -2\psi_- + m_{\rm FP}^2 r^2(\phi_- + 4\mu)\,, \tag{A.8b}$$

$$0 = r\psi_-' - m_{\rm FP}^2 r^2(\psi_- + \phi_- + 4\mu + 2r\mu')\,, \tag{A.8c}$$

upon using the Bianchi constraint (A.7) to eliminate ϕ_-' and ϕ_-'' in terms of ψ_- and ψ_-'. Using the algebraic equation (A.8b) to eliminate ϕ_- from Eq. (A.8c), and solving Eqs. (A.8a) and (A.8c) for ψ_- and μ leads to

$$\psi_-' = -2m_{\rm FP}^2\, r\mu\,, \quad \mu' = -\frac{(2+m_{\rm FP}^2\, r^2)\psi_- + 2m_{\rm FP}^2\, r^2\mu}{2m_{\rm FP}^2\, r^3}\,. \tag{A.9}$$

These represent two coupled first-order differential equations, which are solved by

$$\begin{aligned}
\phi_- &= \frac{C_1 e^{-m_{\rm FP}\, r}}{r}\,,\\
\psi_- &= -\frac{C_1(1+m_{\rm FP}\, r)e^{-m_{\rm FP}\, r}}{2r}\,,\\
\mu &= -\frac{C_1\left(1+m_{\rm FP}^2\, r + m_{\rm FP}^2 r^2\right)e^{-m_{\rm FP}\, r}}{4m_{\rm FP}^2 r^3}\,,
\end{aligned} \tag{A.10}$$

where the solution for ϕ_- is determined by Eq. (A.8b). Here, C_1 is a constant of integration, which we will determine later. We already fixed the other constant of integration by requiring that the fields $r \to \infty$ to ensure asymptotical proportionality.

It remains to solve for the fields ϕ_+ and ψ_+. The second set of linearly independent Einstein equations can be arranged to

$$\begin{aligned} 0 &= (\bar{\alpha}^2 - 1)(\psi_- + r\psi_-') + (1 + \bar{\alpha}^2)(\psi_+ + r\psi_+') - 2(1 + \bar{\alpha}^2)\Lambda r^2 \,, \\ 0 &= (\bar{\alpha}^2 - 1)\psi_- - (1 + \bar{\alpha}^2)(\psi_+ - r\phi_+') + 2(1 + \bar{\alpha}^2)\Lambda r^2 \,, \\ 0 &= (\bar{\alpha}^2 - 1)\psi_-' - (1 + \bar{\alpha}^2)(\psi_+' - \phi_+' - r\phi_+'' - 4\Lambda r) \end{aligned} \tag{A.11}$$

Using the solutions Eq. (A.10) to eliminate ψ_+, these equations admit the following solutions:

$$\begin{aligned} \phi_+ &= -\frac{2\Lambda r^2}{3} - \frac{2C_2}{r} - \frac{C_1 e^{-m_{\mathrm{FP}}\, r}}{(1 + \bar{\alpha}^2) r} \,, \\ \psi_+ &= \frac{2\Lambda r^2}{3} + \frac{2C_2}{r} + \frac{C_1 (1 + m_{\mathrm{FP}}\, r) e^{-m_{\mathrm{FP}}\, r}}{2(1 + \bar{\alpha}^2) r} \,, \end{aligned} \tag{A.12}$$

where C_2 is another constant of integration. The other constant of integration has be fixed to ensure regularity in the limit $r \to \infty$.

We solved the set of differential equations in terms of $\phi_\pm$, $\psi_\pm$, and μ. Solving (A.6) for the original metric functions, we arrive at

$$\begin{aligned} \mu &= -\frac{C_1 (1 + m_{\mathrm{FP}}\, r + m_{\mathrm{FP}}^2 r^2) e^{-m_{\mathrm{FP}}\, r}}{4 m_{\mathrm{FP}}^2 r^3} \,, \\ \phi_{\mathrm{g}} &= -\frac{\Lambda r^2}{3} - \frac{C_2}{r} - \frac{C_1 \bar{\alpha}^2 e^{-m_{\mathrm{FP}}\, r}}{(1 + \bar{\alpha}^2) r} \,, \\ \phi_{\mathrm{f}} &= -\frac{\Lambda r^2}{3} - \frac{C_2}{r} + \frac{C_1 e^{-m_{\mathrm{FP}}\, r}}{(1 + \bar{\alpha}^2) r} \,, \\ \psi_{\mathrm{g}} &= \frac{\Lambda r^2}{3} + \frac{C_2}{r} + \frac{C_1 \bar{\alpha}^2 (1 + m_{\mathrm{FP}}\, r) e^{-m_{\mathrm{FP}}\, r}}{2(1 + \bar{\alpha}^2) r} \,, \\ \psi_{\mathrm{f}} &= \frac{\Lambda r^2}{3} + \frac{C_2}{r} - \frac{C_1 (1 + m_{\mathrm{FP}}\, r) e^{-m_{\mathrm{FP}}\, r}}{2(1 + \bar{\alpha}^2) r} \,. \end{aligned} \tag{A.13}$$

These linearised solutions coincide with the result of [331,332] for $\Lambda = 0$, as expected. After having derived solutions valid inside the Vainshtein radius, we specify the constants of integration. The final results are presented in Eq. (3.35).

Compton regime

In Section 3.2, we discussed that the linearised solutions do not describe scales smaller than the Vainshtein radius, $r \ll r_{\mathrm{V}}$. To find solutions valid in this regime, we keep all nonlinearities in μ and consider scales smaller than the Compton wavelength, $r \ll m_{\mathrm{FP}}^{-1}$. That means we assume $m_{\mathrm{FP}}^2 r^2 \times \{|\psi_{\mathrm{g,f}}|, |\phi_{\mathrm{g,f}}|\} \ll 1$ in the modified Einstein equations (A.3) and (A.4). In the following, we seek solutions that are valid outside the compact object.

Let us start with the metric functions in $g_{\mu\nu}$. With the aforementioned approximations, the tt-component of Eq. (A.3) is integrated to

$$\psi_{\mathrm{g}} = \frac{r_{\mathrm{S}}}{r} + \frac{\bar{\alpha}^2 m_{\mathrm{FP}}^2}{1 + \bar{\alpha}^2} r^2 \left(\mu + \beta\mu^2 + \frac{\gamma}{3}\mu^3\right) \,. \tag{A.14}$$

We fixed the other constants of integration by requiring regularity at the surface of the compact object and at the origin $r = 0$. The rr-component of Eq. (A.3) simplifies with this solution to

$$r\phi_{\mathrm{g}}' = \frac{r_{\mathrm{S}}}{r} - \frac{\bar{\alpha}^2 m_{\mathrm{FP}}}{1 + \bar{\alpha}^2} r^2 \left(\mu - \frac{\gamma}{3}\mu^3\right) \,. \tag{A.15}$$

Coming to the functions defining $f_{\mu\nu}$, the tt-component of Eq. (A.4) is integrated to

$$\psi_{\mathrm{f}} = -\frac{m_{\mathrm{FP}}^2}{1+\bar{\alpha}^2}\frac{r^2}{1+\mu}\left(\mu + (1+\beta)\mu^2 + \frac{1+\beta+\gamma}{3}\mu^3\right). \tag{A.16}$$

One constant of integration has already been fixed by demanding regularity at the origin $r = 0$. The rr-component of Eq. (A.4) simplifies with the above result to

$$r\phi_{\mathrm{f}}' = \frac{m_{\mathrm{FP}}^2}{1+\bar{\alpha}^2}\frac{r^2(r+r\mu)'}{(1+\mu)^2}\left(\mu + 2\mu^2 + \frac{2+2\beta-\gamma}{3}\mu^3\right). \tag{A.17}$$

We found solutions for all quantities that appear in the Bianchi constraint (A.5) except μ and μ'. Plugging our solutions in Eqs. (A.14) to (A.17) into Eq. (A.5), μ' drops out and what remains is the following algebraic polynomial for μ [331, 332]:

$$\begin{aligned}
&-9(1+\bar{\alpha}^2)\mu \\
&-2\left(9(1+\bar{\alpha}^2)(1+\beta)\right)\mu^2 \\
&-\left(10+9\bar{\alpha}^2+2(17+18\bar{\alpha}^2)\beta+6(1+\bar{\alpha}^2)\beta^2+4(1+\bar{\alpha}^2)\gamma\right)\mu^3 \\
&-2\left(1+(7+9\bar{\alpha}^2)\beta+6(1+\bar{\alpha}^2)\beta^2+4(1+\bar{\alpha}^2)\gamma\right)\mu^4 \\
&-\left(2(1+2\gamma)\beta+2(1+3\bar{\alpha}^2)\beta^2+2(1+2\bar{\alpha}^2)\gamma-(1+\bar{\alpha}^2)\gamma^2\right)\mu^5 \\
&+2\bar{\alpha}^2\gamma^2\mu^6+\bar{\alpha}^2\gamma^2\mu^7 \\
&= 3\left(\frac{r_{\mathrm{V}}}{r}\right)^3(1+\bar{\alpha}^2)(1+\mu)^2(1-\gamma\mu^2).
\end{aligned} \tag{A.18}$$

As before, $r_{\mathrm{V}} = (r_{\mathrm{S}}/m_{\mathrm{FP}}^2)^{1/3}$ denotes the Vainshtein radius. The left hand side of this equation defines the polynomial $P(\mu)$ in Eq. (3.38). In total, this is a 7th order polynomial in μ, which gives rise to seven real- or complex-valued roots, which we already discussed in Section 3.2 following [331].

Matching the analytic solutions

As last step, we have to match the linear and nonlinear solutions on scales, where both are valid. This is the case for $r_{\mathrm{V}} \ll r \ll m_{\mathrm{FP}}^{-1}$. This allows to determine the constants of integration C_1 and C_2.

First, we linearise the nonlinear solutions Eqs. (A.14), (A.16) and (A.18) for $|\mu| \ll 1$. Keeping only the lowest-order term in Eq. (A.18) leads to $3\mu = -(r_{\mathrm{V}}/r)^3$, which we plug into Eqs. (A.14) and (A.16). Summarising, this leads to

$$\mu = -\frac{r_{\mathrm{S}}}{3m_{\mathrm{FP}}^2 r^3}, \quad \psi_{\mathrm{g}} = \frac{(3+2\bar{\alpha}^2)r_{\mathrm{S}}}{3(1+\bar{\alpha}^2)r}, \quad \psi_{\mathrm{f}} = \frac{r_{\mathrm{S}}}{3(1+\bar{\alpha}^2)r}. \tag{A.19}$$

Next, we expand the linear solutions Eq. (A.13) for $r \ll m_{\mathrm{FP}}^{-1}$, which leads to

$$\mu = -\frac{C_1}{4m_{\mathrm{FP}}^2 r^3}, \quad \psi_{\mathrm{g}} = \frac{\bar{\alpha}^2 C_1 + 2(1+\bar{\alpha}^2)C_2}{2(1+\bar{\alpha}^2)r}, \quad \psi_{\mathrm{f}} = -\frac{C_1 - 2(1+\bar{\alpha}^2)C_2}{2(1+\bar{\alpha}^2)r}. \tag{A.20}$$

Comparing Eq. (A.19) to Eq. (A.19) unveils that the constants of integration must be given by

$$C_1 = \frac{4r_{\mathrm{S}}}{3}, \quad C_2 = \frac{r_{\mathrm{S}}}{1+\bar{\alpha}^2}. \tag{A.21}$$

Plugged into the full linearised solutions in Eq. (A.13) yields the explicit expressions presented in Eq. (3.35).

Bibliography

[1] I. Newton, *Philosophiæ Naturalis Principia Mathematica*, Jussu Societatis Regiæ ac Typis Joseph Streater, London, England (1687).

[2] A. Einstein, *The Field Equations of Gravitation*, *Sitzungsber. Preuss. Akad. Wiss. Berlin (Math. Phys.)* **1915** (1915) 844.

[3] D. Hilbert, *Die Grundlagen der Physik. 1.*, *Gott. Nachr.* **27** (1915) 395.

[4] A. Einstein, *The Foundation of the General Theory of Relativity*, *Annalen Phys.* **49** (1916) 769.

[5] A. Einstein, *Explanation of the Perihelion Motion of Mercury from the General Theory of Relativity*, *Sitzungsber. Preuss. Akad. Wiss. Berlin (Math. Phys.)* **1915** (1915) 831.

[6] A. Einstein, *Lens-Like Action of a Star by the Deviation of Light in the Gravitational Field*, *Science* **84** (1936) 506.

[7] D. Walsh, R.F. Carswell and R.J. Weymann, *0957 + 561 A, B - Twin quasistellar objects or gravitational lens*, *Nature* **279** (1979) 381.

[8] A. Einstein, *Approximative Integration of the Field Equations of Gravitation*, *Sitzungsber. Preuss. Akad. Wiss. Berlin (Math. Phys.)* **1916** (1916) 688.

[9] A. Einstein, *Über Gravitationswellen*, *Sitzungsber. Preuss. Akad. Wiss. Berlin (Math. Phys.)* **1918** (1918) 154.

[10] R.A. Hulse and J.H. Taylor, *Discovery of a pulsar in a binary system*, *Astrophys. J. Lett.* **195** (1975) L51.

[11] LIGO Scientific, Virgo collaboration, *Observation of Gravitational Waves from a Binary Black Hole Merger*, *Phys. Rev. Lett.* **116** (2016) 061102 [1602.03837].

[12] K. Schwarzschild, *On the gravitational field of a mass point according to Einstein's theory*, *Sitzungsber. Preuss. Akad. Wiss. Berlin (Math. Phys.)* **1916** (1916) 189 [physics/9905030].

[13] Event Horizon Telescope collaboration, *First M87 Event Horizon Telescope Results. I. The Shadow of the Supermassive Black Hole*, *Astrophys. J. Lett.* **875** (2019) L1 [1906.11238].

[14] F. Zwicky, *Die Rotverschiebung von extragalaktischen Nebeln*, *Helv. Phys. Acta* **6** (1933) 110.

[15] V.C. Rubin and W.K. Ford, Jr., *Rotation of the Andromeda Nebula from a Spectroscopic Survey of Emission Regions*, *Astrophys. J.* **159** (1970) 379.

[16] K.C. Freeman, *On the disks of spiral and SO Galaxies*, *Astrophys. J.* **160** (1970) 811.

[17] Supernova Search Team collaboration, *Observational evidence from supernovae for an accelerating universe and a cosmological constant*, *Astron. J.* **116** (1998) 1009 [astro-ph/9805201].

[18] Supernova Cosmology Project collaboration, *Measurements of* Ω *and* Λ *from 42 high redshift supernovae*, *Astrophys. J.* **517** (1999) 565 [astro-ph/9812133].

[19] Y.B. Zeldovich, *Cosmological Constant and Elementary Particles*, *JETP Lett.* **6** (1967) 316.

[20] S. Weinberg, *The Cosmological Constant Problem*, *Rev. Mod. Phys.* **61** (1989) 1.

[21] G. Dvali and C. Gomez, *Quantum Compositeness of Gravity: Black Holes, AdS and Inflation*, *JCAP* **01** (2014) 023 [1312.4795].

[22] G. Dvali and C. Gomez, *Quantum Exclusion of Positive Cosmological Constant?*, *Annalen Phys.* **528** (2016) 68 [1412.8077].

[23] G. Dvali, C. Gomez and S. Zell, *Quantum Break-Time of de Sitter*, *JCAP* **06** (2017) 028 [1701.08776].

[24] G. Obied, H. Ooguri, L. Spodyneiko and C. Vafa, *De Sitter Space and the Swampland*, 1806.08362.

[25] G. Dvali and C. Gomez, *On Exclusion of Positive Cosmological Constant*, *Fortsch. Phys.* **67** (2019) 1800092 [1806.10877].

[26] S.K. Garg and C. Krishnan, *Bounds on Slow Roll and the de Sitter Swampland*, *JHEP* **11** (2019) 075 [1807.05193].

[27] H. Ooguri, E. Palti, G. Shiu and C. Vafa, *Distance and de Sitter Conjectures on the Swampland*, *Phys. Lett. B* **788** (2019) 180 [1810.05506].

[28] G. Dvali, C. Gomez and S. Zell, *Quantum Breaking Bound on de Sitter and Swampland*, *Fortsch. Phys.* **67** (2019) 1800094 [1810.11002].

[29] S.W. Hawking and R. Penrose, *The Singularities of gravitational collapse and cosmology*, *Proc. Roy. Soc. Lond. A* **314** (1970) 529.

[30] G. 't Hooft and M.J.G. Veltman, *One loop divergencies in the theory of gravitation*, *Ann. Inst. H. Poincare Phys. Theor. A* **20** (1974) 69.

[31] S. Deser and P. van Nieuwenhuizen, *Nonrenormalizability of the Quantized Einstein-Maxwell System*, *Phys. Rev. Lett.* **32** (1974) 245.

[32] S. Deser and P. van Nieuwenhuizen, *Nonrenormalizability of the Quantized Dirac-Einstein System*, *Phys. Rev. D* **10** (1974) 411.

[33] S. Deser, H.-S. Tsao and P. van Nieuwenhuizen, *One Loop Divergences of the Einstein Yang-Mills System*, *Phys. Rev. D* **10** (1974) 3337.

[34] M.H. Goroff and A. Sagnotti, *Quantum gravity at two loops*, *Phys. Lett. B* **160** (1985) 81.

[35] A.E.M. van de Ven, *Two loop quantum gravity*, *Nucl. Phys. B* **378** (1992) 309.

[36] J.F. Donoghue, *Introduction to the effective field theory description of gravity*, in *Advanced School on Effective Theories*, 6, 1995 [gr-qc/9512024].

[37] C.P. Burgess, *Quantum gravity in everyday life: General relativity as an effective field theory*, *Living Rev. Rel.* **7** (2004) 5 [gr-qc/0311082].

[38] R. Blumenhagen, D. Lüst and S. Theisen, *Basic concepts of string theory*, Theoretical and Mathematical Physics, Springer, Heidelberg, Germany (2013), 10.1007/978-3-642-29497-6.

[39] M. Ostrogradsky, *Mémoires sur les équations différentielles, relatives au problème des isopérimètres*, *Mem. Acad. St. Petersbourg* **6** (1850) 385.

[40] A. Pais and G.E. Uhlenbeck, *On Field theories with nonlocalized action*, *Phys. Rev.* **79** (1950) 145.

[41] S.N. Gupta, *Gravitation and Electromagnetism*, *Phys. Rev.* **96** (1954) 1683.

[42] S. Weinberg, *Photons and gravitons in perturbation theory: Derivation of Maxwell's and Einstein's equations*, *Phys. Rev.* **138** (1965) B988.

[43] S. Deser, *Selfinteraction and gauge invariance*, *Gen. Rel. Grav.* **1** (1970) 9 [gr-qc/0411023].

[44] D.G. Boulware and S. Deser, *Classical General Relativity Derived from Quantum Gravity*, *Annals Phys.* **89** (1975) 193.

[45] R.P. Feynman, F.B. Morinigo, W.G. Wagner and B. Hatfield, *Feynman lectures on gravitation*, Addison–Wesley (1996).

[46] M. Fierz and W. Pauli, *On relativistic wave equations for particles of arbitrary spin in an electromagnetic field*, *Proc. Roy. Soc. Lond. A* **173** (1939) 211.

[47] D. Boulware and S. Deser, *Can gravitation have a finite range?*, *Phys. Rev. D* **6** (1972) 3368.

[48] C. de Rham and G. Gabadadze, *Generalization of the Fierz-Pauli Action*, *Phys. Rev. D* **82** (2010) 044020 [1007.0443].

[49] C. de Rham, G. Gabadadze and A.J. Tolley, *Resummation of Massive Gravity*, *Phys. Rev. Lett.* **106** (2011) 231101 [1011.1232].

[50] S. Hassan and R.A. Rosen, *Resolving the Ghost Problem in non-Linear Massive Gravity*, *Phys. Rev. Lett.* **108** (2012) 041101 [1106.3344].

[51] S. Hassan and R.A. Rosen, *Confirmation of the Secondary Constraint and Absence of Ghost in Massive Gravity and Bimetric Gravity*, *JHEP* **04** (2012) 123 [1111.2070].

[52] S. Hassan and R.A. Rosen, *Bimetric Gravity from Ghost-free Massive Gravity*, *JHEP* **02** (2012) 126 [1109.3515].

[53] J.A. Wheeler and K. Ford, *Geons, black holes, and quantum foam: A life in physics*, New York: Norton (1998).

[54] C.W. Misner, K.S. Thorne and J.A. Wheeler, *Gravitation*, W. H. Freeman, San Francisco (1973).

[55] R.M. Wald, *General Relativity*, Chicago Univ. Pr., Chicago, USA (1984), 10.7208/chicago/9780226870373.001.0001.

[56] S.M. Carroll, *Spacetime and Geometry*, Cambridge University Press (7, 2019), 10.1017/9781108770385.

[57] M.P. Hobson, G.P. Efstathiou and A.N. Lasenby, *General relativity: An introduction for physicists*, Cambridge (2006).

[58] N. Straumann, *General Relativity*, Graduate Texts in Physics, Springer, Dordrecht (2013), 10.1007/978-94-007-5410-2.

[59] M. Bartelmann, *General relativity*, Heidelberg University Publishing (2019), 10.17885/heiup.534.

[60] A. Einstein, *Cosmological Considerations in the General Theory of Relativity*, *Sitzungsber. Preuss. Akad. Wiss. Berlin (Math. Phys.)* **1917** (1917) 142.

[61] S. Weinberg, *Gravitation and Cosmology: Principles and Applications of the General Theory of Relativity*, John Wiley and Sons, New York (1972).

[62] J.A. Peacock, *Cosmological physics*, Cambridge University Press (1999).

[63] B. Ryden, *Introduction to cosmology*, Cambridge University Press (1970), 10.1017/9781316651087.

[64] V. Mukhanov, *Physical Foundations of Cosmology*, Cambridge University Press, Oxford (2005).

[65] D. Saadeh, S.M. Feeney, A. Pontzen, H.V. Peiris and J.D. McEwen, *How isotropic is the Universe?*, *Phys. Rev. Lett.* **117** (2016) 131302 [1605.07178].

[66] R. Maartens, *Is the Universe homogeneous?*, *Phil. Trans. Roy. Soc. Lond. A* **369** (2011) 5115 [1104.1300].

[67] A. Friedman, *On the Curvature of space*, *Z. Phys.* **10** (1922) 377.

[68] A. Friedmann, *On the Possibility of a world with constant negative curvature of space*, *Z. Phys.* **21** (1924) 326.

[69] G. Lemaitre, *A Homogeneous Universe of Constant Mass and Growing Radius Accounting for the Radial Velocity of Extragalactic Nebulae*, *Gen. Rel. Grav.* **45** (2013) 1635.

[70] G. Lemaitre, *A homogeneous universe of constant mass and increasing radius accounting for the radial velocity of extra-galactic nebulae*, *Mon. Not. Roy. Astron. Soc.* **91** (1931) 483.

[71] H.P. Robertson, *Kinematics and World-Structure*, *Astrophys. J.* **82** (1935) 284.

[72] H.P. Robertson, *Kinematics and World-Structure. 2*, *Astrophys. J.* **83** (1935) 187.

[73] H.P. Robertson, *Kinematics and World-Structure. 3*, *Astrophys. J.* **83** (1936) 257.

[74] A.G. Walker, *On Milne's Theory of World-Structure*, *Proc. London Math. Soc.* **s2-42** (1937) 90.

[75] Planck collaboration, *Planck 2018 results. VI. Cosmological parameters*, *Astron. Astrophys.* **641** (2020) A6 [1807.06209].

[76] F. Zwicky, *On the Masses of Nebulae and of Clusters of Nebulae*, *Astrophys. J.* **86** (1937) 217.

[77] S.M. Faber and R.E. Jackson, *Velocity dispersions and mass to light ratios for elliptical galaxies*, *Astrophys. J.* **204** (1976) 668.

[78] D. Clowe, M. Bradac, A.H. Gonzalez, M. Markevitch, S.W. Randall, C. Jones et al., *A direct empirical proof of the existence of dark matter*, *Astrophys. J. Lett.* **648** (2006) L109 [astro-ph/0608407].

[79] C.J. Copi, D.N. Schramm and M.S. Turner, *Big bang nucleosynthesis and the baryon density of the universe*, *Science* **267** (1995) 192 [astro-ph/9407006].

[80] J.R. Primack, *Dark matter and structure formation*, in *Midrasha Mathematicae in Jerusalem: Winter School in Dynamical Systems*, 7, 1997 [astro-ph/9707285].

[81] G. Bertone, D. Hooper and J. Silk, *Particle dark matter: Evidence, candidates and constraints*, *Phys. Rept.* **405** (2005) 279 [hep-ph/0404175].

[82] X. Calmet and I. Kuntz, *What is modified gravity and how to differentiate it from particle dark matter?*, *Eur. Phys. J. C* **77** (2017) 132 [1702.03832].

[83] M. Milgrom, *A Modification of the Newtonian dynamics as a possible alternative to the hidden mass hypothesis*, *Astrophys. J.* **270** (1983) 365.

[84] B. Famaey and S. McGaugh, *Modified Newtonian Dynamics (MOND): Observational Phenomenology and Relativistic Extensions*, *Living Rev. Rel.* **15** (2012) 10 [1112.3960].

[85] J. Martin, *Everything You Always Wanted To Know About The Cosmological Constant Problem (But Were Afraid To Ask)*, *Comptes Rendus Physique* **13** (2012) 566 [1205.3365].

[86] G. 't Hooft, *Naturalness, chiral symmetry, and spontaneous chiral symmetry breaking*, *NATO Sci. Ser. B* **59** (1980) 135.

[87] C.P. Burgess, *The Cosmological Constant Problem: Why it's hard to get Dark Energy from Micro-physics*, in *100e Ecole d'Ete de Physique: Post-Planck Cosmology*, pp. 149–197, 2015, DOI [1309.4133].

[88] S.M. Carroll, W.H. Press and E.L. Turner, *The Cosmological constant*, *Ann. Rev. Astron. Astrophys.* **30** (1992) 499.

[89] A.D. Dolgov, *The Problem of vacuum energy and cosmology*, in *4th Paris Cosmology Colloquium*, pp. 161–175, 6, 1997 [astro-ph/9708045].

[90] N. Straumann, *The Mystery of the cosmic vacuum energy density and the accelerated expansion of the universe*, *Eur. J. Phys.* **20** (1999) 419 [astro-ph/9908342].

[91] S. Weinberg, *The Cosmological constant problems*, in *4th International Symposium on Sources and Detection of Dark Matter in the Universe (DM 2000)*, pp. 18–26, 2, 2000 [astro-ph/0005265].

[92] S.M. Carroll, *The Cosmological constant*, *Living Rev. Rel.* **4** (2001) 1 [astro-ph/0004075].

[93] S.E. Rugh and H. Zinkernagel, *The Quantum vacuum and the cosmological constant problem*, *Stud. Hist. Phil. Sci. B* **33** (2002) 663 [hep-th/0012253].

[94] T. Padmanabhan, *Cosmological constant: The Weight of the vacuum*, *Phys. Rept.* **380** (2003) 235 [hep-th/0212290].

[95] J. Yokoyama, *Issues on the cosmological constant*, in *12th Workshop on General Relativity and Gravitation*, 5, 2003 [gr-qc/0305068].

[96] J. Polchinski, *The Cosmological Constant and the String Landscape*, in *23rd Solvay Conference in Physics: The Quantum Structure of Space and Time*, pp. 216–236, 3, 2006 [hep-th/0603249].

[97] E.J. Copeland, M. Sami and S. Tsujikawa, *Dynamics of dark energy*, *Int. J. Mod. Phys. D* **15** (2006) 1753 [hep-th/0603057].

[98] P. Brax, *Gif Lectures on Cosmic Acceleration*, 0912.3610.

[99] J. Sola, *Cosmological constant and vacuum energy: old and new ideas*, *J. Phys. Conf. Ser.* **453** (2013) 012015 [1306.1527].

[100] C. Vafa, *The String landscape and the swampland*, hep-th/0509212.

[101] T.D. Brennan, F. Carta and C. Vafa, *The String Landscape, the Swampland, and the Missing Corner*, *PoS* **TASI2017** (2017) 015 [1711.00864].

[102] E. Palti, *The Swampland: Introduction and Review*, *Fortsch. Phys.* **67** (2019) 1900037 [1903.06239].

[103] Y. Akrami, R. Kallosh, A. Linde and V. Vardanyan, *The Landscape, the Swampland and the Era of Precision Cosmology*, *Fortsch. Phys.* **67** (2019) 1800075 [1808.09440].

[104] R. Blumenhagen, C. Kneissl and A. Makridou, *De Sitter Quantum Breaking, Swampland Conjectures and Thermal Strings*, 2011.13956.

[105] G. Dvali, *S-Matrix and Anomaly of de Sitter*, *Symmetry* **13** (2020) 3 [2012.02133].

[106] E. Witten, *Quantum gravity in de Sitter space*, in *Strings 2001: International Conference*, 6, 2001 [hep-th/0106109].

[107] J.L. Bernal, L. Verde and A.G. Riess, *The trouble with H_0*, *JCAP* **10** (2016) 019 [1607.05617].

[108] E. Di Valentino et al., *Snowmass2021 - Letter of interest cosmology intertwined II: The hubble constant tension*, *Astropart. Phys.* **131** (2021) 102605 [2008.11284].

[109] E. Di Valentino, O. Mena, S. Pan, L. Visinelli, W. Yang, A. Melchiorri et al., *In the Realm of the Hubble tension − a Review of Solutions*, 2103.01183.

[110] M.J. Reid, D.W. Pesce and A.G. Riess, *An Improved Distance to NGC 4258 and its Implications for the Hubble Constant*, *Astrophys. J. Lett.* **886** (2019) L27 [1908.05625].

[111] K.C. Wong et al., *H0LiCOW – XIII. A 2.4 per cent measurement of H0 from lensed quasars: 5.3σ tension between early- and late-Universe probes*, *Mon. Not. Roy. Astron. Soc.* **498** (2020) 1420 [1907.04869].

[112] ACT collaboration, *The Atacama Cosmology Telescope: DR4 Maps and Cosmological Parameters*, *JCAP* **12** (2020) 047 [2007.07288].

[113] A.G. Riess, *The Expansion of the Universe is Faster than Expected*, *Nature Rev. Phys.* **2** (2019) 10 [2001.03624].

[114] M. Chevallier and D. Polarski, *Accelerating universes with scaling dark matter*, *Int. J. Mod. Phys. D* **10** (2001) 213 [gr-qc/0009008].

[115] E.V. Linder, *Exploring the expansion history of the universe*, *Phys. Rev. Lett.* **90** (2003) 091301 [astro-ph/0208512].

[116] E. Di Valentino, *A combined analysis of the H_0 late time direct measurements and the impact on the Dark Energy sector*, *Mon. Not. Roy. Astron. Soc.* **502** (2021) 2065 [2011.00246].

[117] H. van Dam and M. Veltman, *Massive and massless Yang-Mills and gravitational fields*, *Nucl. Phys. B* **22** (1970) 397.

[118] V. Zakharov, *Linearized gravitation theory and the graviton mass*, *JETP Lett.* **12** (1970) 312.

[119] A. Vainshtein, *To the problem of nonvanishing gravitation mass*, *Phys. Lett. B* **39** (1972) 393.

[120] S. Hassan and R.A. Rosen, *On Non-Linear Actions for Massive Gravity*, *JHEP* **07** (2011) 009 [1103.6055].

[121] D. Lovelock, *The Einstein tensor and its generalizations*, *J. Math. Phys.* **12** (1971) 498.

[122] D. Lovelock, *The four-dimensionality of space and the einstein tensor*, *J. Math. Phys.* **13** (1972) 874.

[123] K. Hinterbichler, *Theoretical Aspects of Massive Gravity*, *Rev. Mod. Phys.* **84** (2012) 671 [1105.3735].

[124] E. Babichev and C. Deffayet, *An introduction to the Vainshtein mechanism*, *Class. Quant. Grav.* **30** (2013) 184001 [1304.7240].

[125] C. de Rham, *Massive Gravity*, *Living Rev. Rel.* **17** (2014) 7 [1401.4173].

[126] A. Schmidt-May and M. von Strauss, *Recent developments in bimetric theory*, *J. Phys. A* **49** (2016) 183001 [1512.00021].

[127] R.P. Woodard, *Avoiding dark energy with 1/r modifications of gravity*, *Lect. Notes Phys.* **720** (2007) 403 [astro-ph/0601672].

[128] M. Ferraris, M. Francaviglia and C. Reina, *Variational formulation of general relativity from 1915 to 1925 "Palatini's method" discovered by Einstein in 1925*, *Gen. Relat. Gravit.* **14** (1982) 243.

[129] P.G. Bergmann and J.H.M. Brunings, *Non-Linear Field Theories II. Canonical Equations and Quantization*, *Rev. Mod. Phys.* **21** (1949) 480.

[130] P.A.M. Dirac, *Generalized Hamiltonian dynamics*, *Can. J. Math.* **2** (1950) 129.

[131] J.L. Anderson and P.G. Bergmann, *Constraints in covariant field theories*, *Phys. Rev.* **83** (1951) 1018.

[132] B. Díaz, D. Higuita and M. Montesinos, *Lagrangian approach to the physical degree of freedom count*, *J. Math. Phys.* **55** (2014) 122901 [1406.1156].

[133] N. Kiriushcheva and S.V. Kuzmin, *The Hamiltonian formulation of General Relativity: Myths and reality*, *Central Eur. J. Phys.* **9** (2011) 576 [0809.0097].

[134] V. Errasti Díez, M. Maier, J.A. Méndez-Zavaleta and M. Taslimi Tehrani, *Lagrangian constraint analysis of first-order classical field theories with an application to gravity*, *Phys. Rev. D* **102** (2020) 065015 [2007.11020].

[135] F. Sbisà, *Classical and quantum ghosts*, *Eur. J. Phys.* **36** (2015) 015009 [1406.4550].

[136] T. Clifton, P.G. Ferreira, A. Padilla and C. Skordis, *Modified Gravity and Cosmology*, *Phys. Rept.* **513** (2012) 1 [1106.2476].

[137] A. Joyce, B. Jain, J. Khoury and M. Trodden, *Beyond the Cosmological Standard Model*, *Phys. Rept.* **568** (2015) 1 [1407.0059].

[138] K. Koyama, *Cosmological Tests of Modified Gravity*, *Rept. Prog. Phys.* **79** (2016) 046902 [1504.04623].

[139] L. Amendola and S. Tsujikawa, *Dark Energy: Theory and Observations*, Cambridge University Press (1, 2015).

[140] G.W. Horndeski, *Second-order scalar-tensor field equations in a four-dimensional space*, *Int. J. Theor. Phys.* **10** (1974) 363.

[141] C. Deffayet, X. Gao, D.A. Steer and G. Zahariade, *From k-essence to generalised Galileons*, *Phys. Rev. D* **84** (2011) 064039 [1103.3260].

[142] J. Gleyzes, D. Langlois, F. Piazza and F. Vernizzi, *Healthy theories beyond Horndeski*, *Phys. Rev. Lett.* **114** (2015) 211101 [1404.6495].

[143] D. Langlois and K. Noui, *Degenerate higher derivative theories beyond Horndeski: evading the Ostrogradski instability*, *JCAP* **02** (2016) 034 [1510.06930].

[144] J. Ben Achour, M. Crisostomi, K. Koyama, D. Langlois, K. Noui and G. Tasinato, *Degenerate higher order scalar-tensor theories beyond Horndeski up to cubic order*, *JHEP* **12** (2016) 100 [1608.08135].

[145] G. Tasinato, *Cosmic Acceleration from Abelian Symmetry Breaking*, *JHEP* **04** (2014) 067 [1402.6450].

[146] L. Heisenberg, *Generalization of the Proca Action*, *JCAP* **05** (2014) 015 [1402.7026].

[147] J. Beltran Jimenez and L. Heisenberg, *Derivative self-interactions for a massive vector field*, *Phys. Lett. B* **757** (2016) 405 [1602.03410].

[148] V. Errasti Díez, B. Gording, J.A. Méndez-Zavaleta and A. Schmidt-May, *Maxwell-Proca theory: Definition and construction*, *Phys. Rev. D* **101** (2020) 045009 [1905.06968].

[149] V. Errasti Díez, B. Gording, J.A. Méndez-Zavaleta and A. Schmidt-May, *Complete theory of Maxwell and Proca fields*, *Phys. Rev. D* **101** (2020) 045008 [1905.06967].

[150] M. Hull, K. Koyama and G. Tasinato, *Covariantized vector Galileons*, *Phys. Rev. D* **93** (2016) 064012 [1510.07029].

[151] E. Allys, P. Peter and Y. Rodriguez, *Generalized SU(2) Proca Theory*, *Phys. Rev. D* **94** (2016) 084041 [1609.05870].

[152] J. Beltran Jimenez and L. Heisenberg, *Generalized multi-Proca fields*, *Phys. Lett. B* **770** (2017) 16 [1610.08960].

[153] J. Beltrán Jiménez, C. de Rham and L. Heisenberg, *Generalized Proca and its Constraint Algebra*, *Phys. Lett. B* **802** (2020) 135244 [1906.04805].

[154] A. Gallego Cadavid, Y. Rodriguez and L.G. Gómez, *Generalized SU(2) Proca theory reconstructed and beyond*, *Phys. Rev. D* **102** (2020) 104066 [2009.03241].

[155] L. Heisenberg, *A systematic approach to generalisations of General Relativity and their cosmological implications*, *Phys. Rept.* **796** (2019) 1 [1807.01725].

[156] K. Hinterbichler and R.A. Rosen, *Interacting Spin-2 Fields*, *JHEP* **07** (2012) 047 [1203.5783].

[157] S.F. Hassan, A. Schmidt-May and M. von Strauss, *Metric Formulation of Ghost-Free Multivielbein Theory*, 1204.5202.

[158] K. Nomura and J. Soda, *When is Multimetric Gravity Ghost-free?*, *Phys. Rev. D* **86** (2012) 084052 [1207.3637].

[159] C. Deffayet, J. Mourad and G. Zahariade, *A note on 'symmetric' vielbeins in bimetric, massive, perturbative and non perturbative gravities*, *JHEP* **03** (2013) 086 [1208.4493].

[160] J. Noller, J.H.C. Scargill and P.G. Ferreira, *Interacting spin-2 fields in the Stückelberg picture*, *JCAP* **02** (2014) 007 [1311.7009].

[161] J.H.C. Scargill, J. Noller and P.G. Ferreira, *Cycles of interactions in multi-gravity theories*, *JHEP* **12** (2014) 160 [1410.7774].

[162] J. Noller and J.H.C. Scargill, *The decoupling limit of Multi-Gravity: Multi-Galileons, Dualities and More*, *JHEP* **05** (2015) 034 [1503.02700].

[163] C. de Rham and A.J. Tolley, *Vielbein to the rescue? Breaking the symmetric vielbein condition in massive gravity and multigravity*, *Phys. Rev. D* **92** (2015) 024024 [1505.01450].

[164] J.H.C. Scargill and J. Noller, *Strong-coupling scales and the graph structure of multi-gravity theories*, *JHEP* **01** (2016) 029 [1511.02877].

[165] S.F. Hassan and A. Schmidt-May, *Interactions of multiple spin-2 fields beyond pairwise couplings*, *Phys. Rev. Lett.* **122** (2019) 251101 [1804.09723].

[166] LIGO Scientific, Virgo, Fermi-GBM, INTEGRAL collaboration, *Gravitational Waves and Gamma-rays from a Binary Neutron Star Merger: GW170817 and GRB 170817A*, *Astrophys. J. Lett.* **848** (2017) L13 [1710.05834].

[167] P. Creminelli and F. Vernizzi, *Dark Energy after GW170817 and GRB170817A*, *Phys. Rev. Lett.* **119** (2017) 251302 [1710.05877].

[168] J. Sakstein and B. Jain, *Implications of the Neutron Star Merger GW170817 for Cosmological Scalar-Tensor Theories*, *Phys. Rev. Lett.* **119** (2017) 251303 [1710.05893].

[169] J.M. Ezquiaga and M. Zumalacárregui, *Dark Energy After GW170817: Dead Ends and the Road Ahead*, *Phys. Rev. Lett.* **119** (2017) 251304 [1710.05901].

[170] T. Baker, E. Bellini, P.G. Ferreira, M. Lagos, J. Noller and I. Sawicki, *Strong constraints on cosmological gravity from GW170817 and GRB 170817A*, *Phys. Rev. Lett.* **119** (2017) 251301 [1710.06394].

[171] Y. Iwasaki, *Consistency condition for propagators*, *Phys. Rev. D* **2** (1970) 2255.

[172] V.I. Ogievetsky and I.V. Polubarinov, *Interacting field of spin 2 and the Einstein equations*, *Annals Phys.* **35** (1965) 167.

[173] C. de Rham, G. Gabadadze and A.J. Tolley, *Helicity decomposition of ghost-free massive gravity*, *JHEP* **11** (2011) 093 [1108.4521].

[174] N. Arkani-Hamed, H. Georgi and M.D. Schwartz, *Effective field theory for massive gravitons and gravity in theory space*, *Annals Phys.* **305** (2003) 96 [hep-th/0210184].

[175] J.H. Jun and I. Kang, *Instability of Flat Space for Massive Gravitational Fields*, *Phys. Rev. D* **34** (1986) 1005.

[176] T. Damour, I.I. Kogan and A. Papazoglou, *Spherically symmetric space-times in massive gravity*, *Phys. Rev. D* **67** (2003) 064009 [hep-th/0212155].

[177] E. Babichev, C. Deffayet and R. Ziour, *The Vainshtein mechanism in the Decoupling Limit of massive gravity*, *JHEP* **05** (2009) 098 [0901.0393].

[178] E. Babichev, C. Deffayet and R. Ziour, *Recovering General Relativity from massive gravity*, *Phys. Rev. Lett.* **103** (2009) 201102 [0907.4103].

[179] E. Babichev, C. Deffayet and R. Ziour, *The Recovery of General Relativity in massive gravity via the Vainshtein mechanism*, *Phys. Rev. D* **82** (2010) 104008 [1007.4506].

[180] L. Alberte, A.H. Chamseddine and V. Mukhanov, *Massive Gravity: Resolving the Puzzles*, *JHEP* **12** (2010) 023 [1008.5132].

[181] T. Damour and I.I. Kogan, *Effective Lagrangians and universality classes of nonlinear bigravity*, *Phys. Rev. D* **66** (2002) 104024 [hep-th/0206042].

[182] R.L. Arnowitt, S. Deser and C.W. Misner, *The Dynamics of general relativity*, *Gen. Rel. Grav.* **40** (2008) 1997 [gr-qc/0405109].

[183] P. Creminelli, A. Nicolis, M. Papucci and E. Trincherini, *Ghosts in massive gravity*, *JHEP* **09** (2005) 003 [hep-th/0505147].

[184] N. Arkani-Hamed, S. Dimopoulos and G.R. Dvali, *The Hierarchy problem and new dimensions at a millimeter*, *Phys. Lett. B* **429** (1998) 263 [hep-ph/9803315].

[185] I. Antoniadis, N. Arkani-Hamed, S. Dimopoulos and G.R. Dvali, *New dimensions at a millimeter to a Fermi and superstrings at a TeV*, *Phys. Lett. B* **436** (1998) 257 [hep-ph/9804398].

[186] R. Gregory, V.A. Rubakov and S.M. Sibiryakov, *Opening up extra dimensions at ultra large scales*, *Phys. Rev. Lett.* **84** (2000) 5928 [hep-th/0002072].

[187] G.R. Dvali, G. Gabadadze and M. Porrati, *Metastable gravitons and infinite volume extra dimensions*, *Phys. Lett. B* **484** (2000) 112 [hep-th/0002190].

[188] G.R. Dvali, G. Gabadadze and M. Porrati, *4-D gravity on a brane in 5-D Minkowski space*, *Phys. Lett. B* **485** (2000) 208 [hep-th/0005016].

[189] G.R. Dvali, G. Gabadadze, M. Kolanovic and F. Nitti, *The Power of brane induced gravity*, *Phys. Rev. D* **64** (2001) 084004 [hep-ph/0102216].

[190] C. de Rham, S. Hofmann, J. Khoury and A.J. Tolley, *Cascading Gravity and Degravitation*, *JCAP* **02** (2008) 011 [0712.2821].

[191] C. de Rham, G. Dvali, S. Hofmann, J. Khoury, O. Pujolas, M. Redi et al., *Cascading gravity: Extending the Dvali-Gabadadze-Porrati model to higher dimension*, *Phys. Rev. Lett.* **100** (2008) 251603 [0711.2072].

[192] V.A. Rubakov and P.G. Tinyakov, *Infrared-modified gravities and massive gravitons*, *Phys. Usp.* **51** (2008) 759 [0802.4379].

[193] S.F. Hassan, S. Hofmann and M. von Strauss, *Brane Induced Gravity, its Ghost and the Cosmological Constant Problem*, *JCAP* **01** (2011) 020 [1007.1263].

[194] G. Gabadadze, *General Relativity With An Auxiliary Dimension*, *Phys. Lett. B* **681** (2009) 89 [0908.1112].

[195] C. de Rham, *Massive gravity from Dirichlet boundary conditions*, *Phys. Lett. B* **688** (2010) 137 [0910.5474].

[196] C. de Rham and G. Gabadadze, *Selftuned Massive Spin-2*, *Phys. Lett. B* **693** (2010) 334 [1006.4367].

[197] S.F. Hassan and R.A. Rosen, *Exact Solution to the 'Auxiliary Extra Dimension' Model of Massive Gravity*, *Phys. Lett. B* **702** (2011) 90 [1104.1373].

[198] S. Hassan, R.A. Rosen and A. Schmidt-May, *Ghost-free Massive Gravity with a General Reference Metric*, *JHEP* **02** (2012) 026 [1109.3230].

[199] M. Mirbabayi, *A Proof Of Ghost Freedom In de Rham-Gabadadze-Tolley Massive Gravity*, *Phys. Rev. D* **86** (2012) 084006 [1112.1435].

[200] A. Golovnev, *On the Hamiltonian analysis of non-linear massive gravity*, *Phys. Lett. B* **707** (2012) 404 [1112.2134].

[201] J. Kluson, *Remark About Hamiltonian Formulation of Non-Linear Massive Gravity in Stuckelberg Formalism*, *Phys. Rev. D* **86** (2012) 124005 [1202.5899].

[202] S.F. Hassan, A. Schmidt-May and M. von Strauss, *Proof of Consistency of Nonlinear Massive Gravity in the Stückelberg Formulation*, *Phys. Lett. B* **715** (2012) 335 [1203.5283].

[203] J. Kluson, *Non-Linear Massive Gravity with Additional Primary Constraint and Absence of Ghosts*, *Phys. Rev. D* **86** (2012) 044024 [1204.2957].

[204] C. Deffayet, J. Mourad and G. Zahariade, *Covariant constraints in ghost free massive gravity*, *JCAP* **01** (2013) 032 [1207.6338].

[205] J. Kluson, *Note About Hamiltonian Formalism for General Non-Linear Massive Gravity Action in Stuckelberg Formalism*, *Int. J. Mod. Phys. A* **28** (2013) 1350160 [1209.3612].

[206] S. Alexandrov, *Canonical structure of Tetrad Bimetric Gravity*, *Gen. Rel. Grav.* **46** (2014) 1639 [1308.6586].

[207] A. Golovnev, *On non-perturbative analysis of massive and bimetric gravity*, *AIP Conf. Proc.* **1606** (2015) 299 [1401.6343].

[208] S. Deser, M. Sandora, A. Waldron and G. Zahariade, *Covariant constraints for generic massive gravity and analysis of its characteristics*, *Phys. Rev. D* **90** (2014) 104043 [1408.0561].

[209] S.F. Hassan and A. Lundkvist, *Analysis of constraints and their algebra in bimetric theory*, *JHEP* **08** (2018) 182 [1802.07267].

[210] C. de Rham, J.T. Deskins, A.J. Tolley and S.-Y. Zhou, *Graviton Mass Bounds*, *Rev. Mod. Phys.* **89** (2017) 025004 [1606.08462].

[211] G. D'Amico, C. de Rham, S. Dubovsky, G. Gabadadze, D. Pirtskhalava and A.J. Tolley, *Massive Cosmologies*, *Phys. Rev. D* **84** (2011) 124046 [1108.5231].

[212] A.E. Gümrükçüoğlu, C. Lin and S. Mukohyama, *Open FRW universes and self-acceleration from nonlinear massive gravity*, *JCAP* **11** (2011) 030 [1109.3845].

[213] A.E. Gümrükçüoğlu, C. Lin and S. Mukohyama, *Cosmological perturbations of self-accelerating universe in nonlinear massive gravity*, *JCAP* **03** (2012) 006 [1111.4107].

[214] A. De Felice, A.E. Gümrükçüoğlu and S. Mukohyama, *Massive gravity: nonlinear instability of the homogeneous and isotropic universe*, *Phys. Rev. Lett.* **109** (2012) 171101 [1206.2080].

[215] B. Vakili and N. Khosravi, *Classical and quantum massive cosmology for the open FRW universe*, *Phys. Rev. D* **85** (2012) 083529 [1204.1456].

[216] M. von Strauss, A. Schmidt-May, J. Enander, E. Mörtsell and S.F. Hassan, *Cosmological Solutions in Bimetric Gravity and their Observational Tests*, *JCAP* **03** (2012) 042 [1111.1655].

[217] S. Alexandrov, K. Krasnov and S. Speziale, *Chiral description of ghost-free massive gravity*, *JHEP* **06** (2013) 068 [1212.3614].

[218] V.O. Soloviev and M.V. Tchichikina, *Bigravity in Kuchar's Hamiltonian formalism. 2. The special case*, *Phys. Rev. D* **88** (2013) 084026 [1302.5096].

[219] J. Klusoň, *Hamiltonian Formalism of Bimetric Gravity In Vierbein Formulation*, *Eur. Phys. J. C* **74** (2014) 2985 [1307.1974].

[220] T. Kugo and N. Ohta, *Covariant Approach to the No-ghost Theorem in Massive Gravity*, *PTEP* **2014** (2014) 043B04 [1401.3873].

[221] L. Bernard, C. Deffayet, A. Schmidt-May and M. von Strauss, *Linear spin-2 fields in most general backgrounds*, *Phys. Rev. D* **93** (2016) 084020 [1512.03620].

[222] S.F. Hassan and M. Kocic, *On the local structure of spacetime in ghost-free bimetric theory and massive gravity*, *JHEP* **05** (2018) 099 [1706.07806].

[223] S.F. Hassan, A. Schmidt-May and M. von Strauss, *On Consistent Theories of Massive Spin-2 Fields Coupled to Gravity*, *JHEP* **05** (2013) 086 [1208.1515].

[224] A. Higuchi, *Forbidden Mass Range for Spin-2 Field Theory in De Sitter Space-time*, *Nucl. Phys. B* **282** (1987) 397.

[225] A. Higuchi, *Massive Symmetric Tensor Field in Space-times With a Positive Cosmological Constant*, *Nucl. Phys. B* **325** (1989) 745.

[226] Y. Akrami, S.F. Hassan, F. Könnig, A. Schmidt-May and A.R. Solomon, *Bimetric gravity is cosmologically viable*, *Phys. Lett. B* **748** (2015) 37 [1503.07521].

[227] E. Babichev, L. Marzola, M. Raidal, A. Schmidt-May, F. Urban, H. Veermäe et al., *Heavy spin-2 Dark Matter*, *JCAP* **09** (2016) 016 [1607.03497].

[228] Y. Yamashita, A. De Felice and T. Tanaka, *Appearance of Boulware–Deser ghost in bigravity with doubly coupled matter*, *Int. J. Mod. Phys. D* **23** (2014) 1443003 [1408.0487].

[229] C. de Rham, L. Heisenberg and R.H. Ribeiro, *On couplings to matter in massive (bi-)gravity*, *Class. Quant. Grav.* **32** (2015) 035022 [1408.1678].

[230] Y. Akrami, T.S. Koivisto, D.F. Mota and M. Sandstad, *Bimetric gravity doubly coupled to matter: theory and cosmological implications*, *JCAP* **10** (2013) 046 [1306.0004].

[231] Y. Akrami, T.S. Koivisto and A.R. Solomon, *The nature of spacetime in bigravity: two metrics or none?*, *Gen. Rel. Grav.* **47** (2015) 1838 [1404.0006].

[232] Q.-G. Huang, R.H. Ribeiro, Y.-H. Xing, K.-C. Zhang and S.-Y. Zhou, *On the uniqueness of the non-minimal matter coupling in massive gravity and bigravity*, *Phys. Lett. B* **748** (2015) 356 [1505.02616].

[233] L. Heisenberg, *More on effective composite metrics*, *Phys. Rev. D* **92** (2015) 023525 [1505.02966].

[234] S. Melville and J. Noller, *Generalised matter couplings in massive bigravity*, *JHEP* **01** (2016) 094 [1511.01485].

[235] M. Lüben and A. Schmidt-May, *Ghost-Free Completion of An Effective Matter Coupling in Bimetric Theory*, *Fortsch. Phys.* **66** (2018) 1800031 [1804.04671].

[236] S.F. Hassan, M. Kocic and A. Schmidt-May, *Absence of ghost in a new bimetric-matter coupling*, 1409.1909.

[237] J. Enander, A.R. Solomon, Y. Akrami and E. Mörtsell, *Cosmic expansion histories in massive bigravity with symmetric matter coupling*, *JCAP* **01** (2015) 006 [1409.2860].

[238] A. Schmidt-May, *Mass eigenstates in bimetric theory with matter coupling*, *JCAP* **01** (2015) 039 [1409.3146].

[239] C. de Rham, L. Heisenberg and R.H. Ribeiro, *Ghosts and matter couplings in massive gravity, bigravity and multigravity*, *Phys. Rev. D* **90** (2014) 124042 [1409.3834].

[240] A.E. Gümrükçüoğlu, L. Heisenberg and S. Mukohyama, *Cosmological perturbations in massive gravity with doubly coupled matter*, *JCAP* **02** (2015) 022 [1409.7260].

[241] A.R. Solomon, J. Enander, Y. Akrami, T.S. Koivisto, F. Könnig and E. Mörtsell, *Cosmological viability of massive gravity with generalized matter coupling*, *JCAP* **04** (2015) 027 [1409.8300].

[242] L. Heisenberg, *Quantum corrections in massive bigravity and new effective composite metrics*, *Class. Quant. Grav.* **32** (2015) 105011 [1410.4239].

[243] X. Gao and D. Yoshida, *Coupling between Galileon and massive gravity with composite metrics*, *Phys. Rev. D* **92** (2015) 044057 [1412.8471].

[244] D. Comelli, M. Crisostomi, K. Koyama, L. Pilo and G. Tasinato, *Cosmology of bigravity with doubly coupled matter*, *JCAP* **04** (2015) 026 [1501.00864].

[245] A.E. Gümrükçüoğlu, L. Heisenberg, S. Mukohyama and N. Tanahashi, *Cosmology in bimetric theory with an effective composite coupling to matter*, *JCAP* **04** (2015) 008 [1501.02790].

[246] L. Blanchet and L. Heisenberg, *Dark Matter via Massive (bi-)Gravity*, *Phys. Rev. D* **91** (2015) 103518 [1504.00870].

[247] L. Blanchet and L. Heisenberg, *Dipolar Dark Matter with Massive Bigravity*, *JCAP* **12** (2015) 026 [1505.05146].

[248] M. Lagos and J. Noller, *New massive bigravity cosmologies with double matter coupling*, *JCAP* **01** (2016) 023 [1508.05864].

[249] P. Brax, A.-C. Davis and J. Noller, *Dark Energy and Doubly Coupled Bigravity*, *Class. Quant. Grav.* **34** (2017) 095014 [1606.05590].

[250] P. Brax, A.-C. Davis and J. Noller, *Gravitational Waves in Doubly Coupled Bigravity*, *Phys. Rev. D* **96** (2017) 023518 [1703.08016].

[251] P. Brax, S. Cespedes and A.-C. Davis, *Signatures of graviton masses on the CMB*, *JCAP* **03** (2018) 008 [1710.09818].

[252] Y. Akrami, P. Brax, A.-C. Davis and V. Vardanyan, *Neutron star merger GW170817 strongly constrains doubly coupled bigravity*, *Phys. Rev. D* **97** (2018) 124010 [1803.09726].

[253] M.S. Volkov, *Hairy black holes in theories with massive gravitons*, *Lect. Notes Phys.* **892** (2015) 161 [1405.1742].

[254] A.R. Solomon, *Cosmology Beyond Einstein*, Ph.D. thesis, Cambridge U., Cham, 2015. 1508.06859. 10.1007/978-3-319-46621-7.

[255] E. Babichev, L. Marzola, M. Raidal, A. Schmidt-May, F. Urban, H. Veermäe et al., *Bigravitational origin of dark matter*, *Phys. Rev. D* **94** (2016) 084055 [1604.08564].

[256] M.S. Volkov, *Cosmological solutions with massive gravitons in the bigravity theory*, *JHEP* **01** (2012) 035 [1110.6153].

[257] D. Comelli, M. Crisostomi, F. Nesti and L. Pilo, *FRW Cosmology in Ghost Free Massive Gravity*, *JHEP* **03** (2012) 067 [1111.1983].

[258] V. Baccetti, P. Martin-Moruno and M. Visser, *Massive gravity from bimetric gravity*, *Class. Quant. Grav.* **30** (2013) 015004 [1205.2158].

[259] S.F. Hassan, A. Schmidt-May and M. von Strauss, *Particular Solutions in Bimetric Theory and Their Implications*, *Int. J. Mod. Phys. D* **23** (2014) 1443002 [1407.2772].

[260] M. Högås and E. Mörtsell, *Constraints on bimetric gravity. Part I. Analytical constraints*, *JCAP* **05** (2021) 001 [2101.08794].

[261] M.S. Volkov, *Exact self-accelerating cosmologies in the ghost-free bigravity and massive gravity*, *Phys. Rev. D* **86** (2012) 061502 [1205.5713].

[262] M.S. Volkov, *Exact self-accelerating cosmologies in the ghost-free massive gravity – the detailed derivation*, *Phys. Rev. D* **86** (2012) 104022 [1207.3723].

[263] Y. Akrami, T.S. Koivisto and M. Sandstad, *Accelerated expansion from ghost-free bigravity: a statistical analysis with improved generality*, *JHEP* **03** (2013) 099 [1209.0457].

[264] M.S. Volkov, *Self-accelerating cosmologies and hairy black holes in ghost-free bigravity and massive gravity*, *Class. Quant. Grav.* **30** (2013) 184009 [1304.0238].

[265] F. Könnig, A. Patil and L. Amendola, *Viable cosmological solutions in massive bimetric gravity*, *JCAP* **03** (2014) 029 [1312.3208].

[266] A. De Felice, A.E. Gümrükçüoğlu, S. Mukohyama, N. Tanahashi and T. Tanaka, *Viable cosmology in bimetric theory*, *JCAP* **06** (2014) 037 [1404.0008].

[267] K.-i. Maeda and M.S. Volkov, *Anisotropic universes in the ghost-free bigravity*, *Phys. Rev. D* **87** (2013) 104009 [1302.6198].

[268] H. Nersisyan, Y. Akrami and L. Amendola, *Consistent metric combinations in cosmology of massive bigravity*, *Phys. Rev. D* **92** (2015) 104034 [1502.03988].

[269] C. García-García, A.L. Maroto and P. Martín-Moruno, *Cosmology with moving bimetric fluids*, *JCAP* **12** (2016) 022 [1608.06493].

[270] D. Comelli, M. Crisostomi and L. Pilo, *Perturbations in Massive Gravity Cosmology*, *JHEP* **06** (2012) 085 [1202.1986].

[271] G. Tasinato, K. Koyama and G. Niz, *Vector instabilities and self-acceleration in the decoupling limit of massive gravity*, *Phys. Rev. D* **87** (2013) 064029 [1210.3627].

[272] D. Comelli, M. Crisostomi and L. Pilo, *FRW Cosmological Perturbations in Massive Bigravity*, *Phys. Rev. D* **90** (2014) 084003 [1403.5679].

[273] G. Cusin, R. Durrer, P. Guarato and M. Motta, *A general mass term for bigravity*, *JCAP* **04** (2016) 051 [1512.02131].

[274] F. Könnig, Y. Akrami, L. Amendola, M. Motta and A.R. Solomon, *Stable and unstable cosmological models in bimetric massive gravity*, *Phys. Rev. D* **90** (2014) 124014 [1407.4331].

[275] F. Könnig, *Higuchi Ghosts and Gradient Instabilities in Bimetric Gravity*, *Phys. Rev. D* **91** (2015) 104019 [1503.07436].

[276] M. Fasiello and A.J. Tolley, *Cosmological Stability Bound in Massive Gravity and Bigravity*, *JCAP* **12** (2013) 002 [1308.1647].

[277] M. Lüben, A. Schmidt-May and J. Smirnov, *Vainshtein Screening in Bimetric Cosmology*, *Phys. Rev. D* **102** (2020) 123529 [1912.09449].

[278] Y. Yamashita and T. Tanaka, *Mapping the ghost free bigravity into braneworld setup*, *JCAP* **06** (2014) 004 [1401.4336].

[279] B. Ratra and P.J.E. Peebles, *Cosmological Consequences of a Rolling Homogeneous Scalar Field*, *Phys. Rev. D* **37** (1988) 3406.

[280] R.R. Caldwell, R. Dave and P.J. Steinhardt, *Cosmological imprint of an energy component with general equation of state*, *Phys. Rev. Lett.* **80** (1998) 1582 [astro-ph/9708069].

[281] K. Hinterbichler, M. Trodden and D. Wesley, *Multi-field galileons and higher co-dimension branes*, *Phys. Rev. D* **82** (2010) 124018 [1008.1305].

[282] C. de Rham, G. Gabadadze, L. Heisenberg and D. Pirtskhalava, *Nonrenormalization and naturalness in a class of scalar-tensor theories*, *Phys. Rev. D* **87** (2013) 085017 [1212.4128].

[283] C. de Rham, L. Heisenberg and R.H. Ribeiro, *Quantum Corrections in Massive Gravity*, *Phys. Rev. D* **88** (2013) 084058 [1307.7169].

[284] R.R. Caldwell, *A Phantom menace?*, *Phys. Lett. B* **545** (2002) 23 [astro-ph/9908168].

[285] G.W. Gibbons, *Phantom matter and the cosmological constant*, hep-th/0302199.

[286] K.J. Ludwick, *The viability of phantom dark energy: A review*, *Mod. Phys. Lett. A* **32** (2017) 1730025 [1708.06981].

[287] S.M. Carroll, A. De Felice and M. Trodden, *Can we be tricked into thinking that w is less than -1?*, *Phys. Rev. D* **71** (2005) 023525 [astro-ph/0408081].

[288] C. Csaki, N. Kaloper and J. Terning, *The Accelerated acceleration of the Universe*, *JCAP* **06** (2006) 022 [astro-ph/0507148].

[289] P. Creminelli, G. D'Amico, J. Norena and F. Vernizzi, *The Effective Theory of Quintessence: the w<-1 Side Unveiled*, *JCAP* **02** (2009) 018 [0811.0827].

[290] V. Baccetti, P. Martin-Moruno and M. Visser, *Null Energy Condition violations in bimetric gravity*, *JHEP* **08** (2012) 148 [1206.3814].

[291] S.V. Sushkov and M.S. Volkov, *Giant wormholes in ghost-free bigravity theory*, *JCAP* **06** (2015) 017 [1502.03712].

[292] Mörtsell, Edvard, *Cosmological histories in bimetric gravity: A graphical approach*, *JCAP* **02** (2017) 051 [1701.00710].

[293] P.H. Frampton, K.J. Ludwick and R.J. Scherrer, *The Little Rip*, *Phys. Rev. D* **84** (2011) 063003 [1106.4996].

[294] P.H. Frampton, K.J. Ludwick and R.J. Scherrer, *Pseudo-rip: Cosmological models intermediate between the cosmological constant and the little rip*, *Phys. Rev. D* **85** (2012) 083001 [1112.2964].

[295] S. Nojiri, S.D. Odintsov and S. Tsujikawa, *Properties of singularities in (phantom) dark energy universe*, *Phys. Rev. D* **71** (2005) 063004 [hep-th/0501025].

[296] E. Mörtsell and S. Dhawan, *Does the Hubble constant tension call for new physics?*, *JCAP* **09** (2018) 025 [1801.07260].

[297] M. Lindner, K. Max, M. Platscher and J. Rezacek, *Probing alternative cosmologies through the inverse distance ladder*, *JCAP* **10** (2020) 040 [2002.01487].

[298] A. Caravano, M. Lüben and J. Weller, *Combining cosmological and local bounds on bimetric theory*, 2101.08791.

[299] M. Högås and E. Mörtsell, *Constraints on bimetric gravity. Part II. Observational constraints*, *JCAP* **05** (2021) 002 [2101.08795].

[300] N. Khosravi, H.R. Sepangi and S. Shahidi, *Massive cosmological scalar perturbations*, *Phys. Rev. D* **86** (2012) 043517 [1202.2767].

[301] M. Berg, I. Buchberger, J. Enander, E. Mörtsell and S. Sjors, *Growth Histories in Bimetric Massive Gravity*, *JCAP* **12** (2012) 021 [1206.3496].

[302] Y. Sakakihara, J. Soda and T. Takahashi, *On Cosmic No-hair in Bimetric Gravity and the Higuchi Bound*, *PTEP* **2013** (2013) 033E02 [1211.5976].

[303] F. Könnig and L. Amendola, *Instability in a minimal bimetric gravity model*, *Phys. Rev. D* **90** (2014) 044030 [1402.1988].

[304] A.R. Solomon, Y. Akrami and T.S. Koivisto, *Linear growth of structure in massive bigravity*, *JCAP* **10** (2014) 066 [1404.4061].

[305] M. Lagos and P.G. Ferreira, *Cosmological perturbations in massive bigravity*, *JCAP* **12** (2014) 026 [1410.0207].

[306] V.F. Mukhanov, H.A. Feldman and R.H. Brandenberger, *Theory of cosmological perturbations. Part 1. Classical perturbations. Part 2. Quantum theory of perturbations. Part 3. Extensions*, *Phys. Rept.* **215** (1992) 203.

[307] M. Lagos, M. Bañados, P.G. Ferreira and S. García-Sáenz, *Noether Identities and Gauge-Fixing the Action for Cosmological Perturbations*, *Phys. Rev. D* **89** (2014) 024034 [1311.3828].

[308] K. Aoki, K.-i. Maeda and R. Namba, *Stability of the Early Universe in Bigravity Theory*, *Phys. Rev. D* **92** (2015) 044054 [1506.04543].

[309] E. Mörtsell and J. Enander, *Scalar instabilities in bimetric gravity: The Vainshtein mechanism and structure formation*, *JCAP* **10** (2015) 044 [1506.04977].

[310] M. Högås, F. Torsello and E. Mörtsell, *On the stability of bimetric structure formation*, *JCAP* **04** (2020) 046 [1910.01651].

[311] G. Cusin, R. Durrer, P. Guarato and M. Motta, *Gravitational waves in bigravity cosmology*, *JCAP* **05** (2015) 030 [1412.5979].

[312] L. Amendola, F. Könnig, M. Martinelli, V. Pettorino and M. Zumalacarregui, *Surfing gravitational waves: can bigravity survive growing tensor modes?*, *JCAP* **05** (2015) 052 [1503.02490].

[313] M. Johnson and A. Terrana, *Tensor Modes in Bigravity: Primordial to Present*, *Phys. Rev. D* **92** (2015) 044001 [1503.05560].

[314] G. Cusin, R. Durrer, P. Guarato and M. Motta, *Inflationary perturbations in bimetric gravity*, *JCAP* **09** (2015) 043 [1505.01091].

[315] Y. Sakakihara and J. Soda, *Primordial Gravitational Waves in Bimetric Gravity*, *JCAP* **09** (2015) 015 [1504.04969].

[316] M. Fasiello and R.H. Ribeiro, *Mild bounds on bigravity from primordial gravitational waves*, *JCAP* **07** (2015) 027 [1505.00404].

[317] J. Adamek, R. Durrer and V. Tansella, *Lensing signals from Spin-2 perturbations*, *JCAP* **01** (2016) 024 [1510.01566].

[318] Y. Sakakihara and T. Tanaka, *Primordial fluctuations from inflation in dRGT bimetric theory of gravity*, *JCAP* **09** (2016) 033 [1605.05790].

[319] M. Biagetti, E. Dimastrogiovanni and M. Fasiello, *Possible signatures of the inflationary particle content: spin-2 fields*, *JCAP* **10** (2017) 038 [1708.01587].

[320] E. Dimastrogiovanni, M. Fasiello and G. Tasinato, *Probing the inflationary particle content: extra spin-2 field*, *JCAP* **08** (2018) 016 [1806.00850].

[321] G. Goon, K. Hinterbichler, A. Joyce and M. Trodden, *Shapes of gravity: Tensor non-Gaussianity and massive spin-2 fields*, *JHEP* **10** (2019) 182 [1812.07571].

[322] A. De Felice, T. Nakamura and T. Tanaka, *Possible existence of viable models of bi-gravity with detectable graviton oscillations by gravitational wave detectors*, *PTEP* **2014** (2014) 043E01 [1304.3920].

[323] T. Narikawa, K. Ueno, H. Tagoshi, T. Tanaka, N. Kanda and T. Nakamura, *Detectability of bigravity with graviton oscillations using gravitational wave observations*, *Phys. Rev. D* **91** (2015) 062007 [1412.8074].

[324] K. Max, M. Platscher and J. Smirnov, *Gravitational Wave Oscillations in Bigravity*, *Phys. Rev. Lett.* **119** (2017) 111101 [1703.07785].

[325] K. Max, M. Platscher and J. Smirnov, *Decoherence of Gravitational Wave Oscillations in Bigravity*, *Phys. Rev. D* **97** (2018) 064009 [1712.06601].

[326] E. Ayón-Beato, D. Higuita-Borja, J.A. Méndez-Zavaleta and G. Velázquez-Rodríguez, *Exact ghost-free bigravitational waves*, *Phys. Rev. D* **97** (2018) 084045 [1801.06764].

[327] J.B. Jiménez, J.M. Ezquiaga and L. Heisenberg, *Probing cosmological fields with gravitational wave oscillations*, *JCAP* **04** (2020) 027 [1912.06104].

[328] D. Comelli, M. Crisostomi, F. Nesti and L. Pilo, *Spherically Symmetric Solutions in Ghost-Free Massive Gravity*, *Phys. Rev. D* **85** (2012) 024044 [1110.4967].

[329] M.S. Volkov, *Hairy black holes in the ghost-free bigravity theory*, *Phys. Rev. D* **85** (2012) 124043 [1202.6682].

[330] J. Enander and E. Mörtsell, *Strong lensing constraints on bimetric massive gravity*, *JHEP* **10** (2013) 031 [1306.1086].

[331] E. Babichev and M. Crisostomi, *Restoring general relativity in massive bigravity theory*, *Phys. Rev. D* **88** (2013) 084002 [1307.3640].

[332] J. Enander and E. Mörtsell, *On stars, galaxies and black holes in massive bigravity*, *JCAP* **11** (2015) 023 [1507.00912].

[333] K. Aoki, K.-i. Maeda and M. Tanabe, *Relativistic stars in bigravity theory*, *Phys. Rev. D* **93** (2016) 064054 [1602.02227].

[334] M. Platscher and J. Smirnov, *Degravitation of the Cosmological Constant in Bigravity*, *JCAP* **03** (2017) 051 [1611.09385].

[335] M. Lüben, E. Mörtsell and A. Schmidt-May, *Bimetric cosmology is compatible with local tests of gravity*, *Class. Quant. Grav.* **37** (2020) 047001 [1812.08686].

[336] J. Enander, Y. Akrami, E. Mörtsell, M. Renneby and A.R. Solomon, *Integrated Sachs-Wolfe effect in massive bigravity*, *Phys. Rev. D* **91** (2015) 084046 [1501.02140].

[337] S. Dhawan, A. Goobar, E. Mörtsell, R. Amanullah and U. Feindt, *Narrowing down the possible explanations of cosmic acceleration with geometric probes*, *JCAP* **07** (2017) 040 [1705.05768].

[338] M. Hohmann, *Post-Newtonian parameter γ and the deflection of light in ghost-free massive bimetric gravity*, *Phys. Rev. D* **95** (2017) 124049 [1701.07700].

[339] M. Platscher, J. Smirnov, S. Meyer and M. Bartelmann, *Long Range Effects in Gravity Theories with Vainshtein Screening*, *JCAP* **12** (2018) 009 [1809.05318].

[340] M. Lüben, A. Schmidt-May and J. Weller, *Physical parameter space of bimetric theory and SN1a constraints*, *JCAP* **09** (2020) 024 [2003.03382].

[341] N. Chow and J. Khoury, *Galileon Cosmology*, *Phys. Rev. D* **80** (2009) 024037 [0905.1325].

[342] C. de Rham and L. Heisenberg, *Cosmology of the Galileon from Massive Gravity*, *Phys. Rev. D* **84** (2011) 043503 [1106.3312].

[343] E. Fischbach and C. Talmadge, *The Search for Non-Newtonian Gravity*, Springer-Verlag New York (1999), 10.1007/978-1-4612-1438-0.

[344] E. Adelberger, B.R. Heckel and A. Nelson, *Tests of the gravitational inverse square law*, *Ann. Rev. Nucl. Part. Sci.* **53** (2003) 77 [hep-ph/0307284].

[345] C.D. Hoyle, D.J. Kapner, B.R. Heckel, E.G. Adelberger, J.H. Gundlach, U. Schmidt et al., *Sub-millimeter tests of the gravitational inverse-square law*, *Phys. Rev.* **D70** (2004) 042004 [hep-ph/0405262].

[346] E. Adelberger, J. Gundlach, B. Heckel, S. Hoedl and S. Schlamminger, *Torsion balance experiments: A low-energy frontier of particle physics*, *Prog. Part. Nucl. Phys.* **62** (2009) 102.

[347] C.M. Will, *The Confrontation between General Relativity and Experiment*, *Living Rev.Rel.* **17** (2014) 4 [1403.7377].

[348] J. Murata and S. Tanaka, *A review of short-range gravity experiments in the LHC era*, *Class. Quant. Grav.* **32** (2015) 033001 [1408.3588].

[349] G. D'Agostini, *Probability and measurement uncertainty in physics: A Bayesian primer*, hep-ph/9512295.

[350] R. Trotta, *Applications of Bayesian model selection to cosmological parameters*, *Mon. Not. Roy. Astron. Soc.* **378** (2007) 72 [astro-ph/0504022].

[351] R. Trotta, *Bayes in the sky: Bayesian inference and model selection in cosmology*, *Contemp. Phys.* **49** (2008) 71 [0803.4089].

[352] A.R. Liddle, *Statistical methods for cosmological parameter selection and estimation*, *Ann. Rev. Nucl. Part. Sci.* **59** (2009) 95 [0903.4210].

[353] M. Kerscher and J. Weller, *On Model Selection in Cosmology*, *SciPost Phys. Lect. Notes* **9** (2019) 1 [1901.07726].

[354] T. Bayes, Rev., *An essay toward solving a problem in the doctrine of chances*, *Phil. Trans. Roy. Soc. Lond.* **53** (1764) 370.

[355] N. Metropolis, A.W. Rosenbluth, M.N. Rosenbluth, A.H. Teller and E. Teller, *Equation of state calculations by fast computing machines*, *J. Chem. Phys.* **21** (1953) 1087.

[356] W.K. Hastings, *Monte Carlo Sampling Methods Using Markov Chains and Their Applications*, *Biometrika* **57** (1970) 97.

[357] N. Christensen and R. Meyer, *Bayesian methods for cosmological parameter estimation from cosmic microwave background measurements*, astro-ph/0006401.

[358] N. Christensen, R. Meyer, L. Knox and B. Luey, *II. Bayesian methods for cosmological parameter estimation from cosmic microwave background measurements*, *Class. Quant. Grav.* **18** (2001) 2677 [astro-ph/0103134].

[359] G. Schwarz, *Estimating the Dimension of a Model*, *Annals Statist.* **6** (1978) 461.

[360] R.E. Kass and A.E. Raftery, *Bayes Factors*, *J. Am. Statist. Assoc.* **90** (1995) 773.

[361] D.J. Fixsen, *The Temperature of the Cosmic Microwave Background*, *Astrophys. J.* **707** (2009) 916 [0911.1955].

[362] V.F. Shvartsman, *Density of relict particles with zero rest mass in the universe*, *Pisma Zh. Eksp. Teor. Fiz.* **9** (1969) 315.

[363] G. Steigman, D.N. Schramm and J.E. Gunn, *Cosmological Limits to the Number of Massive Leptons*, *Phys. Lett. B* **66** (1977) 202.

[364] N.Y. Gnedin and O.Y. Gnedin, *Cosmological neutrino background revisited*, *Astrophys. J.* **509** (1998) 11 [astro-ph/9712199].

[365] G. Mangano, G. Miele, S. Pastor, T. Pinto, O. Pisanti and P.D. Serpico, *Relic neutrino decoupling including flavor oscillations*, *Nucl. Phys. B* **729** (2005) 221 [hep-ph/0506164].

[366] P.F. de Salas and S. Pastor, *Relic neutrino decoupling with flavour oscillations revisited*, *JCAP* **07** (2016) 051 [1606.06986].

[367] SDSS collaboration, *Improved cosmological constraints from a joint analysis of the SDSS-II and SNLS supernova samples*, *Astron. Astrophys.* **568** (2014) A22 [1401.4064].

[368] W. Hu and N. Sugiyama, *Small scale cosmological perturbations: An Analytic approach*, *Astrophys. J.* **471** (1996) 542 [astro-ph/9510117].

[369] G. Efstathiou and J.R. Bond, *Cosmic confusion: Degeneracies among cosmological parameters derived from measurements of microwave background anisotropies*, *Mon. Not. Roy. Astron. Soc.* **304** (1999) 75 [astro-ph/9807103].

[370] A. Kosowsky, M. Milosavljevic and R. Jimenez, *Efficient cosmological parameter estimation from microwave background anisotropies*, *Phys. Rev. D* **66** (2002) 063007 [astro-ph/0206014].

[371] Y. Wang and P. Mukherjee, *Observational Constraints on Dark Energy and Cosmic Curvature*, *Phys. Rev. D* **76** (2007) 103533 [astro-ph/0703780].

[372] WMAP collaboration, *Five-Year Wilkinson Microwave Anisotropy Probe (WMAP) Observations: Cosmological Interpretation*, *Astrophys. J. Suppl.* **180** (2009) 330 [0803.0547].

[373] O. Elgaroy and T. Multamaki, *On using the CMB shift parameter in tests of models of dark energy*, *Astron. Astrophys.* **471** (2007) 65 [astro-ph/0702343].

[374] Z. Zhai, C.-G. Park, Y. Wang and B. Ratra, *CMB distance priors revisited: effects of dark energy dynamics, spatial curvature, primordial power spectrum, and neutrino parameters*, *JCAP* **07** (2020) 009 [1912.04921].

[375] R. Durrer, *The Cosmic Microwave Background*, Cambridge University Press, 2 ed. (12, 2020), 10.1017/9781316471524.

[376] L. Chen, Q.-G. Huang and K. Wang, *Distance Priors from Planck Final Release*, *JCAP* **02** (2019) 028 [1808.05724].

[377] F. Beutler, C. Blake, M. Colless, D.H. Jones, L. Staveley-Smith, L. Campbell et al., *The 6dF Galaxy Survey: Baryon Acoustic Oscillations and the Local Hubble Constant*, *Mon. Not. Roy. Astron. Soc.* **416** (2011) 3017 [1106.3366].

[378] A.J. Ross, L. Samushia, C. Howlett, W.J. Percival, A. Burden and M. Manera, *The clustering of the SDSS DR7 main Galaxy sample – I. A 4 per cent distance measure at* $z = 0.15$, *Mon. Not. Roy. Astron. Soc.* **449** (2015) 835 [1409.3242].

[379] BOSS collaboration, *The clustering of galaxies in the completed SDSS-III Baryon Oscillation Spectroscopic Survey: cosmological analysis of the DR12 galaxy sample*, *Mon. Not. Roy. Astron. Soc.* **470** (2017) 2617 [1607.03155].

[380] J.E. Bautista et al., *The SDSS-IV extended Baryon Oscillation Spectroscopic Survey: Baryon Acoustic Oscillations at redshift of 0.72 with the DR14 Luminous Red Galaxy Sample*, *Astrophys. J.* **863** (2018) 110 [1712.08064].

[381] G.-B. Zhao et al., *The clustering of the SDSS-IV extended Baryon Oscillation Spectroscopic Survey DR14 quasar sample: a tomographic measurement of cosmic structure growth and expansion rate based on optimal redshift weights*, *Mon. Not. Roy. Astron. Soc.* **482** (2019) 3497 [1801.03043].

[382] A. Lewis, *GetDist: a Python package for analysing Monte Carlo samples*, 1910.13970.

[383] C. Talmadge, J. Berthias, R. Hellings and E. Standish, *Model Independent Constraints on Possible Modifications of Newtonian Gravity*, *Phys. Rev. Lett.* **61** (1988) 1159.

[384] D.E. Smith, D.C. Christodoulidis, R. Kolenkiewicz, P.J. Dunn, S.M. Klosko, M.H. Torrence et al., *A global geodetic reference frame from LAGEOS ranging (SL5.1AP)*, *J. Geophys. Res.* **90** (1985) 9221.

[385] J.O. Dickey et al., *Lunar Laser Ranging: A Continuing Legacy of the Apollo Program*, *Science* **265** (1994) 482.

[386] J. Thomas, P. Kasameyer, O. Fackler, D. Felske, R. Harris, J. Kammeraad et al., *Testing the inverse-square law of gravity on a 465-m tower*, *Phys. Rev. Lett.* **63** (1989) 1902.

[387] J. Kammeraad, P. Kasameyer, O. Fackler, D. Felske, R. Harris, M. Millett et al., *New results from Nevada: A Test of Newton's law using the BREN tower and a high density ground gravity survey*, in *10th Moriond Workshop: New and Exotic Phenomena*, pp. 245–254, 1990.

[388] G.W. Gibbons and B.F. Whiting, *Constraints on Unification Theories Imposed by Measurements of Newtonian Gravity*, *Nature* **291** (1981) 636.

[389] A. Cornaz, B. Hubler and W. Kuendig, *Determination of the gravitational constant at an effective interaction distance of 112-m*, *Phys. Rev. Lett.* **72** (1994) 1152.

[390] B. Hubler, A. Cornaz and W. Kuendig, *Determination of the gravitational constant with a lake experiment: New constraints for nonNewtonian gravity*, *Phys. Rev. D* **51** (1995) 4005.

[391] G.G. Luther and W.R. Towler, *Redetermination of the Newtonian Gravitational Constant G*, *Phys. Rev. Lett.* **48** (1982) 121.

[392] J.K. Hoskins, R.D. Newman, R. Spero and J. Schultz, *Experimental tests of the gravitational inverse square law for mass separations from 2-cm to 105-cm*, *Phys. Rev. D* **32** (1985) 3084.

[393] S.J. Smullin, A.A. Geraci, D.M. Weld, J. Chiaverini, S.P. Holmes and A. Kapitulnik, *New constraints on Yukawa-type deviations from Newtonian gravity at 20 microns*, *Phys. Rev. D* **72** (2005) 122001 [hep-ph/0508204].

[394] D.J. Kapner, T.S. Cook, E.G. Adelberger, J.H. Gundlach, B.R. Heckel, C.D. Hoyle et al., *Tests of the gravitational inverse-square law below the dark-energy length scale*, *Phys. Rev. Lett.* **98** (2007) 021101 [hep-ph/0611184].

[395] S.K. Lamoreaux, *Demonstration of the Casimir force in the 0.6 to 6 micrometers range*, *Phys. Rev. Lett.* **78** (1997) 5.

[396] A.O. Sushkov, W.J. Kim, D.A.R. Dalvit and S.K. Lamoreaux, *New Experimental Limits on Non-Newtonian Forces in the Micrometer Range*, *Phys. Rev. Lett.* **107** (2011) 171101 [1108.2547].

[397] R.S. Decca, D. Lopez, H.B. Chan, E. Fischbach, D.E. Krause and C.R. Jamell, *Constraining new forces in the Casimir regime using the isoelectronic technique*, *Phys. Rev. Lett.* **94** (2005) 240401 [hep-ph/0502025].

[398] R.S. Decca, D. Lopez, E. Fischbach, G.L. Klimchitskaya, D.E. Krause and V.M. Mostepanenko, *Tests of new physics from precise measurements of the Casimir pressure between two gold-coated plates*, *Phys. Rev. D* **75** (2007) 077101 [hep-ph/0703290].

[399] T. Ederth, *Template-stripped gold surfaces with 0.4-nm rms roughness suitable for force measurements: Application to the Casimir force in the 20-100-nm range*, *Phys. Rev. A* **62** (2000) 062104 [quant-ph/0008009].

[400] V.M. Mostepanenko and M. Novello, *Constraints on nonNewtonian gravity from the Casimir force measurements between two crossed cylinders*, *Phys. Rev. D* **63** (2001) 115003 [hep-ph/0101306].

[401] B.W. Harris, F. Chen and U. Mohideen, *Precision measurement of the Casimir force using gold surfaces*, *Phys. Rev. A* **62** (2000) 052109 [quant-ph/0005088].

[402] J.N. Israelachvili and D. Tabor, *The measurement of van der Waals dispersion forces in the range 1.5 to 130 nm*, *Proc. R. Soc. Lond. A* **331** (1972) 19.

[403] M. Bordag, V.M. Mostepanenko and I.Y. Sokolov, *On the strengthening of restrictions on hypothetical Yukawa type forces with extremely small range of action*, *Phys. Lett. A* **187** (1994) 35.

[404] J. Bergé, M. Pernot-Borràs, J.-P. Uzan, P. Brax, R. Chhun, G. Métris et al., *MICROSCOPE's constraint on a short-range fifth force*, 2102.00022.

[405] C.M. Will and K. Nordtvedt, Jr., *Conservation Laws and Preferred Frames in Relativistic Gravity. I. Preferred-Frame Theories and an Extended PPN Formalism*, *Astrophys. J.* **177** (1972) 757.

[406] C.M. Will, *The Confrontation between General Relativity and Experiment*, *Living Rev. Rel.* **17** (2014) 4 [1403.7377].

[407] A.S. Bolton, S. Burles, L.V.E. Koopmans, T. Treu and L.A. Moustakas, *The sloan lens acs survey. 1. a large spectroscopically selected sample of massive early-type lens galaxies*, *Astrophys. J.* **638** (2006) 703 [astro-ph/0511453].

[408] T. Treu, L. Koopmans, A. Bolton, S. Burles and L. Moustakas, *The sloan-lens acs survey. 2. stellar populations and internal structure of early-type lens galaxies*, *Astrophys. J.* **640** (2006) 662 [astro-ph/0512044].

[409] L.V.E. Koopmans, T. Treu, A.S. Bolton, S. Burles and L.A. Moustakas, *The sloan lens acs survey. 3. the structure and formation of early-type galaxies and their evolution since z~1*, *Astrophys. J.* **649** (2006) 599 [astro-ph/0601628].

[410] A.S. Bolton, S. Rappaport and S. Burles, *Constraint on the Post-Newtonian Parameter gamma on Galactic Size Scales*, *Phys. Rev. D* **74** (2006) 061501 [astro-ph/0607657].

[411] B. Bertotti, L. Iess and P. Tortora, *A test of general relativity using radio links with the Cassini spacecraft*, *Nature* **425** (2003) 374.

[412] J.K. Bloomfield, C. Burrage and A.-C. Davis, *Shape dependence of Vainshtein screening*, *Phys. Rev. D* **91** (2015) 083510 [1408.4759].

[413] D. Baumann and L. McAllister, *Inflation and String Theory*, Cambridge Monographs on Mathematical Physics, Cambridge University Press (5, 2015), 10.1017/CBO9781316105733, [1404.2601].

[414] P. Agrawal, G. Obied, P.J. Steinhardt and C. Vafa, *On the Cosmological Implications of the String Swampland*, *Phys. Lett. B* **784** (2018) 271 [1806.09718].

[415] L. Heisenberg, M. Bartelmann, R. Brandenberger and A. Refregier, *Dark Energy in the Swampland*, *Phys. Rev. D* **98** (2018) 123502 [1808.02877].

[416] D. Lüst and E. Palti, *A Note on String Excitations and the Higuchi Bound*, *Phys. Lett. B* **799** (2019) 135067 [1907.04161].

[417] T. Noumi, T. Takeuchi and S. Zhou, *String Regge trajectory on de Sitter space and implications to inflation*, *Phys. Rev. D* **102** (2020) 126012 [1907.02535].

[418] M. Scalisi, *Inflation, Higher Spins and the Swampland*, *Phys. Lett. B* **808** (2020) 135683 [1912.04283].

[419] C. Bachas and I. Lavdas, *Massive Anti-de Sitter Gravity from String Theory*, *JHEP* **11** (2018) 003 [1807.00591].

[420] S. Ferrara, A. Kehagias and D. Lüst, *Bimetric, Conformal Supergravity and its Superstring Embedding*, *JHEP* **05** (2019) 100 [1810.08147].

[421] D. Klaewer, D. Lüst and E. Palti, *A Spin-2 Conjecture on the Swampland*, *Fortsch. Phys.* **67** (2019) 1800102 [1811.07908].

[422] C. De Rham, L. Heisenberg and A.J. Tolley, *Spin-2 fields and the weak gravity conjecture*, *Phys. Rev. D* **100** (2019) 104033 [1812.01012].

[423] C. Bachas, *Massive AdS Supergravitons and Holography*, *JHEP* **06** (2019) 073 [1905.05039].

[424] I. Lavdas and D. Lüst, *Massive gravitons on the Landscape and the AdS Distance Conjecture*, 2007.08913.

[425] M. Lüben and D. Lüst, *Higuchi bound on slow-roll inflation and the swampland*, *JHEP* **09** (2020) 055 [2003.10494].

[426] D. Baumann, *Inflation*, in *Theoretical Advanced Study Institute in Elementary Particle Physics: Physics of the Large and the Small*, 7, 2009, DOI [0907.5424].

[427] J. Martin, C. Ringeval and V. Vennin, *Encyclopædia Inflationaris*, *Phys. Dark Univ.* **5-6** (2014) 75 [1303.3787].

[428] S. Deser and R.I. Nepomechie, *Gauge Invariance Versus Masslessness in De Sitter Space*, *Annals Phys.* **154** (1984) 396.

[429] S.F. Hassan, A. Schmidt-May and M. von Strauss, *On Partially Massless Bimetric Gravity*, *Phys. Lett. B* **726** (2013) 834 [1208.1797].

[430] G. Alestas, L. Kazantzidis and L. Perivolaropoulos, H_0 *tension, phantom dark energy, and cosmological parameter degeneracies*, *Phys. Rev. D* **101** (2020) 123516 [2004.08363].

[431] E. Di Valentino, A. Melchiorri and J. Silk, *Investigating Cosmic Discordance*, *Astrophys. J. Lett.* **908** (2021) L9 [2003.04935].

[432] A. Joyce, L. Lombriser and F. Schmidt, *Dark Energy Versus Modified Gravity*, *Ann. Rev. Nucl. Part. Sci.* **66** (2016) 95 [1601.06133].

[433] K. Aoki and S. Mukohyama, *Massive gravitons as dark matter and gravitational waves*, *Phys. Rev. D* **94** (2016) 024001 [1604.06704].

[434] DES, SPT collaboration, *Cosmological constraints from DES Y1 cluster abundances and SPT multiwavelength data*, *Phys. Rev. D* **103** (2021) 043522 [2010.13800].

[435] DESI collaboration, *The Dark Energy Spectroscopic Instrument (DESI)*, 1907.10688.

[436] L. Amendola et al., *Cosmology and fundamental physics with the Euclid satellite*, *Living Rev. Rel.* **21** (2018) 2 [1606.00180].

[437] A. Weltman et al., *Fundamental physics with the Square Kilometre Array*, *Publ. Astron. Soc. Austral.* **37** (2020) e002 [1810.02680].

[438] LSST Science, LSST Project collaboration, *LSST Science Book, Version 2.0*, 0912.0201.

[439] CMB-S4 collaboration, *CMB-S4 Science Book, First Edition*, 1610.02743.

[440] T. Matsumura et al., *Mission design of LiteBIRD*, *J. Low Temp. Phys.* **176** (2014) 733 [1311.2847].

[441] P. Brax, C. Burrage and A.-C. Davis, *Laboratory Tests of the Galileon*, *JCAP* **09** (2011) 020 [1106.1573].

[442] P. Brax, C. Burrage and A.-C. Davis, *Laboratory constraints*, *Int. J. Mod. Phys. D* **27** (2018) 1848009.

[443] L. Hui, A. Nicolis and C. Stubbs, *Equivalence Principle Implications of Modified Gravity Models*, *Phys. Rev. D* **80** (2009) 104002 [0905.2966].

[444] B. Jain and J. VanderPlas, *Tests of Modified Gravity with Dwarf Galaxies*, *JCAP* **10** (2011) 032 [1106.0065].

[445] L. Hui and A. Nicolis, *Proposal for an Observational Test of the Vainshtein Mechanism*, *Phys. Rev. Lett.* **109** (2012) 051304 [1201.1508].

[446] T. Hiramatsu, W. Hu, K. Koyama and F. Schmidt, *Equivalence Principle Violation in Vainshtein Screened Two-Body Systems*, *Phys. Rev. D* **87** (2013) 063525 [1209.3364].

[447] K. Koyama and J. Sakstein, *Astrophysical Probes of the Vainshtein Mechanism: Stars and Galaxies*, *Phys. Rev. D* **91** (2015) 124066 [1502.06872].

[448] B. Falck, K. Koyama and G.-B. Zhao, *Cosmic Web and Environmental Dependence of Screening: Vainshtein vs. Chameleon*, *JCAP* **07** (2015) 049 [1503.06673].

[449] P. Brax and A.-C. Davis, *Distinguishing modified gravity models*, *JCAP* **10** (2015) 042 [1506.01519].

[450] J. Sakstein, B. Jain, J.S. Heyl and L. Hui, *Tests of Gravity Theories Using Supermassive Black Holes*, *Astrophys. J. Lett.* **844** (2017) L14 [1704.02425].

[451] B. Falck, K. Koyama, G.-B. Zhao and M. Cautun, *Using Voids to Unscreen Modified Gravity*, *Mon. Not. Roy. Astron. Soc.* **475** (2018) 3262 [1704.08942].

[452] T. Baker, J. Clampitt, B. Jain and M. Trodden, *Void Lensing as a Test of Gravity*, *Phys. Rev. D* **98** (2018) 023511 [1803.07533].

[453] C. Burrage, J. Dombrowski and D. Saadeh, *The shape dependence of Vainshtein screening in the cosmic matter bispectrum*, *JCAP* **10** (2019) 023 [1905.06260].

[454] H. Desmond, B. Jain and J. Sakstein, *Local resolution of the Hubble tension: The impact of screened fifth forces on the cosmic distance ladder*, *Phys. Rev. D* **100** (2019) 043537 [1907.03778].

[455] C. Burrage and J. Dombrowski, *Constraining the cosmological evolution of scalar-tensor theories with local measurements of the time variation of G*, *JCAP* **07** (2020) 060 [2004.14260].

[456] P. Brax, L. Heisenberg and A. Kuntz, *Unveiling the Galileon in a three-body system : scalar and gravitational wave production*, *JCAP* **05** (2020) 012 [2002.12590].

[457] J. Sakstein, *Astrophysical tests of screened modified gravity*, *Int. J. Mod. Phys. D* **27** (2018) 1848008 [2002.04194].

[458] T. Baker et al., *Novel Probes Project: Tests of gravity on astrophysical scales*, *Rev. Mod. Phys.* **93** (2021) 015003 [1908.03430].

[459] A. Adams, N. Arkani-Hamed, S. Dubovsky, A. Nicolis and R. Rattazzi, *Causality, analyticity and an IR obstruction to UV completion*, *JHEP* **10** (2006) 014 [hep-th/0602178].

[460] C. de Rham, S. Melville, A.J. Tolley and S.-Y. Zhou, *UV complete me: Positivity Bounds for Particles with Spin*, *JHEP* **03** (2018) 011 [1706.02712].

[461] K. Hinterbichler, A. Joyce and R.A. Rosen, *Massive Spin-2 Scattering and Asymptotic Superluminality*, *JHEP* **03** (2018) 051 [1708.05716].

[462] C. de Rham, S. Melville and A.J. Tolley, *Improved Positivity Bounds and Massive Gravity*, *JHEP* **04** (2018) 083 [1710.09611].

[463] J. Bonifacio, K. Hinterbichler, A. Joyce and R.A. Rosen, *Massive and Massless Spin-2 Scattering and Asymptotic Superluminality*, *JHEP* **06** (2018) 075 [1712.10020].

[464] C. de Rham, S. Melville, A.J. Tolley and S.-Y. Zhou, *Positivity Bounds for Massive Spin-1 and Spin-2 Fields*, *JHEP* **03** (2019) 182 [1804.10624].

[465] L. Alberte, C. de Rham, A. Momeni, J. Rumbutis and A.J. Tolley, *Positivity Constraints on Interacting Spin-2 Fields*, *JHEP* **03** (2020) 097 [1910.11799].

[466] L. Alberte, C. de Rham, S. Jaitly and A.J. Tolley, *Positivity Bounds and the Massless Spin-2 Pole*, *Phys. Rev. D* **102** (2020) 125023 [2007.12667].

[467] S. Melville and J. Noller, *Positivity in the Sky: Constraining dark energy and modified gravity from the UV*, *Phys. Rev. D* **101** (2020) 021502 [1904.05874].

[468] A. Barreira, B. Li, C.M. Baugh and S. Pascoli, *Linear perturbations in Galileon gravity models*, *Phys. Rev. D* **86** (2012) 124016 [1208.0600].

[469] A. Barreira, B. Li, W.A. Hellwing, C.M. Baugh and S. Pascoli, *Nonlinear structure formation in the Cubic Galileon gravity model*, *JCAP* **10** (2013) 027 [1306.3219].

[470] B. Li, A. Barreira, C.M. Baugh, W.A. Hellwing, K. Koyama, S. Pascoli et al., *Simulating the quartic Galileon gravity model on adaptively refined meshes*, *JCAP* **11** (2013) 012 [1308.3491].

[471] A. Barreira, B. Li, C.M. Baugh and S. Pascoli, *Spherical collapse in Galileon gravity: fifth force solutions, halo mass function and halo bias*, *JCAP* **11** (2013) 056 [1308.3699].

[472] J. Braden, C. Burrage, B. Elder and D. Saadeh, *φenics: Vainshtein screening with the finite element method*, *JCAP* **03** (2021) 010 [2011.07037].

[473] M. Kocic, *Geometric mean of bimetric spacetimes*, *Class. Quant. Grav.* **38** (2021) 075023 [1803.09752].

[474] M. Kocic, *Causal propagation of constraints in bimetric relativity in standard 3+1 form*, *JHEP* **10** (2019) 219 [1804.03659].

[475] M. Kocic, A. Lundkvist and F. Torsello, *On the ratio of lapses in bimetric relativity*, *Class. Quant. Grav.* **36** (2019) 225013 [1903.09646].

[476] F. Torsello, M. Kocic, M. Högås and E. Mörtsell, *Covariant BSSN formulation in bimetric relativity*, *Class. Quant. Grav.* **37** (2020) 025013 [1904.07869].

[477] M. Kocic, F. Torsello, M. Högås and E. Mörtsell, *Spherical dust collapse in bimetric relativity: Bimetric polytropes*, 1904.08617.

[478] F. Torsello, *The mean gauges in bimetric relativity*, *Class. Quant. Grav.* **36** (2019) 235010 [1904.09297].

[479] F. Torsello, `bimEX`*: A Mathematica package for exact computations in* $3+1$ *bimetric relativity*, *Comput. Phys. Commun.* **247** (2020) 106948 [1904.10464].

[480] M. Kocic, F. Torsello, M. Högås and E. Mörtsell, *Initial data and first evolutions of dust clouds in bimetric relativity*, *Class. Quant. Grav.* **37** (2020) 165010.

[481] X. Chu and C. Garcia-Cely, *Self-interacting Spin-2 Dark Matter*, *Phys. Rev. D* **96** (2017) 103519 [1708.06764].

[482] E.G.M. Ferreira, *Ultra-Light Dark Matter*, 2005.03254.

[483] K. Aoki and K.-i. Maeda, *Condensate of Massive Graviton and Dark Matter*, *Phys. Rev. D* **97** (2018) 044002 [1707.05003].

[484] L. Marzola, M. Raidal and F.R. Urban, *Oscillating Spin-2 Dark Matter*, *Phys. Rev. D* **97** (2018) 024010 [1708.04253].

[485] K. Aoki, K.-i. Maeda, Y. Misonoh and H. Okawa, *Massive Graviton Geons*, *Phys. Rev. D* **97** (2018) 044005 [1710.05606].

[486] F.R. Urban, *Dark Matter with Genuine Spin-2 Fields*, *Universe* **4** (2018) 90.

[487] J.M. Armaleo, D. López Nacir and F.R. Urban, *Binary pulsars as probes for spin-2 ultralight dark matter*, *JCAP* **01** (2020) 053 [1909.13814].

[488] J.M. Armaleo, D. López Nacir and F.R. Urban, *Pulsar timing array constraints on spin-2 ULDM*, *JCAP* **09** (2020) 031 [2005.03731].

[489] J.M. Armaleo, D. López Nacir and F.R. Urban, *Searching for spin-2 ULDM with gravitational waves interferometers*, *JCAP* **04** (2021) 053 [2012.13997].

[490] F. Piazza and C. Marinoni, *Model for gravitational interaction between dark matter and baryons*, *Phys. Rev. Lett.* **91** (2003) 141301 [hep-ph/0304228].

[491] J. Henrichs, M. Lembo, F. Iocco and L. Amendola, *Testing gravity with the Milky Way: Yukawa potential*, 2010.15190.